Nonperturbative dynamics of quantum fields in de Sitter spacetime

Gabriel Moreau

UNIVERSITÉ DE PARIS



Thèse préparée à l'Université de Paris

École doctorale des Sciences de la Terre et de l'Environnement et Physique de l'Univers - ED n°560

Laboratoire AstroParticules et Cosmologie (APC) - Groupe Théorie

---

Nonperturbative dynamics of quantum fields in de Sitter spacetime

---

Thèse de doctorat de Physique de l'Univers

Gabriel MOREAU

dirigée par Julien SERREAU

présentée et soutenue publiquement le 11 septembre 2020
devant le jury composé de :

Bertrand DELAMOTTE Directeur de recherche (CNRS, LPTMC)	Examinateur
Arttu RAJANTIE Professor (Imperial College London)	Rapporteur
Gerasimos RIGOPOULOS Lecturer (Newcastle University)	Rapporteur
Julien SERREAU Maître de conférence (Université de Paris, APC)	Directeur de thèse
Danièle STEER Professeure (Université de Paris, APC)	Présidente du jury
Vincent VENNIN Chargé de recherche (CNRS, APC)	Examinateur

Acknowledgments

I would like to thank all the people who helped me during this long journey.

I start with my supervisor Julien Serreau for his support on the scientific and non-scientific aspects of the PhD. He introduced me to a variety of topics with patience and pedagogy, and managed to create a welcoming and stimulating atmosphere which made the whole experience truly enjoyable. I also learned a lot from his intellectual rigour and honesty. For all that I am infinitely grateful.

I also thank the jury members, Bertrand Delamotte, Danièle Steer and Vincent Vennin, and I am especially grateful to Arttu Rajantie and Gerasimos Rigopoulos for accepting to be my referees and for their careful reading of the present manuscript. I also thank them for the discussions we had during the past three years.

Throughout this thesis, I have benefited from the stimulating atmosphere of the theory group at the APC laboratory. I have a special thought for all the PhD students of the APC that I have encountered over the years, and who made the work environment a lot more fun.

Teaching was also a great experience and I thank the pedagogical teams I had the pleasure to work with.

I finally thank my family, and Charlotte, for their support throughout these demanding times.

Abstract

The study of quantum field theory in de Sitter spacetime is notably motivated by the success of inflation, and the possibility to test fundamental physics through cosmological experiments. Going beyond the usual linearized description, one has to use nonperturbative methods to circumvent the infrared and secular divergences arising from the gravitational amplification of superhorizon modes. This thesis first focuses on the backreaction of an $O(N)$ quantum scalar theory on the background geometry, related to the cosmological constant problem, as such divergences may signal an instability of de Sitter space towards a Minkowski spacetime. Our study uses the functional renormalization group (FRG) and shows a finite backreaction in the presence of interactions, which saturates as a result of the nonperturbative generation of a mass. The FRG methods also allows to probe a large parameter space, including the case of a massless minimally coupled field and symmetry breaking potentials, and concludes in favor of the stability of de Sitter in all case. The second main topic of the thesis is the effect of selfinteractions on scalar field correlators correlators at separate spacetime points, in the infrared limit. The spacetime dependence gives access to several interesting physical quantities such as power spectra, relaxation time, or decoherence time. The stochastic formalism is considered. A functional formulation, in terms of a one-dimensional supersymmetric field theory, is obtained through the Janssen-de Dominic procedure, and we use it as an effective field theory to compute the correlators with different techniques. The FRG is first implemented beyond the usual local potential approximation (LPA) to second order in the derivative expansion, as the LPA is known to give a too simplistic result for the spacetime dependence of the correlators. We compare with exact analytical results in the context of a $1/N$ expansion and with numerical results for the case of a single $(N = 1)$ massless minimally coupled field. We typically obtain a ten percent accuracy in both cases for the correlation time (or length), at large spacetime separation. The aforementioned analytic results in the $1/N$ expansion are computed solving the Schwinger-Dyson equations at next-to-leading order (NLO). We obtain the two- and four-point field correlators and the results are shown to coincide with the one obtained in the original Lorentzian field theory. Finally, the $1/N$ expansion is applied directly to the Fokker-Planck formulation of the stochastic approach, which is phrased as an equivalent, Schrödinger-like, eigenvalue problem. The correponding spectrum is entirely computed at NLO, giving access to the spacetime dependence of any correlator.

Résumé

L'étude des champs quantiques en espace-temps de Sitter est notamment motivée par le succès de la théorie de l'inflation, et la possibilité de réaliser des tests de physique fondamentale à travers des expériences de cosmologie. Pour aller au delà de la description linéarisée habituelle, il est nécessaire d'utiliser des méthodes non-perturbatives, pour s'affranchir des divergences infrarouges ou séculaires, elles-mêmes conséquences de l'amplification gravitationnelle des modes super-horizon. Cette thèse se concentre tout d'abord sur le problème de la rétroaction d'une théorie $O(N)$ de champs scalaires quantiques sur la géométrie ambiante, en lien avec le problème de la constante cosmologique, les divergences précédemment citées pouvant révéler une instabilité de l'espace-temps de Sitter relaxant vers un espace-temps de Minkowski. On utilise ici le groupe de renormalisation fonctionnel (GRF), and on montre que la rétroaction est toujours finie malgré la présence d'interactions. Le mécanisme de saturation est intrinsèquement non-perturbatif et résulte de la génération d'une masse pour le champ scalaire. Le GRF permet de sonder un large espace de paramètres, incluant notamment le cas d'un champ sans masse minimalement couplé et des potentiels à symétrie brisée, et conclu à la stabilité de de Sitter dans tous les cas. L'autre thématique majeure concerne les effets des auto-interactions sur les corrélateurs du champ scalaire pris en différents points de l'espace-temps, dans la limite infrarouge. La dépendance dans les coordonnées d'espace-temps donne accès à diverses quantités physiques d'intérêt, comme des spectres de puissance, des temps de relaxation, ou de décohérence. Le formalisme stochastique est utilisé dans ce cadre. Une formulation fonctionnelle en terme d'une théorie unidimensionnelle supersymétrique est obtenue avec la procédure de Janssen-de Dominicis, et est utilisée comme une théorie des champs effective pour le calcul des corrélateurs via différentes techniques. Le GRF est d'abord implémenté au delà de l'approximation du potentiel local (APL) usuelle au deuxième ordre dans le développement dérivatif, l'APL donnant un résultat trop simplistes pour la dépendance en espace-temps des corrélateurs. On compare ensuite avec des résultats analytiques obtenus dans le contexte d'un développement $1/N$, et numériques pour un seul champ ($N = 1$) sans masse et minimalement couplé. On obtient typiquement une précision de l'ordre de dix pourcent dans ces deux cas pour le temps (ou la longueur) de corrélation à grandes séparations d'espace-temps. Les résultats analytiques précédemment mentionnés dans le développement $1/N$ sont également calculés par la résolution des équations de Schwinger-Dyson, à l'ordre sous dominant (OSD). On obtient les corrélateurs du champ à deux et quatre points, et on constate que le résultat co-

incide avec le calcul fait dans la théorie des champs Lorentzienne originale. Enfin, un développement $1/N$ est appliqué directement à la formulation en terme d'une équation de Fokker-Planck de l'approche stochastique, exprimée comme un problème équivalent d'une équation aux valeurs propres de type équation de Schrödinger. Le spectre associé est calculé en intégralité à l'OSD, et donne accès à la dépendance en espace-temps de tous les corrélateurs de la théorie.

Contents

Contents **v**

Introduction **1**

1 Context and motivations **5**
1.1 From the Big Bang to inflation . . . 5
1.1.1 Cosmological standard model . . . 6
1.1.2 Problems . . . 8
1.1.3 Inflation . . . 11
1.2 Semi-classical theory . . . 13
1.2.1 De Sitter geometry . . . 14
1.2.2 In-in formalism . . . 15
1.2.3 Bunch-Davies vacuum and quantization . . . 17
1.2.4 Infrared amplification . . . 19
1.3 The functional renormalization group . . . 22
1.3.1 Principle . . . 22
1.3.2 Wetterich equation . . . 24
1.3.3 Approximation strategies and regulator . . . 25

2 Backreaction **27**
2.1 Self-consistent metric . . . 28
2.1.1 Regularized semiclassical Einstein equations . . . 28
2.1.2 Symmetries and the regulator . . . 30
2.1.3 Hubble parameter . . . 31
2.2 Flow equations . . . 31
2.2.1 Flow of the effective potential . . . 32
2.2.2 Flow of the Hubble parameter . . . 34
2.3 Interesting limits . . . 36
2.3.1 Gaussian case . . . 36
2.3.2 large N interacting case . . . 38
2.3.3 Finite N case . . . 46
2.4 Conclusion . . . 50

3 Model A and FRG **52**

3.1 Stochastic formalism . . . 53
3.1.1 Coarse graining . . . 54
3.1.2 Classicalization . . . 55
3.1.3 Stochastic noise . . . 56
3.1.4 Light fields in slow-roll . . . 58
3.1.5 Generalization to several fields . . . 60
3.2 Functional formulation . . . 61
3.2.1 Janssen-de Dominicis integral . . . 62
3.2.2 Supersymmetry . . . 63
3.3 General properties of correlators . . . 64
3.3.1 Supersymmetry constraints . . . 64
3.3.2 Fluctuation-dissipation relation . . . 67
3.3.3 Causality . . . 68
3.4 FRG for the model A . . . 69
3.4.1 Flow of the effective potential . . . 69
3.4.2 Flow at second order in the derivative expansion . . . 72
3.4.3 Convergence of the derivative expansion . . . 74
3.5 Conclusion . . . 80

4 Model A and eigenvalues **81**
4.1 Fokker-Planck formulation of the stochastic formalism . . . 82
4.1.1 Eigenvalue problem . . . 82
4.1.2 Mass hierarchy and correlators . . . 83
4.2 Diagrammatic resummations with the Janssen-de Dominicis path integral 85
4.2.1 Perturbative expansion . . . 86
4.2.2 $1/N$ expansion . . . 90
4.2.3 Discussion . . . 95
4.3 $1/N$ expansion of the Fokker-Planck equation . . . 98
4.3.1 Gaussian case . . . 99
4.3.2 Interacting case . . . 100
4.3.3 Discussion . . . 102
4.3.4 Comparison to finite N results . . . 103
4.4 Conclusion . . . 107

Conclusion **109**

A Flow of the inverse propagator **113**
A.1 Four-point vertex contribution . . . 113
A.2 Three-point vertex contribution . . . 115

B Self-energy at three-loop order **118**

C $1/N$ expansion of the Fokker-Planck eigenvalue problem at higher-order **121**
C.1 Computation of the spectrum at next-to-leading order . . . 121

C.2 Eigenvalues at NNLO 124

Bibliography **126**

Introduction

Quantum field theory (QFT) in curved spacetime, *i.e.*, in the presence of a nontrivial background geometry, is believed to give a good approximation of the yet unknown quantum theory of gravity in numerous contexts where the typical energy scales are well below the Planck scale [1]. Among its most celebrated result is the correct description of the production of inhomogeneities from quantum fluctuations in the primordial Universe. This leads, in turn, to the observed spectrum for temperature fluctuation in the Cosmic Microwave Background (CMB) [2], which seeds all the subsequent structure formation in the Universe. Indeed, the inflationary phase, initially introduced to tackle some problems of the cosmological standard model [3–6], relies on an exponential expansion, which dramatically amplifies the small quantum fluctuations up to cosmological scales. This phase being approximately described by de Sitter spacetime, the inclusion of quantum effects in such a geometry is important for at least two reasons. It is theoretically motivated by the need for a coherent description of higher order corrections, to understand the success of the actual description. Also, the increasing precision in cosmological experiments opens interesting perspective to test quantum effects at a fundamental level.

The computation leading to the well-known scale invariant power spectrum for the inflaton field is, so far, essentially based on a linearized description [7, 8]. Going to higher orders in the perturbative expansion is in principle required by the presence of non-linearities, either in the form of interactions of the inflaton field, or intrinsic to the relativistic theory of gravitation. However, the computation of loop diagrams in a de Sitter background is plagued by the very amplification mechanism that makes inflation so appealing. It materializes as a huge particle production in the infrared (superhorizon) sector of the theory [9–12], which turns out as problematic divergences in loop integrals [11, 13, 14]. The latter cannot be treated through the usual perturbative renormalization procedure developed in flat spacetime, they rather signal nonperturbative effects, and nontrivial physics in the infrared.

The proper treatment of these divergences has been an active subject of research in the past four decades, with renewed interest in the recent years, and has lead to different nonperturbative approaches and studies of the nonlinearities. One of the first techniques introduced in this context is the stochastic formalism [15–18]. It describes the dynamics of superhorizon modes in terms of a Langevin equation, sourced by the modes coming out of the horizon during the expansion. This formalism has been shown to resum the leading logarithm contributions of the diagrammatic computations [11, 19,

20], leading to genuinly nonperturbative results. In parallel, several QFT techniques, initially developed to tackle nonperturbative effects in flat spacetime, have been developed over the years [21–42]. Among them, those which will be used throughout this thesis are the $1/N$ expansion and the functional renormalization group (FRG) [43–45]. The latter is specifically designed to treat infared physics, and is used in a variety of situations, ranging from critical phenomena [46, 47] to quantum gravity [48]. It has been systematically studied for interacting test scalar fields in de Sitter spacetime at the Local Potential Approximation (LPA) [39], and has been shown to coincide in some appropriate limits with the stochastic results.

As a particular manifestation of the infrared divergences, secular divergences that grows in terms of the cosmic time appear to be very generic in cosmological setups [13, 14]. Such behavior is often encountered in nonequilibrium QFT as an artifact of the perturbative approach, which disappears after an appropriate resummation [49–51], and similar methods can be implemented in de Sitter [29, 34, 35]. Simultaneously, in de Sitter, such large loop contributions could lead to important backreaction effects on the geometry, and have sometimes been considered as a sign of possible instability of such spacetime [10, 12, 52–62]. This type of backreaction effect is often considered as a possible solution to the cosmological constant problem [63–65], as it gives a dynamical screening process. However, similarly to what happens in the nonequilibrium QFT setup, this could be an artifact of an invalid pertubative expansion. Studying this idea in de Sitter using an appropriate extension of the FRG approach for test scalar fields is one of the main topic of this thesis. The use of FRG is motivated by the fact that it does not deal directly with secular divergencies but, instead, with the equivalent infrared divergences in momentum space. In particular, this allows to consider stability along the renormalization flow rather than a time coordinate, so as to preserve the symmetries of spacetime.

Even in the case of test scalar fields, explicit nonperturbative computations have been restricted so far essentially to one-point functions, and there are few explicit results for more complicated correlators, depending on different spacetime points. Another goal of the present thesis is to compute such correlators, which give access to a variety of physical quantities, *e.g.*, relaxation times, decoherence times, or power spectra of various operators.

For example, the FRG computation in the LPA predicts the so-called dynamical mass, which measures the amplitude of the local field fluctuations in a Hubble patch, but it gives an incorrect answer for unequal time quantities, such as the field autocorrelation time. We investigate the FRG beyond the LPA, testing in particular whether going to higher order in the derivative expansion improves the result. The computation for the Lorentzian QFT proves difficult [40], as one needs to compute the flow equation of the complete theory before considering the infrared regime which we are interested in. An alternative is to consider an effective theory that describes the infrared, such as the stochastic formalism. Applying the FRG to the latter has been shown to correctly reproduce the infrared limit of the original QFT approach in the LPA [42]. In this thesis, we follow this line, and extend this computation, using the fact that the stochastic ap-

proach is nothing but a particular case of the model A in the classification of Hohenberg and Halperin [66]. The latter has been extensively studied in statistical physics, using in particular the FRG [67, 68]. The starting point is a functional formulation of the stochastic equation, derived with the Janssen-de Dominicis (JdD) procedure [68–70]. In the present context, the JdD path integral is one-dimensional and can be linked with supersymmetric quantum mechanics which has been recently studied with the FRG for a single field [71]. Starting from these existing works, we compute the flow equation for an $O(N)$ model of test scalar fields beyond the LPA at the next order in the derivative expansion. We check that this reproduces the LPA' result, which includes a field independent renormalization for the kinetic term and was computed in the original QFT [40]. The validity of the derivative expansion can then be studied in a $1/N$ expansion of the flow equation, that can be compared to other $1/N$ computations that are also treated in this thesis. The precision for the obtained autocorrelation time is of about ten percent. The same precision is obtained when comparing the single field ($N = 1$) result with known numerical results [18, 72].

The result of the FRG computation shows that analytical results cannot be obtained easily beyond the LPA. Moreover, although the precision on the autocorrelation time could be improved by going to higher order in the derivative expansion, we show that it is not able to reproduce the correct structure of the unequal time propagator. This structure has however been captured correctly by solving the Schwinger-Dyson equations in two specific approximations [34, 35]. We apply this method directly to the JdD path integral formulation of the stochastic formalism. We compute the self-energies for the effective one-dimensional supersymmetric theory, in a perturbative expansion at three-loop order, and to next-to-leading order (NLO) in a $1/N$ expansion. The comparison with the original QFT gives a perfect agreement for the infrared correlators, which shows a nontrivial equivalence with the stochastic formalism, while the computations are much easier for higher orders in the latter framework.

Finally, we turn to the formulation of the stochastic approach in terms of the equivalent Fokker-Planck equation, phrased as en eigenvalue problem [18, 72–74]. This gives a natural explanation to the observed splitted structure of the correlators at NLO [35], in terms of its spectral decomposition. In this language, by solving the Schwinger-Dyson equations, we are able to find the lowest eigenvalues, by direct computation of the correlators. The expressions obtained at leading order (LO) in the $1/N$ expansion have a very simple structure, pointing towards the possibility to obtain the entire spectrum analytically. In principle, the latter can be used to reconstruct all observables. We thus investigate a $1/N$ expansion directly at the level of the Fokker-Planck equation, and explicitly compute the eigenvalues and eigenfunctions up to NLO (and NNLO for some quantities). To test the validity of the $1/N$ expansion, we solve numerically the eigenvalue problem in the case of a massless field for arbitrary values of N, down to $N = 1$. The comparison between the numerical results and the $1/N$ expansion shows a good agreement down to low values of N, including $N = 1$ for some cases.

The thesis is organized as follows. In the first chapter, we recall the motivations for introducing an inflationary phase to the cosmological standard model, which is ap-

proximately described by de Sitter spacetime. We then present some technical aspects concerning the semi-classical approach, in particular the quantization of the free massive field, to comment one central aspect of quantum fluctuations in de Sitter, namely the gravitational amplification of infrared modes. The final tool we introduce is the FRG, formulated in the effective average action formalism.

We then move on to the study of the backreaction problem in the second chapter. We first introduce a minimal extension to the case of an $O(N)$ theory of test scalar fields. It amounts to consider a classical metric renormalized only by the scalars quantum fluctuations, discarding in particular the metric fluctuations such as the graviton. We derive the regularized semi-classical Einstein equations, and use them to compute the renormalization flow of the Hubble rate in the deep infrared limit. The flow is dominated by the effective potential, which is computed from a zero-dimensional theory. The FRG allows to consider several initial potentials and we explore different regimes, either Gaussian, or deeply nonperturbative, possibly with spontaneous symmetry breaking at the classical level. The large-N limit of the RG flow is also considered, as it gives simple analytical formulas that give interesting physical insight.

In the third chapter, after a brief derivation of the stochastic formalism, the JdD procedure is described. Some general consequences on the correlators are then discussed, and we extract different constraints in the infrared which gives both interesting interpretations in terms of properties of thermal systems, and useful relations for subsequent computations. The FRG is then implemented, and we can show that the flow of the effective potential is exactly captured in the LPA. The flow of the effective action is then computed at second order in the derivative expansion, and the convergence is discussed in special cases.

Finally, the last chapter focus on two different approaches to extract analytical results for the correlators in a $1/N$ expansion. A first direct computation solves the Schwinger-Dyson equations at NLO to resum a class of diagrams. The second computation formulates a $1/N$ expansion of the Fokker-Planck equation, formulated as an eigenvalue problem, and we compute the entire spectrum at NNLO.

1 Context and motivations

Contents

1.1 From the Big Bang to inflation . . . 5
1.1.1 Cosmological standard model . . . 6
1.1.2 Problems . . . 8
1.1.3 Inflation . . . 11
1.2 Semi-classical theory . . . 13
1.2.1 De Sitter geometry . . . 14
1.2.2 In-in formalism . . . 15
1.2.3 Bunch-Davies vacuum and quantization . . . 17
1.2.4 Infrared amplification . . . 19
1.3 The functional renormalization group . . . 22
1.3.1 Principle . . . 22
1.3.2 Wetterich equation . . . 24
1.3.3 Approximation strategies and regulator . . . 25

This chapter is devoted to the context and motivations of this thesis. Although quantum field theory in curved spacetime can be developed as a relevant subjet in its own right, the specific case of de Sitter is particularly interesting because of its link to cosmology and the inflationary Universe. This will be the topic of Sec. 1.1. The following section 1.2 will be concerned with the technical setup necessary to the semi-classical treatment of quantum fields in a curved background. As this work is about nonperturbative treatments, we will give a general introduction to the principle of the FRG in Sec. 1.3.

1.1 From the Big Bang to inflation

This introduction to cosmology is brief and partial, and mainly focus on understanding how inflation comes as a solution to several theoretical problems of the standard approach to cosmology. What makes inflation particularly interesting is that, on top of solving several fine-tuning issues, it has observable signatures in the Cosmic Microwave Background (CMB) that are directly related to quantum effects in the early Universe.

1.1.1 Cosmological standard model

It is remarkable that, although we lack a complete description of physics at intermediate scales, the Universe at very large scales can be described with good accuracy by the equations of general relativity, together with a fundamental assumption of homogeneity and isotropy, valid at large distances. This approach gives rise to the cosmological standard model, also called Λ-CDM, which we now discuss.

The basic equations describing the dynamics of the Universe are the Einstein equations,

$$G_{\mu\nu} = \frac{8\pi G}{3} T_{\mu\nu} \,. \tag{1.1}$$

Using the assumed symmetries of spacetime, we can specialize them to a Friedman-Lemaître-Robertson-Walker (FLRW) metric expressed in cosmic time t and comoving distances x

$$\mathrm{d}s^2 = -\mathrm{d}t^2 + a(t)^2 \mathrm{d}\vec{x}^2 \,, \tag{1.2}$$

where $a(t)$ is the scale factor, describing the expansion of space as time flows. The spatial part can be expressed in spherical coordinates as

$$\mathrm{d}\vec{x}^2 = \frac{\mathrm{d}r^2}{1 - Kr^2} + r^2 \left(\mathrm{d}\theta^2 + \sin^2\theta \mathrm{d}\phi^2\right) \,, \tag{1.3}$$

with K the spatial curvature which can be either open, flat or closed (resp. $K = -1, 0$, or 1). The energy-momentum tensor can be taken to describe a perfect fluid with energy density ρ and pressure P to give the Friedmann equations

$$H^2 = \left(\frac{\dot{a}}{a}\right)^2 = \frac{8\pi G}{3}\rho - \frac{K}{a^2} \,, \tag{1.4}$$

$$\frac{\ddot{a}}{a} = -\frac{4\pi G}{3}(\rho + 3P) \,, \tag{1.5}$$

where we introduced the Hubble expansion rate $H \equiv \dot{a}/a$.

We can rewrite the first Friedmann equation (1.4) making use of the critical density ρ_{crit}, defined in terms of the Hubble rate

$$\rho_{\mathrm{crit}} = \frac{3H^2}{8\pi G} \,. \tag{1.6}$$

The different matter components of the Universe are described as several coexisting fluids and we introduce the density parameters

$$\Omega_m = \frac{\rho_m}{\rho_{\mathrm{crit}}}, \quad \Omega_r = \frac{\rho_r}{\rho_{\mathrm{crit}}} \quad \text{and} \quad \Omega_\Lambda = \frac{\rho_\Lambda}{\rho_{\mathrm{crit}}} \,, \tag{1.7}$$

respectively for the matter, radiation and dark energy densities. Each of these species has a different equation of state, expressed in the form $P = w\rho$, and $w = 0$ (resp. $1/3$, -1) for matter (resp. radiation, dark energy). The continuity equation for a perfect

fluid, which is obtained either by combining Eqs. (1.4) and (1.5), or by using the conservation of the energy-momentum tensor, is

$$\dot{\rho} + 3H(\rho + P) = 0 \, . \tag{1.8}$$

Assuming each fluid to be independent, we deduce that their energy densities simply behave as a power law $\rho \propto a^{-3(1+w)}$. Using the notation $\Omega_K = -K/(aH)^2$ for the spatial curvature, we end up with

$$\frac{H^2}{H_0^2} = \left[\Omega_{m,0} \left(\frac{a_0}{a} \right)^3 + \Omega_{r,0} \left(\frac{a_0}{a} \right)^4 + \Omega_{\Lambda,0} + \Omega_{K,0} \left(\frac{a_0}{a} \right)^2 \right] . \tag{1.9}$$

where the quantity today are denoted with a 0 subscript. As the expansion goes on, one can see that the different species are diluted at a different rate, leading to a succession of eras where the Universe energy content is dominated by a single species, see Fig. 1.1, where we used actual experimental data [2, 75],

$$\Omega_{m,0} = 0.32, \quad \Omega_{r,0} = 9.4 \, 10^{-5}, \quad \Omega_{\Lambda,0} = 0.68, \quad |\Omega_{K,0}| \lesssim 0.01 \, . \tag{1.10}$$

These values are constrained by independent data, including large scale structures survey and baryon acoustic oscillation, type IA supernovæ and CMB temperature. In this logic, the Universe has been in a radiation dominated era, before reaching the matter-radiation equality time, after which matter became predominant. A most surprising conclusion coming out of the data is that we entered lately in a phase of accelerated expansion, dominated by the dark energy, which is now supposed to represent around 70 percent of the Universe energy content, although its exact nature is not precisely known.

One important moment in the history of the Universe is the recombination, which is qualitatively defined as follows. In the early past, the Universe was in a hot and dense state. Cooling off as a result of expansion, it reached a point where the matter and radiation content formed a plasma of nucleons, electrons and photons. This kind of medium, from an optical point of view, is opaque, meaning that the photons scatter too much on the charged particles to propagate on long distances. At some point, however, the temperature gets low enough for hydrogen atoms to form. As electrons are bound together with protons, the cross section with photons is drastically reduced, so that radiation can propagate freely. This precise moment happened around 370000 years after the Big Bang and is called the recombination time.

This leads to a crucial cosmological observable, called the CMB, composed of the primordial photons freely propagating from recombination time isotropically towards us, with a perfect black-body spectrum redshifted by the subsequent expansion. This radiation encodes a lot of valuable information about the Λ-CDM model parameters, and about earlier stages of the Universe, as we will describe in the following.

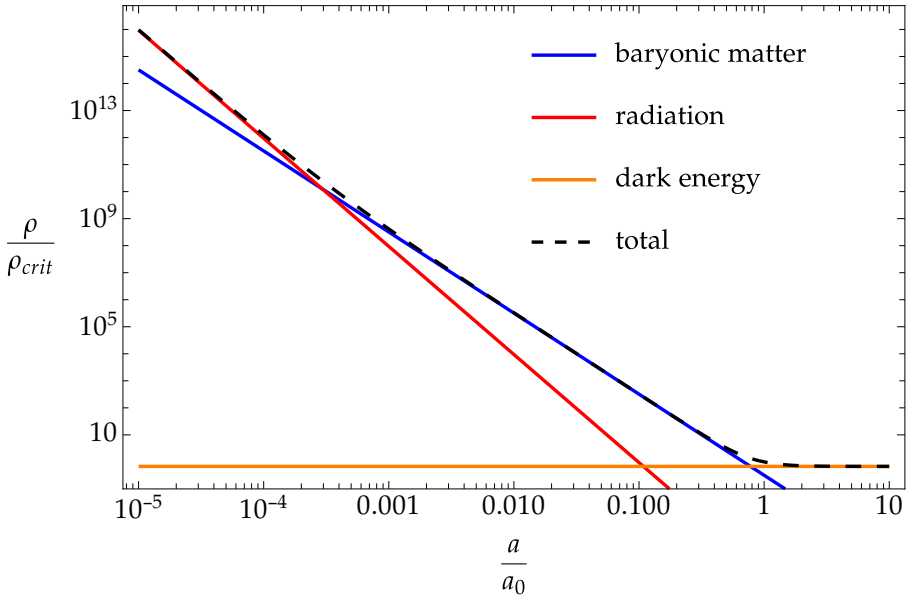

Figure 1.1: Time evolution of the energy density of the different matter components of the Universe, together with the total energy density, in units of the critical density ρ_{crit}. The numerical values are extrapolated from the experimental data (1.10). The equivalence time corresponds to the crossing of the red and blue curves, corresponding to the radiation and baryonic matter.

1.1.2 Problems

Despite its many successes, the Λ-CDM model has some theoretical flaws. We will mention two of these problems, which are both formulated as fine tuning issues, and thus appear physically unnatural.

The horizon problem is related to the large scale homogeneity of the Universe, observed in the CMB. Although homogeneity underlies the whole description, the cosmological standard model by itself does not provide a natural explanation for it. Because the size of causally connected patches, meaning regions of space which share a common history, is very small at recombination time, it is not possible to find a dynamical explanation for, *e.g.*, the observed constant value of the CMB temperature.

Let us show this in more detail. Because it travels along null geodesics, the physical distance covered at time t_f by a photon emitted at time t_i is

$$d(t_f, t_i) = a(t_f) \int_{t_i}^{t_f} \frac{\mathrm{d}t}{a(t)} \,. \tag{1.11}$$

In particular, the maximal size of a causally connected region, or the horizon size, at recombination, will be given by Eq. (1.11) with t_i the time of the Big Bang t_{BB}, and t_f the recombination time t_{rec}.

For us, recombination appears on a spherical surface at constant time and radius, called the last scattering surface. This spatial hypersurface has a metric which is given by the following projection

$$\mathrm{d}s^2 = a^2(t_{\mathrm{rec}}) r_{\mathrm{rec}}^2 \left(\mathrm{d}\theta^2 + \sin^2\theta \mathrm{d}\phi^2\right) \tag{1.12}$$

where $a(t_{\mathrm{rec}})r_{\mathrm{rec}}$ is the radius of the sphere, expressed as the physical distance between the observer, located at the origin, and the last scattering surface. It is easily expressed as the following integral

$$a(t_{\mathrm{rec}})r_{\mathrm{rec}} = a(t_{\mathrm{rec}}) \int_{t_{\mathrm{rec}}}^{t_0} \frac{\mathrm{d}t}{a(t)} \,, \tag{1.13}$$

with t_0 our observing time today. Putting everything together, the angular size of a causally connected patch on the observed map of the CMB is given by

$$\Delta\Omega = \frac{\int_{t_{\mathrm{BB}}}^{t_{\mathrm{rec}}} \mathrm{d}t\, a^{-1}(t)}{\int_{t_{\mathrm{rec}}}^{t_0} \mathrm{d}t\, a^{-1}(t)} \,. \tag{1.14}$$

Numerical computation of this quantity for a Λ-CDM Universe can be achieved using the Friedmann equation (1.4). We first express the integral over $1/a(t)$ as

$$\int_{t_i}^{t_f} \frac{\mathrm{d}t}{a(t)} = \int_{a_i}^{a_f} \frac{\mathrm{d}a}{a^2 H_0 \sqrt{\sum_i \Omega_{i,0} (a_0/a)^{3(1+w_i)}}} \,, \tag{1.15}$$

and we use the value of the scale factor at recombination time, which is $a_{\mathrm{rec}}/a_0 = a(t_{\mathrm{rec}})/a_0 \simeq 1/1091$ [2], to get $\Delta\Omega \simeq 0.02$ rad $= 1.16°$. The fact that the observed value of the CMB temperature is uniform in every directions up to relative fluctuations of order 10^{-5}, while the expected angular size of the regions of the sky which share a common past is of the order of a few degrees is called the horizon problem and is depicted in Fig. 1.2. Solving this problem would require some serious fine tuning of the initial conditions of the Universe to ensure that each independent patch of the sky shares common initial conditions up to five order of magnitudes.

A different, although similar, problem is the so-called flatness problem, which stems from the experimental value of $\Omega_{K,0}$. During the expansion, this quantity scales as a^{-2}. We write the Friedmann equation (1.4) in terms of $\Omega_{\mathrm{tot}} = \Omega_m + \Omega_r + \Omega_\Lambda$,

$$1 - \Omega_{\mathrm{tot}} = \Omega_K \,. \tag{1.16}$$

At very early times, the Universe was dominated by radiation, so that $\Omega_{\mathrm{tot}} \simeq \Omega_r$, which gives, using the continuity equation for the radiation energy density together with its equation of state

$$\frac{\Omega_{\mathrm{tot}}}{\Omega_K} \simeq \frac{\Omega_{r,0}}{\Omega_{K,0}} \left(\frac{a_0}{a}\right)^2 . \tag{1.17}$$

Combining Eqs. (1.16) and (1.17), together with the fact that $a \ll a_0$ at early times, we end up with

$$\Omega_K \simeq \frac{\Omega_{K,0}}{\Omega_{r,0}} \left(\frac{a}{a_0}\right)^2 . \tag{1.18}$$

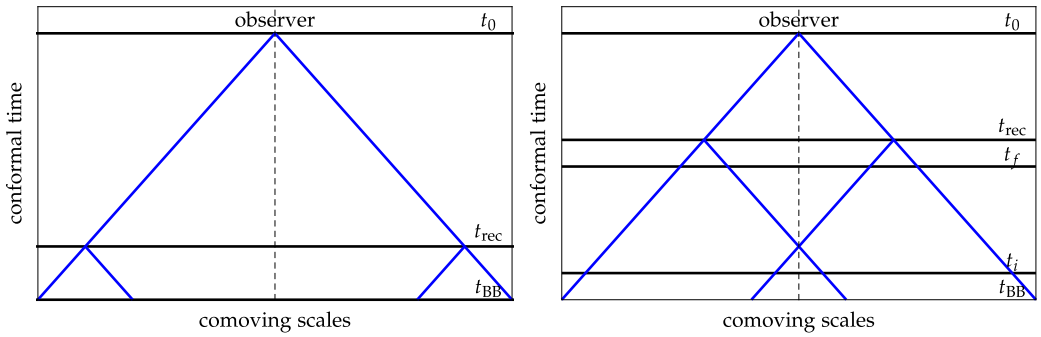

Figure 1.2: The horizon problem is easily understood in terms of spacetime diagrams in conformal time, defined later in Sec. 1.2.1, and comoving scales. The observer is at the origin and the blue lines represent null geodesics. The left diagram corresponds to the situation in the Λ-CDM model, where the two photons coming from opposite directions from the last scattering surface do not have any intersection between their past light cones. Adding the inflationary phase between t_i and t_f corresponds to extending this diagram towards negative conformal time and is represented in the right diagram. Provided this phase lasts long enough, the past light cones of the two photons now has an overlap in the infinite past.

This, again, requires a fine-tuned value of Ω_K in the early Universe in order for today's Universe to be flat enough, *i.e.* to get the experimental value $|\Omega_{K,0}| \lesssim 0.01$.

Both of these problems can be cured by adding an inflationary phase [3], taking place before the radiation dominated epoch, defined as a phase with accelerating expansion

$$\ddot{a} > 0 \,. \tag{1.19}$$

According to the second Friedmann equation (1.5), provided the Universe is dominated by a single perfect fluid, this would correspond to an equation of state with $w < -1/3$.

For a Universe dominated by a fluid with a given w between t_i and t_f, the integral appearing in Eq. (1.11) gives a contribution proportional to

$$\int_{t_i}^{t_f} \frac{\mathrm{d}t}{a} \propto \frac{a_f^{\frac{1}{2}(1+3w)} - a_i^{\frac{1}{2}(1+3w)}}{1+3w} \,. \tag{1.20}$$

Now for standard matter, $w > -1/3$, pushing t_i to very early time bring the lower bound contribution of the integral to small values

$$a_i^{\frac{1}{2}(1+3w)} \to 0 \,, \tag{1.21}$$

whereas it can take large values if the fluid is of the type $w < -1/3$. An early phase dominated by such a fluid would bring a significant contribution in the numerator in the angular size of a causally connected patch (1.14), solving the horizon problem. The graphic representation of this phenomenon is given in Fig. 1.2.

Similarly, for the flatness problem, the previous computation for the spatial curvature energy density at early time, see Eq. (1.18), is modified in a Universe dominated by a non standard fluid F between a time t_i and a time t_f. Denoting the quantities at t_i and t_f with a corresponding subscript we have

$$\Omega_{K,f} = \frac{1}{1 + \frac{\Omega_{F,i}}{\Omega_{K,i}} \left(\frac{a_f}{a_i}\right)^{-(1+3w)}} \,. \tag{1.22}$$

When $w < -1/3$, whatever spatial curvature we start with initially, it is diluted by the accelerated expansion and can give arbitrarily small values for $\Omega_{K,f}$ provided this phase lasts long enough.

Introducing a phase of accelerated expansion, the so-called inflationary phase, gives an elegant dynamical explanation to the observed flatness of the Universe, and provides a space for a possible causal mechanism explaining the large-scale homogeneity. Both of these apparently unrelated fine-tuning problems are thus solved simultaneously. Some important questions remain, however, about the precise nature of this nonstandard fluid F, and the mechanism allowing to fall back to the cosmological standard model afterwards. As a final remark, although the recent phase of acceleration could also cure these problem in principle, its duration is too small to explain the observed values, and the fine-tuning problem remains.

1.1.3 Inflation

We saw that introducing a phase of accelerated expansion that lasts for a sufficient number of e-folds after the Big-Bang helps solving some issues of the Λ-CDM model. It turns out that it is pretty easy to describe a fluid with an equation of state $w < -1/3$ using a single scalar field dominated by its potential energy [4–6]. This scalar field is called the inflaton. Consider a classical action of the type

$$S[\phi] = -\int_x \left[\frac{1}{2}\partial_\mu\phi\partial^\mu\phi + V(\phi)\right] , \tag{1.23}$$

where $\int_x = \int \mathrm{d}^D x \sqrt{-g}$, g is the determinant of the metric, and D is the spacetime dimension. The energy-momentum tensor can be written as in the perfect fluid case with the following energy density and pressure

$$\rho_\phi = \frac{\dot\phi^2}{2} + V(\phi) \,, \tag{1.24}$$

$$P_\phi = \frac{\dot\phi^2}{2} - V(\phi) \,, \tag{1.25}$$

where the spatial derivatives are discarded due to the homogeneity and isotropy. We get the desired equation of state provided $\dot\phi^2 < V(\phi)$ so that $\rho_\phi + 3P_\phi < 0$.

An interesting limit is the so-called slow-roll regime, which is widely used in model building for inflation. It consists qualitatively in expanding in the time derivatives of

the scalar field, taking the following limit

$$\dot{\phi}^2 \ll V(\phi) \,, \tag{1.26}$$

which means $w = -1$. Although the slow-roll in itself is not necessary, it leads to lower values of w, corresponding to shorter inflation, in the sense that less e-folds are required to solve the horizon and flatness problems [76]. The first Friedmann equation at leading order in the slow-roll regime reads

$$H^2 = \frac{8\pi G}{3} V(\phi) \,, \tag{1.27}$$

which means that H is almost constant. This corresponds to a de Sitter Universe[1]. The equation governing the dynamics of the inflaton field is simply the Klein-Gordon equation

$$\ddot{\phi} + 3H\dot{\phi} + V'(\phi) = 0 \,. \tag{1.28}$$

Moreover, the slow-roll approximation further assumes

$$\ddot{\phi} \ll H\dot{\phi} \,, \tag{1.29}$$

and we end up with

$$3H\dot{\phi} + V'(\phi) = 0 \,, \tag{1.30}$$

which can be solved together with Eq. (1.27) to give the spacetime dynamics at leading order in slow-roll.

Another important feature of inflation is its prediction for the CMB anisotropies spectrum, which we describe schematically here. Indeed, as already mentioned, precise measurements of the CMB reveals small inhomogeneities, of the order of 10^{-5} relatively to the average temperature of the radiation [2]. These are well described by taking into account the quantum fluctuations of the inflaton and of the metric. The usual computation, considering the smallness of the perturbations, is to do a perturbative expansion for the metric and the scalar field.

The leading order gives the classical solutions we juste described, with a quasi-de Sitter Universe. Going beyond requires a careful treatment of the gauge redundancies. For the scalar part of the perturbations, this leads to the definition of a specific gauge invariant quantity, the Mukhanov-Sasaki variable, composed of first order perturbations coming from the metric and the scalar field [7, 8]. Because of the perturbative treatment, its dynamics is the one of a free massless field in de Sitter spacetime. As we will later describe, this leads, after quantization, to a scale invariant power spectrum for the inflationary perturbations, together with the dramatic amplification of the fluctuations as a result of the expansion of the geometry.

The subsequent history of these perturbations is then sketched in Fig. 1.3. The relevant scales exits the horizon before the end of inflation, and are frozen until horizon

[1] More accurately, it is a subpatch of de Sitter called the expanding Poincaré patch, see Sec. 1.2.1

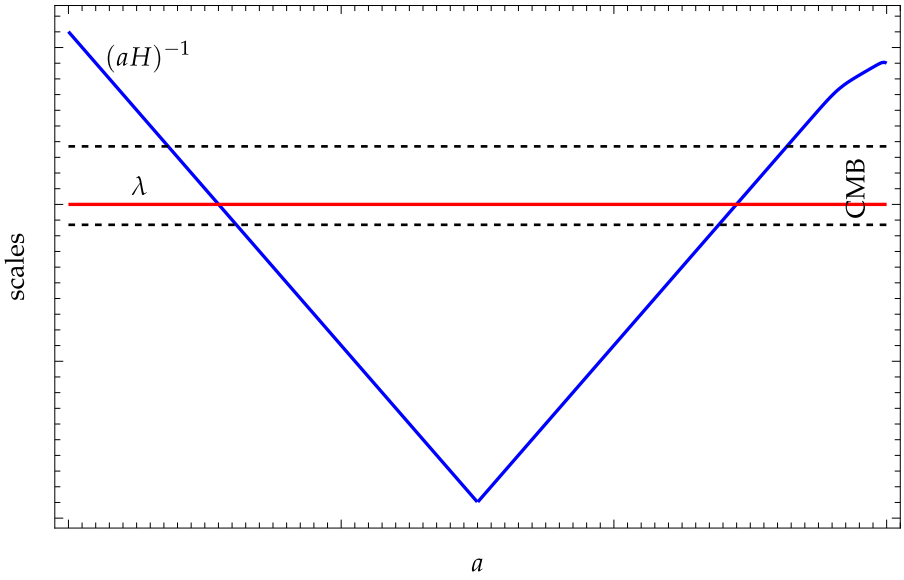

Figure 1.3: Sketch of the history of the inflationary perturbations. The horizon scale $(aH)^{-1}$ is depicted in blue, and the decreasing left part corresponds to the inflation epoch, while the increasing right part is the standard evolution of the Universe. The modes observed in the CMB are between the dashed lines, and the red line represent one particular mode, amplified by the gravitational expansion, frozen after horizon exit and turning into temperature fluctuations in the CMB.

reentry during the radiation dominated era [77–79]. Then, the amplified fluctuations of spacetime gives rise to macroscopic variations in the recombination process, which translates into fluctuations of the temperature of the blackbody spectrum of the CMB temperature [80], in very good agreement with the experimental result.

1.2 Semi-classical theory

The framework of quantum fields in curved spacetime is a semi-classical approach, which consider a non trivial gravitational background described by general relativity, together with a quantum content. It is motivated by the fact that such an effective approach should be valid for energy scales well below the Planck mass, at which the quantum gravity effects become relevant [1]. It should be recovered, in the end, as a limit of an ultraviolet complete theory of quantum gravity.

In addition to the motivations coming from cosmology, the specific case of de Sitter spacetime is of particular theoretical interest, as its symmetries are essential in solving technical difficulties, related, *e.g.* to quantization. This makes de Sitter one of the simplest situation for practical computations.

1.2.1 De Sitter geometry

De Sitter spacetime in D dimensions can be defined as the Lorentzian sphere of radius H^{-1} in $D+1$ dimensions, defined through the following implicit equation

$$-X_0^2 + \sum_{i=1}^{D} X_i^2 = H^{-2} \,. \tag{1.31}$$

It arises as a maximally symmetric solution of the Einstein equations in the vacuum in the presence of a positive cosmological constant

$$G_{\mu\nu} + \Lambda g_{\mu\nu} = 0 \,, \tag{1.32}$$

provided

$$\Lambda = \frac{(D-1)(D-2)}{2} H^2 \,. \tag{1.33}$$

In cosmology, the description of the inflationary phase, which is said to be quasi-de Sitter in the slow-roll approximation, relies only on a subpart of de Sitter spacetime called the expanding Poincaré patch (EPP). The remaining half is called the contracting Poincaré patch, and will not be considered in the following.

The EPP can be viewed as a specific case of a FLRW spacetime, with a constant Hubble rate H, with a cosmic time such that

$$t \in]-\infty, +\infty[\,. \tag{1.34}$$

This means that the scale factor in the previous metric (1.2) is simply given in terms of the cosmic time as $a(t) = e^{Ht}$. In these coordinates, the spatial translations and rotations are explicitly realized, but the time translation symmetry of the de Sitter geometry is not manifest due to the explicit time dependence of the scale factor. In fact, it is a general property of de Sitter spacetime that the generators of spatial and temporal translations do not commute. Physically, this translates, for example, into the gravitational redshift, and on a technical level, it has crucial consequences for the quantization and QFT computations, as we will see in Sec. 1.2.3.

Another interesting coordinate system makes use of the conformal time, defined as $\mathrm{d}\eta = \mathrm{d}t/a(t)$, so that the metric is conformally flat

$$\mathrm{d}s^2 = a(\eta)\left(-\mathrm{d}\eta^2 + \mathrm{d}\vec{x}^2\right) \,, \tag{1.35}$$

and the scale factor can be expressed as $a(\eta) = -1/(H\eta)$. The conformal times is such that

$$\eta \in]-\infty, 0[\,. \tag{1.36}$$

The last coordinate system we mention is the Painlevé-Gullstrand one, defined in terms of the cosmic time and the physical coordinate $\vec{r} = a(t)\vec{x}$, so that

$$\mathrm{d}s^2 = -(1 - H^2\vec{r}^2)\mathrm{d}t^2 - 2H\,\mathrm{d}t\,\vec{r}\cdot\mathrm{d}\vec{r} + \mathrm{d}\vec{r}^2 \,. \tag{1.37}$$

In these coordinates, the spatial homogeneity is no longer explicit, but the time translation invariance is, as the metric coefficient no longer depend on the time variable t.

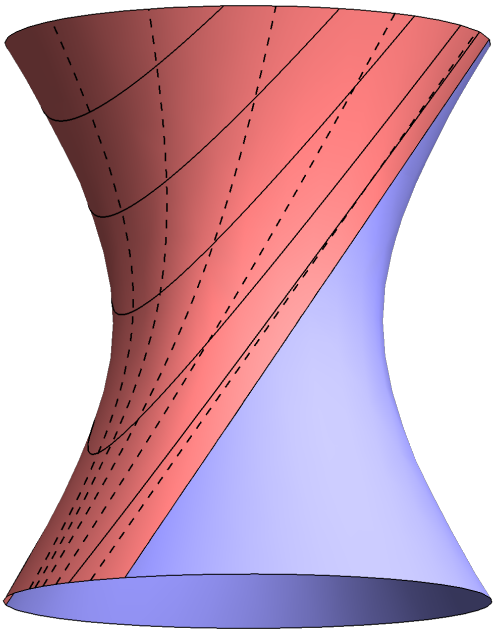

Figure 1.4: Representation of the $1+1$ dimensional de Sitter spacetime embedded in the three dimensional Euclidean space. The vertical direction is used as a time direction. The EPP is colored in red, while the contracting Poincaré patch is in blue. The black lines correspond to constant cosmic time t, while the dashed lines represent constant comoving distance x.

1.2.2 In-in formalism

De Sitter spacetime, despite being maximally symmetric, differs from flat spacetime on the fact that the generators of spatial and temporal translations do not commute. Contrarily to what is usually done in QFT in Minkowski spacetime, we cannot codiagonalize space and time translations by going to Fourier space and introducing a four momentum. This procedure is necessary to define asymptotic states in the infinite past and infinite future, and to compute overlaps between incoming and outgoing quantum states, or S-matrix elements, relevant for scattering amplitudes.

The preferred method is to use spatial homogeneity only and treat the time dependence as a nonequilibrium problem[2] [49]. The in-in, or Schwinger-Keldysh [81, 82], formalism, is adapted to such problems, as it computes the expectation value of operators in a given initial quantum state as a path integral over a time contour $\mathcal{C}$.

Let us briefly discuss how the formalism is obtained in the case of a single scalar field in the Heisenberg picture. We start with the expectation value of some Heisenberg

[2]Note that although the time translation invariance will no longer appear explicitly, it is not *a priori* broken.

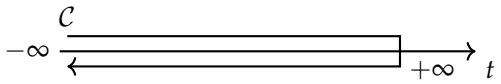

Figure 1.5: Time contour for the cosmic time used in the in-in formalism.

operator $\mathcal{O}_H$ in an initial quantum state $|\Omega\rangle$. Upon insertion of several complete sets of eigenstates of the field operator, labeled as $|\varphi, t\rangle$, we get

$$\langle\Omega|\mathcal{O}_H|\Omega\rangle = \int \mathrm{d}\varphi_1\,\mathrm{d}\varphi_2\,\mathrm{d}\varphi_3\,\langle\varphi_2,t_2|\Omega\rangle\,\langle\Omega|\varphi_3,t_3\rangle\,\langle\varphi_3,t_3|\mathcal{O}_H|\varphi_1,t_1\rangle\,\langle\varphi_1,t_1|\varphi_2,t_2\rangle\ . \tag{1.38}$$

Taking $t_{2/3} < t_1$, the product $\langle\varphi_3,t_3|\mathcal{O}_H|\varphi_1,t_1\rangle\,\langle\varphi_1,t_1|\varphi_2,t_2\rangle$ can be computed as a product of path integral, one going from t_3 to t_1 and one going back from t_1 to t_2, with the appropriate boundary conditions. Taking $t_{2/3}$ to the infinite past and t_1 to the infinite future, these two integrals can be formulated as a single one defined on a contour $\mathcal{C}$ going from the infinite past to the infinite future and back, see Fig. 1.5. If $|\Omega\rangle$ is defined as the vacuum of the noninteracting field in the infinite past[3] (see next section for a more precise definition), the remaining expectation values $\langle\varphi_2,t_2|\Omega\rangle\,\langle\Omega|\varphi_3,t_3\rangle$ can be shown [83] to contribute as some $i\varepsilon$-term, quadratic in the fields, that are added to the action. This in turns defines a prescription for the computation of the propagator, which ends up being the time ordered propagator for our boundary conditions.

In the end, the action is typically written as

$$S[\hat{\phi}] = -\int_x \left(\frac{1}{2}g^{\mu\nu}\partial_\mu\hat{\phi}\partial_\nu\hat{\phi} + V(\hat{\phi}) + i\varepsilon\,\text{terms}\right), \tag{1.39}$$

with the following integration measure $\int_x = \int_{\mathcal{C}} \mathrm{d}t \int \mathrm{d}^d\vec{x}\,\sqrt{-g}$, where $D \equiv d+1$ and the time variable now runs over the contour.

It is also useful for the following computations to define covariant notations for the functional derivative

$$\frac{\delta_c}{\delta\phi} = \frac{1}{\sqrt{-g}}\frac{\delta}{\delta\phi}\,, \tag{1.40}$$

as well as the Dirac distribution

$$\delta_c(x-y) = \frac{\delta_{\mathcal{C}}(t_x - t_y)\delta^{(d)}(\vec{x}-\vec{y})}{\sqrt{-g}}\,, \tag{1.41}$$

where $\delta_{\mathcal{C}}(t)$ is the Dirac distribution on the contour.

From there, we define the usual machinery of quantum field theory in terms of path integrals using a microscopic action $S[\hat{\phi}]$, depending on the scalar field. First, the functional quantities $\mathcal{Z}$ and $\mathcal{W}$ are defined as

$$\mathcal{Z}[j] = e^{-i\mathcal{W}[j]} = \int \mathcal{D}\hat{\phi}\exp\left(iS[\hat{\phi}] - i\int_x j\hat{\phi}\right), \tag{1.42}$$

[3]It is not necessary here to chose the vacuum state, however the state has to be defined in the infinite past so that the interactions are turned on adiabatically later.

in terms of a source field j. Successive functional derivatives of $\mathcal{Z}$ (resp. $\mathcal{W}$) will extract the different Green functions (resp. connected Green functions). Both sets contains all the information of the theory, in the sense that any observable can in principle be built from these functions.

Of particular interest are the various two-point functions. The time-ordered two-point function in the presence of external current j is simply obtained by taking two derivatives of $\mathcal{W}$ with respect to the source

$$G(x,y) = i\frac{\delta_c^2 \mathcal{W}}{\delta j(x) j(y)} = \left\langle \hat{\phi}(x)\hat{\phi}(y) \right\rangle_j - \left\langle \hat{\phi}(x) \right\rangle_j \left\langle \hat{\phi}(y) \right\rangle_j \ , \tag{1.43}$$

with the eigenvalue $\langle\rangle_j$ computed for a given external current j. The reason why we obtained this particular correlator from the path integral is related to the choice of boundary conditions hidden in the $i\varepsilon$-terms, itself related to a choice of vacuum state. This point will be discussed in the next section. For now, we just introduce several other correlators which will be used throughout this work.

The statistical and the spectral correlators are denoted by $F(x,y)$ and $\rho(x,y)$. They are defined as

$$G(x,y) = F(x,y) - \frac{i}{2}\text{sign}_{\mathcal{C}}(t_x - t_y)\rho(x,y) \ , \tag{1.44}$$

where $\text{sign}_{\mathcal{C}}$ is the sign function on the contour. Finally the retarded and advanced correlator are defined as

$$G_R(x,y) = \theta_{\mathcal{C}}(t_x - t_y)\rho(x,y) \quad \text{and} \quad G_A(x,y) = G_R(y,x) \ , \tag{1.45}$$

where $\theta_{\mathcal{C}}$ is the Heaviside distribution defined on the time contour.

These correlators can also be expressed in terms of Heisenberg field operators ϕ_H, with the quantum state $|\Omega\rangle$, using the time ordering operator on the contour $\mathcal{T}_{\mathcal{C}}$,

$$G(x,y) = \langle\Omega|\mathcal{T}_{\mathcal{C}}\phi_H(x)\phi_H(y)|\Omega\rangle - \langle\Omega|\phi_H(x)|\Omega\rangle \langle\Omega|\phi_H(y)|\Omega\rangle \ , \tag{1.46}$$

$$F(x,y) = \frac{1}{2}\langle\Omega|\{\phi_H(x),\phi_H(y)\}|\Omega\rangle \ , \tag{1.47}$$

$$\rho(x,y) = i\langle\Omega|[\phi_H(x),\phi_H(y)]|\Omega\rangle \ . \tag{1.48}$$

1.2.3 Bunch-Davies vacuum and quantization

The previous expressions rely on the definition of a vacuum state, that we have not made precise so far. To do so, we describe quickly the quantization procedure of a free massive scalar field in de Sitter. The classical action is

$$S[\hat{\phi}] = -\int_x \left[\frac{1}{2}(\partial\hat{\phi})^2 + m^2\hat{\phi}^2\right] , \tag{1.49}$$

and the associated equation of motion for the scalar field is

$$(-\Box + m^2)\hat{\phi} = 0 \ , \tag{1.50}$$

where the box operator reads, in terms of the background metric $\Box = \frac{1}{\sqrt{-g}}\partial_\mu g^{\mu\nu}\sqrt{-g}\partial_\nu$. In conformal time, Eq. (1.50) reads

$$\left(\partial_\eta^2 - \frac{D-2}{\eta}\partial_\eta - \partial_{\vec{x}}^2 + a^2(\eta)m^2\right)\hat{\phi} = 0\,. \tag{1.51}$$

Solving this equation can be achieved by going to spatial Fourier space, introducing the comoving momentum $\vec{k}$,

$$\hat{\phi}(\eta,\vec{x}) = \int_{\vec{k}}\left(\phi_k(\eta)e^{i\vec{k}\cdot\vec{x}}a_{\vec{k}} + \phi_k^\star(\eta)e^{-i\vec{k}\cdot\vec{x}}a_{\vec{k}}^\dagger\right)\,, \tag{1.52}$$

with $\int_{\vec{k}} = \int\frac{\mathrm{d}^d\vec{k}}{(2\pi)^d}$, and $a_{\vec{k}}$ and $a_{\vec{k}}^\dagger$ are simple constant Fourier coefficients at this point. The mode function $\phi_k(\eta)$ verifies the following equation

$$\left(\partial_\eta^2 - \frac{D-2}{\eta}\partial_\eta + k^2 + a^2(\eta)m^2\right)\phi_k(\eta) = 0\,, \tag{1.53}$$

which has a general solution in terms of the Hankel function of the first kind, denoted H_ν. We get

$$\phi_k(\eta) = a(\eta)^{\frac{1-d}{2}}\frac{\sqrt{-\eta\pi}}{2}[\alpha_k H_\nu(-k\eta) + \beta_k H_\nu^\star(-k\eta)]\,, \tag{1.54}$$

with two integration constants α_k and β_k, and we define the parameter ν as

$$\nu = \sqrt{\frac{d^2}{4} - \frac{m^2}{H^2}}\,. \tag{1.55}$$

Following the canonical quantization procedure, we promote the field to an operator ϕ_H. The Fourier decomposition (1.52) is now expressed in terms of creation $a_{\vec{k}}^\dagger$ and annihilation $a_{\vec{k}}$ operator, and we impose the commutation relation

$$\left[a_{\vec{k}}, a_{\vec{k}'}^\dagger\right] = (2\pi)^d\delta^{(d)}(\vec{k}-\vec{k}')\,. \tag{1.56}$$

The mode functions have to verify the Wronskian relation

$$\phi_k\partial_\eta\phi_k^\star - \phi_k^\star\partial_\eta\phi_k = i\,, \tag{1.57}$$

to get the usual commutation relations for the field operator. The vacuum state corresponding to this particular set of creation and annihilation operators is defined as

$$a_{\vec{k}}\left|\Omega\right\rangle = 0\,. \tag{1.58}$$

In flat space, the constants α_k and β_k are chosen so that the Hamiltonian is diagonalized. This selects the positive frequency solutions, which leads to the construction of quantum states with a well defined particle number. In curved space, the situation is more complicated, as there may be no globally defined time-like Killing vector, and if

one is available, as in de Sitter spacetime, it does not commute with the spatial symmetries and in particular cannot be codiagonalized. Thus we cannot define the positive frequency modes and the notion of the number of particles in a given quantum state is no well defined in general.

Different choices for α_k and β_k are thus equally acceptable, and as they corresponds to different sets of creation and annihilation operators, they give rise to different vacuum states. However, Eq. (1.57) gives the following constraint

$$|\alpha_k|^2 - |\beta_k|^2 = 1 \,, \tag{1.59}$$

which means that the different possibilities are related by Bogolyubov transformations. Looking for symmetric states, the isometries impose that these coefficients are independent of k [10, 29], and the resulting vacuum states form a (complex) one-parameter family called the α-vacua [10, 84].

Although there is no global determination of the positive frequency states, it is possible to require positive frequency solutions in the infinite past $-k\eta \gg 1$, meaning that the physical momentum $p \equiv k/a(\eta)$ is such that $p \gg H$. This condition can also be interpreted as constraining the behavior at short distance (or high energy), in units of H, to be equivalent to Minkowski space. This is physically motivated by the equivalence principle, as for scales below any typical distance scale of the background geometry, the latter appears as effectively flat. We have the following asymptotic behavior for the Hankel functions

$$H_\nu(-k\eta) \sim \sqrt{\frac{-2}{\pi k\eta}} e^{-ik\eta - i\vartheta_\nu} \quad \text{with} \quad \vartheta_\nu = \frac{\pi}{2}\left(\nu + \frac{1}{2}\right) \,, \tag{1.60}$$

and the positive frequency in the infinite past is defined as

$$\phi_k(\eta) \sim a(\eta)^{\frac{1-d}{2}} \frac{e^{-ik\eta}}{\sqrt{2k}} \,, \tag{1.61}$$

which is obtained for $\alpha_k = e^{i\vartheta_\nu}$ and $\beta_k = 0$. The corresponding state is called the Bunch-Davies (BD) vacuum, and will be used throughout this manuscript. In addition to the short distance behavior, this choice of vacuum state does not break any isometry, by construction. As an additional remark, BD is an attractor state in the EPP of de Sitter [85]. Other (non vacuum or less symmetric) states have often been considered in the literature [85–88]. In this thesis, we stick to the standard choice of BD vacuum.

1.2.4 Infrared amplification

We turn to the two-point function of the free scalar field, to underline a specificity of QFT in de Sitter spacetime, namely the gravitational infrared amplification.

The power spectrum of the scalar field operator is defined as

$$\left\langle \hat{\phi}(\eta, \vec{x}) \hat{\phi}(\eta, \vec{x}) \right\rangle = \int \mathrm{d} \log k \, \mathcal{P}(\eta, k) \,. \tag{1.62}$$

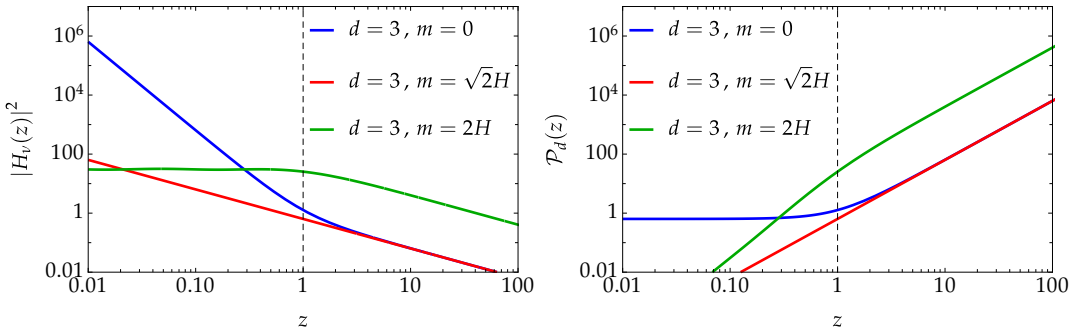

Figure 1.6: Plot of the modulus squared of the Hankel function of the first kind (left), corresponding to the mode occupation of the scalar field, together with the associated power spectrum (right), for various masses: Light case (blue), conformal case (red) and heavy case (green). The variable z is the physical momentum in units of H.

With the mode function (1.54) in the Bunch-Davies vacuum we get

$$\begin{aligned}\mathcal{P}_d(\eta,k) &= \frac{k^d\Omega_d}{(2\pi)^d}|\phi_k(\eta)|^2 \\ &= \frac{H^{d-1}\Omega_d\pi}{4(2\pi)^d}(-k\eta)^d|H_\nu(-k\eta)|^2\,,\end{aligned} \tag{1.63}$$

with $\Omega_d = 2\pi^{d/2}/\Gamma(d/2)$. Note that the power spectrum is actually a function of $p/H = -k\eta$, the physical momentum in units of H.

The asymptotic behaviors in the ultraviolet (UV) and infrared (IR) limits are as follows

$$\begin{cases}\mathcal{P}_d(p) \sim H^{2\nu-1}C_{d,\nu}p^{d-2\nu} & \text{for} \quad p \ll H\,,\\ \mathcal{P}_d(p) \sim C'_d p^{d-1} & \text{for} \quad p \gg H\,,\end{cases} \tag{1.64}$$

with the constant coefficients equal to

$$C_{d,\nu} = \frac{\Omega_d[2^\nu\Gamma(\nu)]^2}{2(2\pi)^{d+1}} \quad \text{and} \quad C'_d = \frac{\Omega_d}{2(2\pi)^d}\,. \tag{1.65}$$

By construction, in the BD state, the UV limit is similar to the flat spacetime behavior, as it reproduces the appropriate mode function. The IR limit however, exhibits a modified spectrum, which signals the gravitational amplification of the mode function on super-horizon scales. For $\nu = 1/2$, we see that the UV and IR asymptotic behavior are the same. In fact, this case, called the conformal case, exhibits a dilatation symmetry which allows one to scale out the cosmic expansion. Physical observables are the same as in Minkowski vacuum. Note, also, that the massless limit leads to $\nu \approx d/2$, which cancels the power law in the IR power spectrum and gives the well known scale invariance that is observed in the CMB. This is summarized in Fig. 1.6.

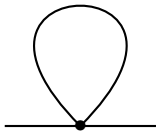

Figure 1.7: One loop tadpole diagram, which features an infrared divergence.

This IR amplification can be viewed as gravitational particle production on super-horizon scales. It is similar in nature to the Schwinger effect, where pairs of charged particles are produced in the presence of an external electric field. It is physically interpreted as virtual pairs of particles, created from quantum fluctuations of the vacuum, which are unable to recombine because the external field strength pulls them apart, thus forming a real pair [10, 59, 61].

There are several important consequences to this long distance behavior of the mode functions. First, we mentioned the remarkable feature of scale invariance of the power spectrum which is needed for a successful theory of inflation. However, at the same time, this makes computations difficult when it comes to quantum (loop) corrections. Let us show how in the case of a $\lambda\phi^4$ self-interaction for a light scalar field $m \ll H$. If we try to apply perturbation theory, we have to compute loop diagrams, such as in Fig. 1.7. This diagram is proportional to $G(x,x)$, which we already expressed in terms of the power spectrum and the mode functions in Eqs. (1.62) and (1.63). Introducing a UV cutoff Λ on physical spatial momenta we get in real space and up to a numerical factor

$$G(x,x) \propto \int_0^{\Lambda/H} \mathrm{d}z\, z^{d-1} |H_\nu(z)|^2 \,. \tag{1.66}$$

This loop integral has UV divergences, which can be treated with the usual perturbative renormalization tools. If we compute its infrared contribution up to a scale $\mu \ll H$ so that we can use the asymptotic form of the Hankel function we get, developing in terms of the mass m and of μ, see for example [36],

$$\begin{aligned} \int_0^{\mu/H} \mathrm{d}z\, z^{d-1} |H_\nu(z)|^2 &= \frac{2^{2\nu}\Gamma(\nu)^2}{\pi^2(d-2\nu)} \Big(\frac{\mu}{H}\Big)^{d-2\nu} + \mathcal{O}\big((\mu/H)^2\big) \\ &= \frac{2^{d-2}}{\pi}\left[\frac{1}{2\varepsilon} + c + \log\frac{\mu}{H}\right] + \mathcal{O}\big(\varepsilon, (\mu/H)^2\big) \,, \end{aligned} \tag{1.67}$$

with $\varepsilon = d/2 - \nu$, $c = 2 - \gamma - \log 2$ and γ is the Euler constant. This diverges as $\varepsilon \to 0$, or equivalently $m \to 0$, and is an example of infrared divergence in de Sitter spacetime. It is again a direct consequence of the infrared amplification of the mode function.

Had we started with a massless scalar field, we could have tried to regulate the logarithmic infrared divergence in integral (1.66) with a cutoff on the comoving momenta, as is often done in the literature [11, 13]. Because the integration variable z is the physical momentum in units of H, the cutoff introduces a time dependence which translates

into a logarithm of the scale factor. This term, and hence the diagram contribution, grows with time and is an example of a secular divergence appearing in loop integrals [13, 14]. Such secular divergences are actually generic features in non equilibrium systems [49].

Because of these problems, perturbation theory has a limited range of applicability in an expanding spacetime. These divergences are not specific to de Sitter and appear for example in flat spacetime in out-of-equilibrium computations. A number of tools have been developed to tackle these, which are able to resum infinite series of diagrams. Indeed, in a number of situations, the apparent divergence is an artifact of the perturbative expansion. For these reasons, we will introduce one of these tools, the functional renormalization group method.

1.3 The functional renormalization group

Among the several nonperturbative techniques in QFT is the FRG. It has interesting applications in de Sitter spacetime, as it is well designed to manage infrared divergences. We summarize here its main ideas and methods, using the example of a scalar field, in a fixed de Sitter background.

1.3.1 Principle

Wilson's renormalization group (RG) implements the coarse graining idea which underlies the renormalization procedure [89]. Instead of developing in terms of diagrams with loop integrals involving all energy scales, which produce UV and potentially IR divergences, Wilson's RG progressively integrates out momentum shells to build an effective theory for long wavelength modes, where the short wavelength have been integrated out. There are different implementations of this principle, and the one we consider here, based on the effective action, has been developed in [43, 90–96], see [44] for a pedagogical introduction and [45] for a recent review. Technically, it transforms the problem of computing path integrals into a (functional) differential problem which, although difficult to solve, can serve as a basis to implement powerful nonperturbative approximation schemes.

The effective action is defined as the Legendre transform of the generating functional $\mathcal{W}[j]$,

$$\Gamma[\phi] = -\mathcal{W}[j] + \int_x j\phi \,, \tag{1.68}$$

with the classical field ϕ defined as

$$\phi(x) = \frac{\delta_c \mathcal{W}}{\delta j(x)} = \langle \hat{\phi}(x) \rangle \,. \tag{1.69}$$

Successive functional derivatives of the effective action generate the vertex functions, which can be related to the correlation functions, so that $\Gamma[\phi]$ contains all the information of the theory.

To integrate the scales progressively we use a regulator term of the form,

$$\Delta S_\kappa[\hat{\phi}] = \frac{1}{2}\int_{xy} \hat{\phi}(x) R_\kappa(x,y)\hat{\phi}(y) \ . \tag{1.70}$$

The kernel $R_\kappa(x,y)$ is chosen such that it freezes selectively the modes below the scale κ by giving them a mass of order κ^2, leaving modes higher than κ essentially untouched, see Fig. 1.8. In particular, in the limit $\kappa \to 0$, the regulator vanishes, leaving the theory unchanged.

Adding the regulator to the action, the generating functional $\mathcal{W}$ inherits a dependence on κ,

$$e^{-i\mathcal{W}_\kappa[j]} = \int \mathcal{D}\hat{\phi}\, e^{iS[\hat{\phi}] - i\int_x j\hat{\phi} + i\Delta S_\kappa[\hat{\phi}]} \ , \tag{1.71}$$

building a continuum of theories where the modes above κ fluctuate freely and are integrated out while the modes below κ are frozen. The latter are thus progressively integrated out as κ is decreased. The effective action is modified by subtracting a regulator term

$$\Gamma_\kappa[\phi] = -\mathcal{W}_\kappa[j] + \int_x j\phi - \Delta S_\kappa[\phi] \ , \tag{1.72}$$

so as to interpolate between the correct limits for extremal values of κ. Indeed, in general,

$$e^{i\Gamma_\kappa[\phi]} = \int \mathcal{D}\hat{\phi}\, e^{iS[\hat{\phi}] - i\int_x j(\hat{\phi}-\phi) + i\Delta S_\kappa[\hat{\phi}] - i\Delta S_\kappa[\phi]} \ . \tag{1.73}$$

Taking a derivative of (1.72) with respect to ϕ, we get

$$j_\kappa(x) = \frac{\delta_c \Gamma_\kappa}{\delta\phi(x)} + \frac{\delta_c \Delta S_\kappa}{\delta\phi(x)} \ , \tag{1.74}$$

and replace it in the previous path integral. Changing variable $\hat{\phi} = \phi + \tilde{\phi}$ we obtain

$$e^{i\Gamma_\kappa[\phi]} = \int \mathcal{D}\tilde{\phi}\, e^{iS[\phi+\tilde{\phi}] - i\int_x \frac{\delta\Gamma_\kappa}{\delta\phi}\tilde{\phi} + i\Delta S_\kappa[\tilde{\phi}]} \ . \tag{1.75}$$

For κ large compared to all the scales appearing in the problem, the regulator term makes the fluctuation field $\tilde{\phi}$ very heavy, so that it decouples. Integrating it out, we get

$$\Gamma_{\kappa\to\infty}[\phi] \to S[\phi] \ . \tag{1.76}$$

In the opposite limit, $\kappa \to 0$, the regulator vanishes and we end up with the usual effective action, with fluctuations at all scales taken into account

$$\Gamma_{\kappa\to 0}[\phi] = \Gamma[\phi] \ . \tag{1.77}$$

In the end, the continuum of effective theories that we constructed interpolates between the classical theory for $\kappa \to +\infty$ to the full quantum theory with all its quantum fluctuations for $\kappa \to 0$.

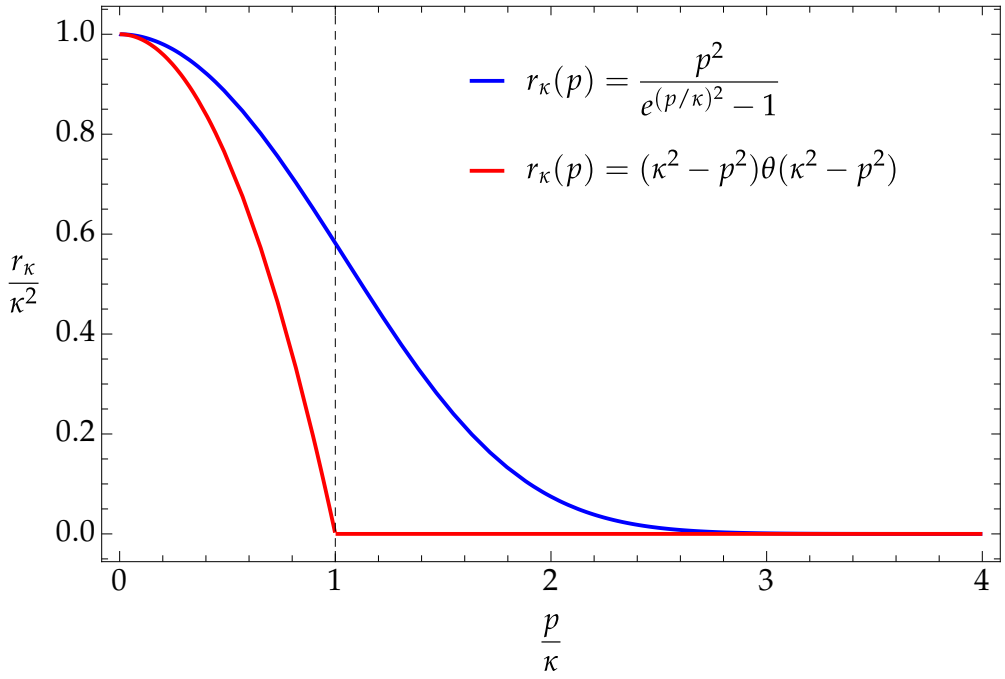

Figure 1.8: Plot of two typical regulator kernels in momentum space.

1.3.2 Wetterich equation

The flow of the effective action is computed from Eqs. (1.71) and (1.72) taking a derivative with respect to κ. For a given ϕ, the source field j has a dependence on κ from Eq. (1.74), so that

$$\partial_\kappa \Gamma_\kappa[\phi] = -\partial_\kappa \mathcal{W}_\kappa[j_\kappa] - \partial_\kappa j_\kappa \frac{\delta_c \mathcal{W}_\kappa}{\delta j} + \partial_\kappa j_\kappa \phi - \partial_\kappa \Delta S_\kappa[\phi] \,. \tag{1.78}$$

Because of Eq. (1.69), the terms in $\partial_\kappa j_\kappa$ cancel out. From Eq. (1.71), we get

$$\partial_\kappa W_\kappa[j] = -\left\langle \partial_\kappa \Delta S_\kappa[\hat{\phi}] \right\rangle_j \,. \tag{1.79}$$

In the end

$$\begin{aligned} \partial_\kappa \Gamma_\kappa[\phi] &= \frac{1}{2} \int_{x,y} \partial_\kappa R_\kappa(x,y) \left[\left\langle \hat{\phi}(x)\hat{\phi}(y) \right\rangle_{j_\kappa} - \phi(x)\phi(y) \right] \\ &= \frac{1}{2} \int_{x,y} \partial_\kappa R_\kappa(x,y) G_\kappa^{j_\kappa}(x,y) \,, \end{aligned} \tag{1.80}$$

with G_κ^j the propagator computed with an external source j. This propagator can be expressed in terms of the vertex functions in order to get a closed equation. Deriving Eq. (1.74) with respect to ϕ, we have

$$\frac{\delta_c j_\kappa(x)}{\delta \phi(y)} = \frac{\delta_c^2 \Gamma_\kappa}{\delta \phi(x) \delta \phi(y)} + R_\kappa(x,y) \tag{1.81}$$

and the left-hand side is obtained deriving Eq. (1.69), applied at j_κ, with respect to ϕ,

$$\int_z \frac{\delta \mathcal{W}_\kappa}{\delta j(x)\delta j(z)} \frac{\delta j_\kappa(z)}{\delta \phi(y)} = \delta(x-y) \ . \tag{1.82}$$

In the end, one has, in matrix notations

$$G_\kappa = i\Big(\Gamma_\kappa^{(2)} + R_\kappa\Big)^{-1} \ , \tag{1.83}$$

and the flow equation becomes

$$\partial_\kappa \Gamma_\kappa = \frac{i}{2}\,\mathrm{tr}\left[\partial_\kappa R_\kappa \Big(\Gamma_\kappa^{(2)} + R_\kappa\Big)^{-1}\right] , \tag{1.84}$$

which is known as the Wetterich equation [90]. Importantly, this equation has a one-loop structure, and the loop integral is regulated both in the UV, by the $\partial_\kappa R_\kappa$ factor, and in the IR, where the additional R_κ in the propagator acts as a regulating mass term.

1.3.3 Approximation strategies and regulator

The Wetterich equation (1.84) is exact so far, but is impossible to solve in general. We have to resort to some approximation strategies in order to extract information. One way to implement such approximations is by injecting a specific ansatz for the effective action. The ansatz has to respect all the symmetries of the action, provided they are not broken by the regulator, and if no anomaly is present.

In de Sitter, we will use the derivative expansion [43, 96], which consists in keeping a functional dependence for the potential part, truncating only the derivative interactions at a given order. For example, the derivative expansion at order ∂^2 for a scalar field with a $\mathbb{Z}_2$ symmetry gives the following ansatz

$$\Gamma_\kappa[\phi] = -\int_x \left[\frac{1}{2} Z_\kappa(\phi)(\partial\phi)^2 + V_\kappa(\phi)\right] . \tag{1.85}$$

The leading order in the derivative expansion, called the local potential approximation (LPA) consists in setting $Z_\kappa(\phi) = 1$. The LPA still includes a kinetic term in order to get the correct interpolation point with the classical action in the UV, but its renormalization is not taken into account.

In de Sitter spacetime, we do not know of a fully de Sitter invariant regulator. More precisely, we cannot reconcile the isometries with an efficient regulation of the loop integral in the RG flow equation (1.84). For example, consider a pure mass term

$$R_\kappa(x,y) \propto f(\kappa)\delta_c(x-y) \ , \tag{1.86}$$

where the function $f(\kappa)$ cannot depend on spacetime coordinates. Choosing $f(\kappa) = \kappa^2$ gives the appropriate behavior in the IR, but does not regulate the UV divergence.

However, we can build regulators that preserve a subgroup of the de Sitter isometries [38], called the affine subgroup, generated by spacetime translations and spatial

rotations. Using the cosmic time together with the physical coordinates (corresponding to the Painlevé-Gullstrand metric), we define the following kernel

$$R_\kappa(x,y) = \delta(t_x - t_y) \int_{\vec{p}} e^{i(\vec{r}_x - \vec{r}_y)\cdot\vec{p}} r_\kappa(p) \ , \tag{1.87}$$

where $r_\kappa(p)$ is a function of the physical momentum which has to verify

$$\begin{cases} r_\kappa(p) \to 0 & \text{for} \quad p \to \infty \ , \\ r_\kappa(p) \sim \kappa^2 & \text{for} \quad p \ll \kappa \ , \end{cases} \tag{1.88}$$

in order to regulate and interpolate correctly. Importantly, a change in the regulating function changes the flow at finite κ, but the asymptotic value at $\kappa = 0$ should not depend on the exact form of r_κ, at least in the exact theory. However, because of the approximation introduced by the truncation, the flow will have different limits when $\kappa \to 0$ for different regulators. An optimal choice for the regulator that leads as close as possible to the exact result has been discussed in [97, 98]. At the LPA level, it is the Litim regulator, which we use in this thesis. However, when going beyond the LPA, we do not study the dependence on the regulator further, and simply stick with this choice.

2 *Backreaction*

Contents

2.1 Self-consistent metric . . . 28
2.1.1 Regularized semiclassical Einstein equations . . . 28
2.1.2 Symmetries and the regulator . . . 30
2.1.3 Hubble parameter . . . 31
2.2 Flow equations . . . 31
2.2.1 Flow of the effective potential . . . 32
2.2.2 Flow of the Hubble parameter . . . 34
2.3 Interesting limits . . . 36
2.3.1 Gaussian case . . . 36
2.3.2 large N interacting case . . . 38
2.3.2.1 Symmetric regime . . . 40
2.3.2.2 Broken-symmetry regime . . . 41
2.3.2.3 Fine tuned parameters . . . 45
2.3.3 Finite N case . . . 46
2.4 Conclusion . . . 50

The infrared amplification in de Sitter spacetime mentionned in Sec. 1.2.4 can be interpreted as a gravitational particle production, in analogy with the Schwinger effect in the presence of a background electric field [10–12]. In the latter case, each pair of charged particles creates a small electric field, which counteracts the background, leading to an overall decrease of the original background field. This nontrivial backreaction is also expected in the gravitational case, where the amplified interacting modes will gravitate and modify the spacetime geometry accordingly.

The study of quantum backreaction in de Sitter spacetime is an important open problem, as it is considered a possible solution to the cosmological constant problem [63–65]. In the framework of semiclassical gravity, the hope is that quantum corrections, coupled to the spacetime geometry through the Einstein equations, could relax the cosmological constant to its small observed value today in a dynamical way.

A conclusive computation faces several difficulties. First, the inclusion of graviton or scalar metric perturbation loop contributions is technically difficult [99–101], coupled to the fact that loop diagrams in this framework contain infrared and secular divergences [11, 13, 14] which need to be resummed using a nonperturbative method,

although this is still debated [100, 102]. A second problem is that a general perturbation of the metric would break de Sitter symmetries and undermine the formalism developed in the previous chapter, which relies on the isometries for the quantization procedure.

Thus, as a first step, we restrict our attention to the possible implication of an interacting $O(N)$ scalar theory, whose infrared sector is expected to have sizeable quantum effects. Motivated by results obtained using FRG on spectator scalar fields [36–39], *i.e.* with a fixed background geometry, we would like to extend the formalism to a backreacting situation to circumvent the limited applicability of perturbation theory. The problem is formulated in a slightly different way, namely by studying the build up of quantum fluctuations and their backreaction not as a function of time but of the RG scale. This has the crucial advantage that we can compute these RG trajectories in the subspace of de Sitter geometries and constant fields configuration, keeping all available symmetries. In the end, we extract the flow of the effective spacetime curvature as the quantum fluctuations are integrated out.

In Sec. 2.1, we discuss the addition of a dynamical (but classical) metric to the FRG formalism, and define the relevant flow that we will compute in Sec. 2.2. Some particular case where analytic calculations are possible, such as the limit where N is large, as well as generic numerical results, are discussed in Sec. 2.3.

2.1 Self-consistent metric

The formulation of QFT in de Sitter spacetime that we described in Sec. 1.2 considered a fixed background geometry, to which were added possible quantum fluctuations. The usual way to make the metric dynamical keeping the semiclassical framework is to use the semiclassical Einstein equation, that relates the Einstein tensor to the expectation value of the energy momentum tensor

$$G_{\mu\nu} = M_P^{-2} \left\langle T_{\mu\nu} \right\rangle \ , \tag{2.1}$$

where we introduced the Planck mass $M_P^2 = 3/(8\pi G)$. Using the FRG formalism, we need to take care of the specific questions regarding the addition of the regulator.

2.1.1 Regularized semiclassical Einstein equations

We first derive the modified semiclassical Einstein equation, using the effective action, in order to clarify the regime of validity of the present approach, and the precise meaning of the considered backreaction we compute.

We start with a microscopic action $S[\hat{\phi}, \hat{g}]$ which now depends on a scalar field $\hat{\phi}$ and a metric $\hat{g}_{\mu\nu}$, where both can in principle fluctuate. For energies well below the Planck mass, the gravity vertices are suppressed, as the derivative interactions dimensions are compensated by powers of the Planck mass. This means that high order diagrams with gravitational interactions can be neglected with respect to low order ones. We also neglect all diagrams involving graviton loops, which we assume not to be amplified in

the infrared contrarily to the scalar field, so that they are subdominant. Whether this is reliable or not is still an open question [57, 100, 102–104].

In practice, this amounts to replacing $\hat{g}$ by its average value $\langle \hat{g} \rangle = g$. All the functional quantities S, $\mathcal{W}$ and Γ now depend on this average metric. To implement the FRG, we add the following quadratic modification to the action

$$\Delta S_\kappa[\hat{\phi}, g] = \frac{1}{2} \operatorname{Tr} R_\kappa[g] \hat{\phi} \hat{\phi} \,, \tag{2.2}$$

where the trace uses the covariant measure and the time contour previously defined, and the regulator kernel R_κ typically depends on the metric.

So far the settings are just those of a regularised field theory, in the geometry described by the metric $g_{\mu\nu}$, with the flow of the effective action described by Eq. (1.84). For our present purposes, the background metric is to be determined self-consistently at each scale κ from the (exact) extremization conditions

$$\left. \frac{\delta_c \Gamma_\kappa[\phi, g]}{\delta \phi(x)} \right|_{\phi_\kappa, g_\kappa} = 0 \,, \quad \left. \frac{\delta_c \Gamma_\kappa[\phi, g]}{\delta g^{\mu\nu}(x)} \right|_{\phi_\kappa, g_\kappa} = 0 \,. \tag{2.3}$$

At the order of approximation considered here for the gravitational fluctuations, this gives the set of regularized semiclassical Klein-Gordon and Einstein equations, which encode the backreaction of the scalar field quantum fluctuations onto the average value of the metric field $g_{\mu\nu}$. The second equation in (2.3) writes, equivalently

$$\left[\left\langle \frac{\delta_c S[\hat{\phi}, g]}{\delta g^{\mu\nu}} \right\rangle + \frac{1}{2} \frac{\delta_c}{\delta g^{\mu\nu}} \operatorname{Tr} R_\kappa[g] G_\kappa[\phi, g_\kappa] \right]_{\phi_\kappa, g_\kappa} = 0 \,, \tag{2.4}$$

where the average $\langle \ldots \rangle_\kappa$ is evaluated at the extremum (ϕ_κ, g_κ) and we stress that the functional derivative in the second regulator term does not act on G_κ.

To be more explicit, let us decompose the action in a pure gravitational term and a matter term as

$$S[\hat{\phi}, g] = S_g[g] + S_m[\hat{\phi}, g] \,, \tag{2.5}$$

and define accordingly

$$M_P^2 G_{\mu\nu} = 2 \frac{\delta_c S_g}{\delta g_{\mu\nu}} \quad \text{and} \quad T_{\mu\nu} = -2 \frac{\delta_c S_m}{\delta g^{\mu\nu}} \,. \tag{2.6}$$

The regularized semiclassical Einstein equation becomes

$$M_P^2 G_{\mu\nu}[g_\kappa] = \left\langle T_{\mu\nu}[\hat{\phi}, g_\kappa] \right\rangle_\kappa + \Delta T^\kappa_{\mu\nu}[\phi_\kappa, g_\kappa] \,. \tag{2.7}$$

The explicit contribution from the regulator reads

$$\Delta T^\kappa_{\mu\nu}(x) = \int_{z,z'} t^\kappa_{\mu\nu}(x; z, z') G_\kappa(z, z') \,, \tag{2.8}$$

where we defined

$$t^{\kappa}_{\mu\nu}(x;z,z') = \left[\frac{1}{2}g_{\mu\nu}(x)\big(\delta_c(x-z)+\delta_c(x-z')\big) - \frac{\delta_c}{\delta g^{\mu\nu}(x)}\right] R_\kappa(z,z') \ . \tag{2.9}$$

As a check, one verifies that a simple mass term, $R_\kappa(z,z') = -m^2\delta_c(z-z')$ yields the expected

$$\Delta T^{\kappa}_{\mu\nu} = -\frac{m^2}{2}g_{\mu\nu}(x)G_\kappa(x,x) \ . \tag{2.10}$$

The general picture is as follows: The progressive integration of the long wavelength scalar field fluctuations through the Wetterich equation (1.84), results in an effective renormalization of the geometry through the extremization conditions (2.3).

2.1.2 Symmetries and the regulator

We now would like to specify the above framework to the maximally symmetric case, with homogeneous sources, that is, homogeneous field configurations ϕ. In order to get a self-consistent Einstein equation we need the condition $\langle T_{\mu\nu}\rangle_\kappa \propto \Delta T^{\kappa}_{\mu\nu} \propto g^{\kappa}_{\mu\nu}$ to be valid along the flow. This would be the case if we had a de Sitter invariant regulator. However, as mentionned in Sec. 1.3.3, we do not know how to choose a regulator invariant under the full de Sitter group that regulates efficiently the UV and IR part of the loop integral in the Wetterich equation.

Still, this issue will not play a role in our analysis for the following reasons. Notice that our choice of regulator (1.87), formulated in terms of an IR cutoff on physical momenta, still preserves the affine subgroup [29]. For the sake of the argument, this allows to consider FLRW solutions and define a scale factor and a corresponding Hubble rate. Moreover, we are interested in the backreaction of the infrared modes of the scalar field, as they are the ones which get amplified, meaning we want to compute the flow for values of κ below a finite value $\kappa_0 \lesssim H_{\kappa_0}$.

Looking back at the first Friedman equation (1.4), for a generic scalar action with a covariant kinetic term and a potential, the expectation value of the first component of the energy momentum tensor has the following contributions, in comoving coordinates

$$\langle T_{00}\rangle = \left\langle \frac{1}{2}\dot{\hat{\phi}}^2 + \frac{1}{2}\left(\frac{\partial_{\vec{x}}\hat{\phi}}{a(t)}\right)^2 + V(\hat{\phi})\right\rangle \ . \tag{2.11}$$

The contributions of the kinetic and gradient terms are dominated by ultraviolet scales [105], so that they will only affect the initial condition of the flow H_{κ_0}. In the infrared regime, the potential term will be the dominant contribution, and it suffices to compute its flow to get an accurate picture.

Additionally, the symmetry breaking induced by the regulator only affects the flow of the derivative terms. Indeed, for the flow of the effective potential, preserving the affine subgroup is enough, as we only need the subspace of constant field configuration. It has been shown, and this will be explained in more details in the following, that the

LPA captures the flow of the effective potential exactly, in the present context. Going beyond the LPA, however, the flow of the derivative terms would be affected by this symmetry issue [40].

Summing up the previous argument, we are interested in infrared effects, where the Hubble rate is mainly renormalized by the contribution from the potential. The flow of the effective potential is obtained exactly using the LPA, despite the symmetry breaking induced by the regulator, which plays no role in the subspace of constant field configurations. Thus, projecting the metric in a de Sitter subspace along the flow is expected to be a good approximation of a more complete computation achieved in a general FLRW metric.

2.1.3 Hubble parameter

This justifies the procedure to specify the above framework to homogeneous field configurations $\phi(x) = \phi$ and de Sitter metric $g_{\mu\nu}(x) = g^H_{\mu\nu}(x)$, characterized by its Hubble scale H only. It is always possible to choose a coordinate system where the H-dependence of the metric appears as a global conformal factor

$$g^H_{\mu\nu}(x) = H^{-2}\tilde{g}_{\mu\nu}(x) \,, \tag{2.12}$$

with $\tilde{g}_{\mu\nu}$ is a fiducial de Sitter metric with Hubble parameter $\tilde{H} = 1$. This is obviously realized for instance in the conformal coordinate system (1.35). It is then possible to express the functional derivative with respect to the metric as a derivative with respect to H, and we have

$$H\partial_H \Gamma_\kappa[\phi, g^H] = 2\int_x g^{\mu\nu}_H(x)\, \frac{\delta\Gamma_\kappa[\phi, g]}{\delta g^{\mu\nu}(x)}\bigg|_{g^H} \,. \tag{2.13}$$

The effective action for constant field depends only on the effective potential

$$\Gamma_\kappa[\phi, g^H] = \int_x V_\kappa(\phi, H) \,, \tag{2.14}$$

and putting this in the extremization conditions for the effective action (2.3), we can determine the physical values using

$$\frac{\partial V_\kappa}{\partial\phi}\bigg|_{\phi_\kappa, H_\kappa} = 0, \quad \frac{\partial(H^{-D}V_\kappa)}{\partial H}\bigg|_{\phi_\kappa, H_\kappa} = 0 \,. \tag{2.15}$$

This transforms the semiclassical Einstein equations into semiclassical Friedmann equations corresponding to the one with a derivative with respect to H in Eq. (2.15), as we will show more explicitly in the following.

2.2 Flow equations

We now have a consistent way to compute the effect of the quantum corrections coming from the scalar field on the metric, in a preferred subspace where it is maximally

symmetric. Although this is not a fully general perturbation, it can still test whether de Sitter space is dynamically relaxed to a flat metric. The key ingredient is the flow of the effective potential which has been studied in [36–39]. We will be interested only in the infrared part of this flow, from an initial value $\kappa_0 \lesssim H_{\kappa_0}$ to the limit where we take κ to 0.

2.2.1 Flow of the effective potential

We recall here the main results regarding the effective potential for an $O(N)$ scalar theory in the LPA in a de Sitter background [36–39]. Take the following ansatz

$$\Gamma_\kappa[\phi, g^H] = -\int_x \left[\frac{1}{2} g_H^{\mu\nu} \partial_\mu \phi^a \partial_\nu \phi^a + N U_\kappa(\chi, H)\right] , \tag{2.16}$$

where $\chi = \phi^a\phi^a/(2N)$ and $NU_\kappa = V_\kappa$ is the complete effective potential where we have factored out a N for later purposes. We choose a regulator diagonal in field space, acting as a cutoff on the physical momenta $p = k/a(\eta)$, see (1.87). In particular, the Litim regulating function

$$r_\kappa(p) = (\kappa^2 - p^2)\theta(\kappa^2 - p^2) , \tag{2.17}$$

allows to perform the momentum integral in the flow equation analytically and get a simple expression for the beta function of the potential.

The flow equation for U_κ is obtained from Eq. (1.84), for constant field ϕ

$$N\partial_\kappa U_\kappa = \frac{1}{2}\int_{\vec{k}} \partial_\kappa r_\kappa\left(\frac{k}{a(\eta)}\right) G_\kappa^{aa}(\eta, \eta, \vec{k}) , \tag{2.18}$$

in terms of the spatial Fourier transform of the propagator of the regularized theory. The inverse propagator can be decomposed in transverse and longitudinal parts. Using the projectors in field space

$$P^t_{ab} = \delta_{ab} - \frac{\phi_a\phi_b}{\phi^2} , \quad P^l_{ab} = \frac{\phi_a\phi_b}{\phi^2} , \tag{2.19}$$

we get from the ansatz $\Gamma^{(2)}_{\kappa,ab} = P^t_{ab}\Gamma^{(2)}_{t,\kappa} + P^l_{ab}\Gamma^{(2)}_{l,\kappa}$, where

$$\Gamma^{(2)}_{t/l,\kappa}(x, y) = (-\Box + m^2_{t/l,\kappa})\delta(x - y) , \tag{2.20}$$

and the transverse and longitudinal masses are nothing but the curvatures of the effective potential in the appropriate directions

$$m^2_{t,\kappa} = \partial_\chi U_\kappa \quad \text{and} \quad m^2_{l,\kappa} = \partial_\chi U_\kappa + 2\chi\partial^2_\chi U_\kappa . \tag{2.21}$$

The computation of the transverse and longitudinal part of the propagator is thus identical to the single field case, where the curvature of the potential is replace by its appropriate component.

We summarize here the single field computation, in terms of the curvature of the effective potential $m_\kappa^2 = V_\kappa''$. The spatial Fourier transform of the propagator at equal time can be expressed in terms of mode functions v_k

$$G_\kappa(\eta, \eta, \vec{k}) = |v_k(\eta)|^2 \,. \tag{2.22}$$

and for our choice of regulator, v_k satisfies the following Klein-Gordon equation

$$\left[\partial_\eta^2 - \frac{D-2}{\eta}\partial_\eta + k^2 + a(\eta)^2 m_\kappa^2 + a(\eta)^2 r_\kappa\left(\frac{k}{a(\eta)}\right)\right] v_k(\eta) = 0 \,. \tag{2.23}$$

For $k/a(\eta) \geq \kappa$, the regulator vanishes and the equation can be solved exactly as in the free field case, using the Bunch-Davies condition. For $k/a(\eta) \leq \kappa$ the Litim regulator cancels the gradient term, and replaces it by a mass term $a(\eta)^2\kappa^2$. We have

$$\begin{cases} v_k(\eta) = a(\eta)^{\frac{1-d}{2}} \dfrac{\sqrt{-\eta\pi}}{2} e^{i\vartheta_{\nu_\kappa}} H_{\nu_\kappa}(-k\eta), \quad \dfrac{k}{a(\eta)} \geq \kappa \\ v_k(\eta) = a(\eta)^{\frac{1-d}{2}} \dfrac{\sqrt{-\eta\pi}}{2} e^{i\vartheta_{\nu_\kappa}} \left[c_\kappa^+ \left(\dfrac{k}{a(\eta)\kappa}\right)^{\bar{\nu}_\kappa} + c_\kappa^- \left(\dfrac{a(\eta)\kappa}{k}\right)^{\bar{\nu}_\kappa}\right], \quad \dfrac{k}{a(\eta)} \leq \kappa \,, \end{cases} \tag{2.24}$$

where

$$\nu_\kappa = \sqrt{\frac{d^2}{4} - \frac{m_\kappa^2}{H^2}}, \quad \bar{\nu}_\kappa^2 = \nu_\kappa^2 - \frac{\kappa^2}{H^2} \,, \tag{2.25}$$

and

$$c_\kappa^\pm = \frac{1}{2}\left[H_{\nu_\kappa}\left(\frac{\kappa}{H}\right) \pm \frac{\kappa}{H\bar{\nu}_\kappa} H'_{\nu_\kappa}\left(\frac{\kappa}{H}\right)\right] \,, \tag{2.26}$$

to ensure the continuity of the mode function v_k and its time derivative at $k/a(\eta) = \kappa$.

The transverse and longitudinal parts of the propagator are obtained substituting $m_\kappa^2 \to m_{t/l,\kappa}^2$ in the previous expressions. Going back to Eq. (2.18), the beta function is now a sum of two contributions

$$N\kappa\partial_\kappa U_\kappa = \beta(m_{l,\kappa}^2, \kappa) + (N-1)\beta(m_{t,\kappa}^2, \kappa) \,, \tag{2.27}$$

where

$$\beta(m^2, \kappa) = \frac{\pi\Omega_d}{16d(2\pi)^d} \frac{\kappa^{d+2}}{H^d(\kappa^2 + m^2)} B_d(\nu_\kappa, \kappa) \,, \tag{2.28}$$

and [37, 39]

$$\begin{aligned} B_d(\nu, \kappa) = e^{-\pi \operatorname{Im}\nu} \Bigg[& \left(d^2 - 2\nu^2 + 2\left(\frac{\kappa}{H}\right)^2\right)\left|H_\nu\left(\frac{\kappa}{H}\right)\right|^2 + 2\left(\frac{\kappa}{H}\right)^2\left|H'_\nu\left(\frac{\kappa}{H}\right)\right|^2 \\ & -2d\frac{\kappa}{H}\operatorname{Re}\left(H_\nu^*\left(\frac{\kappa}{H}\right)H'_\nu\left(\frac{\kappa}{H}\right)\right)\Bigg] \,. \end{aligned} \tag{2.29}$$

In the deep infrared, $\kappa \ll H$, and when the curvature of the potential is small $m_{t/l,\kappa}^2 \ll H^2$, this beta function can be approximated as [36, 39]

$$\beta(m^2, \kappa) \approx \frac{H^D}{\Omega_{D+1}} \frac{\kappa^2}{\kappa^2 + m^2} \,. \tag{2.30}$$

As pointed out in [36, 39], the beta function (2.30) is similar to that of a zero-dimensional Euclidean theory. This effective dimensional reduction results, again, from the strong gravitational amplification of infrared scalar fluctuations[1]. This points out a simple effective description for the infrared physics, through the following generating functional

$$e^{N\mathcal{V}_D \mathcal{W}_\kappa(j,H)} = \int \mathrm{d}^N\hat{\phi}\, e^{-N\mathcal{V}_D\left[U_{\rm in}(\hat{\chi},H)+\kappa^2\hat{\chi}-j\cdot\hat{\phi}\right]} , \tag{2.31}$$

where $\mathcal{V}_D = \Omega_{D+1}/H^D$, $\hat{\chi} = \hat{\phi}^2/(2N)$ and $U_{\rm in}$ is to be specified below. It is easy to check that the regularized effective potential U_κ, defined in terms of $\chi = \phi^2/2N$ as the modified Legendre transform

$$U_\kappa(\chi,H) + \kappa^2\chi = -\mathcal{W}_\kappa(j,H) + j\cdot\phi , \tag{2.32}$$

satisfies Eq. (2.27) and thus coincide with the effective potential of our initial problem provided one adjusts $U_{\rm in}$ in Eq. (2.31) to match the initial condition at $\kappa = \kappa_0$.

2.2.2 Flow of the Hubble parameter

Moving on to compute the flow of H_κ, we choose a particular initial condition for the flow by specifying the potential $U_{\rm in}$ as

$$U_{\rm in}(\hat{\chi},H) = g(H) + \mu^2(H)\hat{\chi} + \frac{\lambda}{2}\hat{\chi}^2 , \tag{2.33}$$

where

$$g(H) = \alpha - \frac{\beta}{2}H^2 + \frac{\gamma}{4}H^4 \quad \text{and} \quad \mu^2(H) = m^2 + \zeta H^2 . \tag{2.34}$$

The function $g(H)$ contains the terms coming from the gravitational part of the action. In a de Sitter metric, the constant and H^2 terms reflect the standard Einstein-Hilbert action with cosmological constant, while the H^4 describes a term quadratic in the curvature tensor (*e.g.* R^2), which could for example be induced by loop effects in the UV. We shall see that it does not play a role here when $D = 4$. The parameters α and β are related to the cosmological constant Λ and the Planck mass as

$$N\alpha = \Lambda M_P^2 \quad \text{and} \quad N\beta = D(D-1)M_P^2 . \tag{2.35}$$

The effective mass function $\mu(H)$ includes a possible nonminimal coupling to the Ricci scalar $R = D(D-1)H^2$. In terms of the standard normalization, $m^2 + \xi R$, we have

$$\zeta = D(D-1)\xi . \tag{2.36}$$

[1] The dimensional reduction can be understood comparing with the flow equation of a Euclidean scalar theory in a D dimensional flat space. In that case, the flow equation reads

$$\beta(m^2,\kappa) \propto \frac{\kappa^{D+2}}{\kappa^2 + m^2}$$

and the deep infrared result in de Sitter space corresponds to the specific case when $D = 0$.

Again, we have extracted the convenient factors of N for later use.

The minimum of the effective potential, Eq. (2.15), is now determined in terms of our new variables as

$$\left.\frac{\partial U_\kappa}{\partial \phi_a}\right|_{\chi_\kappa, H_\kappa} = 0, \quad \left.\frac{\partial (H^{-D} U_\kappa)}{\partial H}\right|_{\chi_\kappa, H_\kappa} = 0 \tag{2.37}$$

which, using the integral representation (2.31) are equivalent to the implicit relations

$$\begin{cases} \left\langle H\partial_H (H^{-D} U_{\text{in}}) \right\rangle_\kappa = D H_\kappa^{-D} \kappa^2 [\langle \hat{\chi} \rangle_\kappa - \chi_\kappa] \\ \phi_\kappa^a = \left\langle \hat{\phi}^a \right\rangle_\kappa \ , \end{cases} \tag{2.38}$$

where the expectation values are to be computed with the measure in (2.31), evaluated with the source $N j^a = \kappa^2 \phi_\kappa^a$, and $H = H_\kappa$. The term proportional to κ^2 is the explicit contribution from the regulator, which we saw in Eq. (2.8). Importantly, Eqs. (2.38) are implicit relations for H_κ and χ_κ, as both are needed to compute the expectation values on the right-hand side.

On the left-hand side of the first member of Eqs. (2.38), the initial potential will generate expectation values for quadratic and quartic operators in the fields. The latter can be eliminated using the following property, valid for any function u for which the integral exists and the boundary terms vanish, obtained through an integration by part

$$\int \mathrm{d}^N \hat{\phi}\, e^{-u(\hat{\phi})} \hat{\phi}^a \frac{\partial u}{\partial \hat{\phi}^a} = N \int \mathrm{d}^N \hat{\phi}\, e^{-u(\hat{\phi})} \ . \tag{2.39}$$

Using this with $u(\hat{\phi}) = N \mathcal{V}_D (U_{\text{in}}(\hat{\chi}) + \kappa^2 \hat{\chi} - j \cdot \hat{\phi})$, we obtain

$$\langle \hat{\chi} \partial_{\hat{\chi}} U_{\text{in}} \rangle_\kappa + \kappa^2 (\langle \hat{\chi} \rangle - \chi) = \frac{H^D}{2\Omega_{D+1}} \ . \tag{2.40}$$

With the initial conditions (2.33), this gives

$$\lambda \left\langle \hat{\chi}^2 \right\rangle_\kappa = \frac{H_\kappa^D}{2\Omega_{D+1}} - \mu^2(H) \left\langle \hat{\chi} \right\rangle_\kappa - \kappa^2 (\left\langle \hat{\chi} \right\rangle_\kappa - \chi_\kappa) \ . \tag{2.41}$$

which we inject in the first implicit relation in Eq. (2.38) to get

$$\begin{aligned} D\alpha - \frac{D-2}{2}\beta H^2 + \frac{D H_\kappa^D}{4\Omega_{D+1}} + \frac{D}{2}(m^2 + \kappa^2)[\langle \hat{\chi} \rangle_\kappa - \chi_\kappa] + \frac{D}{2} m^2 \chi_\kappa \\ = \frac{D-4}{2}\Big(\frac{\gamma}{2} H^4 + \zeta H^2 \left\langle \hat{\chi} \right\rangle_\kappa \Big) \ . \end{aligned} \tag{2.42}$$

To solve this equation, in addition to computing the average value $\phi_\kappa^a = \left\langle \hat{\phi}^a \right\rangle_\kappa$, we only need the two-point correlator of the zero dimensional theory $G_\kappa^{ab} = \left\langle \hat{\phi}^a \hat{\phi}^b \right\rangle_\kappa -$

$\phi^a_\kappa \phi^b_\kappa$. Again, this propagator has a transverse and longitudinal part, which can be expressed in terms of the effective potential, inverting the two-point vertex function. We have a sum of two contributions

$$\langle \hat{\chi} \rangle_\kappa - \chi_\kappa = \frac{G^{aa}_\kappa}{2N} = \frac{H^D_\kappa}{2N\Omega_{D+1}} \left[\frac{1}{\bar{m}^2_{l,\kappa} + \kappa^2} + \frac{N-1}{\bar{m}^2_{t,\kappa} + \kappa^2} \right] , \tag{2.43}$$

with the longitudinal and transverse masses defined as in Eq. (2.21) and evaluated at the physical point $\bar{m}_{t/l,\kappa} = m_{t/l,\kappa}(\chi_\kappa, H_\kappa)$.

These equations simplify further in $D = 4$. In particular, the right-hand side of Eq. (2.42) cancels, which leads to the following regulated semiclassical Friedmann equation,

$$4\alpha - \beta H^2_\kappa + \frac{H^4_\kappa}{\Omega} + 2(m^2 + \kappa^2)[\langle \hat{\chi} \rangle_\kappa - \chi_\kappa] + 2m^2 \chi_\kappa = 0 , \tag{2.44}$$

where the volume factor is $\Omega = 8\pi^2/3$. It is to be compared with the classical result

$$H^2_{\rm cl} = \frac{4\alpha}{\beta} , \tag{2.45}$$

for a symmetric state with $\chi_\kappa = 0$.

It is interesting to note that similar equations have been obtained recently in a completely different context [106], namely using holographic methods to integrate out a QFT living in a constant curvature spacetime and compute its backreaction on the ambient geometry.

2.3 Interesting limits

We now compute and comment on the solutions to this flow equation. To have a better understanding of the physics at stake, we will study two particular cases where the effective potential can be computed analytically namely the case of a Gaussian potential, and the limit when N is large (*i.e.* the leading order in a $1/N$ expansion). The generic case for a finite number of interacting fields can be solved numerically and will be discussed in the end.

2.3.1 Gaussian case

For a Gaussian theory, $\lambda = 0$, the generating function of the cumulants $\mathcal{W}_\kappa$, defined in (2.31), can be computed exactly,

$$\mathcal{W}_\kappa(j, H) = -g(H) + \frac{N j^2}{2\mu^2_\kappa(H)} - \frac{H^D}{2\Omega_{D+1}} \log\left(\frac{\Omega_{D+1}\mu^2_\kappa(H)}{H^D 2\pi} \right) . \tag{2.46}$$

where we introduced the regulated effective mass function $\mu^2_\kappa(H) = \mu^2(H) + \kappa^2$. From there we take the Legendre transform (2.32), expressed in terms of

$$\phi^a = \partial_{j^a} \mathcal{W}_\kappa = \frac{N j^a}{\mu^2_\kappa(H)} \quad \text{or} \quad \chi = \frac{N j^2}{2\mu^4_\kappa(H)} , \tag{2.47}$$

to get

$$U_\kappa(\chi, H) = g(H) + \mu^2(H)\chi + \frac{H^D}{2\Omega_{D+1}} \log\left(\frac{\Omega_{D+1}\mu_\kappa^2(H)}{H^D 2\pi}\right) . \tag{2.48}$$

The effective potential is the sum of the classical potential, corrected by the one-loop logarithm, which is the only quantum correction in the Gaussian case. The argument of the logarithm should in principle be dimensionless, which can be done by means of an arbitrary mass scale that should be included to make the integration measure dimensionless in Eq. (2.31). We do not need to worry about this here, as we will be mostly interested in derivatives of $H^{-D}U_\kappa$, insensitive to this additional constant.

Using this expression to compute the physical minimum, Eq. (2.37), the average field cancels $\phi_\kappa^a = 0$, and we find the following equation for H_κ, in $D = 4$

$$4\alpha - \beta H_\kappa^2 + \frac{H_\kappa^4}{\Omega}\left(1 + \frac{m^2 + \kappa^2}{\bar{\mu}_\kappa^2}\right) = 0 , \tag{2.49}$$

with $\bar{\mu}_\kappa = \mu_\kappa(H_\kappa)$ the mass function at the minimum. This equation matches with the semiclassical Friedmann equation, Eq. (2.44), as we know that $\chi_\kappa = 0$ and

$$\langle\hat{\chi}\rangle_\kappa = \frac{H_\kappa^4}{2\Omega\bar{\mu}_\kappa^2} . \tag{2.50}$$

As expected, H_κ does not flow when the non minimal coupling ζ is taken to zero, as the κ dependence simplifies in Eq. (2.49)

$$4\alpha - \beta H_\kappa^2 + \frac{2H_\kappa^4}{\Omega} = 0 . \tag{2.51}$$

However, the Hubble rate is not equal to its classical value, as it is corrected by the one-loop contribution which gives the H_κ^4 term. Out of the two solutions of the quadratic equation (2.51), only one is compatible with the range of validity of the semiclassical approximation, $H_\kappa^2 \ll \beta$. We get

$$H_\kappa^2 = \frac{\beta\Omega}{4}\left(1 - \sqrt{1 - \frac{32\alpha}{\beta^2\Omega}}\right) \approx H_{\rm cl}^2 + \frac{2H_{\rm cl}^4}{\beta\Omega} . \tag{2.52}$$

We see that the quantum correction is actually small with respect to the classical value, and is already present at the ultraviolet scale κ_0.

Adding the non minimal coupling, a nontrivial flow exists, that leads to a finite value of the Hubble rate as κ goes to zero. The renormalization can be either positive or negative, depending on the sign of ζ: For $\zeta < 0$, the curvature is increased, and vice versa for $\zeta > 0$, see Fig. 2.1.

As a final remark, for $\alpha = 0$, meaning in the absence of cosmological constant, $H_\kappa = 0$ is a fixed point of the flow equation, corresponding to flat spacetime. This, however, goes beyond the range of validity of our approach, where the effective potential curvature is supposedly small compared to H_κ at each scale. Nonetheless, it is reassuring to check that Minkowski spacetime is a fixed point of the flow.

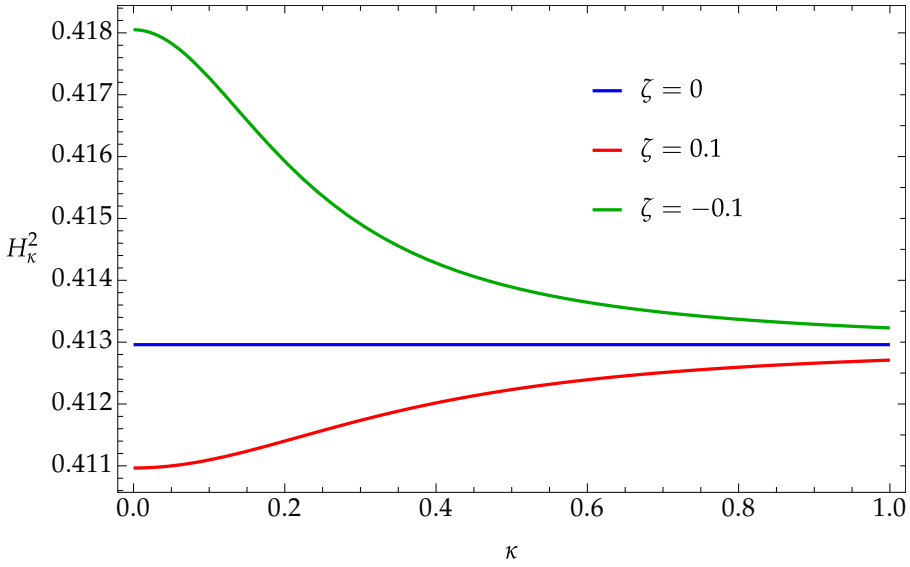

Figure 2.1: Flow of the Hubble parameter H_κ^2 as a function of the regulating scale κ. We consider Gaussian initial conditions $\lambda = 0$, the gravitational parameters are chosen as $\beta = 1$ and $\alpha = 0.1$, and the mass is chosen as $m^2 = 0.1$, while the non minimal coupling ζ is varied between positive and negative values. Even for $\zeta = 0$, the value of H_κ^2 is not the classical value and receives a one-loop correction, so that the blue curve is not exactly at $H_{\rm cl}^2 = 0.4$.

2.3.2 large N interacting case

Another interesting limit is when we take $N \to \infty$, in which case the computation can be done analytically. The function $\mathcal{W}_\kappa$ can again be computed exactly, introducing an auxiliary field σ (here a simple real variable), with a normalized Gaussian weight,

$$\int \mathrm{d}\sigma \sqrt{\frac{N\mathcal{V}_D}{\pi}} e^{-N\mathcal{V}_D(\sigma - i\sqrt{\frac{\lambda}{2}}\hat{\chi})^2} = 1 \,. \tag{2.53}$$

The factors are chosen so that when we insert this integral in Eq. (2.31), the $\hat{\chi}^2$ term in the initial potential is cancelled, and we can perform the gaussian integral over $\hat{\phi}$. We get

$$e^{N\mathcal{V}_D\mathcal{W}_\kappa(j,H)} = \int \mathrm{d}\sigma \sqrt{\frac{N\mathcal{V}_D}{\pi}} e^{-N\mathcal{V}_D F(z,j,H)} \,, \tag{2.54}$$

and we expressed the function F in terms of a new variable $z = \mu_\kappa^2(H) - i\sqrt{2\lambda}\sigma$, so that

$$F(z,j,H) = g(H) - \left(\frac{z - \mu_\kappa^2(H)}{2\lambda}\right)^2 + \frac{1}{2\mathcal{V}_D}\log\left(\frac{\mathcal{V}_D z}{2\pi}\right) - \frac{Nj^2}{2z} \,. \tag{2.55}$$

At leading-order in $1/N$, the integral over σ can be performed using the saddle point approximation. The result is easily expressed in terms of the minimum $\bar{z}$ of F, obtained

through $\partial_z F\big|_{\bar{z}} = 0$,

$$\mathcal{W}_\kappa(j, H) = -F(\bar{z}, j, H) \,. \tag{2.56}$$

The Legendre transform is expressed in terms of

$$\phi^a = \partial_{j^a} \mathcal{W}_\kappa = N j^a / \bar{z} \,. \tag{2.57}$$

Taking a derivative of Eq. (2.32) with respect to ϕ^a, we find that $\bar{z}$ is equal to the regularized transverse mass $M_\kappa^2 \equiv m_{t,\kappa}^2 + \kappa^2$. It is expressed in terms of χ and H as

$$M_\kappa^2(\chi, H) = \frac{\mu_\kappa^2(H) + \lambda\chi}{2} + \sqrt{\left(\frac{\mu_\kappa^2(H) + \lambda\chi}{2}\right)^2 + \frac{\lambda H^D}{2\Omega_{D+1}}} \,. \tag{2.58}$$

Finally, the effective potential is

$$U_\kappa(\chi, H) = g(H) - \kappa^2\chi + \frac{M_\kappa^4(\chi, H) - \mu_\kappa^4(H)}{2\lambda} + \frac{H^D}{2\Omega_{D+1}} \log\left(\frac{\Omega_{D+1} M_\kappa^2(\chi, H)}{2\pi e}\right) \,. \tag{2.59}$$

This result coincides with the Gaussian limit when $\lambda \to 0$.

Again, we can derive the flow of H_κ from there, computing directly the physical minimum through Eqs. (2.37). In $D = 4$, we get the following equation for H_κ

$$4\alpha - \beta H_\kappa^2 + \frac{2}{\lambda}(\bar{M}_\kappa^2 - \bar{\mu}_\kappa^2)(\bar{M}_\kappa^2 + m^2 + \kappa^2) = 4\kappa^2\chi_\kappa \,, \tag{2.60}$$

with $\bar{M}_\kappa^2 = M_\kappa^2(\chi_\kappa, H_\kappa)$, and using the expression for χ_κ, obtained from $\partial_{\phi^a} U_\kappa = \phi_\kappa^a \partial_\chi U_\kappa = 0$. Either $\phi_\kappa^a = 0$ and $\chi_\kappa = 0$, which corresponds to the symmetric phase, or $\bar{m}_{t,\kappa}^2 = 0$, corresponding to the broken-symmetry regime. In both cases, we know that

$$m_{t,\kappa}^2 \chi_\kappa = 0 \,, \tag{2.61}$$

and from the expression (2.58) of $\bar{M}_\kappa^2$, we get

$$\bar{M}_\kappa^4 - (\bar{\mu}_\kappa^2 + \lambda\chi_\kappa)\bar{M}_\kappa^2 - \frac{\lambda H_\kappa^D}{2\Omega_{D+1}} = 0 \,. \tag{2.62}$$

Using Eqs. (2.61) and (2.62) in Eq. (2.60), we end up with, in $D = 4$,

$$4\alpha - \beta H_\kappa^2 + \frac{H_\kappa^4}{\Omega}\left(1 + \frac{m^2 + \kappa^2}{\bar{m}_{t,\kappa}^2 + \kappa^2}\right) + 2m^2\chi_\kappa = 0 \,. \tag{2.63}$$

We can check that Eq. (2.63) coincide with the semiclassical Friedmann equation, Eq. (2.44), at leading order in a $1/N$ expansion.

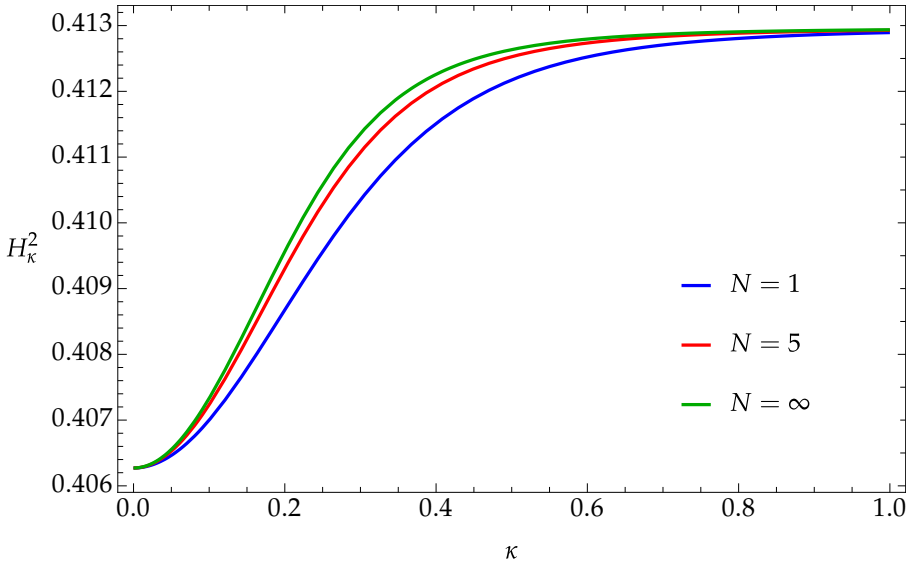

Figure 2.2: Flow of H_κ^2 in the massless minimally coupled case, $m^2 = \zeta = 0$, for various values of N. The other parameters are set to $\beta = 1$, $\alpha = 0.1$ and $\lambda = 1$. The negative renormalization is induced by the generation of a mass. The flow is frozen once the regulating scale goes below this generated mass, around $\kappa \approx \bar{m}_{t,\kappa=0} \approx 0.2$. The result obtained for finite values of N can be seen to be very similar to the large-N limit, even for low values of N.

2.3.2.1 Symmetric regime

Let us first study the symmetric regime, where $\chi_\kappa = 0$. In that case, the regularized transverse mass is

$$\bar{M}_\kappa^2 = \frac{\bar{\mu}_\kappa^2}{2} + \sqrt{\frac{\bar{\mu}_\kappa^4}{4} + \frac{\lambda H_\kappa^4}{2\Omega}} \,, \tag{2.64}$$

and the flow equation (2.63) reads

$$4\alpha - \beta H_\kappa^2 + \frac{H_\kappa^4}{\Omega}\left(1 + \frac{m^2 + \kappa^2}{\bar{M}_\kappa^2}\right) = 0 \,. \tag{2.65}$$

At large values of κ, the regularized transverse curvature can be essentially approximated by $\bar{M}_\kappa^2 \approx \kappa^2$, and the flow equation becomes

$$4\alpha - \beta H_\kappa^2 + 2\frac{H_\kappa^4}{\Omega} = 0 \,, \tag{2.66}$$

which is the same as Eq. (2.51) and gives nothing but the minimally coupled Gaussian solution. This is expected as all fluctuations are effectively frozen in this limit.

We then focus on the massless minimally coupled case, $m = \zeta = 0$, to probe directly the nonperturbative dynamics. Decreasing the value of κ, the transverse mass increases,

which leads to a negative renormalization of H_κ^2, see Fig. 2.2. This can be interpreted as the scalar field drawing energy from the gravitational field. Indeed, while the field is initially massless, a mass is gravitationally generated by the interactions. As κ is taken to zero, the generated mass is

$$m_{t,\kappa=0}^2 = \sqrt{\frac{\lambda H_{\kappa=0}^4}{2\Omega}} \,, \tag{2.67}$$

and saturates to a finite value, while $H_{\kappa=0}^2$ is obtained through

$$4\alpha - \beta H_{\kappa=0}^2 + \frac{H_{\kappa=0}^4}{\Omega} = 0 \,. \tag{2.68}$$

The solution reads

$$H_{\kappa=0}^2 = \frac{\beta\Omega}{2}\left(1 - \sqrt{1 - \frac{16\alpha}{\beta^2\Omega}}\right) \approx H_{\rm cl}^2 + \frac{H_{\rm cl}^4}{\beta\Omega} \,. \tag{2.69}$$

The fact that we obtain a finite value indicates a stabilization of the geometry, as a consequence of this mass generation. Indeed, it gives a new scale below which the flow is effectively frozen. The difference between the asymptotic values is small and it is controlled by the dimensionless parameter

$$\frac{H_{\rm cl}^2}{\beta\Omega} \ll 1 \,, \tag{2.70}$$

whose smallness is a necessary condition for the validity of the present semiclassical approach. Eq. (2.69) is, again, similar to the result obtained in [106] with holographic methods, see their Eq. (4.23). Interestingly, their result is not limited to the semiclassical regime: They explore a wider range of values for α, and they keep the other solution to the quadratic equation as a viable possibility.

The analysis is very similar when taking nonzero values for m^2 and ζ. Actually, the addition of a bare mass tends to freeze the flow earlier, as the second term in factor of the H_κ^4 in Eq. (2.65) will not flow down to zero. The non minimal coupling, as in the Gaussian case, can have nontrivial effects depending on its sign. In particular, a negative value of ζ tends to renormalize positively H_κ^2, competing with the negative renormalization coming from the interactions, see Fig. 2.3.

2.3.2.2 Broken-symmetry regime

In the broken-symmetry regime, the initial potential is chosen so as to have nontrivial minima in χ away from the origin. For a quartic potential this is realized at the classical level under the condition $m^2 + \zeta H_{\kappa_0}^2 < 0$.

The value of χ_κ is determined as a function of H_κ from the cancellation of the transverse mass

$$\partial_\chi U_\kappa \Big|_{\chi_\kappa} = 0 \,, \tag{2.71}$$

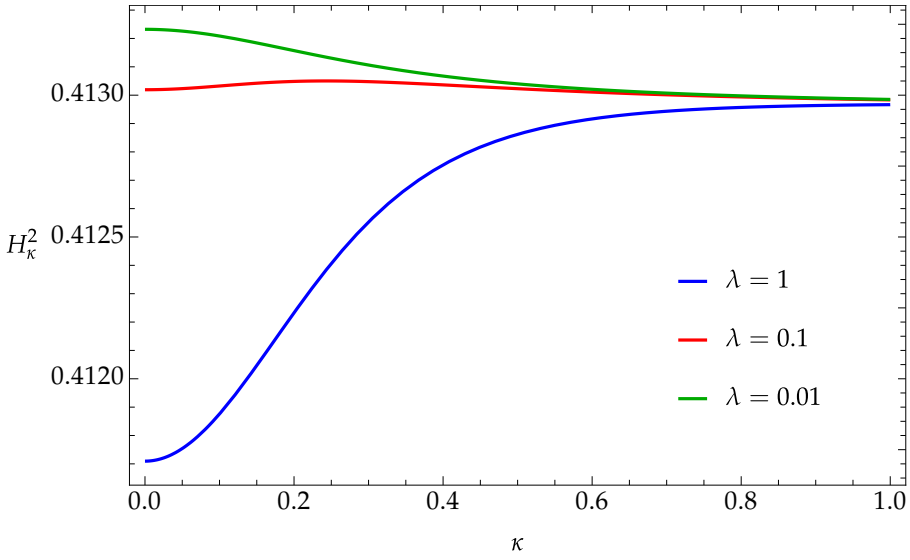

Figure 2.3: Flow of H_κ^2 which displays an interplay between a negative value of the non minimal coupling ζ and the effect of the interactions λ. As the latter is decreased, the positive renormalization induced by a negative ζ becomes the leading effect. The parameters are set to $\beta = 1$, $\alpha = 0.1$, $m^2 = 0.1$, and $\zeta = -0.01$.

which gives, in terms of H_κ,

$$\chi_\kappa = -\frac{m^2 + \zeta H_\kappa^2}{\lambda} - \frac{H_\kappa^4}{2\Omega\kappa^2} \,. \tag{2.72}$$

Injecting this into the flow equation (2.63), it can be expressed in a similar form as for the minimally coupled Gaussian case, Eq. (2.51),

$$4\alpha' - \beta' H_\kappa^2 + 2\frac{H_\kappa^4}{\Omega} = 0 \,, \tag{2.73}$$

with the modified gravitational parameters

$$\alpha' = \alpha - \frac{m^4}{2\lambda} \quad \text{and} \quad \beta' = \beta + \frac{2m^2\zeta}{\lambda} \,, \tag{2.74}$$

and H_κ^2 does not flow, as all explicit dependence in κ has disappeared.

In the limit $N \to \infty$, the dynamics in the broken phase is entirely dominated by the Goldstone transverse modes, which are massless. It appears that these modes do not contribute to the flow of H_κ. This is actually expected from the flow of the effective potential. Indeed, going back to the beta function of the potential in the infrared limit, Eq. (2.30), we know that when the curvature of the potential vanishes in a particular direction,

$$\beta(0, \kappa) = \frac{H^D}{\Omega_{D+1}} \,. \tag{2.75}$$

This means that if the curvature of the potential at a minimum χ_κ is null, then we can derive the minimum condition for H, $\partial_H(H^{-D}U_\kappa)|_{H_\kappa,\chi_\kappa} = 0$, with respect to κ to obtain

$$\partial_\kappa H_\kappa = -\left.\frac{\partial_H(H^{-D}\partial_\kappa U_\kappa)}{\partial_H^2(H^{-D}U_\kappa)}\right|_{\chi_\kappa,H_\kappa} = 0\,. \tag{2.76}$$

where we used Eq. (2.75) to see that the numerator vanishes. As a consequence, a massless mode gives no contribution to the renormalization of the curvature, although it is strongly amplified in the infrared.

Another way to phrase this is to look at the running of the potential at its minimum,

$$U_\kappa(\chi_\kappa, H) = g(H) - \frac{\mu^4(H)}{2\lambda} + \frac{H^4}{2\Omega}\left(1 + \log\left(\frac{\Omega\kappa^2}{2\pi e}\right)\right)\,. \tag{2.77}$$

The only term with an explicit dependence in κ is the logarithm, and it renormalizes the H^4, which does not participate in the renormalization of H_κ^2 in $D = 4$.

The actual value of H_κ^2 is the same as in the minimally coupled Gaussian case, Eq. (2.52), with the replacement $(\alpha, \beta) \to (\alpha', \beta')$. Notice in particular that the classical solution in this case is now

$$H_{\rm cl}'^2 = \frac{4\alpha'}{\beta'}\,. \tag{2.78}$$

These new values do not have the same constraints as the purely gravitational parameters, and we can explore more of the parameter space to see whether the renormalization of H_κ^2 can be made bigger. This will be discussed later.

Before that, an important point is that the symmetry is always restored along the flow at a finite value of κ. Looking at Eq. (2.72), the condition to start the flow in a broken phase is

$$m^2 + \zeta H_{\kappa_0}^2 < -\frac{\lambda H_{\kappa_0}^4}{2\Omega\kappa_0^2}\,, \tag{2.79}$$

and we see that the classical condition has already received a quantum correction, as a consequence of the initial condition being fixed at a finite value of κ. As κ is decreased, this correction grows like $1/\kappa^2$, and the condition for a broken-symmetry regime is always eventually violated. In other words, the symmetry is always restored at a finite scale [36, 38, 39, 107, 108]

$$\kappa_c^2 = -\frac{\lambda H_\kappa^4}{2\Omega(m^2 + \zeta H_\kappa^2)}\,. \tag{2.80}$$

The picture is that, although the symmetry is broken on domains of size below $1/\kappa_c$, it is restored at larger scales as these domains are uncorrelated and the expectation value will average out among these different macroscopic domains. The flow for $\kappa \leq \kappa_c$ is controlled by the previous flow equation for the symmetric regime (2.65), and has already been discussed. The resulting flow is depicted in Fig. 2.4.

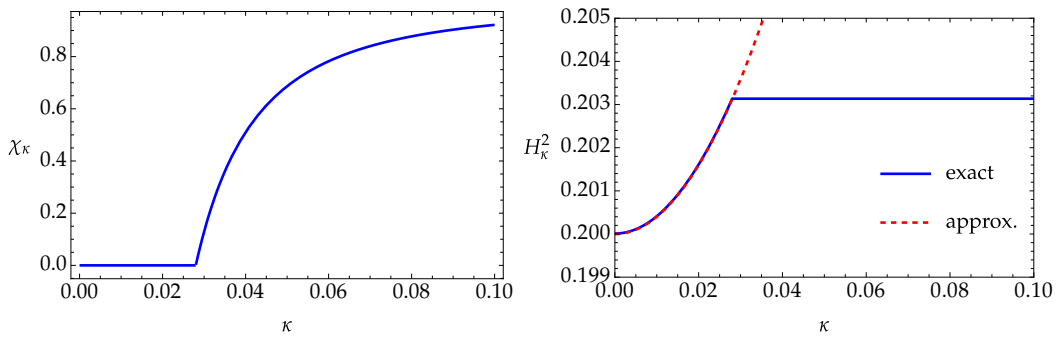

Figure 2.4: Flow of χ_κ (left) and H_κ^2 (right), around the symmetry restoration, happening at $\kappa_c \approx 0.28$. The parameters are chosen as $\beta = 1$, $\alpha = 0.1$, $m^2 = -0.1$, $\zeta = 0$, and $\lambda = 0.1$. This corresponds to the deeply broken regime and the approximate solution of the flow (2.85) is represented as the red dashed line.

An interesting limit where we can obtain simple expressions is the deeply broken phase, when $\left|m^2 + \zeta H_{\kappa_0}^2\right|^2 \gg \lambda H_{\kappa_0}^4$. In that case, the regulated curvature can be expanded for $\kappa \leq \kappa_c$ as

$$\bar{M}_\kappa^2 = \frac{\lambda H_\kappa^4}{2\Omega|\bar{\mu}_\kappa^2|}\left(1 - \frac{\lambda_{\text{eff},\kappa}}{2} + \mathcal{O}\left(\lambda_{\text{eff},\kappa}^2\right)\right), \tag{2.81}$$

in terms of the effective coupling

$$\lambda_{\text{eff},\kappa} = \frac{\lambda H_\kappa^4}{\Omega|\bar{\mu}_\kappa^2|^2}. \tag{2.82}$$

Injecting this expression in the flow equation (2.65) gives, after the symmetry restoration,

$$4\alpha'_\kappa - \beta'_\kappa H_\kappa^2 + \frac{H_\kappa^4}{\Omega}\left(1 - \frac{m^2 + \kappa^2}{\bar{\mu}_\kappa^2}\right) = 0, \tag{2.83}$$

with the regulated modified gravitational parameters

$$\alpha'_\kappa = \alpha - \frac{(m^2+\kappa^2)^2}{2\lambda} \quad \text{and} \quad \beta'_\kappa = \beta + \frac{2\zeta(m^2+\kappa^2)}{\lambda}. \tag{2.84}$$

This is similar to the Gaussian case, Eq. (2.49), with the replacement $(\alpha, \beta) \to (\alpha'_\kappa, \beta'_\kappa)$ and a change of sign for the κ dependent terms in the parenthesis. In particular, when $\left|\zeta H_\kappa^2\right| \ll \left|m^2\right|$, we have the approximate solution

$$H_\kappa^2 = \frac{4\alpha'_\kappa}{\beta'_\kappa}, \tag{2.85}$$

which converges towards the new classical solution (2.78) when $\kappa = 0$

$$H_{\kappa=0}^2 = H_{\text{cl}}'^2. \tag{2.86}$$

This approximate solution is represented together with the actual flow in Fig. 2.4.

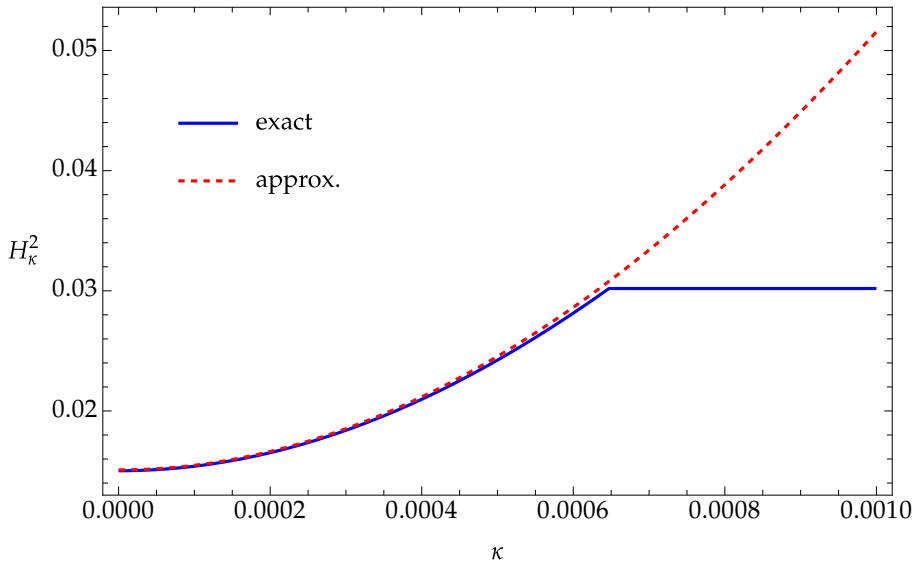

Figure 2.5: Flow of H_κ^2 around the symmetry restoration for the fined tuned parameters $m^2 = -4.47175\,10^{-3}$, $\zeta = 1.113\,10^{-2}$ and $\lambda = 10^{-4}$. The gravitational parameters are $\beta = 1$ and $\alpha = 0.1$. The Hubble parameter is renormalized by an overall factor of two.

2.3.2.3 Fine tuned parameters

As previously mentioned, for generic parameters in the symmetric phase, the renormalization of H_κ^2 is controlled by $H_{\rm cl}^2/(\beta\Omega) \ll 1$, which has to be small for the semiclassical approximation to hold.

In the broken-symmetry regime, the value in the UV is given by

$$H_{\kappa_0}^2 = \frac{\beta'\Omega}{4}\left(1 - \sqrt{1 - \frac{32\alpha'}{\beta'^2\Omega}}\right), \tag{2.87}$$

and to get the solution to Eq. (2.73) which is continuously connected to the classical one, we need to ensure

$$\alpha' > 0\,, \quad \beta' > 0\,, \quad \beta'^2\Omega > 32\alpha'\,. \tag{2.88}$$

After the symmetry restoration, the asymptotic infrared value can be computed from the symmetric phase flow equation (2.83). According to our previous analysis, for generic parameters in the broken phase, both asymptotic values will be close to the classical solution, with corrections controlled by $H_{\rm cl}'^2/(\beta'\Omega) \ll 1$.

We can however fine-tune the parameters so that the quantity $H_{\rm cl}'^2/(\beta'\Omega)$ is of order one, so that the quantum corrections become important, still respecting the aforementioned constraints (2.88) and the semiclassicality condition $0 < H_\kappa^2 \ll \beta$. Thus, we try

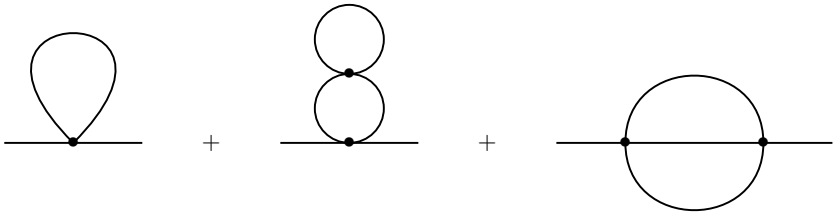

Figure 2.6: Feynman diagrams appearing in the perturbative expansion analysis of the flow of the Hubble parameter, at up to two loop order.

to minimize the determinant in the solution (2.87)

$$0 < 1 - \frac{32\alpha'}{\beta'^2\Omega} \ll 1 \,, \tag{2.89}$$

which leads to $H^2_{\kappa_0} \approx (\beta'\Omega)/4$. Then, the semiclassical constraint tells us that $\alpha' \sim \beta'^2 \ll \beta^2$. Using Eq.(2.88), this means that

$$-\frac{m^2}{\sqrt{\lambda}} \lesssim \sqrt{2\alpha} \quad \text{and} \quad \frac{\zeta}{\sqrt{\lambda}} \lesssim \frac{\beta}{2\sqrt{2\alpha}} \,. \tag{2.90}$$

The value of λ is constrained by the requirement that the curvature of the potential in field space is small in units of the spacetime curvature or, equivalently, of H^2, which at the classical level gives $\left|m^2 + \zeta H^2_{\kappa_0}\right| \ll H^2_{\kappa_0}$. From Eq. (2.90), m^2 and ζ scale as $\sqrt{\lambda}$ for a given α and β which means we have to choose $\lambda \ll 1$. In the end, we can further adjust the parameters for the approximate solution (2.85) to be valid. The result is shown in Fig. 2.5, where, with the choice of parameter, we obtain an overall renormalization of H^2_κ by approximately a factor of two, which is the maximal value we can obtain. The renormalization of H^2_κ never gets bigger, and we do not find any instability, or relaxation towards Minkowski spacetime.

2.3.3 Finite N case

Finally, we turn to the general case, when N is finite. The semiclassical Friedmann equation (2.44) can easily be solved numerically. The general features that we discussed before in the large-N limit are essentially unchanged in the symmetric case. In particular for the massless minimally coupled fields, $m^2 = \zeta = 0$ the asymptotic values are exactly the same for all N. Indeed, looking at (2.44) in the UV, the field is essentially Gaussian with a mass κ^2, and we get Eq. (2.51), which is solved as (2.52), while at $\kappa = 0$, we easily get Eq. (2.69) (see also Fig. 2.2).

It is instructive to compare the observed flow with the result one could obtain from a perturbative expansion in the coupling λ, applied to the zero-dimensional theory. In the regulated massless minimally coupled case, we already computed the tree level

correlator, see Eq. (2.50),

$$\langle\hat{\chi}\rangle_{0,\kappa} = \frac{H_\kappa^4}{2\Omega\kappa^2} \,. \tag{2.91}$$

Again, this is infrared divergent when we take $\kappa \to 0$, and we expect the loop corrections to blow up in this limit. Keeping κ at a high enough value, the perturbative expansion is well behaved, and it is possible to compute standard Feynman diagrams. The dimensionless expansion parameter appearing from loops is, see Eq. (2.82),

$$\frac{\lambda_{\mathrm{eff},\kappa}}{4} = \frac{\lambda\Omega}{H_\kappa^4}\langle\hat{\chi}\rangle_{0,\kappa}^2 \,. \tag{2.92}$$

The one- and two-loop diagrams contributing to the correlator are depicted in Fig. 2.6, and the two-loop result reads, for the correlator,

$$\langle\hat{\chi}\rangle_\kappa = \langle\hat{\chi}\rangle_{0,\kappa}\left(1 - \frac{N+2}{2N}\lambda_{\mathrm{eff},\kappa} + \frac{(N+2)(N+3)}{2N^2}\lambda_{\mathrm{eff},\kappa}^2 + \mathcal{O}(\lambda_{\mathrm{eff},\kappa}^3)\right) , \tag{2.93}$$

and for the transverse mass, using the inversion of the two-point vertex function, see Eq. (2.43),

$$\begin{aligned}\bar{m}_{t,\kappa}^2 &= -\kappa^2 + \frac{H_\kappa^4}{2\Omega\langle\hat{\chi}\rangle_\kappa} \\ &= \kappa^2\left(\frac{N+2}{2N}\lambda_{\mathrm{eff},\kappa} - \frac{(N+4)(N+2)}{4N^2}\lambda_{\mathrm{eff},\kappa}^2 + \mathcal{O}(\lambda_{\mathrm{eff},\kappa}^3)\right) .\end{aligned} \tag{2.94}$$

The equation for H_κ^2, in the symmetric regime,

$$4\alpha - \beta H_\kappa^2 + \frac{H_\kappa^4}{\Omega}\left(1 + \frac{\kappa^2}{\bar{m}_{t,\kappa}^2 + \kappa^2}\right) , \tag{2.95}$$

is then solved perturbatively to get

$$\begin{aligned}\frac{H_\kappa^2}{H_{\kappa_0}^2} = 1 - \frac{N+2}{2N}\frac{H_{\kappa_0}^2}{\beta\Omega - 4H_{\kappa_0}^2}\lambda_{\mathrm{eff},\kappa} + \frac{(N+2)H_{\kappa_0}^2}{2N^2(\beta\Omega - 4H_{\kappa_0}^2)^3}[H_{\kappa_0}^4(34+9N) \\ - 2\beta\Omega H_{\kappa_0}^2(3N+10) + \beta^2\Omega^2(N+3)]\lambda_{\mathrm{eff},\kappa}^2 + \mathcal{O}(\lambda_{\mathrm{eff},\kappa}^3) \,,\end{aligned} \tag{2.96}$$

where $H_{\kappa_0}^2$ is given by the minimally coupled Gaussian solution Eq. (2.52). The one loop contributions leads to a negative renormalization, which could be interpreted as a sign of instability of the geometry, as the correction goes unbounded when we take $\kappa \to 0$. However, when doing so, the effective coupling $\lambda_{\mathrm{eff},\kappa}$ becomes nonperturbative and all terms in the perturbative series are of the same order of magnitude. Taking all loop orders into consideration with a nonperturbative method corresponds to what we did in the previous section with the FRG procedure in the large-N limit, and gives a saturating flow for H_κ^2, as a consequence of the nonperturbative generation of a mass which freezes the flow of H_κ at a finite value, see Fig. 2.7.

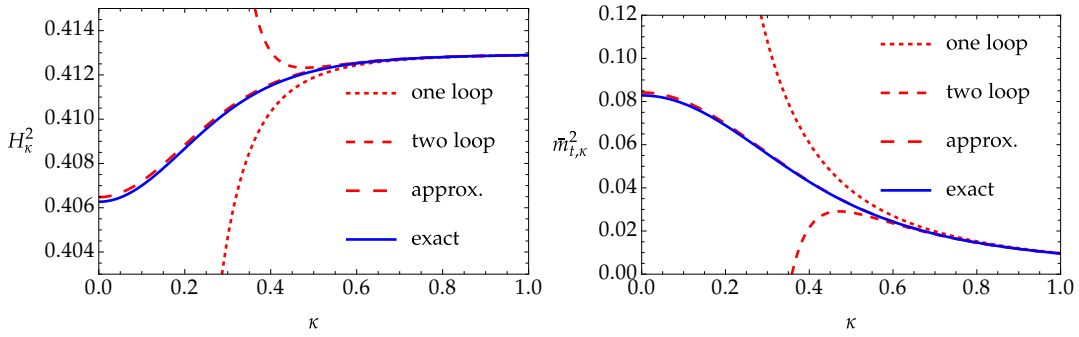

Figure 2.7: Flow of H_κ^2 (left) and the transverse mass (right) in the massless minimally coupled case, for $N = 1$, and $\lambda = 1$. The gravitational parameters are $\beta = 1$, $\alpha = 0.1$. The dashed lines corresponds to the first and second order in the loop expansion and diverge as κ is decreased. The approximate red dashed curve corresponds to the leading order in a development in $H_{\kappa_0}^2/(\beta\Omega)$, which is small in the semiclassical framework: The value of H_κ^2 is obtained from Eq. (2.102), while $\bar{m}_{t,\kappa}^2 = \bar{M}_\kappa^2 - \kappa^2$ is using the analytical solution Eq. (2.100) to compute $\bar{M}_\kappa^2$, evaluated at H_{κ_0}.

In general, the solution can be obtained using the integral representation of the generating functional (2.31). In the symmetric regime, starting with the following integral

$$\mathcal{Z}(A,B) = \int_0^\infty \mathrm{d}\hat{\chi}\, \hat{\chi}^{N/2-1} e^{-A\hat{\chi} - \frac{B\hat{\chi}^2}{2}} , \tag{2.97}$$

we have

$$\langle \hat{\chi} \rangle_\kappa = -\partial_A \log \mathcal{Z}(A,B) , \tag{2.98}$$

with

$$A = N\mathcal{V}_D \bar{\mu}_\kappa^2 \quad \text{and} \quad B = N\mathcal{V}_D \lambda . \tag{2.99}$$

The result can be expressed in terms of the confluent hypergeometric function of the second kind $U(a,b,c)$, as

$$\frac{\langle \hat{\chi} \rangle_\kappa}{\langle \hat{\chi} \rangle_{0,\kappa}} = \frac{\bar{\mu}_\kappa^2}{\bar{M}_\kappa^2} = \frac{N}{2\lambda_{\mathrm{eff},\kappa}} \frac{U\left(\frac{N+4}{4}, \frac{3}{2}, \frac{N}{2\lambda_{\mathrm{eff},\kappa}}\right)}{U\left(\frac{N}{4}, \frac{1}{2}, \frac{N}{2\lambda_{\mathrm{eff},\kappa}}\right)} . \tag{2.100}$$

We can check that Eq. (2.100) gives the correct asymptotic expressions in the limit $N \to \infty$, and for $N = 1$. Also, in the massless minimally coupled case, we find for finite N

$$\frac{\bar{M}_{\kappa=0}^2}{H_{\kappa=0}^2} = \frac{\Gamma\left(\frac{N}{4}\right)}{\Gamma\left(\frac{N+2}{4}\right)} \sqrt{\frac{\lambda N}{8\Omega}} , \tag{2.101}$$

with the expected non analytic dependence in the coupling λ [18].

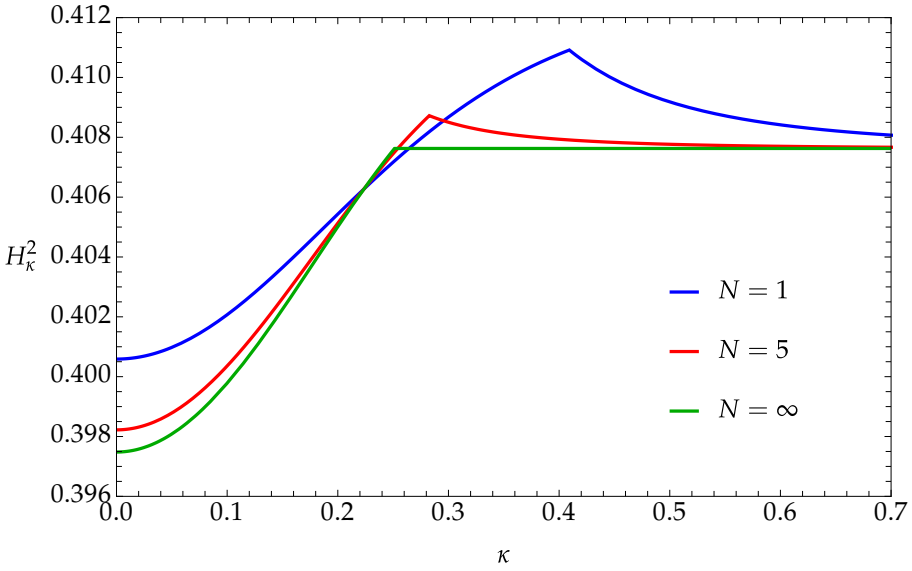

Figure 2.8: Flow of H_κ^2 in the broken-symmetry regime for various values of N, for $m^2 = -0.05$, $\zeta = 0$ and $\lambda = 1$. We also chose $\beta = 1$ and $\alpha = 0.1$. The flow in the broken phase is entirely due to the longitudinal mode, and is suppressed as N is increased, up to the limit $N \to \infty$, where only the massless transverse modes contribute.

Alhtough we do not have an analytic solution for H_κ in general, we can obtain a simple expression by developing in $H_{\kappa_0}^2/(\beta\Omega)$, which is small in the semiclassical approach. In the massless minimally coupled case, we get

$$\frac{H_\kappa^2}{H_{\kappa_0}^2} = 1 - \frac{H_{\kappa_0}^2}{\beta\Omega}\left(1 - \frac{\kappa^2}{\bar{M}_{\kappa,H_{\kappa_0}}^2}\right) + \mathcal{O}\left(\frac{H_{\kappa_0}^4}{(\beta\Omega)^2}\right), \tag{2.102}$$

where we added an index to the running regulated curvature to signify that it should be evaluated at H_{κ_0}. This equation, for large enough κ, relates the development of H_κ to the development of the transverse mass, and we can check that

$$\frac{H_\kappa^2}{H_{\kappa_0}^2} = 1 - \frac{N+2}{2N}\frac{H_{\kappa_0}\lambda_{\mathrm{eff},\kappa}}{\beta\Omega} + \frac{(N+2)(N+3)}{2N^2}\frac{H_{\kappa_0}^2\lambda_{\mathrm{eff},\kappa}^2}{\beta\Omega} + \mathcal{O}\left(\lambda_{\mathrm{eff},\kappa}^3, \frac{H_{\kappa_0}^4}{(\beta\Omega)^2}\right), \tag{2.103}$$

matches with the result from Eq. (2.94). Eq. (2.102) is, however, valid nonperturbatively.

In the broken phase, the main difference with the $N \to \infty$ case is the contribution of the longitudinal mode. Indeed, although it is suppressed by a factor $1/N$, it can modify the flow significantly for a small number of fields. Contrary to what happens in the symmetric phase, the renormalization due to the longitudinal mode only appears as a two-loop effect, which means it increases H_κ^2 along the flow in the presence of interactions, and a nonminimal coupling produces the opposite behavior as before, increasing

(resp. decreasing) H_κ^2 for $\zeta > 0$ (resp. $\zeta < 0$). As before, the symmetry will be restored at a finite value of the coarse graining scale κ, and the subsequent behavior is that of the symmetric regime, see Fig. 2.8.

2.4 Conclusion

To summarize, the FRG framework, previously applied to spectator fields in a fixed de Sitter geometry [36–39], can be extended to a situation where the classical metric is modified by the backreaction of $O(N)$ quantum scalar fields. More precisely, we compute the renormalization of the Hubble parameter, which characterizes the geometry entirely in the subset of de Sitter metrics and constant average field configurations, upon progressive integration of the amplified infrared fluctuating modes, and in the presence of interactions.

The case of a noninteracting minimally coupled field is a fixed point of the renormalization flow, as expected, and the inclusion of either a non minimal coupling ζ to the spacetime curvature, or self interaction λ leads to a nontrivial, but finite, backreaction. The overall amplitude of the effect is generically controlled by $H_{\rm cl}^2/M_P^2 \ll 1$, which is small in the present semiclassical approach and leads to a small renormalization. Although some fine tuning is possible to get a sizeable effect, we see no sign of instability and always get a finite result at the end of the flow.

The nonminimal coupling leads to a positive or negative renormalization depending on its sign. The interactions of the infrared modes tends to draw energy from the gravitational field, and we indeed observe a negative renormalization of the spacetime curvature. In the case of initially massless fields, for which the infrared modes are strongly amplified, the dynamical generation of a mass of order $\sqrt{\lambda H_{\rm cl}^4}$ gives a finite scale below which the fluctuations are effectively frozen and the flow saturates. This effect is nonperturbative in nature and we show that loop computations up to a finite order in perturbation theory lead to misleading results where the corrections grow unbounded. This signals the breakdown of the perturbative approach and the FRG treatment we use provides a resummation of these divergences.

For an initial potential which breaks the $O(N)$ symmetry, the Goldstone modes do not contribute to the backreaction, despite being massless and thus strongly amplified. This is actually the case for any flat direction in the potential and is a rather surprising conclusion of this work. As the symmetry is always restored at a finite scale, the subsequent flow always ends up back in the symmetric case.

There are close correspondances between the present work and results obtained in a recent study using a gauge/gravity duality to compute a similar backreaction problem [106]. Interestingly, the result of [106] is not limited by the semiclassical approximation, and is generally valid for positive and negative constant curvature space.

Finally, although we observe an overall saturation of the renormalization of the scalar curvature, and thus to a stabilization of the metric, in our specific context, the present computation is in no way a definitive conclusion to the problem of the cos-

mological constant. In particular, an accurate treatment of the metric perturbations [57, 109–111], or the use of a quantum state which is not de Sitter invariant [87, 88, 112–114], are not taken into account here.

3 Model A and FRG

Contents

3.1 Stochastic formalism . . . 53
3.1.1 Coarse graining . . . 54
3.1.2 Classicalization . . . 55
3.1.3 Stochastic noise . . . 56
3.1.4 Light fields in slow-roll . . . 58
3.1.5 Generalization to several fields . . . 60
3.2 Functional formulation . . . 61
3.2.1 Janssen-de Dominicis integral . . . 62
3.2.2 Supersymmetry . . . 63
3.3 General properties of correlators . . . 64
3.3.1 Supersymmetry constraints . . . 64
3.3.2 Fluctuation-dissipation relation . . . 67
3.3.3 Causality . . . 68
3.4 FRG for the model A . . . 69
3.4.1 Flow of the effective potential . . . 69
3.4.2 Flow at second order in the derivative expansion . . . 72
3.4.3 Convergence of the derivative expansion . . . 74
3.5 Conclusion . . . 80

One of the first, and most prominent, nonperturbative approach to compute infrared quantum effects for scalar fields in de Sitter spacetime is the stochastic formalism, developed in [15–18]. It gives an effective description of the long-wavelength (superhorizon) physics in terms of a Langevin stochastic equation. The infrared modes behave classically as a result of the gravitational amplification, and are subject to a random noise, coming from the expansion of subhorizon modes as they grow out of the horizon. This effective description has been shown to resum the leading infrared logarithms appearing in the perturbative expansion of the original quantum field theory [11, 19, 20], and thus leads to genuinely nonperturbative results.

There are several ways to extract information from this stochastic equation. The one which is usually considered is to solve the equivalent Fokker-Planck equation in terms of an eigenvalue problem [18, 72, 73]. This will be discussed in more details in the next chapter. Alternatively, the Langevin equation is a particular case of the so-called

model A in the Hohenberg and Halperin classification of nonequilibrium dynamical systems [66]. An approach has been developed in this context which leads to a path integral formulation, through the Janssen-de Dominicis (JdD) procedure, in terms of a one-dimensional QFT that features a supersymmetry [68–70].

This last approach can be used as a basis for implementing other methods. In particular, the FRG has been applied to the model A in the context of statistical physics [67, 68], supersymmetric quantum mechanics [71], and in the stochastic formalism [42]. In [42], it has been shown that the LPA flow for the effective potential is identical to the one obtained in the original Lorentzian QFT [37–39]. The LPA has been found to give the exact answer for the effective potential, which encodes all the information about local (equal-time and inside a Hubble patch) fluctuations. One result of the present thesis, described in this chapter, is to clarify why this is so. However, a limitation of the LPA is that it does not correctly predict some important phenomenological quantities such as the field autocorrelation time, which are related to unequal-time correlators. For this reason, it is desirable to go beyond the LPA and investigate the possiblity to get simple (maybe analytical) results for, *e.g.* autocorrelation times. Another motivation is the possibility of unravelling new phenomena. For instance, in flat Euclidean space, the topological Kostherlitz-Thouless transition is not seen at the LPA level but is clearly captured by including the flow of the kinetic (derivative) term in the effective action [46, 47]. The method of choice to go beyond the LPA, that we shall investigate here, is the so-called derivative expansion, where one expands the running effective action in powers of the field derivatives.

Trying to go beyond the LPA in the context of the Lorentzian QFT computation is notably difficult, and actual calculations were only limited to the LPA', where one adds a field independant renormalization to the kinetic term [40]. The computation for the model A appears to be much simpler and the second order of the derivative expansion has already been implemented for a single scalar field in the context of supersymmetric quantum mechanics [71]. It is thus interesting to study the derivative expansion for an $O(N)$ theory in this context.

We recall in Sec. 3.1 the principle of the effective stochastic approach, and the JdD procedure is detailed in Sec. 3.2. General properties of the correlators are then discussed in the light of this path integral formulation in Sec. 3.3. Finally, in Sec. 3.4, we implement the FRG in this context. We first prove that the LPA gives the exact result for the effective potential, and move on to compute the flow to second order in the derivative expansion.

3.1 Stochastic formalism

In this section, we consider a single test scalar field $\hat{\phi}$, with a potential $V(\hat{\phi})$, in a de Sitter background, and work in cosmic time t (see Eq. (1.2) for the metric). The derivation of the stochastic equation is well-known in that case, see for example [18], and we review it here for completeness. We add some considerations on the slow-roll limit which, although they are in essence not new, bring, we believe, an interesting light.

The formalism itself can be generalized in various ways, to an inflaton field, in a slowly rolling FRLW background or even beyond slow-roll [115–119].

3.1.1 Coarse graining

To derive the stochastic Langevin equation obeyed by the coarse-grained scalar field, we use the Hamiltonian formalism. Denoting with a dot the derivative with respect to the cosmic time, the conjugate momentum to the field ϕ_H reads, in terms of the microscopic action,

$$\pi_H = \frac{\delta S}{\delta \dot{\phi}} = a^d \dot{\phi}_H \,, \tag{3.1}$$

and we have the commutation relation $[\phi_H(t,\vec{x}), \pi_H(t,\vec{y})] = \delta^{(d)}(\vec{x}-\vec{y})$. The Hamiltonian is

$$H = \int \mathrm{d}^d\vec{x}\, a^d \left[\frac{1}{2}\left(\frac{\pi_H}{a^d}\right)^2 + \frac{1}{2}\left(\frac{\partial_{\vec{x}}\phi_H}{a}\right)^2 + V(\phi_H)\right] , \tag{3.2}$$

which gives the equations of motion for ϕ_H and π_H

$$\begin{aligned} \dot{\phi}_H &= \frac{\pi_H}{a^d} \,, \\ \frac{\dot{\pi}_H}{a^d} &= \frac{\partial^2_{\vec{x}}\phi_H}{a^2} - V'(\phi_H) \,. \end{aligned} \tag{3.3}$$

The strategy is to separate both the field and its conjugate momentum in short- and long-wavelength parts with respect to a fixed subhorizon physical scale ϵH, with $\epsilon \lesssim 1$, and to integrate out the short-wavelength part. In terms of comoving scales, the separation is done in terms of the following time-dependent quantity

$$k_\epsilon = \epsilon a(t) H \,. \tag{3.4}$$

We define the coarse-grained field $\bar{\phi}$ and momentum $\bar{\pi}$ as

$$\begin{aligned} \phi_H(t,\vec{x}) &= \bar{\phi}(t,\vec{x}) + \int_{\vec{k}} W\left(\frac{k}{k_\epsilon}\right)\left[\phi_k(t) e^{i\vec{k}\cdot\vec{x}} a_{\vec{k}} + \phi_k^*(t) e^{-i\vec{k}\cdot\vec{x}} a^\dagger_{\vec{k}}\right] , \\ \pi_H(t,\vec{x}) &= \bar{\pi}(t,\vec{x}) + \int_{\vec{k}} W\left(\frac{k}{k_\epsilon}\right)\left[\pi_k(t) e^{i\vec{k}\cdot\vec{x}} a_{\vec{k}} + \pi_k^*(t) e^{-i\vec{k}\cdot\vec{x}} a^\dagger_{\vec{k}}\right] , \end{aligned} \tag{3.5}$$

where the window function W is chosen so that $W \sim 0$ for $k \ll k_\epsilon$ and $W \sim 1$ for $k \gg k_\epsilon$. Additionally, the mode functions have been assumed to depend only on the norm of $\vec{k}$, which implies the use of an isotropic quantum state, *e.g.*, the BD vacuum.

The short-wavelength mode functions ϕ_k and π_k corresponds, by definition, to subhorizon modes, which are not gravitationally amplified. As a first approximation we can thus linearize their equations of motion to get

$$\begin{aligned} \dot{\phi}_k &= \frac{\pi_k}{a^d} \,, \\ \frac{\dot{\pi}_k}{a^d} &= -\frac{k^2}{a^2}\phi_k - V''(\bar{\phi})\phi_k \,. \end{aligned} \tag{3.6}$$

We show in the following section that the coarse grained field $\bar{\phi}$ behaves classically. Moreover, if we assume that the typical timescale for $\bar{\phi}$ is much larger than the one for UV modes, we can treat $V''(\bar{\phi})$ as a constant in Eq. (3.6). Eventually, we shall see that this term actually disappears from the noise correlators in the slow-roll limit so we refrain to discuss it in more detail. We simply consider it as a constant in what follows.

Using these in Eqs. (3.3), and neglecting the gradient term for the long-wavelength part we get the following equation for the dynamics of the coarse grained fields

$$\begin{aligned} \dot{\bar{\phi}} &= \frac{\bar{\pi}}{a^d} + \xi_\phi \,, \\ \frac{\dot{\bar{\pi}}}{a^d} &= -V'(\bar{\phi}) + \xi_\pi \,. \end{aligned} \tag{3.7}$$

where we defined the noise terms

$$\begin{aligned} \xi_\phi(t,\vec{x}) &= -\int_{\vec{k}} \dot{W}\left(\frac{k}{k_\epsilon}\right)\left[\phi_k(t)e^{i\vec{k}\cdot\vec{x}}a_{\vec{k}} + \phi_k^*(t)e^{-i\vec{k}\cdot\vec{x}}a_{\vec{k}}^\dagger\right] \,, \\ \xi_\pi(t,\vec{x}) &= -\frac{1}{a^d(t)}\int_{\vec{k}} \dot{W}\left(\frac{k}{k_\epsilon}\right)\left[\pi_k(t)e^{i\vec{k}\cdot\vec{x}}a_{\vec{k}} + \pi_k^*(t)e^{-i\vec{k}\cdot\vec{x}}a_{\vec{k}}^\dagger\right] \,, \end{aligned} \tag{3.8}$$

corresponding to short-wavelength modes exiting the horizon at a given time. Here, the derivative of the window function with respect to time is nonvanishing as a consequence of the time dependence of k_ϵ.

3.1.2 Classicalization

So far, the coarse-grained fields and noises are defined in terms of quantum operators, with nontrivial commutation relations. To interpret Eqs. (3.7) as Langevin equations with random noises (3.8), we need to understand how these quantities become effectively classical.

This quantum-to-classical transition has been described in different ways [86, 118, 120, 121]: It has been linked with the squeezing of the quantum state of the fluctuations in the Schrödinger picture, or as the consequence of a decoherence process. We will only give a hint of the phenomenon here considering the fluctuations of a test field as an isolated system, *i.e.* without decoherence, in the Heisenberg picture, using the BD vacuum. The transition appears as the consequence of the existence of growing and decaying solutions, in terms of time evolution, to the mode function equation. The growing solutions corresponds to a classical behavior that tend to dominate the decaying ones on superhorizon scales. What we mean by classical behavior here is the possibility to neglect the noncommutativity effects [122], which is the case for these specific modes.

We first focus on the noise terms. The mode functions appearing in Eq. (3.8) verify the linearized equation of motion (3.6). Thus the situation is identical to the free massive scalar field case. As we have already seen in Sec. 1.2, in the Bunch-Davies vacuum [see

Eq. (1.54), with $m^2 = V''(\bar{\phi})$],

$$\phi_k(t) = a^{-\frac{d}{2}}(t)\sqrt{\frac{\pi}{4H}}e^{i\vartheta_\nu}H_\nu\left(\frac{k}{a(t)H}\right) . \tag{3.9}$$

Here, the growing and decaying solutions are both contained in the Hankel function H_ν, and can be identified for superhorizon modes to its imaginary and real part respectively. The momentum $\pi_k(t)$, is obtained from the first equation of (3.6). The derivative of the Hankel function satisfies the identity $H'_\nu(z) = H_{\nu-1}(z) - (\nu/z)H_\nu(z)$. For the long-wavelength modes, $k \sim k_\epsilon \ll aH$, we can use $H'_\nu(z \ll 1) \sim -(\nu/z)H_\nu(z)$ which amounts to neglecting the decaying solution[1]. We get

$$\pi_k(t) \sim \left(\nu - \frac{d}{2}\right)Ha^d(t)\phi_k(t) . \tag{3.10}$$

This means in particular that ξ_π is almost proportional to ξ_ϕ, which implies that their equal-time commutator is small compared to their anticommutator.

For a free massive scalar field, this argument directly applies to the coarse-grained field and its conjugate momentum. In that case, the average value of the canonical commutator, proportional to the spectral correlator ρ, will be small compared to the average value of the anticommutator, proportional to the statistical correlator F

$$F(x,y) \gg \rho(x,y) . \tag{3.11}$$

This property can be generalized to interacting fields [122], and is a sufficient condition for a classical field behavior. Indeed, this means that the correlators of the field and the noises can be effectively obtained as the result of an equivalent classical stochastic process, whose dynamics is given by the Langevin equation (3.7): The corrections coming from noncommutation effects can be neglected.

3.1.3 Stochastic noise

To further characterize the noises, we compute the quantum average of the related operators, again in the Bunch-Davies vacuum. As a consequence of the linearization, they have Gaussian statistics. Thus, they are entirely characterized by their two-point function, which we can compute from Eqs. (3.9) and (3.10) with

$$\nu = \sqrt{\frac{d^2}{4} - \frac{V''(\bar{\phi})}{H^2}} . \tag{3.12}$$

We get,

$$\left\langle \xi_f(t,\vec{x})\xi_g(t',\vec{x}')\right\rangle = \int_{\vec{k}} \dot{W}\left(\frac{k}{k_\epsilon(t)}\right)\dot{W}\left(\frac{k}{k_\epsilon(t')}\right)f_k(t)g_k^*(t')e^{i\vec{k}\cdot(\vec{x}-\vec{x}')} , \tag{3.13}$$

[1] In the limit $z \ll 1$, for a real and positive value of ν, the Hankel function is approximated by its growing component, or equivalently its imaginary part, as $H_\nu(z \ll 1) \sim [(2^\nu)\Gamma(\nu)]/[i\pi z^\nu]$. This can be used to show $H'_\nu(z \ll 1) \sim -(\nu/z)H_\nu(z)$.

with f and g which can be either ϕ or π. Because of the symmetries of the Bunch-Davies vacuum, the mode functions only depends on the modulus of the wavevector. We can use isotropic window functions, in order to integrate the angular part of the integral, and we get

$$\left\langle \xi_f(t,\vec{x})\xi_g(t',\vec{x}')\right\rangle = \int \mathrm{d}k\, k^{d-1}\dot{W}\left(\frac{k}{k_\epsilon(t)}\right)\dot{W}\left(\frac{k}{k_\epsilon(t')}\right) f_k(t)g_k^*(t')\mathcal{F}_d(k\left|\vec{x}-\vec{x}'\right|)\ , \quad (3.14)$$

where the function $\mathcal{F}_d$ represent the spatial smearing of the noise correlator, and can be expressed in terms of a Bessel function

$$\mathcal{F}_d(z) = (2\pi)^{-\frac{d}{2}} z^{\frac{2-d}{2}} J_{\frac{d-2}{2}}(z)\ . \quad (3.15)$$

The simplest option for the coarse-graining function is a Heaviside step $W(x) = \theta(x-1)$, which gives,

$$\left\langle \xi_f(t,\vec{x})\xi_g(t',\vec{x}')\right\rangle = \delta(t-t')Hk_\epsilon^d f_{k_\epsilon}(t)g^*_{k_\epsilon}(t)\mathcal{F}_d(k_\epsilon\left|\vec{x}-\vec{x}'\right|)\ . \quad (3.16)$$

For coincident points in space, we find the following numerical factor $\mathcal{F}_d(0) = C_{d,\nu}$, related to the power spectrum, see Eq. (1.65), and it vanishes rapidly for $|\vec{x}-\vec{x}'| \gtrsim k_\epsilon^{-1}$, or superhorizon spatial separations. In the following, we restrict to a single Hubble patch, so that $\mathcal{F} \sim C_{d,\nu}$, and we can discard the spatial dependence.

Therefore, the stochastic noises are just Gaussian white noises with amplitudes related to the different power spectra of ϕ and π. Specifically, using Eqs. (3.9) and (3.10), we have

$$\begin{aligned}
\left\langle \xi_\phi(t)\xi_\phi(t')\right\rangle &= \delta(t-t')C_{d,\nu}\epsilon^{d-2\nu}H^d\ ,\\
\left\langle \xi_\phi(t)\xi_\pi(t')\right\rangle &= \delta(t-t')C_{d,\nu}\left(\nu-\frac{d}{2}\right)\epsilon^{d-2\nu}H^{d+1}\ ,\\
\left\langle \xi_\pi(t)\xi_\pi(t')\right\rangle &= \delta(t-t')C_{d,\nu}\left(\nu-\frac{d}{2}\right)^2\epsilon^{d-2\nu}H^{d+2}\ .
\end{aligned} \quad (3.17)$$

From Eq. (3.17), it is easy to see that in the case of light fields, $\nu \approx d/2$, and the noise term ξ_π can be neglected compared to ξ_ϕ in the Langevin equation. The two-point correlator of ξ_ϕ simplifies to

$$\left\langle \xi_\phi(t)\xi_\phi(t')\right\rangle = \delta(t-t')\frac{2H^d}{d\Omega_{D+1}}\ . \quad (3.18)$$

We see that, as announced above, in the light mass limit where we take $\nu \approx d/2$, the mass term proportional to $V''(\bar{\phi})$ from Eq. (3.6) does not play a role. Combining with Eq. (3.7), and neglecting the appropriate noise terms, we find

$$\ddot{\bar{\phi}} + dH\dot{\bar{\phi}} + V'(\bar{\phi}) = \xi_\phi\ . \quad (3.19)$$

3.1.4 Light fields in slow-roll

As an additional relevant approximation, we consider a slowly rolling scalar field. We saw in Sec. 1.1 that it corresponds to neglecting the second derivative term in Eq. (3.19). In order to make the consequences on the quantum correlators more precise, we now discuss the case of a free field of mass $m \ll H$, which can be solved exactly.

Eq. (3.19) now reads

$$\ddot{\bar{\phi}} + dH\dot{\bar{\phi}} + m^2\bar{\phi} = \xi_\phi \ , \tag{3.20}$$

and we follow the definitions of Eqs. (1.44), (1.47) and (1.48), for the various two-point functions of the spatially smeared field. The spectral correlator

$$\bar{\rho}(t-t') = i\,\langle\Omega|\left[\bar{\phi}(t),\bar{\phi}(t')\right]|\Omega\rangle \ , \tag{3.21}$$

verifies

$$\dot{\bar{\rho}}(t=0) = i\,\langle\Omega|\left[\dot{\bar{\phi}}(t),\bar{\phi}(t)\right]|\Omega\rangle = Z \ , \tag{3.22}$$

as a consequence of the canonical commutation relation, in the presence of an arbitrary field normalization Z for later purposes[2]. It can be computed from the retarded Green's function for the differential operator (3.20), which verifies the following equation

$$(\partial_t^2 + dH\partial_t + m^2)\bar{G}_R(t) = Z\delta(t) \ , \tag{3.23}$$

solved in frequency space as

$$\bar{G}_R(\omega) = \frac{Z}{2\nu H}\left(\frac{i}{\omega + i\omega_+} - \frac{i}{\omega + i\omega_-}\right) \ , \tag{3.24}$$

where

$$\omega_\pm = H\left(\frac{d}{2} \pm \nu\right) \ . \tag{3.25}$$

Using the relation (1.45) between the retarded and spectral correlators, expressed here in real time as $\bar{G}_R(t) = \theta(t)\bar{\rho}(t)$, we get

$$\bar{\rho}(\omega) = 2i\,\mathrm{Im}\,\bar{G}_R(\omega) = \frac{Z}{2\nu H}\left(\frac{2i\omega}{\omega^2+\omega_+^2} - \frac{2i\omega}{\omega^2+\omega_-^2}\right) \ , \tag{3.26}$$

and in real space

$$\bar{\rho}(t) = \frac{Z}{2\nu H}\mathrm{sign}(t)\left(e^{-\omega_-|t|} - e^{-\omega_+|t|}\right) \ . \tag{3.27}$$

As we discussed in Sec. 3.1.2, the spectral correlator is expected to be negligible compared to the statistical one, which means that we can identify[3]

$$\bar{F}(t-t') = \frac{1}{2}\,\langle\Omega|\left\{\bar{\phi}(t),\bar{\phi}(t')\right\}|\Omega\rangle \approx \left\langle\bar{\phi}(t)\bar{\phi}(t')\right\rangle \ . \tag{3.28}$$

[2]The normalization of the smeared field has no reason to be equal to that of the original field, which would correspond to the case when $Z = 1$.

[3]Note that the second equality relies on several identifications between quantum operators and stochastic variables, as explained in Sec. 3.1.2. In the last expression, $\langle\bar{\phi}(t)\bar{\phi}(t')\rangle$, the field is understood as a stochastic variable, and the average is a stochastic average on the classical random noise ξ_ϕ. We keep the same notations for simplicity.

This can be computed from the solution to Eq. (3.20),

$$\bar{\phi}(t) = \bar{\phi}_0(t) + \frac{d}{Z}\int \mathrm{d}t'\, \bar{G}_R(t-t')\xi_\phi(t') \,, \tag{3.29}$$

where $\bar{\phi}_0$ is a solution of the homogeneous equation. It contains the initial conditions and is associated to a transient regime, whereas the integral term, which dominates at long time, will correspond to a stationary regime, independent of the initial conditions. Because we study the stationary regime, $\bar{\phi}_0$ will be discarded in the following. We get

$$\bar{F}(\omega) = \frac{d^2}{Z^2}\mathcal{N}(\omega)\left|\bar{G}_R(\omega)\right|^2 \,, \tag{3.30}$$

where $\mathcal{N}(\omega)$ is the Fourier transform of the $\left\langle \xi_\phi \xi_\phi \right\rangle$ correlator

$$\mathcal{N}(\omega) = \frac{2H^d}{d\Omega_{D+1}} \,. \tag{3.31}$$

In real time, we end up with

$$\bar{F}(t) = \frac{H^d}{\Omega_{D+1}\nu}\left(\frac{e^{-\omega_-|t|}}{2\omega_-} - \frac{e^{-\omega_+|t|}}{2\omega_+}\right) . \tag{3.32}$$

Now, the slow-roll approximation, which amounts to neglecting the second temporal derivative in Eq. (3.19), would only give a single root for the homogeneous equation, $\omega_0 = -im^2/d$, instead of $\omega_\pm$. This is obtained from the complete equation, provided one takes the limit $m \ll H$, for which

$$\omega_+ \approx dH \quad \text{and} \quad \omega_- \approx \frac{m^2}{dH} \,, \tag{3.33}$$

and neglecting the higher order pole ω_+, as $\omega_+ \gg \omega_-$. This corresponds, in real time, to neglecting $e^{-\omega_+|t|} \ll e^{-\omega_-|t|}$,

$$\bar{\rho}(t) = \mathrm{sign}(t)\frac{Ze^{-\frac{m^2}{dH}|t|}}{dH} \,, \quad \bar{F}(t) = \frac{H^D e^{-\frac{m^2}{dH}|t|}}{\Omega_{D+1}m^2} \,. \tag{3.34}$$

This is represented in Fig. 3.1.

One important point is that, in doing so, the canonical commutation relation (3.22) is no longer verified. In fact, the slow-roll approximation amounts to consider a coarse grained-theory which cannot resolve time scales below ω_-^{-1}. As a consequence, the canonical commutation relation (3.22), which requires the presence of both roots $\omega_\pm$, or equivalently involves shorter timescales of order ω_+^{-1}, is lost. This is similar to the neglect of the decaying mode as described in Sec. 3.1.2. Some information about the field normalization remains, however, and can be obtained from the spectral correlator from

$$\bar{\rho}(t = 0^+) = \frac{Z}{dH} \,, \tag{3.35}$$

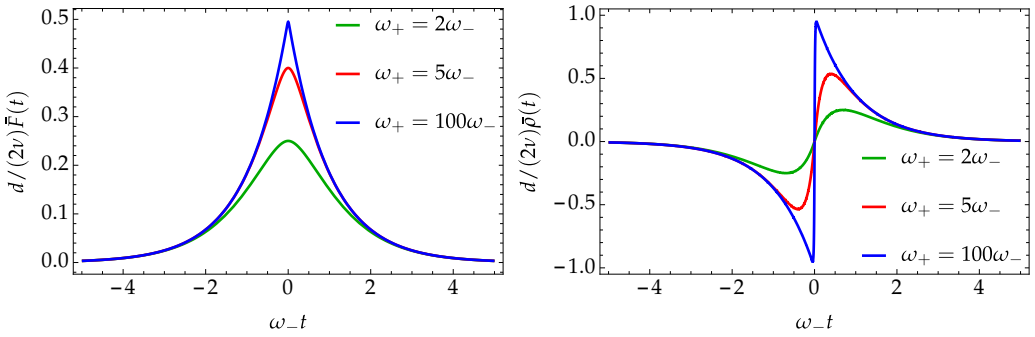

Figure 3.1: Plot of the statistical function $\bar{F}$ (left) and spectral function $\bar{\rho}$ (right) as a function of time in units of ω_-^{-1}. This illustrates the coarse graining resulting from the slow-roll approximation. The functions were rescaled by a factor $d/(2\nu)$ for a nicer plot.

where the limit $t \to 0^+$ is to be understood in units of the relevant timescale ω_-^{-1}.

The effects of the slow-roll limit on the different correlators, computed here in the noninteracting case, will be generalized later to an arbitrary potential and used to prove useful relations on the stochastic correlators defined in the JdD procedure.

3.1.5 Generalization to several fields

We end this section by generalizing the above equations to the case of N light scalar field in slow-roll with an $O(N)$ symmetry. We obtain a system of coupled Langevin equations for the field $\bar{\phi}_a$, with a the field-space index. Because we consider the BD vacuum, which is an $O(N)$ invariant quantum state, the noise correlator computed using Eq. (3.8) is diagonal in field space,

$$\left\langle \xi_\phi^a(t)\xi_\phi^b(t')\right\rangle = \delta_{ab}\delta(t-t')\frac{2H^d}{d\Omega_{D+1}} \,. \tag{3.36}$$

It is useful to rescale the fields and the potential to absorb the different volume factors

$$\bar{\phi}_a \to \sqrt{\frac{2H^d}{d\Omega_{D+1}}}\varphi_a \quad \text{and} \quad V(\bar{\phi}) \to \frac{2H^D}{\Omega_{D+1}}V(\varphi) \,. \tag{3.37}$$

Unless explicitly states, we now exclusively use these rescaled variables in the following.

The Langevin equation in the slow-roll approximation then reads

$$\dot{\varphi}_a(t) + \partial_{\varphi_a}V(t) = \xi_a(t) \,, \tag{3.38}$$

where

$$\left\langle \xi_a(t)\xi_b(t')\right\rangle = \delta_{ab}\delta(t-t') \,. \tag{3.39}$$

The associated one-point probability distribution function (PDF), denoted $P(\varphi_a, t)$, can be shown by standard methods to verify the following Fokker-Planck equation [123],

$$\partial_t P = \partial_{\varphi_a}\left((\partial_{\varphi_a} V)P + \frac{1}{2}\partial_{\varphi_a} P\right) , \tag{3.40}$$

It has an equilibrium distribution $P_{\rm eq}$ which is a solution of

$$\partial_{\varphi_a}\left((\partial_{\varphi_a} V)P_{\rm eq} + \frac{1}{2}\partial_{\varphi_a} P_{\rm eq}\right) = 0 . \tag{3.41}$$

One obtains [18]

$$P_{\rm eq}(\varphi_a) = \frac{1}{\mathcal{N}_{\rm eq}} e^{-2V(\varphi_a)} , \tag{3.42}$$

where $\mathcal{N}_{\rm eq}$ is a normalization factor. The general time-dependent solution tends towards this equilibrium distribution after a long enough time, which will be discussed in the next chapter. This is another manifestation of the fact that the BD vacuum, corresponding to this equilibrium distribution, is an attractor state in the EPP [85].

This equilibrium distribution can be seen as the Boltzmann distribution for a thermal system,

$$P \propto e^{-\beta \mathcal{H}} , \tag{3.43}$$

where $\mathcal{H}$ is the Hamiltonian for the superhorizon field in the Hubble patch under consideration and β is an inverse temperature. It is expressed in terms of the potential as

$$\mathcal{H} = \int \mathrm{d}^d \vec{x}\, V = \frac{\Omega_d}{dH^d} V . \tag{3.44}$$

where we use the fact that the volume of a d-dimensional spherical Hubble patch of radius H^{-1} is $\Omega_d/(dH^d)$. With the rescalings (3.37), the equilibrium distribution (3.42) becomes

$$P_{\rm eq} \propto e^{-\Omega_{D+1} H^{-D} V(\bar{\varphi}_a)} , \tag{3.45}$$

which gives for the inverse temperature

$$\beta = \frac{\Omega_{D+1}}{H^D}\frac{dH^d}{\Omega_d} = \frac{2\pi}{H} . \tag{3.46}$$

This is nothing but the inverse Gibbons-Hawking temperature [124].

3.2 Functional formulation

The Langevin equation (3.38) that we obtained is a particular case of the model A in the classification of Hohenberg and Halperin [66], which has been studied in the context of out-of-equilibrium statistical physics [67, 68]. It can be given an elegant functional formulation through the JdD procedure [69, 70], which provides an efficient starting point for the implementation of various QFT techniques.

3.2.1 Janssen-de Dominicis integral

The expectation value of a given operator $\mathcal{O}(\varphi)$ can be expressed as

$$\langle \mathcal{O}(\varphi) \rangle = \int \mathcal{D}\xi \, P[\xi] \mathcal{O}(\varphi_\xi) \, , \tag{3.47}$$

where φ_ξ is a solution of Eq. (3.38) with given initial condition[4], and

$$P[\xi] = \frac{1}{\sqrt{2\pi}} e^{-\int \mathrm{d}t \frac{1}{2}\xi^2} \, . \tag{3.48}$$

is the normalized probability distribution for the noise, with $\xi^2 = \xi_a \xi_a$. Assuming the uniqueness of the solution to the Langevin equation for a given realization of the noise and a given initial condition, one can write

$$\mathcal{O}(\varphi_\xi) = \int \mathcal{D}\varphi \, \delta[\dot{\varphi}_a + \partial_{\varphi_a} V - \xi_a] \mathcal{J}[\varphi] \mathcal{O}(\varphi) \, , \tag{3.49}$$

where $\mathcal{J}[\varphi] = |\det(\delta_{ab}\partial_t + V_{,ab})|$ is the appropriate functional Jacobian. Under the uniqueness assumption, one can forget the absolute value of the determinant and exponentiate it in terms of Grassmann fields

$$\mathcal{J}[\varphi] = \int \mathcal{D}[\psi, \bar{\psi}] \, e^{i \int \mathrm{d}t \bar{\psi}_a (\delta_{ab}\partial_t + V_{,ab}) \psi_b} \, . \tag{3.50}$$

Similarly, one exponentiates the functional delta as

$$\delta[\dot{\varphi}_a + \partial_{\varphi_a} V - \xi_a] \propto \int \mathcal{D}[i\tilde{\varphi}] \, e^{-\int \mathrm{d}t \tilde{\varphi}_a (\dot{\varphi}_a + \partial_{\varphi_a} V - \xi_a)} \, , \tag{3.51}$$

where the so-called response fields $\tilde{\varphi}_a$ are purely imaginary. Integration over the Gaussian noise finally gives, up to an irrelevant constant factor,

$$\langle \mathcal{O}(\varphi) \rangle = \frac{\int \mathcal{D}[\varphi, i\tilde{\varphi}, \psi, \bar{\psi}] e^{-S_{JdD}[\varphi, \tilde{\varphi}, \psi, \bar{\psi}]} \mathcal{O}(\varphi)}{\int \mathcal{D}[\varphi, i\tilde{\varphi}, \psi, \bar{\psi}] e^{-S_{JdD}[\varphi, \tilde{\varphi}, \psi, \bar{\psi}]}} \, , \tag{3.52}$$

with the following action

$$S_{JdD}[\varphi, \tilde{\varphi}, \psi, \bar{\psi}] = \int \mathrm{d}t \left\{ \tilde{\varphi}_a (\dot{\varphi}_a + \partial_{\varphi_a} V) - \frac{1}{2}\tilde{\varphi}^2 - i\bar{\psi}_a (\delta_{ab}\partial_t + V_{,ab}) \psi_b \right\} . \tag{3.53}$$

This one-dimensional theory with $4N$ fields describes the leading infrared behaviour of the underlying QFT in de Sitter spacetime in the BD vacuum. Alternatively, we can use

[4] We should in principle also average over the initial conditions in Eq. (3.47), reflecting the quantum, and possibly the statistical (for a mixed state) fluctuations in the initial state. Here, we can avoid this procedure and consider an arbitrary fixed initial condition for our random variable because we are only interested in the late-time equilibrium state of the system where all information about the actual initial state has been washed away.

a more symmetric form of the action by changing the variable $\tilde{\varphi}_a \to F_a = i(\dot{\varphi}_a - \tilde{\varphi}_a)$. The action rewrites as

$$S_{JdD}[\varphi, F, \psi, \bar{\psi}] = \int \mathrm{d}t \left\{ \frac{1}{2}\dot{\varphi}_a + \frac{1}{2}F^2 - i\bar{\psi}_a\dot{\psi}_a + iF_a\partial_{\varphi_a}V + \bar{\psi}_a V_{,ab}\psi_b \right\} , \tag{3.54}$$

where, in the stationary state, we can discard the boundary term

$$\int \mathrm{d}t\, 2\dot{\varphi}_a\partial_{\varphi_a}V = \int \mathrm{d}t\, \dot{V} . \tag{3.55}$$

This form of the action clarifies another link, namely its relation to a supersymmetric quantum mechanics after the Wick rotation $t \to i\tau$ [71].

3.2.2 Supersymmetry

The action (3.54) possesses various symmetries, *e.g.* time translation and time reversal in the stationary regime, which can be conveniently encoded in a supersymmetry that mixes the bosonic and fermionic degrees of freedom [68, 71]. This supersymmetry can be made explicit recasting the different fields into a superfield

$$\hat{\Phi}_a(t, \theta, \bar{\theta}) = \varphi_a + \bar{\theta}\psi_a + \bar{\psi}_a\theta + \bar{\theta}\theta F_a , \tag{3.56}$$

living on the superspace $(t, \theta, \bar{\theta})$, with Grassmann variables θ and $\bar{\theta}$. The generators of the supersymmetry can be expressed as

$$Q = i\partial_{\bar{\theta}} + \theta\partial_t \quad \text{and} \quad \bar{Q} = i\partial_\theta + \bar{\theta}\partial_t . \tag{3.57}$$

Introducing the covariant derivatives

$$D = i\partial_{\bar{\theta}} - \theta\partial_t \quad \text{and} \quad \bar{D} = i\partial_\theta - \bar{\theta}\partial_t , \tag{3.58}$$

and the supersymmetric d'Alembertian operator

$$K = \frac{1}{2}[D, \bar{D}] , \tag{3.59}$$

the JdD action can be written as

$$S_{JdD}[\hat{\Phi}] = \int \mathrm{d}z \left\{ \frac{1}{2}\hat{\Phi}K\hat{\Phi} + iV(\hat{\Phi}) \right\} , \tag{3.60}$$

with $z = (t, \theta, \bar{\theta})$, $\mathrm{d}z = \mathrm{d}t\, \mathrm{d}\theta\, \mathrm{d}\bar{\theta}$, and the convention for the Grassmann integration is $\int \mathrm{d}\theta\, \mathrm{d}\bar{\theta}\, \bar{\theta}\theta = 1$.

3.3 General properties of correlators

Various considerations, most importantly the supersymmetry and the causality, allow to put constraints on the correlators of the superfield. Although some of the following properties are well-known in the context of statistical physics, their use in the cosmological context is new and we believe it brings an interesting perspective. We comment here the case of the connected[5] two-point correlator, denoted as

$$G_{12}^{ab}(t_1, t_2) = \left\langle \hat{\Phi}_a(t_1, \theta_1, \bar{\theta}_1) \hat{\Phi}_b(t_2, \theta_2, \bar{\theta}_2) \right\rangle \ . \tag{3.61}$$

In this section, we consider the single field case ($N = 1$) for simplicity, and the generalization to finite N is trivial.

3.3.1 Supersymmetry constraints

The dependence of the propagator G and inverse propogator $\Gamma^{(2)}$ on the Grassmann variables are heavily constrained by the supersymmetry generated by Q and $\bar{Q}$. Using first the anticommutator

$$\left\{Q, \bar{Q}\right\} = 2i\partial_t \ , \tag{3.62}$$

which generates the time translation invariance, we can work in frequency space

$$G_{12}(t_1, t_2) = \int \frac{\mathrm{d}\omega}{2\pi} e^{-i\omega(t_1 - t_2)} G_{12}(\omega) \ , \tag{3.63}$$

The same can be done to define $\Gamma_{12}^{(2)}(\omega)$, and the most general dependence of this correlator on the Grassmann variables can be written *a priori* in terms of six independent functions of the frequency

$$\Gamma_{12}^{(2)}(\omega) = A(\omega) + \bar{\theta}_1\theta_1 B(\omega) + \bar{\theta}_2\theta_2 C(\omega) + \bar{\theta}_1\theta_1\bar{\theta}_2\theta_2 D(\omega) + \bar{\theta}_1\theta_2 E(\omega) + \bar{\theta}_2\theta_1 F(\omega) \ . \tag{3.64}$$

Then, the supersymmetry implies the following Ward identities,

$$\begin{aligned} (Q_1 + Q_2)\Gamma_{12}^{(2)}(\omega) &= 0 \ , \\ (\bar{Q}_1 + \bar{Q}_2)\Gamma_{12}^{(2)}(\omega) &= 0 \ , \end{aligned} \tag{3.65}$$

where the numerical index indicates the Grassmann variable each operator Q and $\bar{Q}$ is acting on. These gives four independent constraints which are solved as

$$\begin{aligned} C(\omega) &= B(\omega) \ , \\ D(\omega) &= \omega^2 A(\omega) \ , \\ E(\omega) &= -B(\omega) - \omega A(\omega) \ , \\ F(\omega) &= -B(\omega) + A(\omega) \ . \end{aligned} \tag{3.66}$$

[5] We consider only connected two-point correlators in the following. For simplicity we do not introduce a special notation.

Renaming $A(\omega) = \eta(\omega)$ and $B(\omega) = i\gamma(\omega)$, the general structure of the two-point vertex reads

$$\Gamma^{(2)}_{12}(\omega) = i\gamma(\omega)\delta_{12} + \eta(\omega)K_\omega\delta_{12} \,, \tag{3.67}$$

where the two Grassmann structures

$$\begin{aligned} \delta_{12} &= (\bar\theta_1 - \bar\theta_2)(\theta_1 - \theta_2) \,, \\ K_\omega\delta_{12} &= 1 + \omega(\bar\theta_2\theta_1 - \bar\theta_1\theta_2) + \omega^2\bar\theta_1\theta_1\bar\theta_2\theta_2 \,, \end{aligned} \tag{3.68}$$

denote, repsectively, the Dirac function in Grassmann coordinates and the supersymmetric d'Alembertian operator $K\delta(z_1 - z_2)$ in frequency space, with $\delta(z_1 - z_2) = \delta(t_1 - t_2)\delta_{12}$.

The superfield propagator is obtained by inversion,

$$\int_2 \Gamma^{(2)}_{12}(\omega)G_{23}(\omega) = \delta_{13} \,, \tag{3.69}$$

with $\int_2 = \int \mathrm{d}\theta_2\,\mathrm{d}\bar\theta_2$, and reads

$$G_{12}(\omega) = \frac{-i\gamma(\omega)\delta_{12} + \eta(\omega)K_\omega\delta_{12}}{\omega^2\eta^2(\omega) + \gamma^2(\omega)} \,. \tag{3.70}$$

Using the decomposition (3.56) of the superfield, we can obtain the correlators for its different components. Using the notation

$$\left\langle \mathcal{A}(t)\mathcal{B}(t')\right\rangle = \int \frac{\mathrm{d}\omega}{2\pi} e^{-i\omega(t-t')}G_{\mathcal{A}\mathcal{B}}(\omega) \,, \tag{3.71}$$

we have

$$G_{\varphi\varphi}(\omega) = \frac{\eta(\omega)}{\omega^2\eta^2(\omega) + \gamma^2(\omega)} \,, \tag{3.72}$$

$$G_{\varphi F}(\omega) = \frac{-i\gamma(\omega)}{\omega^2\eta^2(\omega) + \gamma^2(\omega)} \,, \tag{3.73}$$

and the others can be expressed as

$$\begin{aligned} G_{FF}(\omega) &= \omega^2 G_{\varphi\varphi}(\omega) \,, \\ G_{\psi\bar\psi}(\omega) &= -G_{\varphi F}(\omega) - \omega G_{\varphi\varphi}(\omega) \,, \\ G_{\bar\psi\psi}(\omega) &= G_{\varphi F}(\omega) - \omega G_{\varphi\varphi}(\omega) \,. \end{aligned} \tag{3.74}$$

Using the permutation identity of the superfield correlator, $G_{12}(t) = G_{21}(-t)$, we see that $G_{\varphi\varphi}(\omega)$ and $G_{\varphi F}(\omega)$ are even functions of the frequency. Inverting Eqs. (3.73) in terms of $\gamma(\omega)$ and $\eta(\omega)$ shows that they are both even functions of ω.

Then, from the path integral representation (3.52), we compute the complex conjugate of $\langle\varphi(t)\varphi(t')\rangle$. It only changes the sign of $\tilde\varphi$ in the action S_{JdD}, as the response field is purely imaginary. Making the change of variable $\tilde\varphi \to -\tilde\varphi$ in the numerator and

the denominator gives back the original action, without changing the global sign of the expression, thus showing

$$\big\langle \varphi(t)\varphi(t')\big\rangle^\star = \big\langle \varphi(t)\varphi(t')\big\rangle \ . \tag{3.75}$$

Using the same method to compute $\langle\varphi(t)\tilde{\varphi}(t')\rangle^\star$, again the sign of $\tilde{\varphi}$ is changed in the action as well as in the additional $\tilde{\varphi}$ we are integrating upon. The same change of variable, $\tilde{\varphi} \to -\tilde{\varphi}$ gives back the original correlator and we have

$$\big\langle \varphi(t)\tilde{\varphi}(t')\big\rangle^\star = \big\langle \varphi(t)\tilde{\varphi}(t')\big\rangle \ . \tag{3.76}$$

Thus, both $\langle\varphi(t)\varphi(t')\rangle$ and $\langle\varphi(t)\tilde{\varphi}(t')\rangle$ are real (despite $\tilde{\varphi}$ being imaginary). We get in Fourier space

$$G_{\varphi\varphi}(\omega)^\star = G_{\varphi\varphi}(-\omega) = G_{\varphi\varphi}(\omega) \ , \tag{3.77}$$

and

$$G_{\varphi\tilde{\varphi}}(\omega)^\star = G_{\varphi\tilde{\varphi}}(-\omega) \ . \tag{3.78}$$

From the definition of F, we know that

$$\begin{aligned} G_{\varphi\tilde{\varphi}}(\omega) &= i\big[G_{\varphi F}(\omega) + \omega G_{\varphi\varphi}(\omega)\big] \\ &= \frac{i}{\omega\eta(\omega) + i\gamma(\omega)} \ , \end{aligned} \tag{3.79}$$

and we conclude that

$$G_{\varphi F}(\omega)^\star = -G_{\varphi F}(\omega) \ . \tag{3.80}$$

In the end, $G_{\varphi\varphi}(\omega) \in \mathbb{R}$ and $G_{\varphi F}(\omega) \in i\mathbb{R}$, and we conclude that in frequency space both the functions $\gamma(\omega)$ and $\eta(\omega)$ are real.

We can write down explicitly the expressions for free massive scalar field, *i.e.* for $V(\varphi) = m^2\varphi^2/2$. In that case,

$$\gamma(\omega) = m^2 \quad \text{and} \quad \eta(\omega) = 1 \ , \tag{3.81}$$

and we denote the associated superpropagator as

$$G_{12}^{m^2}(\omega) = \frac{-im^2\delta_{12} + K_\omega\delta_{12}}{\omega^2 + m^4} \ . \tag{3.82}$$

This gives in real space

$$\big\langle \varphi(t)\varphi(t')\big\rangle = \frac{e^{-m^2|t-t'|}}{2m^2} \ , \quad \big\langle \varphi(t)\tilde{\varphi}(t')\big\rangle = \theta(t)e^{-m^2|t-t'|} \ . \tag{3.83}$$

3.3.2 Fluctuation-dissipation relation

As a consequence of the above constraints for the propagator, we can formulate a relation between the fluctuation, encoded in $G_{\varphi\varphi}$, and the dissipation, encoded in the response function $G_{\varphi\tilde{\varphi}}$.

For a free massive scalar field, from Eqs. (3.83), we can identify the expressions of the stochastic correlators with the results for the original Lorentzian QFT using the expressions (3.34), and using the real time relation $\bar{G}_R = \theta(t)\bar{\rho}$. With the rescalings (3.37), we find

$$\bar{G}_R = \frac{Z}{dH} G_{\varphi\tilde{\varphi}} \,, \tag{3.84}$$

and

$$\bar{F} = \frac{2H^d}{d\Omega_{D+1}} G_{\varphi\varphi} \,. \tag{3.85}$$

Note that the correlator $G_{\varphi\tilde{\varphi}}$ is not sensitive to a field rescaling. It follows from the definition (3.51) that the response field $\tilde{\varphi}$ should rescale as the inverse of φ.

Going back to the interacting case, we can define, by analogy, a stochastic spectral function, using the relation in frequency space

$$\rho(\omega) \equiv 2i \,\mathrm{Im}\, G_{\varphi\tilde{\varphi}}(\omega) \,. \tag{3.86}$$

In the free field case, ρ is related to $\bar{\rho}$ as $\bar{\rho} = Z/(dH)\rho$. From Eq. (3.79), the response function is expressed in frequency space in terms of γ and η as

$$G_{\varphi\tilde{\varphi}}(\omega) = \frac{i}{\omega\eta(\omega) + i\gamma(\omega)} \,, \tag{3.87}$$

and we find that

$$\rho(\omega) = 2i\omega G_{\varphi\varphi}(\omega) \,. \tag{3.88}$$

This equation is the fluctuation-dissipation relation, characteristic of a thermal state in the high-temperature, or classical-field, regime. It is the frequency space version of the Einstein relation for the Brownian motion, relating the dissipation coefficient to the noise amplitude [125], which was pointed out in [33, 126] in the context of the stochastic approach in de Sitter.

The above relation (3.88) gives in real space the following limit

$$\rho(t = 0^+) = 1 \,. \tag{3.89}$$

This is the equivalent of Eq. (3.35), which was formulated for a free field, in the interacting case. Indeed, Eq. (3.88) in real time reads

$$\rho(t) = -2\partial_t G_{\varphi\varphi}(t) \,. \tag{3.90}$$

The right-hand side can be computed for $t \to 0^+$,

$$-2\partial_t G_{\varphi\varphi}(t)\Big|_{t=0^+} = -2\left\langle \dot{\varphi}(0^+)\varphi(0)\right\rangle = \left\langle 2\varphi V'(\varphi)\right\rangle \,, \tag{3.91}$$

where we used the Langevin equation (3.38), and the fact that $\langle \xi(0^+)\varphi(0)\rangle$ is zero by causality. The average value $\langle 2\varphi V'(\varphi)\rangle$ can be evaluated with the one-point PDF in equilibrium (3.42). Using the following identity

$$\int_{-\infty}^{+\infty} \mathrm{d}\varphi\, 2\varphi V'(\varphi) e^{-2V} = \int_{-\infty}^{+\infty} \mathrm{d}\varphi\, e^{-2V} \,, \tag{3.92}$$

we find Eq. (3.89).

3.3.3 Causality

One last relation we can prove makes use of causality. It implies in particular that the response function vanishes for negative time separations. Indeed, it is easy to see from the above definition (3.86) that

$$G_{\varphi\tilde{\varphi}}(t) = \theta(t)\rho(t) \,. \tag{3.93}$$

This is also expressed in frequency space as

$$G_{\varphi\tilde{\varphi}}(\omega) = \int_{\omega'} \frac{\rho(\omega')}{\omega - \omega' + i0^+} \,, \tag{3.94}$$

which implies in particular that $G_{\varphi\tilde{\varphi}}(\omega)$ is analytic in the upper half of the complex frequency plane for a well-behaved spectral function $\rho(\omega)$. Using the fluctuation-dissipation relation, Eq. (3.88), we deduce

$$G_{\varphi\tilde{\varphi}}(\omega = 0) = 2\int \frac{\mathrm{d}\omega}{2\pi} G_{\varphi\varphi}(\omega) = 2G_{\varphi\varphi}(t = 0) \,. \tag{3.95}$$

This gives an exact expression for the so-called dynamical mass m_{dyn}, which measures the amplitude of the equal-time fluctuations of the stochastic field within a Hubble patch as

$$G_{\varphi\varphi}(t = 0) = \langle \varphi^2 \rangle \equiv \frac{1}{2m_{\mathrm{dyn}}^2} \,. \tag{3.96}$$

Using the expression of the response function in frequency space (3.87), we find

$$m_{\mathrm{dyn}}^2 = \gamma(0) \,. \tag{3.97}$$

This is analogous to a magnetic susceptibility in statistical field theory, which is the inverse of the response function, here identified as $G_{\varphi\tilde{\varphi}}$, at zero momentum (here frequency). It measures the response of the system to a static perturbation, and should be distinguished from the poles of the propagator, whose relation to correlations between separated spacetime points in the present context will be discussed in Chap. 4.

3.4 FRG for the model A

We saw in Sec. 2.2 the implementation of the FRG to the full Lorentzian QFT, in the LPA. It is interesting to note that the zero-dimensional theory that describes the effective potential in the deep infrared, see Eq. (2.31), can actually be identified with the equilibrium distribution of the Langevin equation (3.42) as

$$e^{N\mathcal{V}_D \mathcal{W}_\kappa(j,H)} = \int \mathrm{d}^N \hat{\phi}\, \hat{P}_{\mathrm{eq}}(\hat{\phi}_a) e^{-\frac{\kappa^2}{2}\hat{\phi}^2 - j\cdot\hat{\phi}} \,, \tag{3.98}$$

where we used the appropriate rescalings (3.37), for which we have

$$\hat{P}_{\mathrm{eq}}(\hat{\phi}_a) = \frac{1}{\mathcal{N}_{\mathrm{eq}}} \exp\big(-\mathcal{V}_D V(\hat{\phi}_a)\big) \,, \tag{3.99}$$

In particular, the cumulants obtained in both formalism will exactly coincide, meaning the LPA on the Lorentzian QFT captures the equilibrium PDF exactly.

This approximation, however, is not well suited for the computation of correlators at different spacetime points, which requires higher orders in the derivative expansion. This corresponds intuitively to pushing the expansion of correlators at higher orders in frequency/momentum space to approximate the time dependence better. Among the technical difficulties for doing so, in the context of the FRG, is the impossibility to diagonalize the Laplace-Beltrami operator due to the noncommutativity of the space and time translations, and the difficulty to construct a regulator function respecting the de Sitter symmetries [40].

These issues can be significantly simplified by applying FRG techniques not to the full QFT but to the effective stochastic theory describing its infrared dynamics. This was implemented first in the cosmological context, for a single scalar spectator in the LPA, in [42], where it was shown that the flow equation exactly coincide with the one obtained in the Lorentzian QFT in the infrared regime. Going beyond the LPA, we will be able to compute unequal-time correlators with better accuracy, and to test the convergence of the derivative expansion on these quantities. The derivative expansion at second order, in the single field case, has already been computed in the context of supersymmetric quantum mechanics [71]. We aim at extending these results to the case of N scalar fields, which will in particular give us access to the large-N limit where analytic nonperturbative results exist [35].

3.4.1 Flow of the effective potential

The first step is to choose a specific regulator which preserves the symmetries of the model A[6]. Following Canet *et al.* [68], we add the following term, quadratic in the

[6]These symmetries are distinct from, although partly related to, the initial de Sitter symmetries, for which a regulator preserving the full group has not yet been found. In particular, in the stochastic approach, the symmetries are formulated in the infrared regime and in a specific coordinate system.

superfields so as not to break the supersymmetry

$$\Delta S_\kappa[\Phi] = \frac{1}{2}\int \mathrm{d}z_1\,\mathrm{d}z_2\, R_\kappa^{ab}(z_1,z_2)\Phi_a(z_1)\Phi_b(z_2)\ . \tag{3.100}$$

Because the theory is now one-dimensional, the loop integrals are well behaved in the UV, which means it is sufficient to choose a simple mass term to regulate the IR,

$$R_\kappa^{ab}(z_1,z_2) = i\kappa^2\delta_{ab}\delta(z_1-z_2)\ . \tag{3.101}$$

We first compute the flow equation of the effective potential in the LPA [42, 71], to show the equivalence with the result obtained in the infrared limit in the Lorentzian QFT. The appropriate ansatz reads

$$\Gamma_\kappa[\Phi] = \int \mathrm{d}z \left\{\frac{1}{2}\Phi_a K \Phi_a + iNU_\kappa(X)\right\}, \tag{3.102}$$

with $X = \Phi^2/(2N)$.

At the end of our computations, we always drop the mean values of the auxiliary fields, and we particularize to constant values of $\phi_a = \langle\varphi_a\rangle$, meaning we take constant values of the superfield $\Phi_a = \phi_a$. The field space structures can be projected using the projectors (2.19) in terms of ϕ.

Again, the flow equation receives two contributions, one coming from the transverse modes and one form the longitudinal modes, whose respective effective masses were defined in Eqs. (2.21) expressed in terms of $\chi = \phi^2/(2N)$. The longitudinal and transverse components of the inverse propagator can be decomposed on the Grassmann structures as in Eq. (3.67), and we have, in the LPA,

$$\gamma_{t/l,\kappa}(\omega) = m^2_{t/l,\kappa} \quad \text{and} \quad \eta_{t/l,\kappa}(\omega) = 1\ . \tag{3.103}$$

The regulator acts as a mass term and adds a κ^2 contribution to the γ components. The propagator can be easily deduced from Eq. (3.70). The flow equation (1.84)[7] yields, for a constant superfield $\Phi_a = \phi_a$, and after factorizing out an infinite volume factor

$$\kappa\partial_\kappa U_\kappa = \frac{\kappa^2}{2N}\left(\frac{N-1}{m^2_{t,\kappa}+\kappa^2} + \frac{1}{m^2_{l,\kappa}+\kappa^2}\right). \tag{3.104}$$

This is identical to Eq. (2.27) and (2.30) in the infrared and small curvature limit, up to a numerical factor stemming from the rescaling (3.37). This equivalence was obtained in [42] for a single scalar field, and the same flow equation was found in the supersymmetric quantum mechanics [71]. Our expression generalizes the result to an $O(N)$ scalar theory.

[7] Notice here that the JdD path integral involves e^{-S} as it is concerned with a classical (stochastic) field theory rather than the e^{iS} of the quantum theory (1.71). In that case, the right hand side of the flow equation (1.84) does not include the factor i in front of the trace.

Interestingly, we can show that this computation can be further generalized at an arbitrary order in the derivative expansion. In general, the ansatz for the derivative expansion at order $2n$ should include all possible terms with n covariant derivative D and n corresponding $\bar{D}$, to get a bosonic quantity. Morevover, the flow of the effective potential only uses the propagator, which we obtain by taking two functional derivatives of the effective action ansatz and inverting the result. Thus, all terms where the derivatives act on more than two different occurrences of the field do not give any contribution. Up to partial integrations, we can thus consider only monomials of the form

$$Y_\kappa^{ab}(\Phi)\Phi_a(D\bar{D})^p\Phi_b \,, \tag{3.105}$$

where $Y_\kappa^{ab}(\Phi)$ is an arbitrary function of the superfield Φ and $p \leq n$. Using the identity

$$D\bar{D} = \frac{1}{2}[D,\bar{D}] + \frac{1}{2}\{D,\bar{D}\} = K - i\partial_t \,, \tag{3.106}$$

together with the fact that $K^2 = -\partial_t^2$, the second functional derivative of Eq. (3.105) at constant superfield $\Phi_a = \phi_a$ will have either zero, or one, occurrence of K, and up to $2n$ powers of time derivatives acting on a Dirac distribution. In frequency space, this corresponds respectively to contributions to $\gamma_\kappa(\omega)$ and $\eta_\kappa(\omega)$ in the form of polynomials in the frequency of degree lower than $2n$[8]. In particular they have no pathological behavior at $\omega = 0$.

Thus, at zero frequency, we have $\gamma_{t/l,\kappa}(\omega) = m^2_{t/l,\kappa}$, which is identical to the LPA case. Using Eq. (3.97), suitably generalized to a finite number of fields and in the presence of a regulator, the dynamical mass is expressed as the sum of a longitudinal and transverse component as

$$\frac{N}{m^2_{\mathrm{dyn},\kappa}} = \frac{N-1}{m^2_{t,\kappa}+\kappa^2} + \frac{1}{m^2_{l,\kappa}+\kappa^2} \,. \tag{3.107}$$

Now the right hand side of the flow equation (1.84), evaluated at constant superfield, gives,

$$\kappa\partial_\kappa U_\kappa = \kappa^2 \left\langle \varphi^2 \right\rangle \,. \tag{3.108}$$

By definition of the dynamical mass,

$$\kappa\partial_\kappa U_\kappa = \frac{\kappa^2}{2m^2_{\mathrm{dyn},\kappa}} \,, \tag{3.109}$$

and together with Eq. (3.107), we find the LPA flow equation (3.104) for the effective potential. We conclude that the effective potential, as it is computed from the LPA flow equation (3.104), is identical at all order in the derivative expansion.

[8] We have shown that these functions are even in general, meaning that they are in fact polynomials in ω^2.

3.4.2 Flow at second order in the derivative expansion

We now turn to the flow of the effective action at second order in the derivative expansion. This computation has been done for a single scalar field in [71]. The appropriate ansatz reads

$$\Gamma_\kappa[\Phi] = \int \mathrm{d}z \left\{ \frac{1}{2} Z_\kappa^{ab}(\Phi) \bar{D}\Phi_a D\Phi_b + iNU(X) \right\} . \tag{3.110}$$

where we introduced a renormalization of the kinetic term, with an arbitrary dependence on the superfield $Z_\kappa^{ab}(\Phi)$. Computing the second field derivative, and evaluating at constant superfield, we get the following expressions for the transverse and longitudinal components of the inverse propagator in frequency space

$$\gamma_{t/l,\kappa}(\chi) = m^2_{t/l,\kappa}(\chi) \quad \text{and} \quad \eta_{t/l,\kappa}(\chi) = z_{t/l,\kappa}(\chi) , \tag{3.111}$$

where $z_{t/l,\kappa}$ are the transverse and longitudinal projections of the field renormalization tensor Z_κ^{ab}, and every function depends on the field value through χ. Thus, the flow of Z_κ^{ab} can be extracted by taking two derivatives of the flow equation (1.84), evaluating at constant superfield, and looking, *e.g.*, at the component of the $K_\omega \delta_{12}$ Grassmann structure[9].

The second derivative of the flow equation yields [43, 44, 68]

$$\kappa\partial_\kappa \Gamma^{(2)}_{12,ab,\kappa}(\omega) = i\kappa^2 (2\mathcal{I}_{12,ab,\kappa}(\omega) - \mathcal{J}_{12,ab,\kappa}(\omega)) , \tag{3.112}$$

with

$$\begin{aligned} \mathcal{I}_{12,ab,\kappa}(\omega) = \int \frac{\mathrm{d}\omega'}{2\pi} \int_{34567} & \Gamma^{(3)}_{134,acd,\kappa}(\omega+\omega',-\omega') \Gamma^{(3)}_{256,bef,\kappa}(\omega',-\omega-\omega') \\ & \times G_{57,eg,\kappa}(\omega') G_{74,gd,\kappa}(\omega') G_{36,cf,\kappa}(\omega+\omega') , \end{aligned} \tag{3.113}$$

$$\mathcal{J}_{12,ab,\kappa}(\omega) = \int \frac{\mathrm{d}\omega'}{2\pi} \int_{345} \Gamma^{(4)}_{1234,abcd,\kappa}(\omega,-\omega',\omega') G_{45,de}(\omega') G_{53,ec}(\omega') , \tag{3.114}$$

corresponding to the contribution from the diagrams of Fig. 3.2.

These Grassmann and frequency intregrals can be computed exactly. Noting with a prime the derivative with respect to χ and omitting the χ dependence for simplicity, we have the following flow equation for $z_{l,\kappa}$,

$$\begin{aligned} \kappa\partial_\kappa z_{l,\kappa} = -\frac{2\kappa^2}{N} \Bigg\{ (N-1) \left(\frac{z_{t,\kappa} - z_{l,\kappa} + \chi z'_{l,\kappa}}{4\chi m^4_{t,\kappa}} - \frac{(m^2_{t,\kappa})'(z_{l,\kappa}-z_{t,\kappa})}{m^6_{t,\kappa}} + \frac{3\chi z_{t,\kappa}[(m^2_{t,\kappa})']^2}{4m^8_{t,\kappa}} \right) \\ + \frac{z'_{l,\kappa} + 2\chi z''_{l,\kappa}}{4m^4_{l,\kappa}} - \frac{(m^2_{l,\kappa})' 2\chi z'_{l,\kappa}}{m^6_{l,\kappa}} + \frac{3\chi z_{l,\kappa}[(m^2_{l,\kappa})']^2}{4m^8_{l,\kappa}} \Bigg\} , \end{aligned} \tag{3.115}$$

[9] Extracting this component can be done by taking the part independent of the Grassmann, for example setting $\theta_{1/2} = \bar{\theta}_{1/2} = 0$.

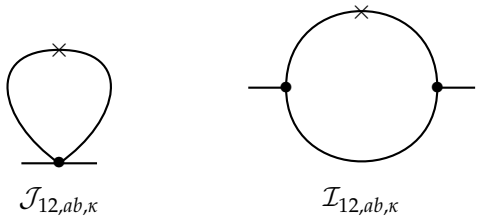

Figure 3.2: Diagrammatic representations of the contributions to the flow of the inverse propagator. The cross represents a regulator insertion, and the dots are the three- and four-point vertex functions.

and for $z_{t,\kappa}$,

$$\begin{aligned}\kappa\partial_\kappa z_{t,\kappa} = -\frac{2\kappa^2}{N}\Bigg\{ &\frac{(N-1)\chi z'_{t,\kappa} + z_{l,\kappa} - z_{t,\kappa}}{4\chi m_{t,\kappa}^4} + \frac{z'_{t,\kappa} + 2\chi z''_{t,\kappa}}{4m_{l,\kappa}^4} - \frac{(z_{l,\kappa} - z_{t,\kappa} - 2\chi z'_{t,\kappa})^2 (z_{l,\kappa} + z_{t,\kappa})}{4\chi \mathcal{M}_\kappa^4} \\ &- \frac{2(m_{t,\kappa}^2)'(z_{l,\kappa} - z_{t,\kappa}) z_{t,\kappa}[(z_{t,\kappa} + z_{l,\kappa}) m_{t,\kappa}^2 + \mathcal{M}_\kappa^2]}{m_{t,\kappa}^4 \mathcal{M}_\kappa^4} \\ &- \frac{2(m_{t,\kappa}^2)' \chi z'_{t,\kappa} z_{l,\kappa}[(z_{t,\kappa} + z_{l,\kappa}) m_{l,\kappa}^2 + M_\kappa^2]}{m_{l,\kappa}^4 \mathcal{M}_\kappa^4} \\ &+ \frac{\chi[(m_{t,\kappa}^2)']^2 z_{l,\kappa} z_{t,\kappa}[(z_{t,\kappa} + z_{l,\kappa}) m_{l,\kappa}^2 m_{t,\kappa}^2 + \mathcal{M}_\kappa^2 (m_{t,\kappa}^2 + m_{l,\kappa}^2)]}{m_{t,\kappa}^4 m_{l,\kappa}^4 \mathcal{M}_\kappa^4} \Bigg\} .\end{aligned} \tag{3.116}$$

where $\mathcal{M}_\kappa^2 = z_{t,\kappa} m_{l,\kappa}^2 + z_{l,\kappa} m_{t,\kappa}^2$. The full calculation is shown in Appendix A. These equations are partial differential equations, as $z_{t,\kappa}$ and $z_{l,\kappa}$ both depend on the composite field value χ. The contribution from the four-point vertex, corresponding to the tadpole diagram of Fig. 3.2, gives the terms where the denominator involves only $m_{t/l,\kappa}^4$, which stems from the loop diagram having only two glued propagators. All other contributions, with the denominator involving higher powers of the masses, or mixing in terms of M_κ^4, come from the sunset diagram of Fig. 3.2. This time, the diagram involves two glued propagators multiplied by a third, which typically produces higher powers of $m_{t/l,\kappa}^2$. Similarly, most of these terms feature insertions of derivatives of the transverse and longitudinal masses, corresponding to the contributions from the three-point vertices.

These flow equations can be compared to known results in several limits. First, for $N = 1$, the transverse component disappears and the longitudinal component verifies

$$\kappa\partial_\kappa z_{l,\kappa} = -2\kappa^2 \left(\frac{\partial_\phi^2 z_{l,\kappa}}{4m_{l,\kappa}^4} - \frac{2\chi \partial_\phi z_{l,\kappa} \partial_\phi^3 U}{m_{l,\kappa}^6} + \frac{3\chi z_{l,\kappa} (\partial_\phi^3 U)^2}{4m_{l,\kappa}^8} \right) . \tag{3.117}$$

This coincides with the result of Ref. [71].

Another comparison, somewhat less trivial, comes from the computation done in the LPA' scheme in the original Lorentzian field theory in the deep infrared regime for light fields [40]. The LPA' is a minimal extension of the LPA where a field renormalization is added, but does not depend on the field. It is obtained as a particular limit of our computation, taking $z_{t,\kappa} = z_{l,\kappa}$, and $z'_{t,\kappa} = 0$. Applying these restrictions to Eq. (3.116), the flow of the transverse part of the inverse propagator becomes an ordinary differential equation given by

$$\frac{\kappa\partial_\kappa z_{t,\kappa}}{z_{t,\kappa}} = \frac{-2\kappa^2}{N}\frac{\chi[(m^2_{t,\kappa})']^2(m^4_{l,\kappa} + 4m^2_{l,\kappa}m^2_{t,\kappa} + m^4_{t,\kappa})}{m^4_{t,\kappa}m^4_{l,\kappa}(m^2_{t,\kappa} + m^2_{l,\kappa})^2} \,. \tag{3.118}$$

This equation coincides with the result obtained in [40] where the authors regulate the spatial physical momenta, similarly to what we did in Sec. 2.2. This is different from our present regulation scheme, as the mass terms (3.101) regulates the frequencies, and the fact that we get the same flow equation, although expected from the de Sitter invariance, is nontrivial. This is a generalization of the similar observation done for the LPA flow in [42].

3.4.3 Convergence of the derivative expansion

In order to test the convergence of the derivative expansion in a nonperturbative regime, we use exact results coming from resummation techniques that will be explained in details later on in Sec. 4.2 and from existing numerical results [18]. Among other things, using a $1/N$ expansion, we compute the inverse propagator, and the four-point vertex function. Thus, we perform a $1/N$ expansion of the flow equations and extract the two- and four- point vertex.

The initial condition is given by the microscopic action and we take the following initial superpotential

$$V(\Phi) = \frac{m^2}{2}\Phi^2 + \frac{\lambda}{8N}\left(\Phi^2\right)^2 \,. \tag{3.119}$$

For simplicity, we only consider parameters in the symmetric regime, meaning $\phi_\kappa = 0$ and $\chi_\kappa = 0$, all along the flow.

There is a technical issue with the way we set the initial condition in actual computations. Formally, the initial value of the effective potential is set to coincide with Eq. (3.119) in the limit $\kappa \to \infty$, where the theory is effectively Gaussian. Initializing the flow at a finite value κ_0 creates small discrepancies, accounting for the fact that we should rather initialize the effective potential by computing the effective potential at κ_0 with a Legendre transform. This technical issue has no influence on the physics, however, and becomes numerically negligible for a high enough value of κ_0.

The leading order (LO) effective potential, has already been computed from the LPA, see Eq. (2.59), and will be denoted here as $u_{0,\kappa}$. At LO, the equation for the transverse part is

$$\kappa\partial_\kappa z_{t,\kappa} = -\kappa^2\frac{z'_{t,\kappa}}{2m^2_{t,\kappa}} \,, \tag{3.120}$$

which is solved by $z_{t,\kappa} = \text{const.}$, independent of κ and χ, fixed to $z_{t,\kappa} = 1$ by the initial conditions (3.110). For the longitudinal part, we define $y_{0,\kappa}$ as

$$z_{l,\kappa} = 1 + 2\chi y_{0,\kappa} + \mathcal{O}\left(\frac{1}{N}\right) . \tag{3.121}$$

Its flow equation is obtained from Eq. (3.115) as

$$\kappa\partial_\kappa y_{0,\kappa} = \frac{-2\kappa^2}{m_{t,\kappa}^4}\left(y'_{0,\kappa} + \frac{4y_{0,\kappa}u''_{0,\kappa}}{m_{t,\kappa}^2} - \frac{3(u''_{0,\kappa})^2}{2m_{t,\kappa}^4}\right) , \tag{3.122}$$

and can be formally solved using the method of characteristics. More precisely, Eq. (3.123) is a transport equation, which we rewrite in the form

$$\partial_\kappa y_{0,\kappa} = a_\kappa(\chi)y'_{0,\kappa}(\chi) + b_\kappa(\chi)y_{0,\kappa}(\chi) + c_\kappa(\chi) , \tag{3.123}$$

with

$$a_\kappa(\chi) = -\frac{2\kappa}{m_{t,\kappa}^4(\chi)} , \quad b_\kappa(\chi) = -\frac{8\kappa u''_{0,\kappa}(\chi)}{m_{t,\kappa}^6(\chi)} \quad \text{and} \quad c_\kappa(\chi) = \frac{3\kappa(u''_{0,\kappa}(\chi))^2}{m_{t,\kappa}^8(\chi)} . \tag{3.124}$$

The solution is expressed in terms of $\zeta_\kappa(\chi)$, defined as the solution of the differential problem

$$\partial_\kappa\zeta_\kappa(\chi) = -a_\kappa(\zeta_\kappa(\chi)) , \quad \zeta_{\kappa_0}(\chi) = \chi . \tag{3.125}$$

where we introduced κ_0 as the scale at which the flow is initialized. The function ζ_κ is formally inverted in terms of $\bar{\chi}_{\kappa,\chi}$

$$\zeta_\kappa(\bar{\chi}_{\kappa,\chi}) = \chi , \tag{3.126}$$

the solution to Eq. (3.123) reads

$$y_{0,\kappa}(\chi) = \int_{\kappa_0}^{\kappa} \mathrm{d}\kappa'\, c_{\kappa'}(\zeta_{\kappa'}(\bar{\chi}_{\kappa',\chi}))e^{\int_{\kappa'}^{\kappa}\mathrm{d}\kappa'' b_{\kappa''}(\zeta_{\kappa''}(\bar{\chi}_{\kappa'',\chi}))} . \tag{3.127}$$

These expressions can be easily computed numerically. Although solving Eq. (3.123) is easy using direct numerical integration of the differential equation, the formal result (3.127) suffers less from discretization issues and was used as a calibration tool.

Now, in terms of the solution to the flow equation (3.123), the LO four-point vertex function for the ansatz (3.110) can be expressed as

$$\Gamma^{(4)}_{1234,abcd,\kappa}(\omega_1,\omega_2,\omega_3) = \frac{1}{N}\delta_{12}\delta_{34}\delta_{ab}\delta_{cd}\mathbb{D}_{13,ac,\kappa}(\omega_1+\omega_3) + \text{perms.} . \tag{3.128}$$

where perms. denotes the appropriate permutations of Grassmann and frequency variables as well as $O(N)$ indices, and

$$\mathbb{D}_{12,ab,\kappa}(\omega) = \delta_{ab}\left[iu''_{0,\kappa}\delta_{12} + y_{0,\kappa}K_\omega\delta_{12}\right]\Big|_{\chi=0} . \tag{3.129}$$

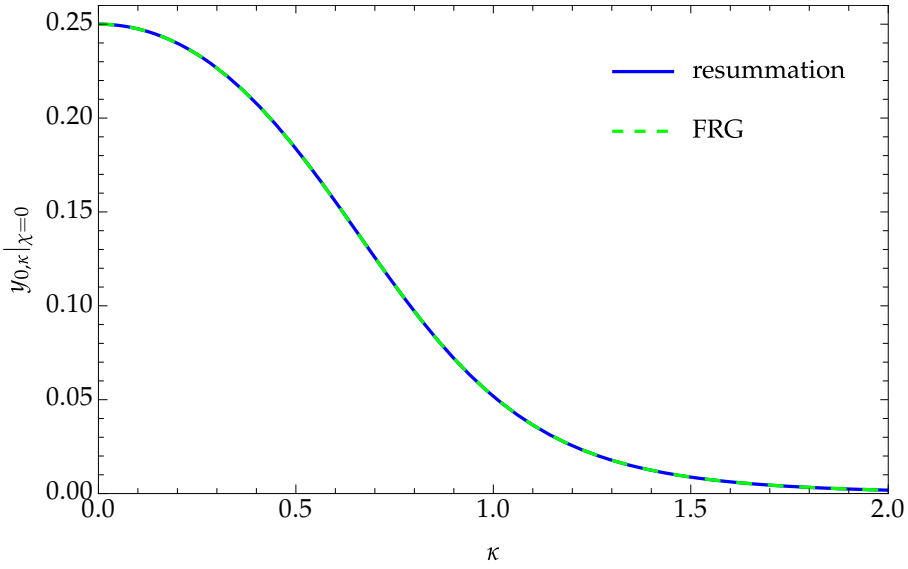

Figure 3.3: Flow of $y_{0,\kappa}$ obtained from the flow equation and the resummation at LO in a $1/N$ expansion. The regulator being a simple mass term, the flow of the resummation result was obtained adding κ^2 to the bare mass and taking $\kappa \to 0$, to compare on a finite range of values. There is a good quantitative agreement between the two results.

The exact LO four-point function obtained through diagram resummations in the next chapter, see Eq. (4.72), is expressed in terms of a free propagator of mass $2M_0^2(1+\tilde{\lambda})$, where

$$M_0^2 = \frac{m^2}{2} + \sqrt{\frac{m^4}{4} + \frac{\lambda}{4}}\,, \tag{3.130}$$

and the effective coupling $\tilde{\lambda}$ is

$$\tilde{\lambda} = \frac{\lambda}{4M_0^4}\,. \tag{3.131}$$

The free propagator of mass m^2 in the symmetric regime, *i.e.* when $\chi = 0$, is diagonal in field space and is expressed in terms of the single field result (3.82) as

$$G^{m^2}_{12,ab}(\omega) = \delta_{ab} G^{m^2}_{12}(\omega)\,. \tag{3.132}$$

In principle we should compare the results only at the end of the flow, at $\kappa = 0$. However, because the regulator (3.101) is a simple mass term, we can reproduce the entire flow by adding a κ^2 to the bare mass. To this end, we define

$$M^2_{0,\kappa} = \frac{m^2+\kappa^2}{2} + \sqrt{\left(\frac{m^2+\kappa^2}{2}\right)^2 + \frac{\lambda}{4}} \quad \text{and} \quad \tilde{\lambda}_\kappa = \frac{\lambda}{4M^4_{0,\kappa}}\,. \tag{3.133}$$

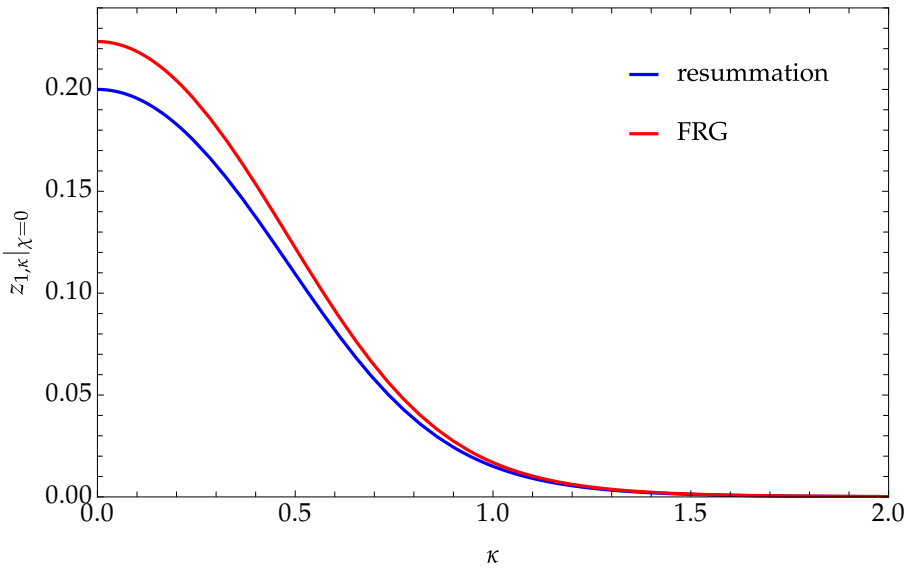

Figure 3.4: Flow of $z_{1,\kappa}$ obtained from the flow equation and the resummation at NLO in a $1/N$ expansion. The regulator being a simple mass term, the flow of the resummation result was obtained adding κ^2 to the bare mass and taking $\kappa \to 0$, to compare on a finite range of values. We see an error of about ten percent for the final value, which can be understood as a consequence of the systematic expansion in the frequencies, which is not able to correctly reproduce the pole structure of the inverse propagator.

This gives

$$\mathbb{D}_{12,ab,\kappa}(\omega) = \delta_{ab}\left[i\lambda\delta_{12} + \frac{\lambda^2}{2M_{0,\kappa}^2} G_{12}^{2M_{0,\kappa}^2(1+\tilde{\lambda}_\kappa)}(\omega)\right] . \tag{3.134}$$

The identification with Eq. (3.128) is done by developing Eq. (3.134) in frequencies, in order to reproduce the derivative expansion. We find that, at zero frequency,

$$y_{0,\kappa}\Big|_{\chi=0} \stackrel{?}{=} \frac{2\tilde{\lambda}_\kappa^2 M_{0,\kappa}^2}{(1+\tilde{\lambda}_\kappa)^2} , \tag{3.135}$$

which is in perfect agreement with the FRG result, see Fig. 3.3. This agreement at LO is expected. Indeed, the diagrammatic computation of the four-point vertex at this order only involves the bare propagator. The structure of the latter, see Eq. (3.82), is correctly captured by the ansatz (3.110). Thus, the final result developed in frequency coincides with the result of the flow.

To test the derivative expansion further, we turn to the two-point vertex at NLO in the $1/N$ expansion. We obtained the LO, for the transverse component as $z_{t,\kappa}^{\mathrm{LO}} = 1$, so that we parametrize the transverse field renormalization as

$$z_{t,\kappa} = 1 + \frac{z_{1,\kappa}}{N} + \mathcal{O}\left(\frac{1}{N^2}\right) , \tag{3.136}$$

and the corresponding flow equation reads

$$\kappa\partial_\kappa z_{1,\kappa} = -\kappa^2 \frac{z'_{1,\kappa}}{2m_{t,k}^4} - 2\kappa^2 \left\{ \frac{y_{0,\kappa}}{2m_{t,\kappa}^4} - \frac{2\chi y_{0,\kappa}^2(1+\chi y_{0,\kappa})}{\mathcal{M}_\kappa^4} - \frac{4\chi u''_{0,\kappa} y_{0,\kappa}(2(1+\chi y_{0,\kappa})m_{t,\kappa}^2 + \mathcal{M}_\kappa^2)}{m_{t,\kappa}^4 \mathcal{M}_\kappa^4} + \frac{2\chi^2 (u''_{0,\kappa})^2 y_{0,\kappa}(2(1+\chi y_{0,\kappa})m_{l,\kappa}^2 m_{t,\kappa}^2 + \mathcal{M}_\kappa^2(m_{t,\kappa}^2 + m_{l,\kappa}^2))}{m_{t,\kappa}^4 m_{l,\kappa}^4 \mathcal{M}_\kappa^4} \right\} . \tag{3.137}$$

This equation can again be formally solved, using the same method as for Eq. (3.127). Defining $d_\kappa(\chi)$ such that Eq. (3.137) reads

$$\partial_\kappa z_{1,\kappa}(\chi) = a_\kappa(\chi) z'_{1,\kappa}(\chi) + d_\kappa(\chi) , \tag{3.138}$$

and $d_\kappa(\chi)$ can be read off (3.137), the solution is expressed in terms of ζ_κ. Using Eqs. (3.125) and (3.126), we get

$$z_{1,\kappa}(\chi) = \int_{\kappa_0}^{\kappa} \mathrm{d}\kappa' \, d_{\kappa'}(\zeta_{\kappa'}(\bar{\chi}_{\kappa',\chi})) . \tag{3.139}$$

Again, in practice, we mostly used this expression to calibrate the direct numerical resolution of the flow equation (3.137) with the appropriate precision, which is more efficient.

The result is directly related to the inverse propagator through Eq. (3.111). The exact NLO expression of the self-energy will be obtained in the next chapter through diagram resummation, see Eq. (4.68). It gives, in terms of the η function,

$$\eta(\omega) = 1 + \frac{2M_0^4}{N} \frac{\tilde{\lambda}^2(3+2\tilde{\lambda})}{(1+\tilde{\lambda})} \frac{1}{\omega^2 + M_0^4(3+2\tilde{\lambda})^2} . \tag{3.140}$$

As before, we extend this expression to a finite κ making use of Eq. (3.133), and we match the derivative expansion result by expanding in the frequency. We get

$$z_{1,\kappa}\Big|_{\chi=0} \stackrel{?}{=} \frac{2\tilde{\lambda}_\kappa^2}{(1+\tilde{\lambda}_\kappa)(3+2\tilde{\lambda}_\kappa)} . \tag{3.141}$$

The comparison with the result from the flow equation is in qualitative agreement, but has a mismatch of around ten percent at $\kappa = 0$, see Fig. 3.4.

This mismatch can be understood as a consequence of the frequency expansion inherent in the derivative expansion. In this case, contrarily to what happened in the LO computation, in addition to the propagator, the diagrammatic computation involves the complete (frequency dependent) four-point vertex. However, the frequency dependence of the latter, see (3.134), is not correctly reproduced by the ansatz (3.110). The FRG computation effectively introduces a frequency expansion of the structure (3.134).

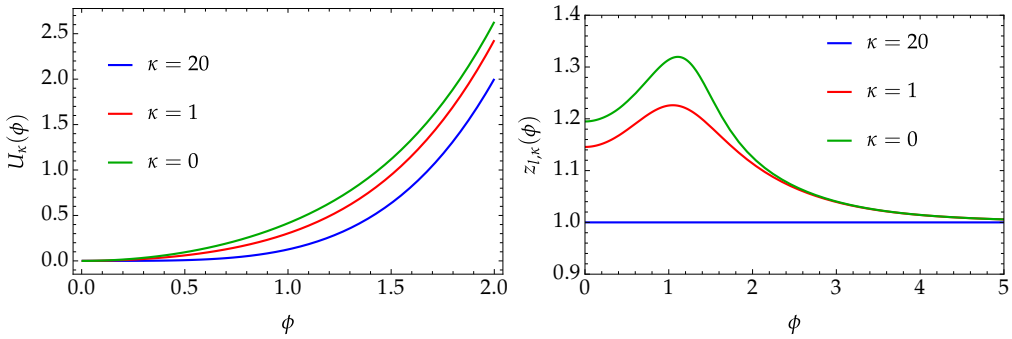

Figure 3.5: Flow of the potential (left) and field renormalization (right) for $N = 1$ massless minimally coupled interacting field, with $\lambda = 1$. The flow should be initialized in the UV, for a large value of κ, for the initial effective potential to coincide with the microscopic one, Eq. (3.119). The effective potential is normalized at zero for $\phi = 0$, to better see the mass generation, appearing as an increasing curvature at the origin.

The systematic expansion in the frequencies spoils the pole structure of the full inverse propagator.

We end this section with a comparison to existing numerical results [18, 72] in the case of a single massless field, $N = 1$ and $m = 0$. Then, only the longitudinal field renormalization $z_{l,\kappa}$ exists, and its flow is described by Eq. (3.117). We use a direct numerical resolution of Eq. (3.117), together with the flow equation of the effective potential (3.104). This leads to $z_{l,\kappa}\big|_{\kappa=0,\phi=0} = 1.18$. The numerical integration of the flow of the potential together with the field renormalization is depicted in that case in Fig. 3.5.

This can be compared with the result coming from the direct numerical resolution of the Langevin equation. In the notations of [18], in order to cancel the effect of the different normalizations, we compute the ratio between the lowest pole of the propagator of φ and the dynamical mass. The pole is computed as $3H\Lambda_1$, while the dynamical mass is $3/(8\pi^2\langle\varphi^2\rangle)$. With the ansatz (3.110), the propagator in frequency space reads

$$G_{\varphi\varphi}(\omega) = \frac{z_{l,\kappa}}{\omega^2 z_{l,\kappa}^2 + m_{l,\kappa}^4}\bigg|_{\kappa=0,\phi=0}, \tag{3.142}$$

giving for the lowest pole in ω, up to a factor i, $m_{l,\kappa}^2/z_{l,\kappa}\big|_{\kappa=0,\phi=0}$, and the dynamical mass $m_{l,\kappa}\big|_{\kappa=0,\phi=0}$. The ratio thus directly gives $z_{l,\kappa}\big|_{\kappa=0,\phi=0}$. Using the numerical values from [18], we find

$$z_{l,\kappa=0}\bigg|_{\phi=0} = \frac{\Gamma(1/4)}{2\Gamma(3/4)\times 1.36859} \approx 1.08092\,. \tag{3.143}$$

Again, we get an agreement of about ten percent with the FRG result.

3.5 Conclusion

In this chapter, the stochastic formalism is first presented, and the well-known description in terms of a Langevin equation is derived, with a special emphasis on the proper way to implement slow-roll at the level of the correlators.

The JdD path-integral formulation of the stochastic formalism allows to study general properties of the correlators for an $O(N)$ scalar theory in the deep infrared. The resulting field theory is a one-dimensional supersymmetric theory with N scalar superfields. The supersymmetry appears as an implementation of several symmetries of the original problem, including the time-translation invariance and the time-reversal symmetry, in the stationary state. The Ward identities associated to the supersymmetry generators, together with a causality constraint, give some relations between the different two-point correlators of the theory, valid in the long distance limit, including a fluctuation-dissipation relation between the spectral and statistical functions. These relations are valid independently of any approximation scheme, and give useful insight for practical computation, notably on the possible Grassmann structures that can appear.

The FRG and its derivative expansion can be implemented using a supersymmetric regulator. As previously observed in [42], the LPA flow of the effective potential obtained in the Lorentzian QFT is recovered in a very simple way. Moreover, the result of [42] can be generalized, showing that this flow equation would not be modified at any order in the derivative expansion, so that it is exactly captured already in the LPA. In the language of nonequilibrium statistical physics, this tells us that the equilibirum state of the Langevin process, which is determined by the effective potential alone, is unaffected by the possible nonequilibrium deviations [67, 68].

Going beyond the LPA, up to second order in the derivative expansion, corresponds to the inclusion of a functional renormalization of the kinetic term. The flow of the latter is obtained in relatively simple way and compares well with the much more challenging computation in the Lorentzian QFT where the latter could only be obtained in a simplified version, the LPA', where one drops the field dependence of the kinetic term renormalization.

Finally, the convergence of the derivative expansion is tested in a limit where analytical results are available, namely at NLO in a $1/N$ expansion and against numerical results for $N = 1$. The integration of the flow equations gives qualitatively correct results for the inverse propagator, and good quantitative predictions for the four-point function. However, the frequency expansion does not correctly capture the actual frequency dependence of the various vertex functions which enter in loop diagrams. Ultimately, this means that the $1/N$ and frequency expansions do not commute, hence the mismatch in detailed comparisons. In practice, in all the cases where we could test it, we found a difference of about ten percents between the result of the flow and the exact result.

4 Model A and eigenvalues

Contents

4.1 Fokker-Planck formulation of the stochastic formalism 82
4.1.1 Eigenvalue problem 82
4.1.2 Mass hierarchy and correlators 83
4.2 Diagrammatic resummations with the Janssen-de Dominicis path integral 85
4.2.1 Perturbative expansion 86
4.2.2 $1/N$ expansion 90
4.2.3 Discussion 95
4.3 $1/N$ expansion of the Fokker-Planck equation 98
4.3.1 Gaussian case 99
4.3.2 Interacting case 100
4.3.3 Discussion 102
4.3.4 Comparison to finite N results 103
4.4 Conclusion 107

Conclusion **109**

A powerful method to extract information from the stochastic formalism uses a reformulation of the Langevin equation in terms of a Fokker-Planck equation for a PDF for the field value at a given time [18]. This can, in turn, be formulated as an eigenvalue problem which, although convenient for implementing a numerical resolution [72, 73], is not analytically solvable in the presence of interactions.

Analytical results can however be obtained in several limits for simple potentials, for instance a perturbative expansion around the Gaussian case [18, 72], or a $1/N$ expansion. Here we will consider a quartic potential. The $1/N$ expansion is particularly interesting as it gives access to strongly nonperturbative regimes [35], where the effects of the interactions can have sizeable physical consequences. We shall present two different ways to obtain these results. The first relies on the path integral formulation introduced in Sec. 3.2. Using specific resummations of diagrams, we can compute several correlators through the Schwinger-Dyson equations [30, 35]. The other approach consists in formulating the $1/N$ expansion directly for the eigenvalue problem.

In the first section 4.1, we recall how the Fokker-Planck equation and its formulation as an eigenvalue problem is obtained, and how it is linked to the structure of the dif-

ferent correlators. Sec. 4.2 is devoted to the computation of some two-point correlators through diagram resummations. The $1/N$ expansion of the Fokker-Planck equation is then presented in Sec. 4.3.

4.1 Fokker-Planck formulation of the stochastic formalism

In this chapter, unless explicitly stated, we use the rescaled variables defined in Eq. (3.37) for the field and the potential.

Starting from the stochastic equation (3.38) for N interacting scalar field with an $O(N)$ symmetry, the associated PDF, $P(\varphi_a, t)$, verifies the Fokker-Planck equation (3.40), which we recall here to be [123]

$$\partial_t P = \partial_{\varphi_a}\left((\partial_{\varphi_a} V) P + \frac{1}{2}\partial_{\varphi_a} P \right) . \tag{4.1}$$

Note that, because we consider the specific case of test scalar field, the Langevin equation (3.38) is linear, meaning that there is no field dependent term multiplying the noise. For linear Langevin equations, we do not need to chose a particular discretization, such as Itô or Stratonovitch, as it has no incidence on the Fokker-Planck equation [123]. This would be different for example for the inflaton, where one has to chose a particular prescription [117], as the Hubble parameter becomes a field dependent factor.

4.1.1 Eigenvalue problem

Eq. (4.1) can be formulated as an eigenvalue problem. For that purpose, we introduce the reduced PDF, $p(\varphi_a, t)$, defined as

$$P(\varphi_a, t) = e^{-V(\varphi_a)} p(\varphi_a, t) , \tag{4.2}$$

which is governed by the Schrödinger-like equation

$$\partial_t p = \frac{1}{2}\Delta_\varphi p - W p , \tag{4.3}$$

where $\Delta_\varphi = \partial_{\varphi_a}\partial_{\varphi_a}$ is the Laplacian in field space, and W is related to V as

$$W = \frac{1}{2}\left[(\partial_{\varphi_a} V)^2 - \Delta_\varphi V \right] . \tag{4.4}$$

For an $O(N)$-symmetric potential, it is convenient to use spherical coordinates in field space. We decompose the angular dependence onto generalized spherical harmonics [127] $Y_{\ell_i}(\theta_i)$, where $\theta_{i=1\ldots N-1}$ denotes the $N-1$ angular variables in field space and the ℓ_i are integers such that

$$|\ell_1| \leq \ell_2 \leq \cdots \leq \ell_{N-1} . \tag{4.5}$$

These harmonics diagonalize the angular part of the Laplacian. The latter is decomposed as

$$\Delta_\varphi = \frac{1}{N}\partial_x^2 + \frac{N-1}{Nx}\partial_x + \frac{\Delta_{S^{N-1}}}{Nx^2} , \tag{4.6}$$

using the rescaled radial variable $x = \sqrt{\varphi^2/N}$. We have, for the angular part,

$$\Delta_{S^{N-1}} Y_{\ell_i}(\theta_i) = -\ell(\ell+N-2) Y_{\ell_i}(\theta_i) \,, \tag{4.7}$$

with $\ell = \ell_{N-1}$. We can thus separate the radial and angular parts and expend the reduced PDF in terms of eigenfunctions $\Psi_{n,\ell}$ of the form

$$\Psi_{n,\ell}(\varphi_a) = \mathcal{R}_{n,\ell}(x) Y_{\ell_i}(\theta_i) e^{-\Lambda_{n,\ell} t} \,, \tag{4.8}$$

where the radial part verifies

$$-\frac{\mathcal{R}''_{n,\ell}}{2N} - \frac{N-1}{2Nx}\mathcal{R}'_{n,\ell} + \left[\frac{\ell(\ell+N-2)}{2Nx^2} + W\right]\mathcal{R}_{n,\ell} = \Lambda_{n,\ell}\mathcal{R}_{n,\ell} \,. \tag{4.9}$$

The index n represent a possible additional quantum number. For example in the Gaussian case, as will be explained in more details in Sec. 4.3, n has to be a positive integer chosen such that $n-\ell$ is even and positive. We expect this to be true also for the quartic potential that we consider here, and it will be explicitly verified in the $1/N$ expansion described in Sec. 4.3.

In general, the differential operator in Eq. (4.3), that acts on the eigenfunctions $\Psi_{n,\ell}(\varphi_a)$, can be factorized as

$$\left(-\frac{1}{2}\Delta_\varphi + W\right)\Psi_{n,\ell} = \left(-\partial_{\varphi_a} + V'\right)\left(-\partial_{\varphi_a} + V'\right)^\dagger \Psi_{n,\ell} \,. \tag{4.10}$$

This differential operator being the square of an operator, it is positive, and its eigenvalues are thus nonnegative. Moreover, from Eq. (4.8), the equilibrium value corresponds to $\Lambda = 0$. We have seen that such an equilibrium exists in Sec. 3.1, see Eq. (3.42), and thus the ground state always verify $\Lambda_{0,0} = 0$.

4.1.2 Mass hierarchy and correlators

Using the decomposition of the reduced PDF in terms of the eigenfunctions (4.8), the unequal time two-point correlator of a given operator $\mathcal{A}(\varphi)$ can be written as

$$G_{\mathcal{A}\mathcal{A}}(t-t') \equiv \left\langle \mathcal{A}(t)\mathcal{A}(t')\right\rangle = \sum_{n\geq 0}\sum_{\ell=0}^{n} C^{\mathcal{A}}_{n,\ell} e^{-\Lambda_{n,\ell}|t-t'|} \,. \tag{4.11}$$

The coefficients $C^{\mathcal{A}}_{n,\ell}$ are computed as the following matrix elements [18, 72],

$$C^{\mathcal{A}}_{n,\ell} = \int \mathrm{d}^N\varphi \Psi_{0,0}(\varphi_a)\mathcal{A}\Psi_{n,\ell}(\varphi_a) \,, \tag{4.12}$$

and depending on the symmetry properties of $\mathcal{A}$, symmetry selection rules [72] will leave only a subset of nonvanishing coefficients.

For example, choosing $\mathcal{A} = \varphi$ will select only the vector channel $\ell = 1$, meaning we only have contributions from the $C^{\varphi}_{2n+1,1}$ coefficients. For $\mathcal{A} = \chi = \varphi^2/(2N)$, the

operator is in the scalar channel, $\ell = 0$, and the nonvanishing contributions will come from the $C^{\chi}_{2n,0}$ coefficients. From the expression (4.11), for a given correlator, it is clear that the late-time (or long-distance) behavior is dominated by the lowest contributing eigenvalue.

For later convenience, we define the rescaled coefficients c^{φ}_{2n+1} and c^{χ}_{2n} as,

$$C^{\varphi}_{2n+1,1} = \frac{c^{\varphi}_{2n+1}}{2\Lambda_{2n+1,1}} \quad \text{and} \quad C^{\chi}_{2n,0} = \frac{c^{\chi}_{2n}}{2\Lambda_{2n,0}} \,, \tag{4.13}$$

and the tree-level propagator of mass m^2 reads, in real-time and in frequency space

$$G_{m^2}(t) = \frac{e^{-m^2|t|}}{2m^2}, \quad G_{m^2}(\omega) = \frac{1}{\omega^2 + m^4} \,. \tag{4.14}$$

In terms of these quantities we can easily express the $\langle\varphi\varphi\rangle$ and the $\langle\chi\chi\rangle$ correlators as

$$\begin{aligned} G_{\varphi\varphi} &= \sum_{n\geq 0} c^{\varphi}_{2n+1} G_{\Lambda_{2n+1,1}} \,, \\ G_{\chi\chi} &= \sum_{n\geq 0} c^{\chi}_{2n} G_{\Lambda_{2n,0}} \,. \end{aligned} \tag{4.15}$$

Using the response field $\tilde{\varphi}$ introduced in the JdD formulation (3.52), the response function $G_{\varphi\tilde{\varphi}}$ was shown to be the analog of the retarded Green function in Sec. 3.3. The functions $G_{\varphi\varphi}(\omega)$ and $G_{\varphi\tilde{\varphi}}(\omega)$ can both be expressed in terms of $\gamma(\omega)$ and $\eta(\omega)$, defined in Eq. (3.67). For a free massive propagator, these are given by $\gamma(\omega) = m^2$ and $\eta(\omega) = 1$. Each tree-level propagator $G_{\Lambda_{2n+1,1}}$ in Eq. (4.15) thus corresponds to a contribution to $G_{\varphi\tilde{\varphi}}$ which, using Eqs. (3.72) and (3.87), gives

$$G_{\varphi\tilde{\varphi}}(\omega) = \sum_{n\geq 0} \frac{i c^{\varphi}_{2n+1}}{\omega + i\Lambda_{2n+1,1}} \,. \tag{4.16}$$

Thus, the coefficients (4.13) and eigenvalues $\Lambda_{n,\ell=0,1}$ can be obtained as poles and residues of the appropriate response function. Using the results shown in Sec. 3.3, we can get general relations on these quantities. Specifically, Eq. (3.89) gives the following sum rule

$$\sum_{n\geq 0} c^{\varphi}_{2n+1} = 1 \,, \tag{4.17}$$

while Eq. (3.97) gives the following expression for the dynamical mass

$$\sum_{n\geq 0} \frac{c^{\varphi}_{2n+1}}{\Lambda_{2n+1,1}} = \frac{1}{m^2_{\text{dyn}}} \,. \tag{4.18}$$

(a)

Figure 4.1: One-loop diagram giving the expression of $C_{12}^{m^2}$ in a free theory. The lines denote the tree-level propagator (4.21).

4.2 Diagrammatic resummations with the Janssen-de Dominicis path integral

We now turn to the actual computations of the $\langle\varphi\varphi\rangle$ and $\langle\chi\chi\rangle$ correlators using the JdD path integral formulation. We consider two different approximation schemes, a perturbative expansion and a $1/N$ expansion, from which we obtain $\Lambda_{2n,0}$ and $\Lambda_{2n+1,1}$ at the relevant order of approximation. These two approximations were already studied in the D-dimensional Lorentzian theory [34, 35], to which we can thus compare our results. The microscopic potential reads, in terms of the superfield,

$$V(\hat{\Phi}) = \frac{m^2}{2}\hat{\Phi}^2 + \frac{\lambda}{8N}(\hat{\Phi}^2)^2 \,. \tag{4.19}$$

We mentioned in Sec. 2.3 that, due to the low dimensionality of the system, no spontaneous symmetry breaking is possible, and thus $\langle\hat{\Phi}_a\rangle = 0$, independently of the sign of the parameter m^2. As a consequence, the two-point correlators is diagonal in field space, *e.g.* $G_{12,ab}(\omega) = \delta_{ab}G_{12}(\omega)$.

We define the self-energy Σ in the following way

$$\Gamma_{12}^{(2)}(\omega) = im^2\delta_{12} + K_\omega\delta_{12} + \Sigma_{12}(\omega) \,. \tag{4.20}$$

We isolated the free field contribution, corresponding to the free superpropagator (3.132), which we recall here to be

$$G_{12}^{m^2}(\omega) = \frac{-im^2\delta_{12} + K_\omega\delta_{12}}{\omega^2 + m^4} \,. \tag{4.21}$$

The supercorrelator of $\hat{X} = \hat{\Phi}^2/(2N)$ is denoted

$$C_{12}(t - t') = \left\langle \hat{X}(t, \bar{\theta}_1, \theta_1)\hat{X}(t', \bar{\theta}_2, \theta_2)\right\rangle \,. \tag{4.22}$$

In the free theory, it is given by the diagram (a) of Fig. 4.1, which is computed in frequency space as

$$C_{12}^{m^2}(\omega) = \frac{1}{2N}\int_{\omega'} G_{12}^{m^2}(\omega - \omega')G_{12}^{m^2}(\omega') = \frac{G_{12}^{2m^2}(\omega)}{2Nm^2} \,, \tag{4.23}$$

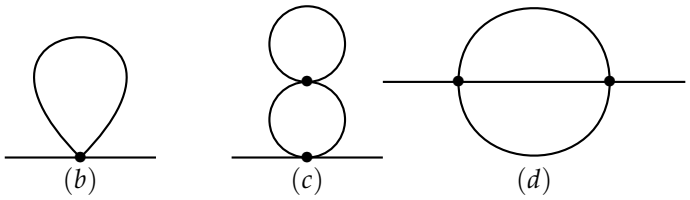

Figure 4.2: Perturbative contributions to the self-energy at one- and two-loop orders. The interaction vertex is represented with a dot and gives a factor $-i\lambda/(8N)$, while the propagator lines are given by the tree-level propagator (4.21).

where we used the relations

$$\begin{aligned} \delta_{12}^2 &= 0 \,, \\ \delta_{12} K_\omega \delta_{12} &= \delta_{12} \,, \\ K_\omega \delta_{12} K_{\omega'} \delta_{12} &= K_{\omega+\omega'} \delta_{12} \,. \end{aligned} \tag{4.24}$$

The scalar component is extracted at $\theta_{1,2} = \bar{\theta}_{1,2} = 0$, and we have

$$G^{m^2}_{\chi\chi}(\omega) = \frac{1}{2Nm^2} \frac{1}{\omega^2 + 4m^2} \,. \tag{4.25}$$

Using the decomposition (4.11), we can read off Eq. (4.14) that

$$\begin{aligned} \Lambda^{\text{free}}_{1,1} &= m^2, \quad c^{\varphi,\text{free}}_{2n+1} = \delta_{n,0} \,, \\ \Lambda^{\text{free}}_{2,0} &= 2m^2, \quad c^{\chi,\text{free}}_{2n} = \frac{\delta_{n,1}}{2Nm^2} \,. \end{aligned} \tag{4.26}$$

This is in agreement with the known spectrum for the Gaussian case [18, 72]

$$\Lambda^{\text{free}}_{n,\ell} = nm^2 \,, \tag{4.27}$$

which we derive explicitly later in Sec. 4.3.

4.2.1 Perturbative expansion

We first compute the self-energy at two-loop order in the perturbative expansion. The three-loop order is computed in Appendix B. The relevant diagrams are shown in Fig. 4.2. Standard diagrammatic rules yield, for the contribution of the one-loop diagram (b) of Fig. 4.2.

$$\Sigma^{(b)}_{12} = \delta_{12} \frac{N+2}{N} \frac{i\lambda}{2} \int \frac{\mathrm{d}\omega}{2\pi} G^{m^2}_{12}(\omega) \,. \tag{4.28}$$

Using the expression (4.21) of the free superpropagator, and the formulas (4.24), the Grassmann algebra gives

$$\Sigma^{(b)}_{12}(\omega) = i \frac{N+2}{N} \frac{\lambda}{2} \mathcal{F}(m^2) \delta_{12} \,, \tag{4.29}$$

where

$$\mathcal{F}(m^2) = \int \frac{\mathrm{d}\omega}{2\pi} \frac{1}{\omega^2 + m^4} = \frac{1}{2m^2} \,. \tag{4.30}$$

This leads to

$$\Sigma_{12}^{(b)}(\omega) = i\frac{N+2}{N}\frac{\lambda}{4m^2}\delta_{12} \,. \tag{4.31}$$

It corresponds to a simple shift in the value of $\gamma(\omega)$, which is nothing but a mass renormalization. This is also the case for the two-loop local contribution coming from diagram (c) of Fig. 4.2 (local meaning that external legs are attached to a single vertex), which reads

$$\Sigma_{12}^{(c)}(\omega) = \left(\frac{N+2}{N}\right)^2 \frac{\lambda^2}{4} \int_3 \int \frac{\mathrm{d}\omega'}{2\pi} G_{13}^{m^2}(\omega') G_{32}^{m^2}(\omega') \int \frac{\mathrm{d}\omega''}{2\pi} G_{33}^{m^2}(\omega'') \,. \tag{4.32}$$

Using again the Grassmann formulas (4.24), we get

$$\begin{aligned} \Sigma_{12}^{(c)}(\omega) &= i\left(\frac{N+2}{N}\right)^2 \frac{\lambda^2}{4} \mathcal{F}'(m^2)\mathcal{F}(m^2)\delta_{12} \\ &= -i\left(\frac{N+2}{N}\right)^2 \frac{\lambda^2}{16m^4}\delta_{12} \,. \end{aligned} \tag{4.33}$$

A nontrivial frequency dependence appears with the nonlocal contribution from diagram (d) of Fig. 4.2, which can be expressed as

$$\Sigma_{12}^{(d)}(\omega) = \frac{\lambda^2}{2}\frac{N+2}{N^2} \int \frac{\mathrm{d}\omega'}{2\pi}\frac{\mathrm{d}\omega''}{2\pi} G_{12}^{m^2}(\omega - \omega' - \omega'') G_{12}^{m^2}(\omega') G_{12}^{m^2}(\omega'') \,. \tag{4.34}$$

The frequency integration is performed using the following identity

$$\int \frac{\mathrm{d}\omega'}{2\pi} G_{12}^{m_A^2}(\omega') G_{12}^{m_B^2}(\omega - \omega') = \frac{1}{2m_{AB}^2} G_{12}^{m_A^2 + m_B^2}(\omega) \,, \tag{4.35}$$

where m_{AB}^2 is the reduced square mass, defined as

$$\frac{1}{m_{AB}^2} = \frac{1}{m_A^2} + \frac{1}{m_B^2} \,. \tag{4.36}$$

Eq. (4.35) expresses the fact that a product of two tree level superpropagators in real space is proportional to a superpropagator with the sum of the two square masses. For example for the $G_{\varphi\varphi}$ component, we have

$$G_{m_A^2}(t) G_{m_B^2}(t) = \frac{1}{2m_{AB}^2} G_{m_A^2 + m_B^2}(t) \,, \tag{4.37}$$

which follows trivially from Eq. (4.14). Using this relation twice on Eq. (4.34) gives

$$\Sigma_{12}^{(d)}(\omega) = \frac{N+2}{N^2}\frac{3\lambda^2}{8m^4} G_{12}^{3m^2}(\omega) \,. \tag{4.38}$$

Putting together Eqs. (4.31), (4.33) and (4.38), we get for the inverse propagator, in terms of the functions γ and η

$$\begin{aligned}\gamma(\omega) &= M^2 - \frac{6\bar{\lambda}^2}{N+2}\frac{3m^6}{\omega^2+9m^4} + \mathcal{O}(\bar{\lambda}^3) \,, \\ \eta(\omega) &= 1 + \frac{6\bar{\lambda}^2}{N+2}\frac{m^4}{\omega^2+9m^4} + \mathcal{O}(\bar{\lambda}^3) \,,\end{aligned} \tag{4.39}$$

where we have introduced the dimensionless coupling

$$\bar{\lambda} = \frac{N+2}{N}\frac{\lambda}{3m^4} \,, \tag{4.40}$$

and the renormalized mass

$$M^2 = m^2\big(1+\bar{\lambda}-\bar{\lambda}^2\big) \,. \tag{4.41}$$

We immediately obtain the expression for the dynamical mass from Eq. (3.97)

$$m^2_{\rm dyn} = \gamma(0) = m^2\left[1+\bar{\lambda}-\frac{N+4}{N+2}\bar{\lambda}^2+\mathcal{O}\big(\bar{\lambda}^3\big)\right] . \tag{4.42}$$

Following Eq. (4.16), we can read the relevant mass hierarchy from the response function, which reads, at this order of approximation,

$$G_{\varphi\tilde{\varphi}}(\omega) = \frac{ic_1^\varphi}{\omega+i\Lambda_{1,1}} + \frac{ic_3^\varphi}{\omega+i\Lambda_{3,1}} + \mathcal{O}\big(\bar{\lambda}^3\big) \,. \tag{4.43}$$

Using Eq. (4.39) we compute the poles

$$\begin{aligned}\Lambda_{1,1} &= m^2\left[1+\bar{\lambda}-\frac{N+5}{N+2}\bar{\lambda}^2+\mathcal{O}\big(\bar{\lambda}^3\big)\right] , \\ \Lambda_{3,1} &= m^2\big[1+\mathcal{O}\big(\bar{\lambda}\big)\big] \,,\end{aligned} \tag{4.44}$$

and the residues

$$\begin{aligned}c_1^\varphi &= 1 - \frac{3\bar{\lambda}^2}{2(N+2)} + \mathcal{O}\big(\bar{\lambda}^3\big) \,, \\ c_3^\varphi &= \frac{3\bar{\lambda}^2}{2(N+2)} + \mathcal{O}\big(\bar{\lambda}^3\big) \,.\end{aligned} \tag{4.45}$$

Notice that we check the sum rule (4.17).

The structure of the propagator, involving only two poles at this order of approximation, precisely coincides with the propagator obtained in the Lorentzian QFT in D dimensions of Ref. [34], which reads

$$G_{\varphi\varphi}(t) = c_+ G_{m_+^2}(t) + c_- G_{m_-^2}(t) \,. \tag{4.46}$$

The expressions of these various masses and coefficients agree with our results provided we identify

$$\begin{aligned}c_+ = c_1^\varphi \,, \quad c_- = c_3^\varphi \,, \\ m_+^2 = \Lambda_{1,1} \,, \quad m_-^2 = \Lambda_{3,1} \,,\end{aligned} \tag{4.47}$$

(e) (f)

Figure 4.3: Two-loop contribution to the $\langle\chi\chi\rangle$ correlator. The diagram (e) is just an effect of the mass renormalization.

with the appropriate rescaling (denoting the quantities of Ref. [34] with a hat)

$$m^2 = \frac{\hat{m}^2}{dH}, \quad \lambda = \frac{2H^{d-1}}{d^2\Omega_{D+1}}\hat{\lambda} \, . \tag{4.48}$$

We now compute the two-loop correction to the $\langle\chi\chi\rangle$ correlator, given by the diagrams of Fig. 4.3. The diagram (e) simply corresponds to the effect of the one-loop renormalization of one propagator line [similarly to the diagram (c) of Fig. 4.2], and can be computed easily. Equivalently, one can use a trick, implicitly including this diagram in the one-loop diagram of Fig. 4.1 by using effective propagator lines with a mass M. The latter is then replaced by its expression (4.41), and the result is expanded systematically at the relevant order. Although this is not necessary here, this method will be useful later in the $1/N$ expansion.

Each loop in the diagram (a) of Fig. 4.1 and the diagram (f) of Fig. 4.3 is given by $C_{12}^{M^2}$, see Eq. (4.23). The sum reads

$$C_{12}^{(a+f)}(\omega) = C_{12}^{M^2}(\omega) - i\lambda(N+2)\int_3 C_{13}^{M^2}(\omega)C_{32}^{M^2}(\omega) \, . \tag{4.49}$$

Using the identity

$$\int_3 G_{13}^{m^2}(\omega)G_{32}^{m^2}(\omega) = \frac{(\omega^2 - m^4)\delta_{12} - 2im^2K_\omega\delta_{12}}{(\omega^2+m^4)^2} \, , \tag{4.50}$$

and extracting the component at vanishing Grassmann variables, we obtain in terms of M,

$$\begin{aligned} G_{\chi\chi}(\omega) &= \frac{1}{2NM^2}\frac{1}{\omega^2+4M^4}\left[1 - \frac{8\bar{\lambda}M^4}{\omega^2+4M^4} + \mathcal{O}(\bar{\lambda}^2)\right] \\ &= \frac{1}{2NM^2}\frac{1}{\omega^2+4M^4(1+\bar{\lambda})^2} + \mathcal{O}(\bar{\lambda}^2) \, . \end{aligned} \tag{4.51}$$

In the second line we used our knowledge of the general structure of the correlator (4.11) to resum the two-loop correction to the χ propagator in the appropriate form (*i.e.* a correction to the corresponding self-energy). We can directly read off the expressions

$$\Lambda_{2,0} = 2m^2\left[1 + 2\bar{\lambda} + \mathcal{O}(\bar{\lambda})\right] \, , \tag{4.52}$$

$$c_2^\chi = \frac{1}{2Nm^2}\left[1 - \bar{\lambda} + \mathcal{O}(\bar{\lambda}^2)\right] \, . \tag{4.53}$$

An important remark is that the present computation with two-loop diagrams, up to order $\bar{\lambda}^2$, only gives access to the LO expression of the subleading eigenvalue $\Lambda_{3,1}$, as the corresponding coefficient c_3^φ is itself of order $\bar{\lambda}^2$. It is interesting to push our perturbative calculation up to three-loop order to get the first correction to $\Lambda_{3,1}$, to compare with the result obtained from the Fokker-Planck approach. This computation is presented in Appendix B, where the reader can find the results obtained for m^2_{dyn}, $\Lambda_{1,1}$, c_1^φ and c_3^φ at three-loop order. We report here the NLO results for the eigenvalues

$$\begin{aligned}
\Lambda_{1,1} &= m^2\big[1+\bar{\lambda}+\mathcal{O}(\bar{\lambda}^2)\big]\,,\\
\Lambda_{2,0} &= 2m^2\big[1+2\bar{\lambda}+\mathcal{O}(\bar{\lambda}^2)\big]\,,\\
\Lambda_{3,1} &= 3m^2\left[1+\frac{5N+22}{3(N+2)}\bar{\lambda}+\mathcal{O}(\bar{\lambda}^2)\right]\,,
\end{aligned} \tag{4.54}$$

which reproduce and generalize to arbitrary N and D the results of Refs. [72, 73].

The present perturbative computation is controlled by the dimensionless parameter $\bar{\lambda} \propto \lambda/m^4$, which blows up as m is taken to zero. As is well-known, perturbative results are thus invalid in this limit, as well as for negative square mass, similarly to the loop computations of Sec. 2.3. The nonperturbative regime can be reached with a $1/N$ expansion, which was also studied in Ref. [35] with the Lorentzian QFT, and that we now compute in the stochastic framework.

4.2.2 $1/N$ expansion

The diagrammatic formulation of the $1/N$ expansion that we now present closely follows the calculation of Ref. [35] in the D-dimensional Lorentzian QFT. The local and nonlocal contributions to the self-energy are treated separately, and the former can be put in an effective squared mass M^2, defined through the following gap equation

$$M^2 = m^2 + \sigma\,, \tag{4.55}$$

where σ is given by the diagram (b) of Fig. 4.2, computed with the full propagator, namely

$$\sigma = \frac{N+2}{N}\frac{\lambda}{2}\int\frac{\mathrm{d}\omega}{2\pi}G_{11}(\omega) = \frac{N+2}{N}\frac{\lambda}{4\gamma(0)}\,. \tag{4.56}$$

Here, we used the fact that $G_{11}(\omega) = G_{\varphi\varphi}(\omega)$ and Eq. (3.97). We first compute the LO contribution in the form $M^2 = M_0^2 + \mathcal{O}(1/N)$. At this order, there is no nonlocal contribution, thus the propagator is simply a tree-level propagator, see Eq. (4.21), with a renormalized mass M_0^2, which corresponds to $\gamma(0) = M_0^2 + \mathcal{O}(1/N)$. Using the LO expressions in Eq. (4.55), we find, keeping the positive solution,

$$M_0^2 = \frac{m^2}{2} + \sqrt{\frac{m^4}{4}+\frac{\lambda}{4}}\,. \tag{4.57}$$

Note that this result coincides, up to the rescalings (4.48), with the curvature of the effective potential at the origin we obtained in the FRG treatment, Eq. (2.64), at vanishing regulator and absorbing the nonminimal coupling into m^2.

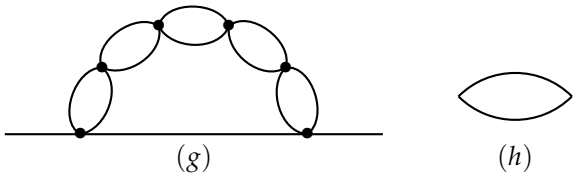

Figure 4.4: The diagram (g) represent the topology of the contributions to the self-energy at NLO in the $1/N$ expansion. The diagram (h) is the single bubble Π_{12}.

The NLO propagator is obtained using the LO propagator $G_{12}^{M_0^2}$ to compute the non-local contribution to the self-energy. This automatically resums the LO local insertions in the internal lines. Then, we have to solve the implicit equation (4.55) with the obtained propagator to get the NLO expression of M_0^2. The nonlocal part is given by the diagrams of the type of diagram (g) in Fig. 4.4, where an arbitrary number of loops are inserted between the two external legs. The one-loop bubble is represented by the diagram (h) and gives a conribution

$$\Pi_{12(\omega)} = \frac{\lambda}{2}\int \frac{\mathrm{d}\omega'}{2\pi} G_{12}^{M_0^2}(\omega') G_{12}^{M_0^2}(\omega-\omega') \,. \tag{4.58}$$

The infinite series of bubbles is summed through the integral equation [30, 35, 122]

$$\mathbb{I}_{12}(\omega) = \Pi_{12}(\omega) + i\int_3 \Pi_{13}(\omega)\mathbb{I}_{32}(\omega) \,. \tag{4.59}$$

The function $\mathbb{I}$ resums the entire chain of bubbles, as represented in Fig. 4.5, where it is depicted as a wiggly line. The NLO nonlocal contribution is obtained in terms of this quantity, and corresponds to the diagram (i) of Fig. 4.5. We get the effective one-loop expression

$$\Sigma_{12}^{(i)}(\omega) = -\frac{\lambda}{N}\int \frac{\mathrm{d}\omega'}{2\pi} G_{12}^{M_0^2}(\omega')\mathbb{I}_{12}(\omega-\omega') \,. \tag{4.60}$$

We now compute explicitly all these quantities. The integral in Eq. (4.58) is computed using the formula (4.35), to get

$$\Pi_{12}(\omega) = -2\tilde{\lambda} M_0^2 G_{12}^{2M_0^2}(\omega) \,, \tag{4.61}$$

in terms of the dimensionless effective coupling

$$\tilde{\lambda} = \frac{\lambda}{4M_0^4} \,. \tag{4.62}$$

which is the large-N analog of the one defined in the perturbative expansion in Eq. (4.40). Writing explicitly the Grassmann structures,

$$\begin{aligned} \Pi_{12}(\omega) &= i\pi_\gamma(\omega)\delta_{12} + \pi_\eta(\omega)K_\omega\delta_{12} \,, \\ \mathbb{I}_{12}(\omega) &= iI_\gamma(\omega)\delta_{12} + I_\eta(\omega)K_\omega\delta_{12} \,, \end{aligned} \tag{4.63}$$

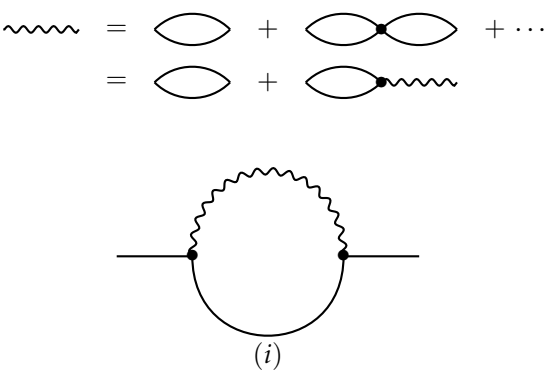

Figure 4.5: Top: Diagrammatic representation of the function $\mathbb{I}_{12}$ which sums the infinite series of bubble diagrams. Bottom: The nonlocal contribution to the self-energy at NLO in the $1/N$ expansion.

we can express Eq. (4.59) as

$$\begin{aligned} I_\gamma(\omega) &= \pi_\gamma(\omega) - \pi_\gamma(\omega) I_\gamma(\omega) + \omega^2 \pi_\eta(\omega) I_\eta(\omega) \,, \\ I_\eta(\omega) &= \pi_\eta(\omega) - \pi_\gamma(\omega) I_\eta(\omega) - \pi_\eta(\omega) I_\gamma(\omega) \,. \end{aligned} \tag{4.64}$$

Using Eq. (4.61), this is solved as

$$\begin{aligned} I_\gamma(\omega) &= 2\tilde{\lambda} M_0^2 \frac{2M_0^2(1+\tilde{\lambda})}{\omega^2 + 4M_0^2(1+\tilde{\lambda})^2} \,, \\ I_\eta(\omega) &= -2\tilde{\lambda} M_0^2 \frac{1}{\omega^2 + 4M_0^2(1+\tilde{\lambda})^2} \,, \end{aligned} \tag{4.65}$$

which can be reassembled as a tree-level propagator with mass $2M_0^2(1+\tilde{\lambda})$, so that

$$\mathbb{I}_{12}(\omega) = -2\tilde{\lambda} M_0^2 G_{12}^{2M_0^2(1+\tilde{\lambda})}(\omega) \,. \tag{4.66}$$

Using, again, Eq. (4.35), we finally get

$$\Sigma_{12}^{(i)}(\omega) = \frac{2M_0^4}{N} \frac{\tilde{\lambda}^2(3+2\tilde{\lambda})}{1+\tilde{\lambda}} G_{12}^{M_0^2(3+2\tilde{\lambda})}(\omega) \,. \tag{4.67}$$

The structure is similar to the two-loop case discussed above, and we get, for $\gamma(\omega)$ and $\eta(\omega)$,

$$\begin{aligned} \gamma(\omega) &= M^2 - \frac{2M_0^4}{N} \frac{\tilde{\lambda}^2(3+2\tilde{\lambda})}{1+\tilde{\lambda}} \frac{M_0^2(3+2\tilde{\lambda})}{\omega^2 + M_0^4(3+2\tilde{\lambda})^2} \,, \\ \eta(\omega) &= 1 + \frac{2M_0^4}{N} \frac{\tilde{\lambda}^2(3+2\tilde{\lambda})}{1+\tilde{\lambda}} \frac{1}{\omega^2 + M_0^4(3+2\tilde{\lambda})^2} \,. \end{aligned} \tag{4.68}$$

The response function is, as before, the sum of two poles, see Eq. (4.43), which at the present order of approximation are

$$\begin{aligned}\Lambda_{1,1} &= M^2\left[1-\frac{1}{N}\frac{\tilde{\lambda}^2(3+2\tilde{\lambda})}{(1+\tilde{\lambda})^2}+\mathcal{O}\left(\frac{1}{N^2}\right)\right],\\ \Lambda_{3,1} &= M^2\left[3+2\tilde{\lambda}+\mathcal{O}\left(\frac{1}{N}\right)\right],\end{aligned} \tag{4.69}$$

with the residues

$$\begin{aligned}c_1^{\varphi} &= 1-\frac{1}{N}\frac{\tilde{\lambda}^2(3+2\tilde{\lambda})}{2N(1+\tilde{\lambda})^3}+\mathcal{O}\left(\frac{1}{N^2}\right),\\ c_3^{\varphi} &= \frac{1}{N}\frac{\tilde{\lambda}^2(3+2\tilde{\lambda})}{2N(1+\tilde{\lambda})^3}+\mathcal{O}\left(\frac{1}{N^2}\right).\end{aligned} \tag{4.70}$$

Similarly to the previous computation, the coefficient c_3^{φ} being of order $1/N$, we only obtain the LO expression for $\Lambda_{3,1}$.

Let us now discuss the $\langle\chi\chi\rangle$ correlator which, at LO, is simply given by the chain of bubbles. Indeed, in the symmetric phase, one has

$$\langle\Phi_A\Phi_B\Phi_C\Phi_D\rangle_{\mathrm{nc}} = G_{AB}G_{CD}+\text{perms.}-G_{AE}G_{BF}G_{CG}G_{DH}\Gamma^{(4)}_{EFGH}\,, \tag{4.71}$$

where $\langle\rangle_{\mathrm{nc}}$ includes the disconnected contributions, perms. denotes the relevant permutations, the capital indices encompass the time variable, the Grassmann variables, and the field space index, and $G_{AB}=\langle\Phi_A\Phi_B\rangle$. We use the LO expression for the four-point vertex function, which is, in frequency space [30],

$$\Gamma^{(4)}_{1234,abcd}(\omega_1,\omega_2,\omega_3) = \frac{1}{N}\delta_{12}\delta_{34}\delta_{ab}\delta_{cd}\mathbb{D}_{13,ac}(\omega_1+\omega_3)+\text{perms.}\,, \tag{4.72}$$

where

$$\mathbb{D}_{12,ab}(\omega) = i\lambda\delta_{ab}[\delta_{12}+i\mathbb{I}_{12}(\omega)]\,. \tag{4.73}$$

Inserting this in Eq. (4.71), and retaining only the LO terms, one obtains, after some simple algebra,

$$C_{12}(\omega) = -\frac{1}{\lambda N}\left[\Pi_{12}(\omega)+i\int_3\Pi_{13}(\omega)\Pi_{32}(\omega)-\int_{34}\Pi_{13}(\omega)\Pi_{34}(\omega)\mathbb{I}_{42}(\omega)\right]. \tag{4.74}$$

Using Eq. (4.59), we finally get

$$\begin{aligned}C_{12}(\omega) &= -\frac{1}{\lambda N}\left[\Pi_{12}(\omega)+i\int_3\Pi_{13}(\omega)\mathbb{I}_{32}(\omega)\right]\\ &= -\frac{1}{\lambda N}\mathbb{I}_{12}(\omega)\,.\end{aligned} \tag{4.75}$$

From this, taking $\theta_{1,2}=\bar{\theta}_{1,2}=0$, we get the connected correlator of χ,

$$G_{\chi\chi}(\omega) = \frac{1}{2NM_0^2}G_{2M_0^2(1+\tilde{\lambda})}(\omega)+\mathcal{O}\left(\frac{1}{N^2}\right), \tag{4.76}$$

and we deduce the LO expressions

$$\Lambda_{2,0} = 2M_0^2(1+\tilde{\lambda}) \,, \tag{4.77}$$

$$c_2^\chi = \frac{2}{N}(1+\tilde{\lambda}) \,. \tag{4.78}$$

Finally, we need to solve Eq. (4.55) to get the NLO expression of the effective mass squared parameter M^2. We use

$$\gamma(0) = M^2\left[1 - \frac{2}{N}\frac{\tilde{\lambda}^2}{1+\tilde{\lambda}} + \mathcal{O}\left(\frac{1}{N^2}\right)\right] , \tag{4.79}$$

from which we obtain

$$M^2 = M_0^2\left[1 + \frac{2}{N}\frac{\tilde{\lambda}(1+\tilde{\lambda}+\tilde{\lambda}^2)}{(1+\tilde{\lambda})^2} + \mathcal{O}\left(\frac{1}{N^2}\right)\right] . \tag{4.80}$$

Collecting the previous formulas, we have for the dynamical mass,

$$m_{\rm dyn}^2 = M_0^2\left[1 + \frac{2}{N}\frac{\tilde{\lambda}}{(1+\tilde{\lambda})^2} + \mathcal{O}\left(\frac{1}{N^2}\right)\right] , \tag{4.81}$$

and for the lowest eigenvalues

$$\begin{aligned}
\Lambda_{1,1} &= M_0^2\left[1 + \frac{1}{N}\frac{\tilde{\lambda}(2-\tilde{\lambda})}{(1+\tilde{\lambda})^2} + \mathcal{O}\left(\frac{1}{N^2}\right)\right] , \\
\Lambda_{2,0} &= M_0^2\left[2 + 2\tilde{\lambda} + \mathcal{O}\left(\frac{1}{N}\right)\right] , \\
\Lambda_{3,1} &= M_0^2\left[3 + 2\tilde{\lambda} + \mathcal{O}\left(\frac{1}{N}\right)\right] .
\end{aligned} \tag{4.82}$$

As for the perturbative results, the above expressions exactly agree with those of the direct QFT calculations in Ref. [35]. In fact, remarkably, the agreement concerns all the intermediate quantities Π, $\mathbb{I}$ and Σ, using the rescalings (4.48) of the parameters and

$$\hat{G} = \frac{d\Omega_{D+1}}{2H^d}G, \quad \hat{\mathbb{I}} = \frac{\Omega_{D+1}}{H^D}\mathbb{I}, \quad \text{and} \quad \hat{\Sigma} = \frac{\Omega_{D+1}}{2dH^{D+1}}\Sigma \,, \tag{4.83}$$

for the different two-point functions. The very same results have also been recently obtained from a QFT calculation in Euclidean de Sitter in Ref. [128]. Such an agreement between the stochastic approach and direct QFT calculations on either Lorentzian or Euclidean de Sitter was already well-known for equal-time correlators, *e.g.* $\langle\varphi^n\rangle$, which measure the local field fluctuations [11, 24, 27]. Although expected on the basis of general arguments [11, 19, 20], the agreement mentioned here for unequal time (nonlocal) correlators is far less trivial. In particular, for nonperturbative approximation schemes, the present results, together with those of Refs. [35] and [128] provide an explicit nontrivial check.

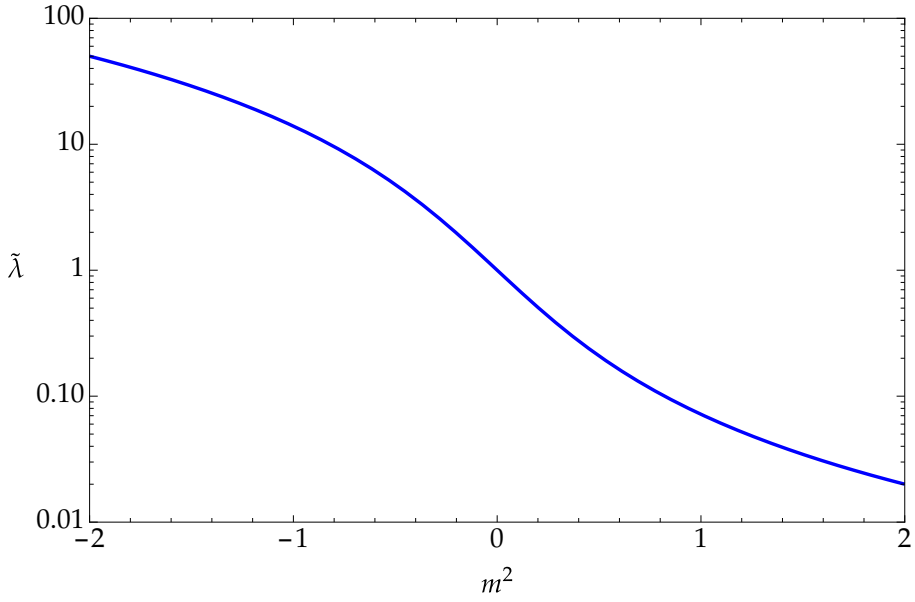

Figure 4.6: Effective coupling $\tilde{\lambda}$ as a function of the bare squared mass m^2. The bare coupling is taken as $\lambda = 1$. The coupling becomes strongly nonperturbative for small and negative values of m^2.

4.2.3 Discussion

We now discuss the previous results in different regimes. First we check that the expressions of the eigenvalues $\Lambda_{n,\ell}$ and the coefficients $c_n^{\varphi/\chi}$ coincide in the limit where both expansion schemes are valid, *i.e.* when $\bar{\lambda}$, defined in Eq. (4.40), is small and N is large. Denoting

$$\bar{\lambda}_\infty = \lim_{N\to\infty} \bar{\lambda} = \frac{\lambda}{4m^4} \,, \tag{4.84}$$

we have $M_0^2 = m^2[1 + \bar{\lambda}_\infty - \bar{\lambda}_\infty^2 + \mathcal{O}(\bar{\lambda}_\infty^3)]$, and $\tilde{\lambda} = \bar{\lambda}_\infty + \mathcal{O}(\bar{\lambda}_\infty^2)$, meaning that the two couplings coincide at LO. We can check for example that $\Lambda_{1,1}$ at NLO, given in Eq. (4.82), has the following expansion,

$$\frac{\Lambda_{1,1}}{m^2} = 1 + \bar{\lambda}_\infty - \bar{\lambda}_\infty^2 + \frac{2\bar{\lambda}_\infty - 7\bar{\lambda}_\infty^2 + 27\bar{\lambda}_\infty^3}{N} + \mathcal{O}\left(\bar{\lambda}_\infty^4, \frac{1}{N^2}\right) . \tag{4.85}$$

which coincides with the three-loop order expression (B.19), given in Appendix B, expanded up to order $1/N$.

The results obtained from the $1/N$ expansion allow us to probe the nonperturbative regime in $\bar{\lambda}$, corresponding to small or negative values of m^2. The effective coupling, which is the actual expansion parameter, and its dependence on m^2 for a fixed value of λ is represented in Fig. 4.6. It becomes of order one for $m^2 = 0$ and becomes larger for

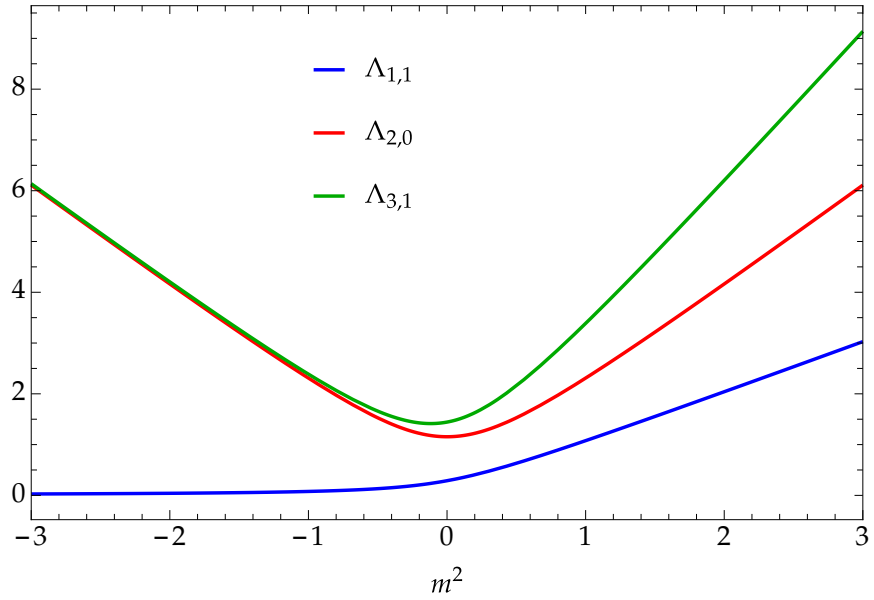

Figure 4.7: The eigenvalues $\Lambda_{1,1}$, $\Lambda_{2,0}$ and $\Lambda_{3,1}$ at LO in the $1/N$ expansion, as a function of the tree-level squared mass m^2 for $\lambda = 1$.

$m^2 < 0$. The LO eigenvalues can be rewritten as

$$\begin{aligned}\Lambda_{1,1} &= \frac{m^2}{2} + \sqrt{\frac{m^4}{4} + \frac{\lambda}{4}}\,,\\ \Lambda_{2,0} &= 4\sqrt{\frac{m^4}{4} + \frac{\lambda}{4}}\,,\\ \Lambda_{3,1} &= \frac{m^2}{2} + 5\sqrt{\frac{m^4}{4} + \frac{\lambda}{4}}\,.\end{aligned} \tag{4.86}$$

They are depicted Fig. 4.7. For small masses, we have

$$\Lambda_{1,1} = \sqrt{\lambda/4}\,, \quad \Lambda_{2,0} = 4\Lambda_{1,1}\,, \quad \Lambda_{3,1} = 5\Lambda_{1,1}\,, \tag{4.87}$$

meaning that all eigenvalues are of the same order of magnitude, and the associated correlators will have relatively large autocorrelation times, particularly in the small coupling limit [1].

For bare potential with spontaneous symmetry breaking, $m^2 < 0$, in the limit of a steep well $\lambda/|m^4| \ll 1$, we find

$$\Lambda_{1,1} = \frac{\lambda}{4|m^2|}, \quad \Lambda_{2,0} = \Lambda_{3,1} = 2|m^2| \gg \Lambda_{1,1}\,. \tag{4.88}$$

[1] Note that the domain of validity of the whole stochastic approach implies that the various mass scales have to be small in units of H. In the massless regime (4.87), this implies that $\lambda/H^4 \ll 1$.

The correlator of the field φ, in the vector sector $\ell = 1$, has a small eigenvalue $\Lambda_{1,1}$ and a large one $\Lambda_{3,1}$ corresponding respectively to the transverse (would-be Goldstone) mode, and the longitudinal mode in the tree-level potential. The fact that the first eigenvalue is nonvanishing is a consequence of the dynamical restoration of the symmetry, or equivalently the effective dimensional reduction of the system. The scalar sector, $\ell = 0$, which encompasses the case of the composite field χ is controlled by the heavy (longitudinal) mode $\Lambda_{2,0}$.

In terms of correlation functions, this means in particular that correlators for scalar operators have a much smaller autocorrelation time than the one in the vector channel, which sees the transverse flat direction. These autocorrelation times can be related to other physical quantities such as a relaxation (or equilibration) time from an excited state to the Bunch-Davies vacuum [74, 129], decoherence timescales [125, 130–132], or to the spectral index of observables [18, 72].

As an illustration of the latter, exploiting the de Sitter invariance, the equal time correlator for large physical distances can be related to the temporal correlator as [18, 72]

$$\langle \mathcal{A}(t,\vec{x}_1)\mathcal{A}(t,\vec{x}_2)\rangle = G_{\mathcal{A}\mathcal{A}}\left(\frac{2}{H}\log(a(t)H|\vec{x}_1-\vec{x}_2|)\right) . \tag{4.89}$$

This is easily translated in terms of the power spectrum $\mathcal{P}_{\mathcal{A}}$, defined as in Eq. (1.62). The spectral tilt is defined as

$$\frac{\log \mathcal{P}_{\mathcal{A}}(k)}{\log k} = n_{\mathcal{A}} - 1 . \tag{4.90}$$

As the long-time behavior is dominated by the lowest eigenvalues appearing in the decomposition (4.11), which we denote by $\Lambda_{\mathcal{A}}$, we end up with

$$n_{\mathcal{A}} - 1 = \frac{2}{H}\Lambda_{\mathcal{A}} . \tag{4.91}$$

In particular, the spectral index for φ is given by $n_\varphi - 1 = 2\Lambda_{1,1}/H$. In the scalar sector, the spectral index for the χ field, or for the density contrast

$$\delta = \frac{V(\varphi) - \langle V(\varphi)\rangle}{\langle V(\varphi)\rangle} , \tag{4.92}$$

is given by $n_\delta - 1 = 2\Lambda_{2,0}/H$.

Finally the comparison between the LO and NLO result for $\Lambda_{1,1}$ is represented in Fig. 4.8, for the extreme case $N = 2$ to emphasize the difference. We see that the correction to the LO value remains small down to low positive values of m^2, which corresponds to nonperturbative regime in the coupling. The NLO correction becomes more important for $m^2 < 0$.

We have to consider $N > 1$ in this case, as the $1/N$ expansion of $\Lambda_{1,1}$ becomes singular in the deeply broken limit for $N = 1$. Indeed, the expression (4.82) gives,

$$\Lambda_{1,1} = \frac{\lambda}{4|m^2|}\left(1 - \frac{1}{N} + \mathcal{O}\left(\frac{1}{N^2}\right)\right) . \tag{4.93}$$

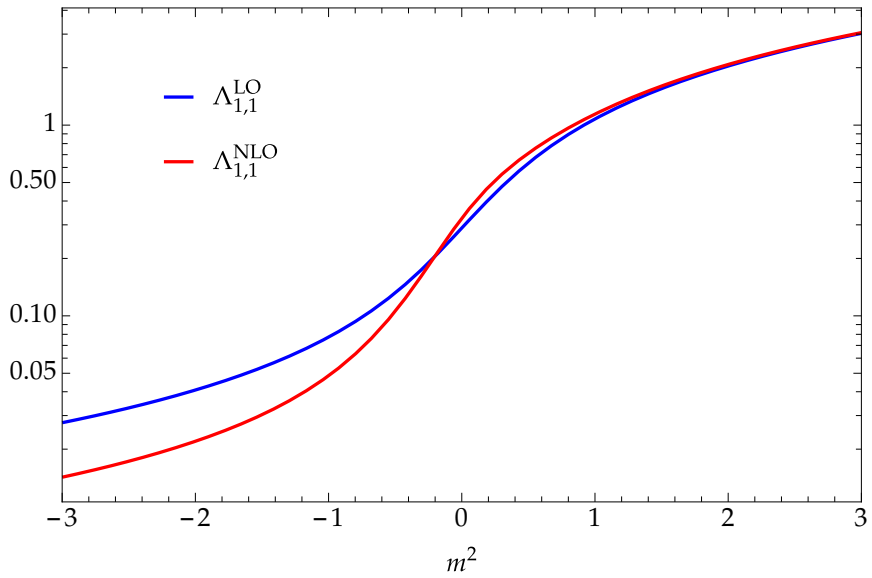

Figure 4.8: The lowest nonzero eigenvalue $\Lambda_{1,1}$ at LO and NLO in the $1/N$ expansion, as a function of m^2 with $\lambda = 1$ and $N = 2$.

In the limit $N \to 1$, $\Lambda_{1,1} \to 0$ and the autocorrelation time diverges. This corresponds to a singular limit for this particular eigenvalue.

4.3 $1/N$ expansion of the Fokker-Planck equation

The LO result for the three eigenvalues (4.82) only involves simple combinations of two quantities, $\tilde{\lambda}$ and M_0^2. This hints at a possible analytical solution for the entire spectrum in the limit $N \to \infty$. However, extracting the spectrum from the calculations of correlators as we did in the previous section is particularly inefficient since, as we have noticed, the contributions from higher-order eigenvalues are suppressed.

This problem can be avoided by the direct resolution of the eigenvalue problem at the level of the Fokker-Planck equation. There, simple quantum mechanical methods can be used to obtain, *e.g.*, the Gaussian spectrum, entirely [18, 72]. In the presence of interactions, the problem can be formulated as an anharmonic oscillator in N dimensions, to which we apply the $1/N$ expansion. Similar situations have been considered in quantum mechanics [133–135], but set up the expansion in slightly different ways, that we shall comment on later. In the stochastic formalism framework, the single field case has been recently thoroughly studied in [72, 73], for a potential with quadratic and quartic terms, possibly with a spontaneous symmetry breaking. First multifield results for a massless theory with quartic interactions at finite N has been obtained numerically in [74].

This motivates the implementation of the $1/N$ expansion directly to the eigenvalue equation (4.9), in order to obtain the entire spectrum analytically. Preparing for a proper

large-N expansion, we need to identify which quantities are to be considered of $\mathcal{O}(1)$, which amounts to chose a point in theory space around which to expand. In this spirit, we use the standard scaling [136], in which we consider φ^2 to be of order N. This makes the potential scale like N, and justifies the definition of the following rescaled potential

$$V(\varphi) = Nv(x) \,, \tag{4.94}$$

and similarly for the corresponding W

$$W(\varphi) \equiv Nw(x) = \frac{1}{2N}\left[N(v')^2 - v'' - (N-1)\frac{v'}{x}\right] \,, \tag{4.95}$$

using the rescaled variable $x = \sqrt{\varphi^2/N}$. As x is of $\mathcal{O}(1)$, we see that taking naively the limit $N \to \infty$ in Eq. (4.9) gives simply $\mathcal{R}(x) = 0$, as the potential term has an additional factor of N and dominates the other terms. This is because the ansatz (4.8) that we plugged into the Fokker-Planck equation still contains some dependence in N that we now discuss. In order to understand how the different quantities scale with N, we begin by investigating the Gaussian case for N finite, which is exactly solvable.

4.3.1 Gaussian case

For a quadratic potential

$$v(x) = \frac{m^2}{2}x^2 \quad \text{and} \quad w(x) = -\frac{m^2}{2} + \frac{m^4}{2}x^2 \,, \tag{4.96}$$

so that, up to a constant shift $-m^2/2$ on the energy levels, Eq. (4.9) is nothing but the radial Schrödinger equation for a symmetric N-dimensional harmonic oscillator with unit mass and pulsation $\omega = m^2$. The spectrum is degenerate in the quantum numbers ℓ_i, and labeled by a nonnegative integer n,

$$\Lambda_{n,\ell} = nm^2 \,. \tag{4.97}$$

The eigenfunctions are obtained in Cartesian coordinates as product of Hermite polynomials. In radial coordinates, they can be written as

$$\mathcal{R}_{n,\ell} = e^{-Nm^2\frac{x^2}{2}} r_{n,\ell} \,, \tag{4.98}$$

where $n - \ell = 2k$ is bound to be a nonnegative even integer and $r_{n,\ell}$ is the finite polynomial

$$r_{n,\ell} = x^\ell \sum_{q=0}^{\frac{n-\ell}{2}} a_q x^{2q} \,. \tag{4.99}$$

The coefficients a_q are determined through the recursion relation

$$(N + 2\ell + 2q)(q+1)a_{q+1} = -2Nm^2(k-q)a_q \,. \tag{4.100}$$

The solution to Eq. (4.100) has a well-defined limit for $N \to \infty$ for n and ℓ fixed. In that case, the recursion relation becomes

$$(q+1)a_{q+1} = -2Nm^2(k-q)a_q \tag{4.101}$$

which is solved as

$$a_q = a_0 C_q^k (-2m^2)^q \,, \tag{4.102}$$

with C_q^k the binomial coefficient. In particular we obtain for the LO radial eigenfunction

$$r_{n,\ell} = a_0 x^\ell (1-2m^2x^2)^{\frac{n-\ell}{2}} \,, \tag{4.103}$$

where the constant a_0 is fixed by requiring the eigenfunction to be normalized.

The first important remark is that the eigenvalues (4.97) do not scale with N. Also, the appropriate radial variable to work with in order to obtain a nontrivial large-N limit is the rescaled variable x. Finally, the exponential term in Eq. (4.98), which is consistent with the naive limit $\mathcal{R} \to 0$ for $N \to \infty$, is necessary to obtain the spectrum, and has to be factored out explicitly to obtain nontrivial solutions.

4.3.2 Interacting case

These prescriptions can be implemented in the interacting case, introducing the reduced radial function $\mathcal{R}_{n,\ell}(x) = e^{-Nv(x)} r_{n,\ell}(x)$, and plugging it in the radial equation (4.9) we obtain

$$-\frac{r''_{n,\ell}}{2N} - \left(\frac{N-1}{2Nx} - v'\right) r'_{n,\ell} + \frac{\ell(\ell+N-2)}{2Nx^2} r_{n,\ell} = \Lambda_{n,\ell} r_{n,\ell} \,, \tag{4.104}$$

which possesses a well defined large N limit. Taking $N \to \infty$, we get

$$-\frac{1-2xv'}{2x} r'_{n,\ell} + \frac{\ell}{2x^2} r_{n,\ell} = \Lambda_{n,\ell} r_{n,\ell} \tag{4.105}$$

which gives the following LO equation

$$(\log r_{n,\ell})' = \frac{\ell - 2x^2\Lambda_{n,\ell}}{x(1-2xv')} \,. \tag{4.106}$$

This can be easily integrated for polynomial potentials in terms of the roots of $(1-2xv')$. We focus on the case of a quartic potential again chosen as

$$v(x) = \frac{m^2}{2}x^2 + \frac{\lambda}{8}x^4 \,, \tag{4.107}$$

which provides simple analytic formulas. Using the identity[2]

$$1 - 2xv'(x) = (1-2m_+^2x^2)(1-2m_-^2x^2) \,, \tag{4.108}$$

[2]The mass scales $m_\pm$ should not be mixed up with those discussed in the resummations (4.46), which were the ones introduced in [34, 35].

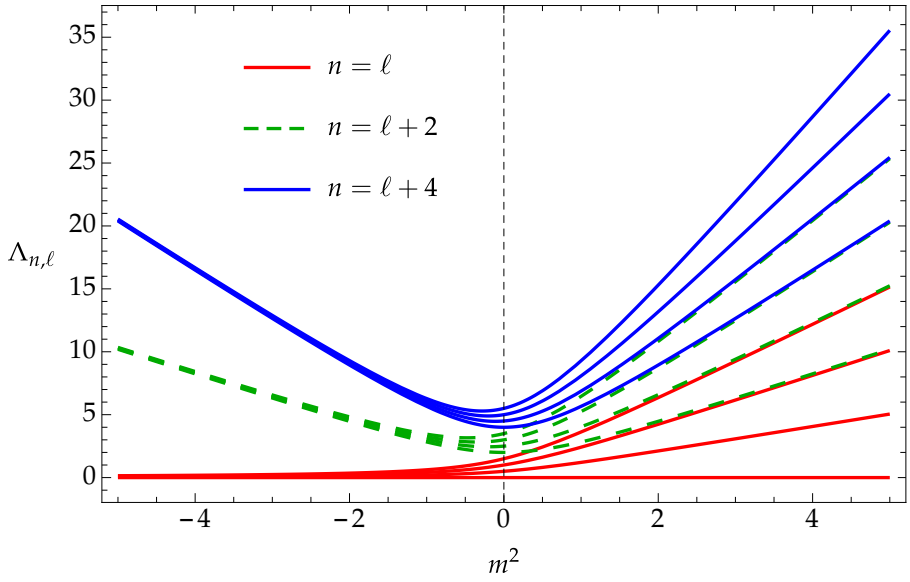

Figure 4.9: LO eigenvalues $\Lambda_{n,\ell}$ as a function of the bare squared mass m^2 for $\lambda = 1$. We show three groups, corresponding to $n = \ell$, $n = \ell + 2$ and $n = \ell + 4$ from bottom to top on the $m^2 = 0$ axis.

where

$$m_\pm^2 = \pm\frac{m^2}{2} + \sqrt{\frac{m^4}{4} + \frac{\lambda}{4}}\,, \tag{4.109}$$

the right hand side of Eq. (4.106) can be decomposed in simple fractions as

$$(\log r'_{n,\ell}) = \frac{\ell}{x} - \frac{4\alpha_+ m_+^2 x}{1 - 2m_+^2 x^2} + \frac{4\alpha_- m_-^2 x}{1 - 2m_-^2 x^2}\,, \tag{4.110}$$

with

$$\alpha_\pm = \frac{\pm\Lambda_{n,\ell} - \ell m_\pm^2}{2(m_+^2 + m_-^2)}\,. \tag{4.111}$$

Integrating Eq. (4.110) is now elementary and yields the leading-order radial function, up to a normalization constant denoted a_0

$$r_{n,\ell}(x) = a_0 x^\ell (1 - 2m_+^2 x^2)^{\alpha_+} (1 - 2m_-^2 x^2)^{\alpha_-}\,. \tag{4.112}$$

The obtained eigenfunctions lead to a normalizable PDF thanks to the exponential factors that were extracted, $P \propto e^{-V} R \propto e^{-2V} r$. Requiring the solutions to be regular for all x selects a discrete subset, as expected from the analogous quantum mechanical problem. Using the fact that $m_\pm^2 \geq 0$, we see that regularity imposes $\alpha_+ = k \in \mathbb{N}$. In turns, this implies that the eigenvalues are indexed by nonnegative integers n and ℓ such that $n - \ell = 2k$, meaning that $n - \ell$ is even and positive. They are given by

$$\Lambda_{n,\ell} = n m_+^2 + (n - \ell) m_-^2\,, \tag{4.113}$$

and the corresponding eigenfunctions are

$$r_{n,\ell}(x) = a_0 x^\ell (1 - 2m_+^2 x^2)^{\frac{n-\ell}{2}} (1 - 2m_-^2 x^2)^{-\frac{n}{2}} . \tag{4.114}$$

Notice that, as expected, the lowest eigenstate of the series has a vanishing eigenvalue, $\Lambda_{0,0} = 0$, which is guaranteed by the symmetries of the system, and corresponds to the equilibrium state with a PDF $P \propto e^{-2V}$.

Eqs. (4.113) and (4.114) completely solve the eigenvalue problem at LO. The present formulation allows one to set up a systematic large-N expansion, and compute higher-orders in $1/N$, some of which are detailed in Appendix C. We report here the NLO result for the eigenvalue as an illustration

$$\Lambda_{n,\ell} = nm_+^2 + (n-\ell)m_-^2 + \frac{\lambda}{4N(m^4+\lambda)}(a_{n,\ell}m_+^2 - b_{n,\ell}m_-^2) + \mathcal{O}\left(\frac{1}{N^2}\right) , \tag{4.115}$$

where

$$a_{n,\ell} = n(3n-2) - \ell(\ell-2) \quad \text{and} \quad b_{n,\ell} = a_{\ell-n,\ell} . \tag{4.116}$$

4.3.3 Discussion

Before commenting on several limits of interest, let us remark that, as expected, the results obtained from this approach coincide with the ones obtained from the direct computations of correlators achieved in Sec. 4.2, or in the D-dimensional QFT [35, 128], where the first eigenvalues $\Lambda_{1,1}$, $\Lambda_{2,0}$ and $\Lambda_{3,1}$ were computed respectively at NLO for the first and LO for the lasts, see Eqs. (4.82). The different variables are related through

$$m_+^2 = M_0^2 \quad \text{and} \quad m_-^2 = -\tilde{\lambda} M_0^2 . \tag{4.117}$$

It is also worth mentioning that in the Gaussian limit, $\lambda = 0$ so that $m_+ = m$ and $m_- = 0$, Eqs. (4.113) and (4.114) gives back the Gaussian result (4.97) and (4.103).

The variation of the spectrum as a function of the mass squared is shown in Fig. 4.9. The perturbative limit is again controlled by λ/m^4 and we have the following expansion

$$\Lambda_{n,\ell} = nm^2 + (2n-\ell)\frac{\lambda}{4m^2} + \mathcal{O}\left(\frac{\lambda}{m^6}\right) , \tag{4.118}$$

which shows the lifting of the Gaussian degeneracy for nonzero λ. The limit $m^2 \to 0$ is again not attainable within the perturbative framework, and one has to use the nonperturabative expression (4.113). This gives

$$\Lambda_{n,\ell} \approx (2n-\ell)\sqrt{\frac{\lambda}{4}} , \tag{4.119}$$

where we see another manifestation of the dynamical mass $m_{\text{dyn}}^2 = \sqrt{\lambda/4}$ gravitationally generated by the interactions. The spectrum (4.119) ressembles to a Gaussian potential with a mass m_{dyn}^2, although the degeneracies are different for each energy level.

The last interesting regime is the broken symmetry regime, $m^2 < 0$, corresponding to a mexican hat potential, which is strongly nonperturbative, due to the massless Goldstone modes. In the deeply broken regime, $\lambda/m^4 \ll 1$, we have $m_+^2 \approx 0$ and the spectrum takes the simple form

$$\Lambda_{n,\ell} = (n-\ell)\left|m^2\right| + \mathcal{O}\left(\lambda/m^2\right) . \tag{4.120}$$

Because $n-\ell$ is an even integer, this is similar, up to the degeneracies, to a Gaussian spectrum, but with a fundamental frequency $2\left|m^2\right|$. The latter corresponds to the curvature of the potential at the nontrivial minimum. Each energy level is now infinitely degenerated, as a consequence of the flat directions in the potential. Finally, for a given ℓ, the eigenvalue $\Lambda_{\ell,\ell}$ is always suppressed,

$$\Lambda_{\ell,\ell} \approx \ell \frac{\lambda}{4|m^2|} \ll \left|m^2\right| , \tag{4.121}$$

leading to a large autocorrelation time (or length) for the higher-order representations, $\ell \geq 1$, in field space. As was previously mentioned, in Sec. 4.2, this is not the case for the scalar channel, $\ell = 0$, which is not sensible to the Goldstone directions and is thus only controlled by the heavy radial mode. The autocorrelation time for scalar operators is thus fixed by the higher energy levels $\Lambda_{2n,0}$, leading to a much smaller value than the other channels.

We end this discussion by commenting on different $1/N$ expansion that have been considered in the literature [133–135]. One important difference with these approaches stems from the fact that the fundamental potential they consider is what we called W, see Eq. (4.9), whereas we started from a potential V, related to W through Eq. (4.4). For a quartic potential V such as (4.107), we obtain the following W, expressed here as Nw, see Eq. (4.95),

$$w(x) = -\frac{m^2}{2} + \left(\frac{m^4}{2} - \frac{N+2}{2N}\frac{\lambda}{2}\right)x^2 + \frac{m^2\lambda}{2}x^4 + \frac{\lambda^2}{8}x^6 , \tag{4.122}$$

which contains terms up to x^6. Although generic sextic potentials have been considered, *e.g.*, in [134], it is not possible in general to deduce a unique corresponding V, and to introduce the reduced radial function (4.104) which we consider here.

4.3.4 Comparison to finite N results

Moving on to the applicability of the present results to finite value of N, we begin by discussing the massless case. Here, we expect possible significant difference with the numerical results at low N, due to the nonperturbative physics, contrary to the Gaussian case where the spectrum is identical for all N. We show some eigenfunctions for the lowest eigenstates in Fig. 4.10, at $m = 0$, with the NLO corrections, and the numerical result, for $N = 2$ and $N = 5$. The agreement is good down to low values of N.

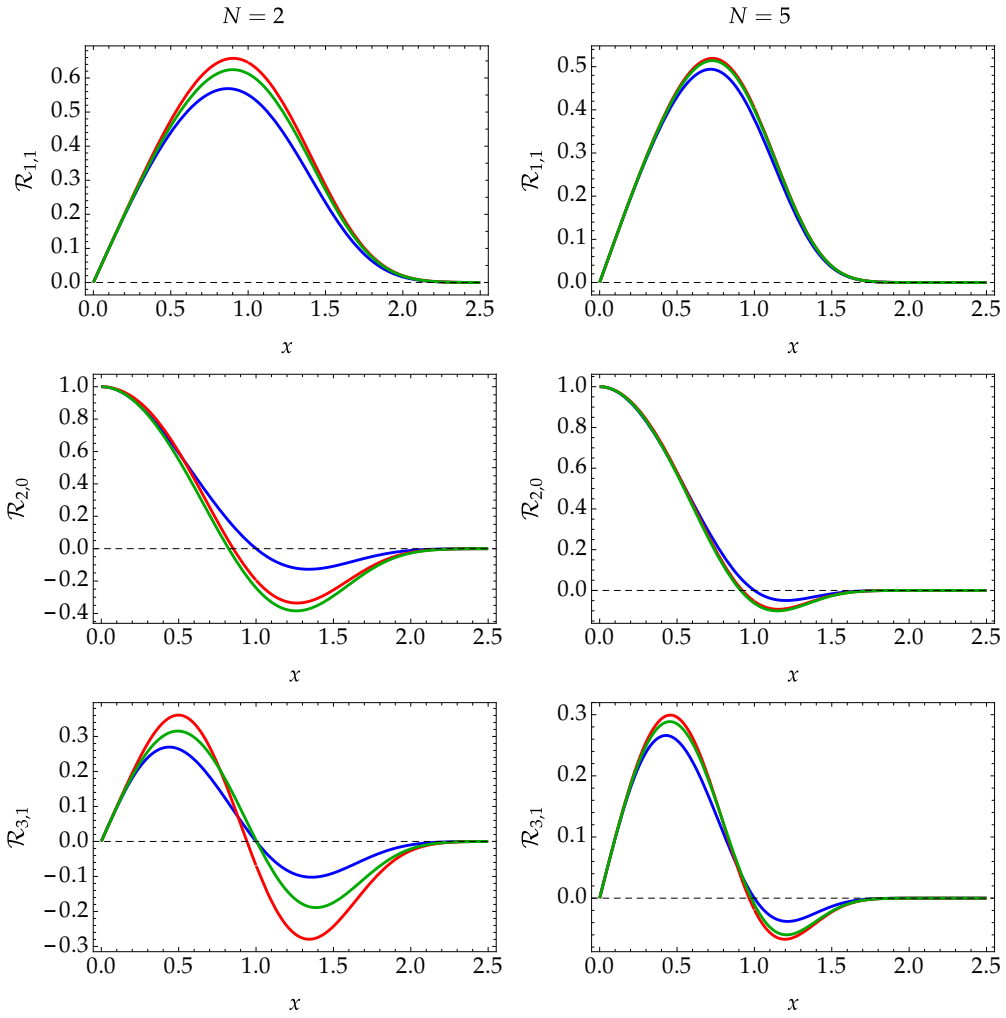

Figure 4.10: The leading order (blue) and next-to-leading order (red) eigenfunctions $\mathcal{R}_{n,\ell}(x)$, together with the exact numerical result (green) for some of the lowest levels for $m^2 = 0$ and $\lambda = 1$, and for various N. Here the normalization is chosen so that either the function or its first nonzero derivative at $x = 0$ is fixed to 1. In practice this means $a_0 = 1/\ell!$.

The numerical results were obtained by solving numerically Eq. (4.104), fixing initial conditions at $x = 0^+$, and determining the eigenvalue that makes the function regular by trials and errors. In practice, we use the fact that when the value of Λ crosses an actual eigenvalue, the divergence of the eigenfunction changes from $+\infty$ to $-\infty$ or vice-versa. This allows to implement a dichotomy procedure on an initial interval, which is progressively narrowed down to the required precision.

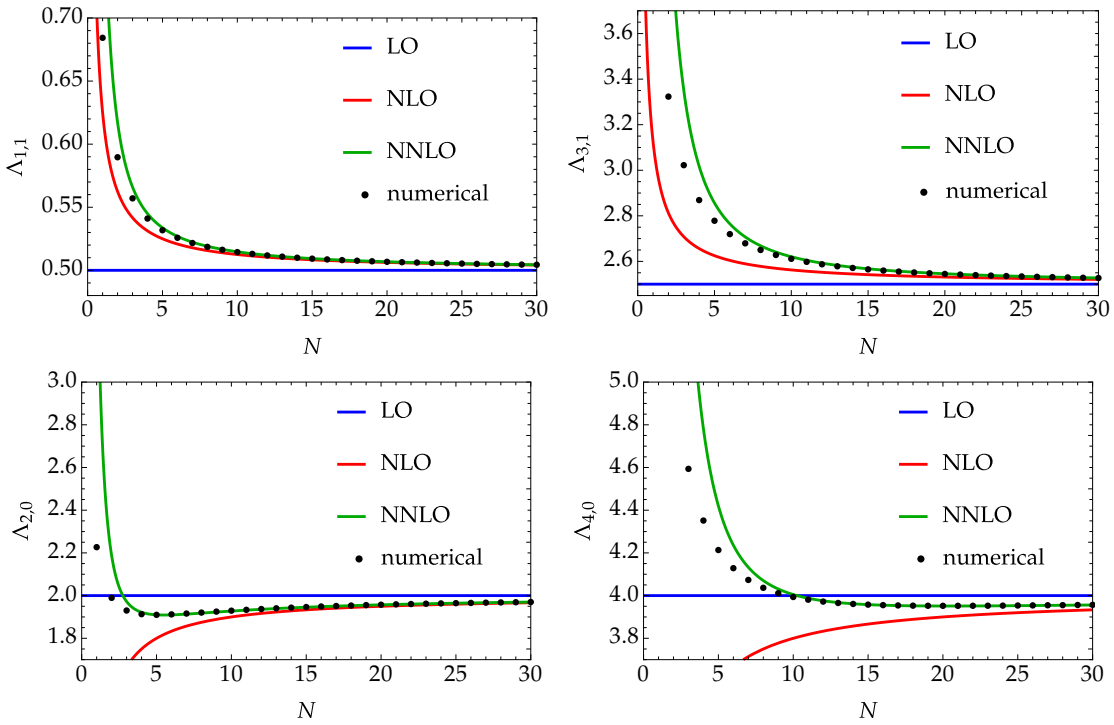

Figure 4.11: First eigenvalues in the scalar and vector channels, for $m^2 = 0$ and $\lambda = 1$, as a function of N. The dots are the exact value coming from a numerical resolution, and we represented the NLO and NNLO corrections.

The explicit formulas for $m^2 = 0$, meaning $m_+^2 = m_-^2 = \sqrt{\lambda/4}$,

$$\frac{\Lambda_{n,\ell}}{\sqrt{\lambda}} = \frac{2n-\ell}{2}\left[1 + \frac{3\ell - 2}{4N} + \mathcal{O}\left(\frac{1}{N^2}\right)\right]. \tag{4.123}$$

Comparison to numerical results is shown in Fig. 4.11. For $\Lambda_{1,1}$, the $1/N$ expansion gives a good qualitative agreement at LO down to relatively low values of N. The agreement becomes quantitative at NLO (or NNLO), and we get a relative error of 8% at NLO for $N = 1$. Looking at Eq. (4.123), the correction in the vector channel $\ell = 1$ is indeed expected to be relatively small at the order $1/N$.

We can also test the scalar channel $\Lambda_{2,0}$, see Fig. 4.11. Again, the LO behaviour gives a correct qualitative estimate, which is improved by the NLO correction, but reaches a relative error of 8% for $N = 4$ and 25% at $N = 1$. In that case, adding the NNLO correction, which is computed in Appendix C, greatly improves the prediction, and the relative error goes down to 10% for $N = 1$.

We now compare, when possible, our results with the ones existing in the literature. While the $N = 1$ case has been studied in great details [18, 72, 73], only of few results exist for $N \geq 2$ [74]. The authors of [74] have presented results for the $N = 2, 3$ cases,

	Num. [74]	Num. (here)	LO	NLO	NNLO
$\hat{\Lambda}_{1,0}^{N=1}$	0.0889	0.0889	0.0650	0.0812	0.110
$\hat{\Lambda}_{1,0}^{N=2}$	0.3656	0.366	0.368	0.276	0.402
$\hat{\Lambda}_{1,0}^{N=3}$	0.4344	0.434	0.450	0.375	0.444
$\hat{\Lambda}_{2,0}^{N=1}$	0.289	0.289	0.260	0.130	0.487
$\hat{\Lambda}_{2,0}^{N=2}$	0.933	0.919	0.735	0.551	1.49
$\hat{\Lambda}_{2,0}^{N=3}$	1.034	1.033	0.900	0.750	1.26

Table 4.1: Comparison between the eigenvalues obtained numerically in Ref. [74] in the first column with our numerical values, and the result from the $1/N$ expansion at the different order of approximation. As expected, the numerical results obtained in the two approaches are very close, and are considered as exact.

for a purely quartic potential, *i.e.* $m = 0$. The coupling $\hat{\lambda}$ in that reference is related to the one here, Eq. (4.107), through

$$\hat{\lambda} = \lambda \frac{d^2 \Omega_{D+1}}{4N} , \tag{4.124}$$

and the authors labeled the quantum states using the integer $k = (n - \ell)/2$. Their eigenvalues are related to ours as

$$\hat{\Lambda}_{k,\ell} = \frac{\Lambda_{2k+\ell,\ell}}{\sqrt{\lambda}} \sqrt{\frac{N}{6\pi^2}} , \tag{4.125}$$

where we specialized to $d = 3$ and we used $\Omega_5 = 8\pi^2/3$. This is valid provided $N \geq 2$. In the $N = 1$ case, there are no angular variables and only eigenvalues with $\ell = 0, 1$ are allowed. One has

$$\begin{aligned} \hat{\Lambda}_{2k} &= \frac{\Lambda_{2k,0}}{\sqrt{\lambda}} \sqrt{\frac{1}{6\pi^2}} , \\ \hat{\Lambda}_{2k+1} &= \frac{\Lambda_{2k+1,1}}{\sqrt{\lambda}} \sqrt{\frac{1}{6\pi^2}} . \end{aligned} \tag{4.126}$$

Numerical comparisons are summarized in 4.1.

The case of a double-well potential ($N = 1$ and $m^2 < 0$) is a bit different. Indeed, the symmetry is discrete, and the relevant physics is driven by the tunneling effects between the minimas rather than the Goldstone modes. The other important point is that the potential appearing in the eigenvalue problem, when formulated in its canonical form (4.9), is not V but rather W. In the standard approach, the radial equation (4.9) is reformulated by eliminating the first derivative term, by means of the redefinition $\mathcal{R}(x) = x^{\frac{1-N}{2}} \psi(x)$, leading to

$$-\frac{1}{2N} \psi'' + W_{\text{eff}} \psi = \Lambda \psi , \tag{4.127}$$

where

$$W_{\text{eff}}(x) = \frac{\ell(\ell+N-2)}{2Nx^2} + \frac{(N-1)(N-3)}{8Nx^2} + W(x)\,. \tag{4.128}$$

Eq. (4.127) is the canonical form of the one-dimensional Schrödinger equation with a potential W_{eff}, up to a factor N in front of the second derivative which arises from the definition of x. As pointed out in [73], in the case $N = 1$, for a double-well potential V with sufficiently deep wells, W exhibits a third minimum at the origin (as a function of φ), in addition to the usual minima at nonzero x. The resulting spectrum is thus, up to exponentially small splittings due to tunneling effects, a superposition of Gaussian spectra from each well at $x = 0$ and $x \neq 0$, with frequencies $\left|m^2\right|$ and $2\left|m^2\right|$ respectively, with a global energy shift of $3\left|m^2\right|/2$ for the central well relatively to the other wells.

For arbitrary $N > 1$, the central well remains, and the potential receives additional centrifugal and geometrical contributions behaving as $\propto 1/x^2$. These contributions shift the central well away from $x = 0$. As N increases, the potential reaches the asymptotic form

$$\frac{W_{\text{eff}}(x)}{N} \approx \frac{1}{8x^2} + \frac{1}{2}\left[(v')^2 - \frac{v'}{x}\right] + \mathcal{O}\left(\frac{1}{N}\right). \tag{4.129}$$

For the quartic potential (4.107), the minima are located at

$$x_-^2 = \frac{1}{2|m^2|} \quad \text{and} \quad x_+^2 = \frac{2\left|m^2\right|}{\lambda}\,. \tag{4.130}$$

The corresponding values of the potential are

$$W_{\text{eff}}(x_-) = \frac{3N\left|m^2\right|}{4} \quad \text{and} \quad W_{\text{eff}}(x_+) = 0\,, \tag{4.131}$$

and it appears that the excitations of the central well are lifted with a factor N compared to the ones of the external well. In the end, the central energy states from the central well decouple in the large-N limit. The potential W_{eff} is shown in Fig. 4.12 together with some of the large-N radial eigenstates $\mathcal{R}_{n,\ell}$.

4.4 Conclusion

Summing up the results of this chapter, two different formulations of the stochastic formalism are used to compute (unequal-time) two-point correlators for an $O(N)$ scalar theory on superhorizon scales. In both cases, nonperturbative analytic results are obtained by means of a $1/N$ expansion. The first approach used the JdD path integral formulation of the Langevin equation. We compute directly some correlators with diagrammatic techniques, using an explicit resummation of the series of bubble diagrams. We can check that these results coincide with other computations done either in the Lorentzian QFT [30, 34, 35] or the Euclidean case [128].

The second approach consists in solving the equivalent eigenvalue problem, coming from the Fokker-Planck equation associated to the stochastic equation. The entire spectrum is computed analytically up to NLO (and NNLO for the eigenvalues) in the $1/N$

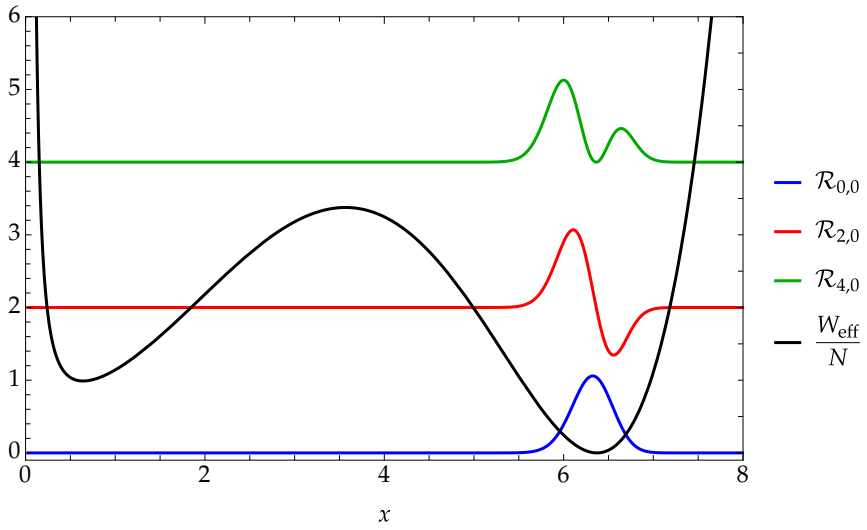

Figure 4.12: Rescaled effective potential $W_{\text{eff}}(x)/N$, with $m^2 = -1$, $\lambda = 0.05$, and $N = 10$, together with the LO eigenfunctions $\mathcal{R}_{n,\ell}$ for the first few values of n at $\ell = 0$. Although another local minimum appears at low x, it is lifted by a factor N and thus gives subleading eigenvalues. The normalization is arbitrary and the eigenfunctions have been upshifted by their respective eigenvalues.

expansion. This problem corresponds to an anharmonic oscillator in N dimensions, and although different large-N limits have been considered before [133–135] they differ from the one proposed here.

The eigenvalues are related to several physical quantities, such as relaxation and decoherence times or spectral indices [72–74, 125, 129–132]. Our results allows us to probe deeply nonperturbative regimes, when the scalars are light, or for potentials with a negative square mass. In this latter case, in the deep potential regime, we find that the autocorrelation time in the scalar channel $\ell = 0$ is strongly suppressed compared to the higher-order channels $\ell \geq 1$. Finally, we find that for the lowest eigenvalues, the $1/N$ expansion offers a qualitative (at LO) and even quantitative (at NLO or NNLO) approximation down to relatively low values of N.

Conclusion

Due to the strong gravitational amplification of the scalar modes on superhorizon scales, the long-distance physics in de Sitter spacetime is highly nontrivial. It is a key ingredient for inflationary physics, to produce the observed scale-invariant spectrum in primordial fluctuations [2], which gives strong motivations to investigate further quantum corrections. Specifically, going beyond the tree-level computation is interesting for theoretical reasons, to explain the experimental success of the actual approximation, and as an interesting playground for fundamental questions on quantum physics. In this context, perturbation theory has a limited range of applicability, and is plagued by infrared divergences, that can take the form of, *e.g.*, low momentum divergences, or secular terms growing as a function of time [13, 14].

Some of these effects are already present in the simplified setups of scalar spectators, where other issues do not intervene, such as, for example, the gauge invariance in the presence of metric fluctuations. Studying the infrared physics in this more basic situations is thus an interesting step to study the specificities of adding interactions and nonlinearities. It can also be used directly in some inflationary scenarios, where spectator fields play an important role [129]. In this thesis, we have investigated interacting test scalar fields in the EPP of a de Sitter background, with and without backreaction of the former on the latter.

The first part of the thesis is concerned with the backreaction of the quantum content on the de Sitter background geometry. This is a possible scenario for solving the cosmological constant problem, through a dynamical screening [63–65]. The intense particle production, seen as a secular effect, could be a sign of a possible instability [10, 12, 52–62], but is also common in nonequilibrium QFT as an artifact of the perturbative expansion [49–51]. This question can be addressed for the backreaction of the infrared modes of an $O(N)$ model, where secular effects are already present. We have extended a previous work using the FRG for interacting test scalar fields [36–40], which resums the infrared divergences, and the stability is considered along the renormalization flow rather than along a time coordinate, thus allowing to preserve de Sitter symmetries.

We have formulated this problem as the computation of the flow of the Hubble parameter, as it gets renormalized by the superhorizon quantum fluctuations. A key role is played by two nonperturbative effects, the symmetry restoration and the dynamical mass generation. The latter phenomenon generates a scale below which the RG flow freezes, which results in the stabilization of the geometry. Interestingly, a recent study of the backreaction problem in the context of holographic renormalization [106]

obtains very similar equations as those presented here. It will be interesting to investigate further the relation between the two approaches. Notably, the study of [106] is, in principle, not constrained by the semiclassical approximation. In the work of [106], the space of solution is larger and features two branches, the "regular" one, that we recover in our approach in the appropriate limit, and the "exotic" one, which lies outside the range of the semiclassical approximation, although it appears as a solution to our flow equation. The conclusion of our approach is that the secular terms, after an appropriate resummation, add up and produce a finite backreaction, preserving the de Sitter geometry. In particular, the scalar curvature does not diverge at a finite scale.

The method proposed in this thesis provides a new way to tackle the question of backreaction. We have limited our attention to the renormalization flow in the subspace of de Sitter geometries, where we have seen no sign of instability. This, however, does not close the discussion and other effects have to be accounted for. In particular, one should include other potentially dangerous fluctuations from the metric [57, 109–111], or consider a quantum state that is not completely de Sitter invariant [87, 88, 112–114].

In the second part of this thesis, we have studied several aspects of the stochastic formalism, focusing on the computation of key dynamical quantities in the presence of interactions, such as the field autocorrelation time. The stochastic description gives an effective theory for the infrared superhorizon physics, that we have applied to an $O(N)$ model of test scalar fields, using the JdD procedure, to obtain a functional formulation in terms of a one-dimensional supersymmetric Euclidean QFT. We have studied the nonperturbative dynamics of this theory by means of FRG techniques, as first proposed in [42], and generalized their LPA study by implementing a systematic derivative expansion [68, 71]. We have given an all-order proof that the flow of the effective potential is exactly given by its LPA expression at all orders. Then, we have computed the flow of the effective action at the second order in the derivative expansion, for arbitrary N, generalizing the result of [71]. Remarkably, the flow equation coincides with the one obtained from the Lorentzian QFT in the LPA', showing that the stochastic approach entirely captures the physics in this approximation scheme.

We could also test the convergence of the derivative expansion in a nonperturbative regime through a $1/N$ expansion of the flow equations compared to the solution of the Schwinger-Dyson equations (also computed in this thesis), and saw that the frequency expansion allowed for a precision of around ten percent for the large time behavior of the inverse propagator at NLO. The same precision was found comparing to existing numerical results in the single field case. This precision is not bad and could be improved by going to higher order. Also, the flow equations may be used in more general contexts, for example to extend the backreaction computation presented in this thesis. However, our present purpose was to investigate whether FRG could bring, similarly to the LPA computation, simple, and possibly analytical access to, *e.g.*, autocorrelation times. From that perspective, our study is not conclusive since the flow equations are not solvable analytically, and the direct numerical resolution of the Langevin (or Fokker-Planck) equation is lighter.

This motivates the last part of this thesis, which focuses on the $1/N$ expansion of

the stochastic formalism, to obtain analytical results for the spacetime dependence of correlators. We have first explored another application of the JdD path integral formulation, solving the Schwinger-Dyson equations at NLO in a $1/N$ expansion, effectively resumming a series of bubble diagrams in the self-energy of the stochastic field. We obtained analytic formulas, which coincide nontrivially with previous Lorentzian [35] or Euclidean [128] QFT computations. This provides an interesting explicit check that the stochastic approach correctly captures such dynamical quantities.

Alternatively, the Fokker-Planck formulation of the stochastic formalism phrases the dynamics in terms of a Schrödinger-like eigenvalue problem. In that context, the spacetime dependence previously obtained through the Schwinger-Dyson computation is interpreted in terms of a spectral decomposition of the correlators. Identifying the large-N limit of the first eigenvalues from the previous diagrammatic computation, they appear to have a simple structure, which hints for a direct computation of the complete spectrum. Indeed, the eigenvalue problem simply corresponds to an anharmonic oscillator in N dimensions. We have set up a $1/N$ expansion of this problem and computed the entire spectrum analytically up to NNLO, extending the result of the diagrammatic computation to virtually all correlators.

This allows to explore unequal-time correlators in the nonperturbative regime. We find that the spectrum for massless fields and in the deeply broken regime ressembles a Gaussian spectrum, however with a modified fundamental frequency, and different degeneracies. The obtained eigenvalues are related to several physical quantities of interest, such as relaxation and decoherence times [74, 125, 129–132], and spectral indices of operators [18, 72]. In particular, in the deeply broken regime, we find that the autocorrelation time in the scalar channel is strongly suppressed compared to higher representations, whose autocorrelation times are large in units of $1/H$. This results in large equilibration/decoherence times, which could have important implications for inflationary models with light spectator fields [131, 132]. Possible such phenomenological consequences remain to be investigated. Finally, we have checked that, at least for the massless case and for low quantum numbers, the results are in good agreement with exact numerical values down to relatively low values of N. A more complete numerical analysis for arbitrary parameters, in the spirit of [72, 73] remains to be done.

This thesis opens a number of prospects for future research. A first possibility is to apply the results obtained for the spectrum in the $1/N$ expansion to specific models of inflation, where several spectator fields are present, and possibly play a role after inflation [129]. This could provide constraints on the interaction potentials of such models, where the configuration of the scalar fields at the end of inflation is important. This calls for a generalization of our previous computation to a situation where the background geometry is a FLRW spacetime in slow-roll, which could have important consequences for the relaxation timescales [129].

Another interesting extension concerns the decoherence processes at stake in the early Universe. This encompasses several distinct situations [125, 130–132, 137, 138], including, *e.g.*, the quantum-to-classical transition caused by spectator fields, acting as an environment for the inflationary fluctuations.

Finally, there are several possible extensions of the FRG in de Sitter spacetime. In particular, it would be interesting to consider higher spin fields, such as the graviton, which fluctuations could play a role in the destabilization of de Sitter [57, 111]. This could be investigated, for instance, by means of an effective theory for the inflationary dynamics [139]. Other possibilities include spinor or vector fields [41, 140]. One last interesting line of development would be to extend the FRG to less symmetric spacetime, especially a FLRW geometry in slow-roll, and extend the previous computations for the backreaction to this more generic case.

A Flow of the inverse propagator

We present here the computation of the flow of the inverse propagator starting from Eq. (3.112). In all this appendix, we do not write explicitly the κ dependence for simplicity, and we always set the superfield at constant value $\Phi(t,\theta,\bar{\theta}) = \phi$ and $X(t,\theta,\bar{\theta}) = \chi = \phi^2/(2N)$.

A.1 Four-point vertex contribution

We first introduce some specific notations. We can decompose the Grassmann and field space structures of the superpropagator as follows,

$$G_{12,ab}(\omega) = \Big[G^t_\gamma(\omega)\delta_{12} + G^t_\eta(\omega)K_\omega\delta_{12}\Big]P^t_{ab} + \Big[G^l_\gamma(\omega)\delta_{12} + G^l_\eta(\omega)K_\omega\delta_{12}\Big]P^l_{ab} \,. \tag{A.1}$$

in terms of the projectors (2.19). Using the ansatz (3.110), we recall the following notations,

$$Z_{ab} = P^t_{ab}z_t + P^l_{ab}z_l \,, \quad m^2_t = \partial_\chi U \,, \quad m^2_l = \partial_\chi U + 2\chi\partial^2_\chi U \,, \tag{A.2}$$

in terms of which we have

$$G^t_\gamma(\omega) = \frac{-im^2_t}{\omega^2 z^2_t + m^4_t} \quad \text{and} \quad G^t_\eta = \frac{z_t}{\omega^2 z^2_t + m^4_t} \,, \tag{A.3}$$

and similarly for the longitudinal part. The function $J_{12,ab}$, defined as

$$J_{12,ab}(\omega) = \int_3 G_{13,ac}(\omega)G_{32,cb}(\omega) \,, \tag{A.4}$$

is decomposed as in (A.1) and gives

$$J^t_\gamma(\omega) = \frac{\omega^2 z^2_t - m^4_t}{\left(\omega^2 z^2_t + m^4_t\right)^2} \quad \text{and} \quad J^t_\eta(\omega) = \frac{-2iz_t m^2_t}{\left(\omega^2 z^2_t + m^4_t\right)^2} \,, \tag{A.5}$$

and the longitudinal part is obtained substituting $t \to l$.

The integral $\mathcal{J}_{12,ab}$, defined in Eq. (3.114), can be expressed as

$$\mathcal{J}_{12,ab}(\omega) = \int \frac{\mathrm{d}\omega'}{2\pi} \int_{34} \Gamma^{(4)}_{1234,abcd}(\omega, -\omega', \omega')J_{43,dc}(\omega') \,. \tag{A.6}$$

In the end, we are not interested in the δ_{12} component, which does not contribute to the flow of Z_{ab}, so we can forget the corresponding terms. Moreover, the function $J_{43,dc}(\omega')$ is symmetric under the exchange of its field space indices, so that the corresponding anti-symmetric component of the four point vertex function under $c \leftrightarrow d$ will not contribute to the integral. Thus, the direct computation of the four-point vertex function gives the following relevant terms

$$\begin{aligned}\Gamma^{(4)}_{1234,abcd}(\omega_2,\omega_3,\omega_4) = \partial_{\phi_c}\partial_{\phi_d}Z_{ab}\Big[&-\frac{1}{2}(\bar{D}_{\omega_2}\delta_{12}D_{\omega_4}\delta_{14}+\bar{D}_{\omega_4}\delta_{14}D_{\omega_2}\delta_{12})\delta_{13}\\ &-\frac{1}{2}(\bar{D}_{\omega_2}\delta_{12}D_{\omega_3}\delta_{13}+\bar{D}_{\omega_3}\delta_{13}D_{\omega_2}\delta_{12})\delta_{14}+\delta_{13}\delta_{14}K_{\omega_2}\delta_{12}\Big]+(\dots)\,,\end{aligned} \tag{A.7}$$

where the $(\dots)$ at the end stands for the terms, proportional to δ_{12} or anti-symmetric in $c \leftrightarrow d$, we discarded, and we recall

$$\begin{aligned}\delta_{12} &= (\bar{\theta}_1-\bar{\theta}_2)(\theta_1-\theta_2)\,,\\ K_\omega\delta_{12} &= 1+\omega(\bar{\theta}_2\theta_1-\bar{\theta}_1\theta_2)+\omega^2\bar{\theta}_2\theta_2\bar{\theta}_1\theta_1\,,\end{aligned} \tag{A.8}$$

and define

$$\begin{aligned}D_\omega\delta_{12} &= i(\theta_1-\theta_2)+i\omega(\bar{\theta}_1-\bar{\theta}_2)\theta_1\theta_2\,,\\ \bar{D}_\omega\delta_{12} &= i(\bar{\theta}_2-\bar{\theta}_2)+i\omega\bar{\theta}_1\bar{\theta}_2(\theta_2-\theta_1)\,.\end{aligned} \tag{A.9}$$

Using the following identity, which follows from simple algebra,

$$\bar{D}_\omega\delta_{12}D_{\omega'}\delta_{13}+\bar{D}_{\omega'}\delta_{13}D_\omega\delta_{12} = \delta_{12}K_{\omega'}\delta_{13}+\delta_{13}K_\omega\delta_{12}-\delta_{23}K_{\omega+\omega'}\delta_{13}\,, \tag{A.10}$$

we can rewrite the four point vertex (A.7) as

$$\Gamma^{(4)}_{1234,abcd}(\omega_2,\omega_3,\omega_4) = \frac{1}{2}\partial_{\phi_c}\partial_{\phi_d}Z_{ab}(\delta_{14}\delta_{23}K_{\omega_2+\omega_3}\delta_{13}+\delta_{13}\delta_{24}K_{\omega_2+\omega_4}\delta_{14})+(\dots)\,. \tag{A.11}$$

Using Eq. (A.11) in Eq. (A.6) and integrating over the Grassmann variables gives,

$$\mathcal{J}_{12,ab} = \frac{1}{2}\int\frac{\mathrm{d}\omega'}{2\pi}\Big[P^t_{cd}J^t_\eta(\omega')+P^l_{cd}J^l_\eta(\omega')\Big]\partial_{\phi_c}\partial_{\phi_d}Z_{ab}K_\omega\delta_{12}+(\dots)\,, \tag{A.12}$$

where we used Eq. (4.24). The frequency integrals are easily obtained

$$\int\frac{\mathrm{d}\omega}{2\pi}J^{t/l}_\eta(\omega) = \frac{1}{2im^4_{t/l}}\,. \tag{A.13}$$

The second derivative of Z_{ab} can be decomposed as

$$\begin{aligned}P^l_{cd}\partial_{\phi_c}\partial_{\phi_d}Z_{ab} &= \frac{1}{N}\Big[(z_t'+2\chi z_t'')P^t_{ab}+(z_l'+2\chi z_l'')P^l_{ab}\Big]\\ P^t_{cd}\partial_{\phi_c}\partial_{\phi_d}Z_{ab} &= \frac{N-1}{N}\Big[z_t'P^t_{ab}+z_l'P^l_{ab}\Big]+\frac{1}{N}\frac{z_l-z_t}{\chi}(P^t_{ab}-(N-1)P^l_{ab})\,.\end{aligned} \tag{A.14}$$

and we finally get, using for $\mathcal{J}_{12,ab}$ a similar decomposition as for Eq. (A.1)

$$\begin{aligned}\mathcal{J}^t_\eta(\omega) &= \frac{1}{2iN}\left(\frac{z_l - z_t + (N-1)\chi z'_t}{\chi m_t^4} + \frac{z'_t + 2\chi z''_t}{m_l^4}\right)\\ \mathcal{J}^l_\eta(\omega) &= \frac{1}{2iN}\left(\frac{(N-1)(z_t - z_l + \chi z'_l)}{\chi m_t^4} + \frac{z'_l + 2\chi z''_l}{m_l^4}\right).\end{aligned} \tag{A.15}$$

A.2 Three-point vertex contribution

Moving on to the computation of $\mathcal{I}_{12,ab}$, defined in Eq. (4.59). We have

$$\mathcal{I}_{12,ab} = \int \frac{\mathrm{d}\omega'}{2\pi} \int_{3456} \Gamma^{(3)}_{134,acd}(\omega+\omega',-\omega')\Gamma^{(3)}_{256,bef}(\omega',-\omega-\omega')J_{54,ed}(\omega')G_{36,cf}(\omega+\omega') \,. \tag{A.16}$$

The direct computation of the three-point vertex function from the ansatz (3.110) gives,

$$\begin{aligned}\Gamma^{(3)}_{123,abc}(\omega_2,\omega_3) = \frac{1}{2}(\partial_{\phi_a}Z_{bc} - \partial_{\phi_b}Z_{ac} - \partial_{\phi_c}Z_{ab})(\bar{D}_{\omega_2}\delta_{12}D_{\omega_3}\delta_{13} + \bar{D}_{\omega_3}\delta_{13}D_{\omega_2}\delta_{12})\\ + \partial_{\phi_b}Z_{ac}\delta_{12}K_{\omega_3}\delta_{13} + \partial_{\phi_c}Z_{ab}\delta_{13}K_{\omega_2}\delta_{12} + iN\partial_{\phi_a}\partial_{\phi_b}\partial_{\phi_c}U\delta_{12}\delta_{13}\,.\end{aligned} \tag{A.17}$$

Using the identity (A.10), we see that there are only four Grassmann structures appearing in the three-point vertex, namely

$$\delta_{12}K_{\omega_3}\delta_{13}, \quad \delta_{13}K_{\omega_2}\delta_{12}, \quad \delta_{23}K_{\omega_2+\omega_3}\delta_{13}, \quad \delta_{12}\delta_{13}\,. \tag{A.18}$$

The integral (A.16) involves several projections of the form $P_{ed}P_{cf}\Gamma^{(3)}_{134,acd}\Gamma^{(3)}_{256,bef}$, where P can be either a transverse or a longitudinal projector. We have four possible combinations in total. Each one can be written in terms of the Grassmann structures (A.18) as

$$\begin{aligned}P_{ed}P_{cf}\Gamma^{(3)}_{134,acd}(\omega+\omega',-\omega')\Gamma^{(3)}_{256,bef}(\omega',-\omega-\omega') = \frac{\chi}{2N}\pi_{ab}\\ \times(\mathcal{A}\delta_{13}K_{-\omega'}\delta_{14} + \mathcal{B}\delta_{14}K_{\omega+\omega'}\delta_{13} + \mathcal{C}\delta_{34}K_{\omega}\delta_{14} + \mathcal{D}\delta_{13}\delta_{14})\\ \times(\mathcal{A}\delta_{26}K_{\omega'}\delta_{25} + \mathcal{B}\delta_{25}K_{-\omega-\omega'}\delta_{26} + \mathcal{C}\delta_{56}K_{-\omega}\delta_{26} + \mathcal{D}\delta_{25}\delta_{26})\,.\end{aligned} \tag{A.19}$$

Denoting by $(t/l, t/l)$ the projection involving the $P^{t/l}_{ed}P^{t/l}_{cf}$ combination, we obtain

$$\begin{aligned}&(t,t), \quad \pi_{ab} = (N-1)P^l_{ab}, \quad \mathcal{A}=\mathcal{B}=z'_t, \quad \mathcal{C} = \frac{z_l - z_t}{\chi} - z'_t, \quad \mathcal{D} = 2iU''\,,\\ &(l,l), \quad \pi_{ab} = P^l_{ab}, \quad \mathcal{A}=\mathcal{B}=\mathcal{C}=z'_l, \quad \mathcal{D} = 2i(3U'' + 2\chi U''')\,,\\ &(t,t), \quad \pi_{ab} = P^t_{ab}, \quad \mathcal{A}=\mathcal{C}=z'_t, \quad \mathcal{B} = \frac{z_l - z_t}{\chi} - z'_t, \quad \mathcal{D} = 2iU''\,,\\ &(t,t), \quad \pi_{ab} = P^t_{ab}, \quad \mathcal{A} = \frac{z_l - z_t}{\chi} - z'_t, \quad \mathcal{B}=\mathcal{C}=z'_t, \quad \mathcal{D} = 2iU''\,.\end{aligned} \tag{A.20}$$

The integration over the Grassmann variables gives, for one particular projection,

$$\begin{aligned}
&\int_{3456} (\mathcal{A}\delta_{13}K_{-\omega'}\delta_{14} + \mathcal{B}\delta_{14}K_{\omega+\omega'}\delta_{13} + \mathcal{C}\delta_{34}K_{\omega}\delta_{14} + \mathcal{D}\delta_{13}\delta_{14}) \\
&\quad \times (\mathcal{B}\delta_{25}K_{-\omega-\omega'}\delta_{26} + \mathcal{A}\delta_{26}K_{\omega'}\delta_{25} + \mathcal{C}\delta_{56}K_{-\omega}\delta_{26} + \mathcal{D}\delta_{25}\delta_{26}) \\
&\quad \times (J_\gamma\delta_{54} + J_\eta K_{\omega'}\delta_{54})(G_\gamma\delta_{36} + G_\eta K_{\omega+\omega'}\delta_{36}) \\
&= 2J_\gamma G_\gamma(\mathcal{A}\mathcal{B} + \mathcal{A}\mathcal{C} + \mathcal{B}\mathcal{C}) + 2J_\gamma G_\eta(\mathcal{A} + \mathcal{C})\mathcal{D} + 2J_\eta G_\gamma(\mathcal{C} + \mathcal{B})\mathcal{D} \\
&\quad + J_\eta G_\eta[\mathcal{D}^2 + (\omega')^2(2\mathcal{C}\mathcal{A} + 2\mathcal{C}\mathcal{B} + \mathcal{A}^2 + \mathcal{B}^2)] + (\dots) \,,
\end{aligned} \tag{A.21}$$

using again Eq. (4.24), and where the dots represent terms proportional to δ_{12}, which do not contribute to the flow of Z_{ab}.

We again decompose $\mathcal{I}_{12,ab}$ as in Eq. (A.1), and first compute $\mathcal{I}^l_\eta$. There are two contributions, coming from the (t,t) and the (l,l) projections. We use the frequency integrals

$$\begin{aligned}
&\int \frac{\mathrm{d}\omega}{2\pi} J^t_\gamma(\omega)G^t_\gamma(\omega) = -\int \frac{\mathrm{d}\omega}{2\pi} J^t_\eta(\omega)G^t_\eta(\omega)\omega^2 = \frac{i}{8m_t^4 z_t} \,, \\
&\int \frac{\mathrm{d}\omega}{2\pi} J^t_\gamma(\omega)G^t_\eta(\omega) = \frac{1}{3}\int \frac{\mathrm{d}\omega}{2\pi} J^t_\eta(\omega)G^t_\gamma(\omega) = -\frac{1}{8m_t^6} \,, \\
&\int \frac{\mathrm{d}\omega}{2\pi} J^t_\eta(\omega)G^t_\eta(\omega) = -\frac{3iz_t}{8m_t^8} \,,
\end{aligned} \tag{A.22}$$

and similarly for the integrals involving the longitudinal components. We get

$$\mathcal{I}^l_\eta = \frac{N-1}{iN}\left(\frac{(z_l - z_t)(m_t^2)'}{m_t^6} - \frac{3\chi z_t\left[(m_t^2)'\right]^2}{4m_t^8}\right) + \frac{1}{iN}\left(\frac{2\chi z_l'(m_l^2)'}{m_l^6} - \frac{3\chi z_l\left[(m_l^2)'\right]^2}{4m_l^8}\right). \tag{A.23}$$

Moving on to I^t_η, we have two contributions coming from the (t,l) and (l,t) projections. We need the following integrals

$$\begin{aligned}
&\int \frac{\mathrm{d}\omega}{2\pi}\left[J^t_\gamma(\omega)G^l_\gamma(\omega) + J^l_\gamma(\omega)G^t_\gamma(\omega)\right] = i\frac{z_l + z_t}{2\mathcal{M}^4} \,, \\
&\int \frac{\mathrm{d}\omega}{2\pi}\left[J^t_\eta(\omega)G^l_\eta(\omega)\omega^2 + J^l_\eta(\omega)G^t_\eta(\omega)\omega^2\right] = -i\frac{z_l + z_t}{2\mathcal{M}^4} \,, \\
&\int \frac{\mathrm{d}\omega}{2\pi}\left[J^t_\gamma(\omega)G^l_\eta(\omega) + J^l_\eta(\omega)G^t_\gamma(\omega)\right] = -\frac{z_l[(z_l + z_t)m_t^2 + \mathcal{M}^2]}{2m_l^4\mathcal{M}^4} \,, \\
&\int \frac{\mathrm{d}\omega}{2\pi}\left[J^l_\gamma(\omega)G^t_\eta(\omega) + J^t_\eta(\omega)G^l_\gamma(\omega)\right] = -\frac{z_t[(z_l + z_t)m_l^2 + \mathcal{M}^2]}{2m_t^4\mathcal{M}^4} \,, \\
&\int \frac{\mathrm{d}\omega}{2\pi}\left[J^t_\eta(\omega)G^l_\eta(\omega) + J^l_\eta(\omega)G^t_\eta(\omega)\right] = -i\frac{z_l z_t[(z_l + z_t)m_l^2 m_t^2 + \mathcal{M}^2(m_l^2 + m_t^2)]}{m_t^4 m_l^4 \mathcal{M}^4} \,,
\end{aligned} \tag{A.24}$$

where $\mathcal{M}^2 = z_t m_l^2 + z_l m_t^2$. In the end, we get

$$\begin{aligned}\mathcal{I}_\eta^t = \frac{1}{iN}\Bigg(&\frac{(z_l - z_t - 2\chi z_t')^2(z_l + z_t)}{4\chi\mathcal{M}^4} + \frac{2(m_t^2)'(z_l - z_t)z_t[(z_t + z_l)m_t^2 + \mathcal{M}^2]}{m_t^4\mathcal{M}^4} \\ &+ \frac{2(m_t^2)'\chi z_t' z_l[(z_t + z_l)m_l^2 + \mathcal{M}^2]}{m_l^4\mathcal{M}^4} \\ &- \frac{\chi[(m_t^2)']^2 z_l z_t[(z_t + z_l)m_l^2 m_t^2 + \mathcal{M}^2(m_t^2 + m_l^2)]}{m_t^4 m_l^4\mathcal{M}^4}\Bigg)\,.\end{aligned} \tag{A.25}$$

Putting together Eqs. (A.15), (A.23) and (A.25) gives the flow equations (3.115) and (3.116).

B Self-energy at three-loop order

In this appendix, we compute $\Lambda_{3,1}$ at order $\mathcal{O}(\lambda)$. Indeed, we saw in Sec. 4.2.1 that taking diagrams up to order $\mathcal{O}(\lambda^2)$ only gives $\Lambda_{3,1}$ at LO because of the subleading coefficient c_3^φ. To extract the $\mathcal{O}(\lambda)$ contribution to $\Lambda_{3,1}$, we need to go to order $\mathcal{O}(\lambda^3)$ for the self-energy. This can be done either by a direct calculation of the relevant local and nonlocal contributions to the latter, or by following the strategy adopted in Sec. 4.2.2. We first compute the nonlocal contributions to the self energy using an effective tree-level propagator with mass M, which is determined self-consistently by solving the gap equation (4.55), at the appropriate order of approximation. As explained before, this automatically takes into account local self-energy insertions in propagator lines.

We start with the only three-loop nonlocal diagram (j) of Fig. B.1. It is expressed as

$$\Sigma_{12}^{(j)}(\omega) = \frac{(N+2)(N+8)}{N^3}\frac{i\lambda^3}{4}\int\frac{\mathrm{d}\omega_1}{2\pi}G_{12}^{M^2}(\omega-\omega_1)\int_3\int\frac{\mathrm{d}\omega_2}{2\pi}G_{13}^{M^2}(\omega_1-\omega_2)G_{13}^{M^2}(\omega_2) \times\int\frac{\mathrm{d}\omega_3}{2\pi}G_{32}^{M^2}(\omega_1-\omega_3)G_{32}^{M^2}(\omega_3)\,. \tag{B.1}$$

Using Eq. (4.35), the integrals on $\omega_{2,3}$ both give a propagator with mass $2M^2$,

$$\Sigma_{12}^{(j)}(\omega) = \frac{(N+2)(N+8)}{N^3}\frac{i\lambda^3}{4M^4}\int\frac{\mathrm{d}\omega_1}{2\pi}G_{12}^{M^2}(\omega-\omega_1)\int_3 G_{13}^{2M^2}(\omega_1)G_{32}^{2M^2}(\omega_1)\,. \tag{B.2}$$

The integral over the Grassmann variable is computed using Eq. (3.68), and the explicit expression of the propagators (3.82). We get

$$\int_3 G_{13}^{2M^2}(\omega_1)G_{32}^{2M^2}(\omega_1) = \frac{(\omega_1^2-4M^4)\delta_{12}+4iM^2K_{\omega_1}\delta_{12}}{(\omega_1^2+4M^4)^2}\,. \tag{B.3}$$

Applying Eqs. (4.24) to multiply this result to $G_{12}^{M^2}$, we end up with

$$\Sigma_{12}^{(j)}(\omega) = \frac{(N+2)(N+8)}{N^3}\frac{i\lambda^3}{4M^4}\int\frac{\mathrm{d}\omega_1}{2\pi}\frac{(\omega_1^2-8M^4)\delta_{12}+4iM^2K_\omega\delta_{12}}{(\omega_1^2+4M^4)^2[(\omega-\omega_1)^2+M^4]}\,. \tag{B.4}$$

We obtain, after integration,

$$\Sigma_{12}^{(j)}(\omega) = -\frac{(N+2)(N+8)}{N^3}\frac{\lambda^3}{32M^8}\left(3iM^2\frac{\omega^2-27M^4}{(\omega^2+9M^4)^2}\delta_{12}+\frac{\omega^2+45M^4}{(\omega^2+9M^4)^2}K_\omega\delta_{12}\right), \tag{B.5}$$

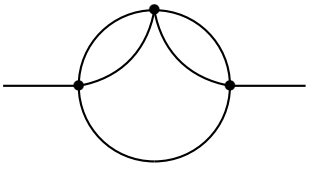

(j)

Figure B.1: Three-loop nonlocal contribution to the self-energy in the perturbative expansion.

which gives the following expressions for γ and η

$$\gamma(\omega) = M^2\left[1 - \frac{3\alpha\lambda^2}{\omega^2+9M^4}\left(1+\beta\lambda\frac{\omega^2-27M^4}{\omega^2+9M^4}\right)\right], \tag{B.6}$$

$$\eta(\omega) = 1 + \frac{\alpha\lambda^2}{\omega^2+9M^4}\left(1-\beta\lambda\frac{\omega^2+45M^4}{\omega^2+9M^4}\right), \tag{B.7}$$

where

$$\alpha = \frac{N+2}{N^2}\frac{3}{8M^4} \quad \text{and} \quad \beta = \frac{N+8}{3N}\frac{1}{4M^4}. \tag{B.8}$$

We then proceed as in Sec. 4.2.1 and compute the roots of $-iG^{-1}_{\varphi\tilde{\varphi}}(\omega) = i\gamma(\omega) + \omega\eta(\omega)$, with

$$-iG^{-1}_{\varphi\tilde{\varphi}}(\omega) = \omega + iM^2 + \frac{\alpha\lambda^2}{\omega+3iM^2}\left(1-\beta\lambda\frac{\omega+9iM^2}{\omega+3iM^2}\right). \tag{B.9}$$

To get the correct perturbative expression for the poles $\Lambda_{1,1}$ and $\Lambda_{3,1}$, and the coefficients c_1^φ and c_3^φ, we have to factorize this expression such that the retarded propagator is decomposed into a sum of free propagators, as in Eq. (4.43). To do this, we write, up to higher-orders terms,

$$-iG^{-1}_{\varphi\tilde{\varphi}}(\omega) = \omega + iM^2 + \frac{\alpha\lambda^2(1-\beta\lambda)}{\omega+3iM^2(1+2\beta\lambda)} + \mathcal{O}\left(\bar{\lambda}^4\right). \tag{B.10}$$

This is the only combination compatible with the decomposition (4.43) in simple fractions. Computing the poles and residue yields

$$\Lambda_{1,1} = M^2\left(1 - \frac{\alpha}{2M^4}\lambda^2 + \frac{2\alpha\beta}{M^4}\lambda^3\right), \tag{B.11}$$

$$\Lambda_{3,1} = 3M^2(1+2\beta\lambda), \tag{B.12}$$

$$c_1^\varphi = 1 - \frac{\alpha\lambda^2(1-\beta\lambda)}{4M^4}, \tag{B.13}$$

$$c_3^\varphi = \frac{\alpha\lambda^2(1-7\beta\lambda)}{4M^4}. \tag{B.14}$$

We now need to compute the effective square mass M^2 at three-loop order. The exact gap equation (4.55) for M^2 reads

$$M^2 = m^2 + \frac{N+2}{N}\frac{\lambda}{4\gamma(0)} , \tag{B.15}$$

where, at the present order of approximation,

$$\gamma(0) = M^2\left(1 - \frac{\alpha\lambda^2}{3M^4} + \frac{\alpha\beta\lambda^3}{M^4}\right) . \tag{B.16}$$

This is readily solved as

$$\frac{M^2}{m^2} = 1 + \bar{\lambda} - \bar{\lambda}^2 + 2\frac{N+3}{N+2}\bar{\lambda}^3 + \mathcal{O}\left(\bar{\lambda}^4\right) . \tag{B.17}$$

We thus find, at three-loop order

$$\frac{m^2_{\rm dyn}}{m^2} = 1 + \bar{\lambda} - \frac{N+4}{N+2}\bar{\lambda}^2 + 2\frac{N^2+9N+20}{(N+2)^2}\bar{\lambda}^3 + \mathcal{O}\left(\bar{\lambda}^4\right) , \tag{B.18}$$

and

$$\frac{\Lambda_{1,1}}{m^2} = 1 + \bar{\lambda} - \frac{N+5}{N+2}\bar{\lambda}^2 + \frac{2N^2+23N+62}{(N+2)^2}\bar{\lambda}^3 + \mathcal{O}\left(\bar{\lambda}^4\right) , \tag{B.19}$$

together with

$$c_3^\varphi = \frac{3\bar{\lambda}^2}{2(N+2)} - \frac{19N+80}{2(N+2)^2}\bar{\lambda}^3 + \mathcal{O}\left(\bar{\lambda}^4\right) , \tag{B.20}$$

and $c_1^\varphi = 1 - c_3^\varphi + \mathcal{O}(\bar{\lambda}^4)$. We also get the $\mathcal{O}(\bar{\lambda})$ correction to $\Lambda_{3,1}$

$$\frac{\Lambda_{3,1}}{3m^2} = 1 + \frac{5N+22}{3(N+2)}\bar{\lambda} + \mathcal{O}(\bar{\lambda}^2) . \tag{B.21}$$

C $1/N$ expansion of the Fokker-Planck eigenvalue problem at higher-order

We presented in Sec. 4.3 a well-defined $N \to \infty$ limit for the eigenvalue problem extracted from the stochastic formalism. This formulation also allows for a systematic $1/N$ expansion, which we illustrate here by explicitely computing the NLO. The following orders can be obtained in a similar fashion, and we discuss the NNLO.

C.1 Computation of the spectrum at next-to-leading order

We start by inserting the $1/N$ expansion of the eigenfunctions and eigenvalues,

$$r = r_0 + \frac{r_1}{N} + \mathcal{O}\left(\frac{1}{N^2}\right) \tag{C.1}$$

$$\Lambda = \Lambda_0 + \frac{\Lambda_1}{N} + \mathcal{O}\left(\frac{1}{N^2}\right) , \tag{C.2}$$

in Eq. (4.104). The LO equation is given by Eq. (4.106), and was solved in Sec. 4.3.2. The LO eigenfunctions and eigenvalues depend on two quantum numbers n and ℓ, and are given in Eqs. (4.113) and (4.114). To keep the formulas simple, we do not write explicitly the dependence in the quantum numbers in the following. We define

$$g = \frac{\ell - 2x^2\Lambda_0}{x(1-2xv')} . \tag{C.3}$$

The NLO equation reads

$$-\left(\frac{1}{2x} - v'\right) r_1' + \left(\frac{\ell}{2x^2} - \Lambda_0^{n,\ell}\right) r_1 = \frac{r_0''}{2} - \frac{r_0'}{2x} - \left[\frac{\ell(\ell-2)}{2x^2} - \Lambda_1\right] r_0 . \tag{C.4}$$

The right-hand side can be written in terms of g using the following relations

$$\begin{aligned} r_0' &= g r_0 , \\ r_0'' &= (g' + g^2) r_0 , \end{aligned} \tag{C.5}$$

together with the factorization (4.108), and we end up with

$$r_1' - g r_1 = h r_0 , \tag{C.6}$$

where

$$h = \frac{xg(1-xg) - x^2 g' + \ell(\ell-2) - 2x^2\Lambda_1}{x(1-2xv')} \,. \tag{C.7}$$

Using the method of variation of constants, we take the following ansatz,

$$r_1(x) = C(x) r_0(x) \,, \tag{C.8}$$

into Eq. (C.6), which yields the equation

$$C' = h \,. \tag{C.9}$$

For the quartic potential (4.107), the function h is a polynomial fraction which can, again, be decomposed into partial fractions. Introducing the notations

$$p_\pm = 1 \mp 2m_\pm^2 x^2 \,, \tag{C.10}$$

with the definition (4.109), the functions r_0 and g can be expressed as

$$r_0 = a_0 x^\ell p_+^{\alpha_+} p_-^{\alpha_-} \,, \tag{C.11}$$

and

$$g = \frac{\ell}{x} + \alpha_+ \frac{p_+'}{p_+} + \alpha_- \frac{p_-'}{p_-} \,, \tag{C.12}$$

with $\alpha_+ = \frac{n-\ell}{2}$ and $\alpha_- = -\frac{n}{2}$. Note also that

$$1 - 2xv' = p_+ p_- \,. \tag{C.13}$$

We obtain, after some calculations,

$$h = \sum_{k=1}^{3} \left[\alpha_k \frac{p_+'}{p_+^k} + \beta_k \frac{p_-'}{p_-^k} \right] \,, \tag{C.14}$$

with the coefficients

$$\begin{aligned} \alpha_1 &= \frac{\Lambda_1}{2M^2} - \frac{m_+^2 m_-^2 (a_{n,\ell} m_+^2 - b_{n,\ell} m_-^2)}{2M^6} \,, \\ \alpha_2 &= (n-\ell) m_+^2 \frac{2(n-\ell)m_-^2 - (n+\ell-2)m_+^2}{2M^4} \,, \\ \alpha_3 &= (n-\ell)(n-\ell-2)\frac{m_+^2}{2M^2} \,, \end{aligned} \tag{C.15}$$

and

$$\begin{aligned} \beta_1 &= -\alpha_1 \,, \\ \beta_2 &= n m_-^2 \frac{2n m_+^2 - (n-2\ell+2)m_-^2}{2M^4} \,, \\ \beta_3 &= n(n+2)\frac{m_-^2}{2M^2} \,, \end{aligned} \tag{C.16}$$

where we defined $M^2 = m_+^2 + m_-^2$ and

$$\begin{aligned} a_{n,\ell} &= n(3n-2) - \ell(\ell-2) \\ b_{n,\ell} &= (n-\ell)(3n-3\ell+2) - \ell(\ell-2)\ . \end{aligned} \tag{C.17}$$

Note that $b_{n,\ell} = a_{\ell-n,\ell}$. We verify explicitly the $+ \leftrightarrow -$ symmetry, obvious from Eqs. (C.12) and (C.13). In particular, we check that the coefficients $\alpha_k \leftrightarrow \beta_k$ under the exchange $m_+^2 \leftrightarrow -m_-^2$ and $n-\ell \leftrightarrow -n$.

With the decomposition (C.14), Eq. (C.9) is readily integrated as

$$C = \alpha_1 \log\frac{p_+}{p_-} - \frac{\alpha_2}{p_+} - \frac{\alpha_3}{2p_+^2} - \frac{\beta_2}{p_-} - \frac{\beta_3}{2p_-^2} + a_1\ , \tag{C.18}$$

with a_1 a free integration constant to be fixed, *e.g.*, by a normalization condition at NLO. As before, at LO, possible singularities are related to the zero of the polynomial p_+. Remembering that the solution we seek is $r_1 = Cr_0$, we see that the p_+^{-1} and p_+^{-2} terms in the first line of Eq. (C.18) contribute as $\alpha_2 p_+^{\alpha_+-1}$ and $\alpha_3 p_+^{\alpha_+-2}$ and are thus potentially singular for $n-\ell = 0$ and $n-\ell = 0,2$, respectively. This singularities are, in fact, absent thanks to the fact that the coefficients α_2 and α_3 vanish for these values of $n-\ell$. The only possible singular behavior comes from the term $\log p_+$ and regularity thus imposes $\alpha_1 = 0$. This fixes Λ_1 as

$$\Lambda_1 = \frac{m_+^2 m_-^2}{M^4}\left(a_{n,\ell}m_+^2 - b_{n,\ell}m_-^2\right)\ . \tag{C.19}$$

The expression (4.115) is obtained using the identities $M^2 = \sqrt{m^4+2\lambda}$ and $m_+^2 m_-^2 = \lambda/2$. Finally, the corresponding eigenfunction reads

$$r_{n,\ell}(x) = \left[1 + \frac{C_{n,\ell}(x)}{N} + \mathcal{O}\left(\frac{1}{N^2}\right)\right] r_0^{n,\ell}(x)\ . \tag{C.20}$$

The above expressions are valid for all values of the parameters m^2 and λ. To end this Section, we present the explicit formulas for the case $m^2 = 0$, where $m_+^2 = m_-^2 = \sqrt{\lambda/2}$. We have

$$\frac{\Lambda_{n,\ell}}{\sqrt{\lambda}} = \frac{2n-\ell}{2}\left[1 + \frac{3\ell-2}{4N} + \mathcal{O}\left(\frac{1}{N^2}\right)\right]\ , \tag{C.21}$$

and the various coefficients in the function $C(x)$ read

$$\begin{aligned} \alpha_2 &= \frac{(n-\ell)(n-3\ell+2)}{8} \\ \alpha_3 &= \frac{(n-\ell)(n-\ell-2)}{4} \\ \beta_2 &= \frac{n(n+2\ell-2)}{8} \\ \beta_3 &= \frac{n(n+2)}{4}\ . \end{aligned} \tag{C.22}$$

As an illustration, the corresponding eigenfunctions are plotted against the LO ones in Fig. 4.10 for $N = 2$. In practice, we observe that the NLO eigenfunctions provide a pretty good approximation of the numerical results down to $N = 2$ for the eigenstates we have computed numerically here, namely, $\mathcal{R}_{1,1}$ and $\mathcal{R}_{2,0}$.

C.2 Eigenvalues at NNLO

The computation at NNLO is very similar to the NLO and we summarize the main steps here. We insert the following $1/N$ expansion

$$\begin{aligned} r &= r_0 + \frac{r_1}{N} + \frac{r_2}{N^2} + \mathcal{O}\left(\frac{1}{N^3}\right) \\ \Lambda &= \Lambda_0 + \frac{\Lambda_1}{N} + \frac{\Lambda_2}{N^2} + \mathcal{O}\left(\frac{1}{N^3}\right) , \end{aligned} \tag{C.23}$$

into Eq. (4.104) and repeat the steps leading to Eq. (C.6). We obtain at NNLO

$$r_2' - g r_2 = \tilde{h} r_0 , \tag{C.24}$$

where we used Eq. (C.5) and (C.8) to get

$$\tilde{h} = \frac{C[\ell(\ell-2) - 2x^2\Lambda_1 + xg(1-xg) - x^2 g'] + xC'(1-2xg) - xC'' - 2x\Lambda_2}{x(1-2xv')} . \tag{C.25}$$

Again, using the variation of constants, we have the following ansatz

$$r_2(x) = \tilde{C}(x) r_0(x) , \tag{C.26}$$

which we plug in Eq. (C.24) to get

$$\tilde{C}' = \tilde{h} . \tag{C.27}$$

The function $\tilde{h}$ is a polynomial fraction which we decompose into partial fraction in inverse powers of $p_\pm$. We end up with

$$\tilde{h} = \sum_{k=1}^{5} \left[\tilde{\alpha}_k \frac{p_+'}{p_+^k} + \tilde{\beta}_k \frac{p_-'}{p_-^k} \right] , \tag{C.28}$$

with twelve numerical coefficients $\tilde{\alpha}_k$ and $\tilde{\beta}_k$. These coefficients can be computed explicitly, however their expression is quite long and not particularly enlightening and we do not give them here. Note the following relation

$$\tilde{\alpha}_1 = \tilde{\beta}_1 . \tag{C.29}$$

The function $\tilde{h}$ is easily integrated to give,

$$\tilde{C} = \tilde{\alpha}_1 \log \frac{p_+}{p_-} - \sum_{k=1}^{4} \left[\frac{\tilde{\alpha}_k}{k p_+^k} + \frac{\tilde{\beta}_k}{k p_-^k} \right] + a_2 , \tag{C.30}$$

up to an integration constant a_2 fixed by the normalization condition at NNLO. We look for regular solutions of the form $r_2 = \tilde{C} r_0$. Potential singularities come from the logarithm as well as $\tilde{\alpha}_k p_+^{-k}$ terms in Eq. (C.30), which gives $\tilde{\alpha}_k p_+^{\alpha_+ - k}$ and could be singular for $n - \ell < 2k$. We check that in those cases, $\tilde{\alpha}_k$ actually vanishes so that there is no singularity. Thus, regular solutions are selected by requiring $\tilde{\alpha}_1 = 0$, which fixes Λ_2 as

$$\Lambda_2 = \frac{2m_+^4 m_-^4}{M^{10}} \left[\tilde{a}_{n,\ell} m_+^4 + \tilde{b}_{n,\ell} m_-^4 + \tilde{c}_{n,\ell} m_+^2 m_-^2 \right] , \tag{C.31}$$

with

$$\begin{aligned} \tilde{a}_{n,\ell} &= (3n-2)(\ell^2 - 2\ell + 2n) - 6n^3 \\ \tilde{b}_{n,\ell} &= -\tilde{a}_{\ell - n, \ell} \\ \tilde{c}_{n,\ell} &= \ell^3 - 9\ell^2(n-1) + 2n(11n^2+6) - 3\ell(11n^2 - 6n + 2) \, . \end{aligned} \tag{C.32}$$

Finally the corresponding eigenfunction reads

$$r_{n,\ell}(x) = \left[1 + \frac{C_{n,\ell}(x)}{N} + \frac{\tilde{C}_{n,\ell}(x)}{N^2} + \mathcal{O}\left(\frac{1}{N^3}\right) \right] r_0^{n,\ell}(x) \, . \tag{C.33}$$

We conclude this computation by giving the expression of the eigenvalue in the massless case, for the scalar sector $\ell = 0$. We have $n = 2k$,

$$\frac{\Lambda_{2k,0}}{\sqrt{\lambda}} = \frac{4k}{2} \left[1 - \frac{1}{2N} + \frac{1 + 10k^2}{8N^2} + \mathcal{O}\left(\frac{1}{N^3}\right) \right] . \tag{C.34}$$

Bibliography

[1] N.D. Birrell and P.C.W. Davies. *Quantum Fields in Curved Space*. Cambridge Monographs on Mathematical Physics. Cambridge, UK: Cambridge Univ. Press, Feb. 1984. ISBN: 978-0-521-27858-4, 978-0-521-27858-4. DOI: 10.1017/CBO9780511622632.

[2] N. Aghanim et al. "Planck 2018 results. VI. Cosmological parameters". In: (July 2018). arXiv: 1807.06209 [astro-ph.CO].

[3] Alan H. Guth. "The Inflationary Universe: A Possible Solution to the Horizon and Flatness Problems". In: *Adv. Ser. Astrophys. Cosmol.* 3 (1987). Ed. by Li-Zhi Fang and R. Ruffini, pp. 139–148. DOI: 10.1103/PhysRevD.23.347.

[4] Andrei D. Linde. "A New Inflationary Universe Scenario: A Possible Solution of the Horizon, Flatness, Homogeneity, Isotropy and Primordial Monopole Problems". In: *Adv. Ser. Astrophys. Cosmol.* 3 (1987). Ed. by Li-Zhi Fang and R. Ruffini, pp. 149–153. DOI: 10.1016/0370-2693(82)91219-9.

[5] Andreas Albrecht and Paul J. Steinhardt. "Cosmology for Grand Unified Theories with Radiatively Induced Symmetry Breaking". In: *Adv. Ser. Astrophys. Cosmol.* 3 (1987). Ed. by Li-Zhi Fang and R. Ruffini, pp. 158–161. DOI: 10.1103/PhysRevLett.48.1220.

[6] Andrei D. Linde. "Chaotic Inflation". In: *Phys. Lett. B* 129 (1983), pp. 177–181. DOI: 10.1016/0370-2693(83)90837-7.

[7] Viatcheslav F. Mukhanov, H.A. Feldman, and Robert H. Brandenberger. "Theory of cosmological perturbations. Part 1. Classical perturbations. Part 2. Quantum theory of perturbations. Part 3. Extensions". In: *Phys. Rept.* 215 (1992), pp. 203–333. DOI: 10.1016/0370-1573(92)90044-Z.

[8] Hideo Kodama and Misao Sasaki. "Cosmological Perturbation Theory". In: *Prog. Theor. Phys. Suppl.* 78 (1984), pp. 1–166. DOI: 10.1143/PTPS.78.1.

[9] Nathan P. Myhrvold. "Runaway Particle Production in De Sitter Space". In: *Phys. Rev. D* 28 (1983), p. 2439. DOI: 10.1103/PhysRevD.28.2439.

[10] E. Mottola. "Particle Creation in de Sitter Space". In: *Phys. Rev. D* 31 (1985), p. 754. DOI: 10.1103/PhysRevD.31.754.

[11] N.C. Tsamis and R.P. Woodard. "Stochastic quantum gravitational inflation". In: *Nucl. Phys. B* 724 (2005), pp. 295–328. DOI: 10.1016/j.nuclphysb.2005.06.031. arXiv: gr-qc/0505115.

[12] Dmitry Krotov and Alexander M. Polyakov. "Infrared Sensitivity of Unstable Vacua". In: *Nucl. Phys. B* 849 (2011), pp. 410–432. DOI: 10.1016/j.nuclphysb.2011.03.025. arXiv: 1012.2107 [hep-th].

[13] Steven Weinberg. "Quantum contributions to cosmological correlations". In: *Phys. Rev. D* 72 (2005), p. 043514. DOI: 10.1103/PhysRevD.72.043514. arXiv: hep-th/0506236.

[14] Steven Weinberg. "Quantum contributions to cosmological correlations. II. Can these corrections become large?" In: *Phys. Rev. D* 74 (2006), p. 023508. DOI: 10.1103/PhysRevD.74.023508. arXiv: hep-th/0605244.

[15] Alexei A. Starobinsky. "STOCHASTIC DE SITTER (INFLATIONARY) STAGE IN THE EARLY UNIVERSE". In: *Lect. Notes Phys.* 246 (1986), pp. 107–126. DOI: 10.1007/3-540-16452-9_6.

[16] Yasusada Nambu and Misao Sasaki. "Stochastic Stage of an Inflationary Universe Model". In: *Phys. Lett. B* 205 (1988), pp. 441–446. DOI: 10.1016/0370-2693(88)90974-4.

[17] Henry E. Kandrup. "STOCHASTIC INFLATION AS A TIME DEPENDENT RANDOM WALK". In: *Phys. Rev. D* 39 (1989), p. 2245. DOI: 10.1103/PhysRevD.39.2245.

[18] Alexei A. Starobinsky and Junichi Yokoyama. "Equilibrium state of a selfinteracting scalar field in the De Sitter background". In: *Phys. Rev. D* 50 (1994), pp. 6357–6368. DOI: 10.1103/PhysRevD.50.6357. arXiv: astro-ph/9407016.

[19] Björn Garbrecht, Gerasimos Rigopoulos, and Yi Zhu. "Infrared correlations in de Sitter space: Field theoretic versus stochastic approach". In: *Phys. Rev. D* 89 (2014), p. 063506. DOI: 10.1103/PhysRevD.89.063506. arXiv: 1310.0367 [hep-th].

[20] Bjorn Garbrecht et al. "Feynman Diagrams for Stochastic Inflation and Quantum Field Theory in de Sitter Space". In: *Phys. Rev. D* 91 (2015), p. 063520. DOI: 10.1103/PhysRevD.91.063520. arXiv: 1412.4893 [hep-th].

[21] Meindert van der Meulen and Jan Smit. "Classical approximation to quantum cosmological correlations". In: *JCAP* 11 (2007), p. 023. DOI: 10.1088/1475-7516/2007/11/023. arXiv: 0707.0842 [hep-th].

[22] C.P. Burgess et al. "Super-Hubble de Sitter Fluctuations and the Dynamical RG". In: *JCAP* 03 (2010), p. 033. DOI: 10.1088/1475-7516/2010/03/033. arXiv: 0912.1608 [hep-th].

[23] C.P. Burgess et al. "Breakdown of Semiclassical Methods in de Sitter Space". In: *JCAP* 10 (2010), p. 017. DOI: 10.1088/1475-7516/2010/10/017. arXiv: 1005.3551 [hep-th].

[24] Arvind Rajaraman. "On the proper treatment of massless fields in Euclidean de Sitter space". In: *Phys. Rev. D* 82 (2010), p. 123522. DOI: 10.1103/PhysRevD.82.123522. arXiv: 1008.1271 [hep-th].

[25] E.T. Akhmedov. "IR divergences and kinetic equation in de Sitter space. Poincare patch: Principal series". In: *JHEP* 01 (2012), p. 066. DOI: 10.1007/JHEP01(2012)066. arXiv: 1110.2257 [hep-th].

[26] Bjorn Garbrecht and Gerasimos Rigopoulos. "Self Regulation of Infrared Correlations for Massless Scalar Fields during Inflation". In: *Phys. Rev. D* 84 (2011), p. 063516. DOI: 10.1103/PhysRevD.84.063516. arXiv: 1105.0418 [hep-th].

[27] M. Beneke and P. Moch. "On "dynamical mass" generation in Euclidean de Sitter space". In: *Phys. Rev. D* 87 (2013), p. 064018. DOI: 10.1103/PhysRevD.87.064018. arXiv: 1212.3058 [hep-th].

[28] Daniel Boyanovsky. "Condensates and quasiparticles in inflationary cosmology: mass generation and decay widths". In: *Phys. Rev. D* 85 (2012), p. 123525. DOI: 10.1103/PhysRevD.85.123525. arXiv: 1203.3903 [hep-ph].

[29] R. Parentani and J. Serreau. "Physical momentum representation of scalar field correlators in de Sitter space". In: *Phys. Rev. D* 87 (2013), p. 045020. DOI: 10.1103/PhysRevD.87.045020. arXiv: 1212.6077 [hep-th].

[30] Julien Serreau and Renaud Parentani. "Nonperturbative resummation of de Sitter infrared logarithms in the large-N limit". In: *Phys. Rev. D* 87 (2013), p. 085012. DOI: 10.1103/PhysRevD.87.085012. arXiv: 1302.3262 [hep-th].

[31] Ahmed Youssef and Dirk Kreimer. "Resummation of infrared logarithms in de Sitter space via Dyson-Schwinger equations: the ladder-rainbow approximation". In: *Phys. Rev. D* 89 (2014), p. 124021. DOI: 10.1103/PhysRevD.89.124021. arXiv: 1301.3205 [gr-qc].

[32] D. Boyanovsky. "Effective field theory during inflation: Reduced density matrix and its quantum master equation". In: *Phys. Rev. D* 92.2 (2015), p. 023527. DOI: 10.1103/PhysRevD.92.023527. arXiv: 1506.07395 [astro-ph.CO].

[33] Ian Moss and Gerasimos Rigopoulos. "Effective long wavelength scalar dynamics in de Sitter". In: *JCAP* 05 (2017), p. 009. DOI: 10.1088/1475-7516/2017/05/009. arXiv: 1611.07589 [gr-qc].

[34] Florian Gautier and Julien Serreau. "Infrared dynamics in de Sitter space from Schwinger-Dyson equations". In: *Phys. Lett. B* 727 (2013), pp. 541–547. DOI: 10.1016/j.physletb.2013.10.072. arXiv: 1305.5705 [hep-th].

[35] Florian Gautier and Julien Serreau. "Scalar field correlator in de Sitter space at next-to-leading order in a 1/N expansion". In: *Phys. Rev. D* 92.10 (2015), p. 105035. DOI: 10.1103/PhysRevD.92.105035. arXiv: 1509.05546 [hep-th].

[36] Julien Serreau. "Effective potential for quantum scalar fields on a de Sitter geometry". In: *Phys. Rev. Lett.* 107 (2011), p. 191103. DOI: 10.1103/PhysRevLett.107.191103. arXiv: 1105.4539 [hep-th].

[37] Ali Kaya. "Exact renormalization group flow in an expanding Universe and screening of the cosmological constant". In: *Phys. Rev. D* 87 (2013), p. 123501. DOI: 10.1103/PhysRevD.87.123501. arXiv: 1303.5459 [hep-th].

[38] Julien Serreau. "Renormalization group flow and symmetry restoration in de Sitter space". In: *Phys. Lett. B* 730 (2014), pp. 271–274. DOI: 10.1016/j.physletb.2014.01.058. arXiv: 1306.3846 [hep-th].

[39] Maxime Guilleux and Julien Serreau. "Quantum scalar fields in de Sitter space from the nonperturbative renormalization group". In: *Phys. Rev. D* 92.8 (2015), p. 084010. DOI: 10.1103/PhysRevD.92.084010. arXiv: 1506.06183 [hep-th].

[40] Maxime Guilleux and Julien Serreau. "Nonperturbative renormalization group for scalar fields in de Sitter space: beyond the local potential approximation". In: *Phys. Rev. D* 95.4 (2017), p. 045003. DOI: 10.1103/PhysRevD.95.045003. arXiv: 1611.08106 [gr-qc].

[41] Francisco Fabián González and Tomislav Prokopec. "Renormalization group approach to scalar quantum electrodynamics on de Sitter". In: (Nov. 2016). arXiv: 1611.07854 [gr-qc].

[42] Tomislav Prokopec and Gerasimos Rigopoulos. "Functional renormalization group for stochastic inflation". In: *JCAP* 08 (2018), p. 013. DOI: 10.1088/1475-7516/2018/08/013. arXiv: 1710.07333 [gr-qc].

[43] Juergen Berges, Nikolaos Tetradis, and Christof Wetterich. "Nonperturbative renormalization flow in quantum field theory and statistical physics". In: *Phys. Rept.* 363 (2002), pp. 223–386. DOI: 10.1016/S0370-1573(01)00098-9. arXiv: hep-ph/0005122.

[44] Bertrand Delamotte. "An Introduction to the nonperturbative renormalization group". In: *Lect. Notes Phys.* 852 (2012), pp. 49–132. DOI: 10.1007/978-3-642-27320-9_2. arXiv: cond-mat/0702365.

[45] N. Dupuis et al. "The nonperturbative functional renormalization group and its applications". In: (June 2020). arXiv: 2006.04853 [cond-mat.stat-mech].

[46] G. Von Gersdorff and C. Wetterich. "Nonperturbative renormalization flow and essential scaling for the Kosterlitz-Thouless transition". In: *Phys. Rev. B* 64 (2001), p. 054513. DOI: 10.1103/PhysRevB.64.054513. arXiv: hep-th/0008114.

[47] P. Jakubczyk, N. Dupuis, and B. Delamotte. "Reexamination of the nonperturbative renormalization-group approach to the Kosterlitz-Thouless transition". In: *Phys. Rev. E* 90.6 (2014), p. 062105. DOI: 10.1103/PhysRevE.90.062105. arXiv: 1409.1374 [cond-mat.stat-mech].

[48] Max Niedermaier and Martin Reuter. "The Asymptotic Safety Scenario in Quantum Gravity". In: *Living Rev. Rel.* 9 (2006), pp. 5–173. DOI: 10.12942/lrr-2006-5.

[49] Juergen Berges. "Introduction to nonequilibrium quantum field theory". In: *AIP Conf. Proc.* 739.1 (2004). Ed. by Mirian Bracco et al., pp. 3–62. DOI: 10.1063/1.1843591. arXiv: hep-ph/0409233.

[50] Juergen Berges and Julien Serreau. "Progress in nonequilibrium quantum field theory". In: *5th Internationa Conference on Strong and Electroweak Matter*. 2003, pp. 111–126. DOI: 10.1142/9789812704498_0011. arXiv: hep-ph/0302210.

[51] Juergen Berges and Julien Serreau. "Progress in nonequilibrium quantum field theory II". In: *6th International Conference on Strong and Electroweak Matter*. 2005, pp. 102–116. DOI: 10.1142/9789812702159_0011. arXiv: hep-ph/0410330.

[52] Alexander m. Polyakov. "PHASE TRANSITIONS AND THE UNIVERSE". In: *Sov. Phys. Usp.* 25 (1982), p. 187. DOI: 10.1070/PU1982v025n03ABEH004529.

[53] L.H. Ford. "Quantum Instability of De Sitter Space-time". In: *Phys. Rev. D* 31 (1985), p. 710. DOI: 10.1103/PhysRevD.31.710.

[54] Ignatios Antoniadis, J. Iliopoulos, and T.N. Tomaras. "Quantum Instability of De Sitter Space". In: *Phys. Rev. Lett.* 56 (1986), p. 1319. DOI: 10.1103/PhysRevLett.56.1319.

[55] Pawel Mazur and Emil Mottola. "Spontaneous Breaking of De Sitter Symmetry by Radiative Effects". In: *Nucl. Phys. B* 278 (1986), pp. 694–720. DOI: 10.1016/0550-3213(86)90058-1.

[56] Ignatios Antoniadis and Emil Mottola. "4-D quantum gravity in the conformal sector". In: *Phys. Rev. D* 45 (1992), pp. 2013–2025. DOI: 10.1103/PhysRevD.45.2013.

[57] N.C. Tsamis and R.P. Woodard. "Relaxing the cosmological constant". In: *Phys. Lett. B* 301 (1993), pp. 351–357. DOI: 10.1016/0370-2693(93)91162-G.

[58] Viatcheslav F. Mukhanov, L.Raul W. Abramo, and Robert H. Brandenberger. "On the Back reaction problem for gravitational perturbations". In: *Phys. Rev. Lett.* 78 (1997), pp. 1624–1627. DOI: 10.1103/PhysRevLett.78.1624. arXiv: gr-qc/9609026.

[59] A.M. Polyakov. "Decay of Vacuum Energy". In: *Nucl. Phys. B* 834 (2010), pp. 316–329. DOI: 10.1016/j.nuclphysb.2010.03.021. arXiv: 0912.5503 [hep-th].

[60] A.M. Polyakov. "Infrared instability of the de Sitter space". In: (Sept. 2012). arXiv: 1209.4135 [hep-th].

[61] Paul R. Anderson and Emil Mottola. "Instability of global de Sitter space to particle creation". In: *Phys. Rev. D* 89 (2014), p. 104038. DOI: 10.1103/PhysRevD.89.104038. arXiv: 1310.0030 [gr-qc].

[62] Paul R. Anderson and Emil Mottola. "Quantum vacuum instability of "eternal" de Sitter space". In: *Phys. Rev. D* 89 (2014), p. 104039. DOI: 10.1103/PhysRevD.89.104039. arXiv: 1310.1963 [gr-qc].

[63] Steven Weinberg. "The Cosmological Constant Problem". In: *Rev. Mod. Phys.* 61 (1989). Ed. by Jong-Ping Hsu and D. Fine, pp. 1–23. DOI: 10.1103/RevModPhys.61.1.

[64] T. Padmanabhan. "Cosmological constant: The Weight of the vacuum". In: *Phys. Rept.* 380 (2003), pp. 235–320. DOI: 10.1016/S0370-1573(03)00120-0. arXiv: hep-th/0212290.

[65] Jerome Martin. "Everything You Always Wanted To Know About The Cosmological Constant Problem (But Were Afraid To Ask)". In: *Comptes Rendus Physique* 13 (2012), pp. 566–665. DOI: 10.1016/j.crhy.2012.04.008. arXiv: 1205.3365 [astro-ph.CO].

[66] P.C. Hohenberg and B.I. Halperin. "Theory of Dynamic Critical Phenomena". In: *Rev. Mod. Phys.* 49 (1977), pp. 435–479. DOI: 10.1103/RevModPhys.49.435.

[67] Leonie Canet and Hugues Chate. "Non-perturbative Approach to Critical Dynamics". In: *J. Phys.* 40 (2007), pp. 1937–1950. DOI: 10.1088/1751-8113/40/9/002. arXiv: cond-mat/0610468.

[68] Leonie Canet, Hugues Chate, and Bertrand Delamotte. "General framework of the non-perturbative renormalization group for non-equilibrium steady states". In: *J. Phys. A* 44 (2011), p. 495001. DOI: 10.1088/1751-8113/44/49/495001. arXiv: 1106.4129 [cond-mat.stat-mech].

[69] Hans-Karl Janssen. "On a Lagrangean for classical field dynamics and renormalization group calculations of dynamical critical properties". In: *Zeitschrift für Physik B Condensed Matter* 23.4 (1976), pp. 377–380.

[70] de Dominicis, c. "Techniques de renormalisation de la théorie des champs et dynamique des phénomènes critiques". In: *J. Phys. Colloques* 37 (1976), pp. C1-247-C1–253. DOI: 10.1051/jphyscol:1976138. URL: https://doi.org/10.1051/jphyscol:1976138.

[71] Franziska Synatschke et al. "Flow Equation for Supersymmetric Quantum Mechanics". In: *JHEP* 03 (2009), p. 028. DOI: 10.1088/1126-6708/2009/03/028. arXiv: 0809.4396 [hep-th].

[72] Tommi Markkanen et al. "Scalar correlation functions in de Sitter space from the stochastic spectral expansion". In: *JCAP* 08 (2019), p. 001. DOI: 10.1088/1475-7516/2019/08/001. arXiv: 1904.11917 [gr-qc].

[73] Tommi Markkanen and Arttu Rajantie. "Scalar correlation functions for a double-well potential in de Sitter space". In: *JCAP* 03 (2020), p. 049. DOI: 10.1088/1475-7516/2020/03/049. arXiv: 2001.04494 [gr-qc].

[74] Peter Adshead et al. "Stochastic evolution of scalar fields with continuous symmetries during inflation". In: (Feb. 2020). arXiv: 2002.07201 [hep-ph].

[75] T.M.C. Abbott et al. "First Cosmology Results using Type Ia Supernovae from the Dark Energy Survey: Constraints on Cosmological Parameters". In: *Astrophys. J. Lett.* 872.2 (2019), p. L30. DOI: 10.3847/2041-8213/ab04fa. arXiv: 1811.02374 [astro-ph.CO].

[76] Vincent Vennin. "Cosmological Inflation: Theoretical Aspects and Observational Constraints". PhD thesis. Paris, Inst. Astrophys., 2014.

[77] Robert H. Brandenberger, Ronald Kahn, and William H. Press. "Cosmological Perturbations in the Early Universe". In: *Phys. Rev. D* 28 (1983), p. 1809. DOI: 10.1103/PhysRevD.28.1809.

[78] D.H. Lyth. "Large Scale Energy Density Perturbations and Inflation". In: *Phys. Rev. D* 31 (1985), pp. 1792–1798. DOI: 10.1103/PhysRevD.31.1792.

[79] Joshua A. Frieman and Michael S. Turner. "Evolution of Density Perturbations Through Cosmological Phase Transitions". In: *Phys. Rev. D* 30 (1984), p. 265. DOI: 10.1103/PhysRevD.30.265.

[80] Viatcheslav F. Mukhanov. "CMB-slow, or how to estimate cosmological parameters by hand". In: *Int. J. Theor. Phys.* 43 (2004). Ed. by E. Gunzig, Viatcheslav F. Mukhanov, and E. Verdaguer, pp. 623–668. DOI: 10.1023/B:IJTP.0000048168.90282.db. arXiv: astro-ph/0303072.

[81] Julian S. Schwinger. "Brownian motion of a quantum oscillator". In: *J. Math. Phys.* 2 (1961), pp. 407–432. DOI: 10.1063/1.1703727.

[82] L.V. Keldysh. "Diagram technique for nonequilibrium processes". In: *Zh. Eksp. Teor. Fiz.* 47 (1964), pp. 1515–1527.

[83] Steven Weinberg. *The Quantum theory of fields. Vol. 1: Foundations*. Cambridge University Press, June 2005. ISBN: 978-0-521-67053-1, 978-0-511-25204-4.

[84] Bruce Allen. "Vacuum States in de Sitter Space". In: *Phys. Rev. D* 32 (1985), p. 3136. DOI: 10.1103/PhysRevD.32.3136.

[85] Paul R. Anderson et al. "Attractor states and infrared scaling in de Sitter space". In: *Phys. Rev. D* 62 (2000), p. 124019. DOI: 10.1103/PhysRevD.62.124019. arXiv: gr-qc/0005102.

[86] J. Lesgourgues, David Polarski, and Alexei A. Starobinsky. "Quantum to classical transition of cosmological perturbations for nonvacuum initial states". In: *Nucl. Phys. B* 497 (1997), pp. 479–510. DOI: 10.1016/S0550-3213(97)00224-1. arXiv: gr-qc/9611019.

[87] E.T. Akhmedov, F.K. Popov, and V.M. Slepukhin. "Infrared dynamics of the massive $\varphi 4$ theory on de Sitter space". In: *Phys. Rev. D* 88 (2013), p. 024021. DOI: 10.1103/PhysRevD.88.024021. arXiv: 1303.1068 [hep-th].

[88] E.T. Akhmedov et al. "Infrared dynamics of massive scalars from the complementary series in de Sitter space". In: *Phys. Rev. D* 96.2 (2017), p. 025002. DOI: 10.1103/PhysRevD.96.025002. arXiv: 1701.07226 [hep-th].

[89] K.G. Wilson and John B. Kogut. "The Renormalization group and the epsilon expansion". In: *Phys. Rept.* 12 (1974), pp. 75–199. DOI: 10.1016/0370-1573(74)90023-4.

[90] C. Wetterich. "Average Action and the Renormalization Group Equations". In: *Nucl. Phys. B* 352 (1991), pp. 529–584. DOI: 10.1016/0550-3213(91)90099-J.

[91] N. Tetradis and C. Wetterich. "Scale dependence of the average potential around the maximum in phi**4 theories". In: *Nucl. Phys. B* 383 (1992), pp. 197–217. DOI: 10.1016/0550-3213(92)90676-3.

[92] N. Tetradis and C. Wetterich. "Critical exponents from effective average action". In: *Nucl. Phys. B* 422 (1994), pp. 541–592. DOI: 10.1016/0550-3213(94)90446-4. arXiv: hep-ph/9308214.

[93] Ulrich Ellwanger. "FLow equations for N point functions and bound states". In: (Sept. 1993). Ed. by B. Geyer and E.-M. Ilgenfritz, pp. 206–211. DOI: 10.1007/BF01555911. arXiv: hep-ph/9308260.

[94] Ulrich Ellwanger. "Flow equations and BRS invariance for Yang-Mills theories". In: *Phys. Lett. B* 335 (1994), pp. 364–370. DOI: 10.1016/0370-2693(94)90365-4. arXiv: hep-th/9402077.

[95] Tim R. Morris. "The Exact renormalization group and approximate solutions". In: *Int. J. Mod. Phys. A* 9 (1994), pp. 2411–2450. DOI: 10.1142/S0217751X94000972. arXiv: hep-ph/9308265.

[96] Tim R. Morris. "The Derivative expansion of the renormalization group". In: *Nucl. Phys. B Proc. Suppl.* 42 (1995), pp. 811–814. DOI: 10.1016/0920-5632(95)00389-Q. arXiv: hep-lat/9411053.

[97] Daniel F. Litim. "Optimized renormalization group flows". In: *Phys. Rev. D* 64 (2001), p. 105007. DOI: 10.1103/PhysRevD.64.105007. arXiv: hep-th/0103195.

[98] Ivan Balog et al. "Convergence of Nonperturbative Approximations to the Renormalization Group". In: *Phys. Rev. Lett.* 123.24 (2019), p. 240604. DOI: 10.1103/PhysRevLett.123.240604. arXiv: 1907.01829 [cond-mat.stat-mech].

[99] N.C. Tsamis and R.P. Woodard. "One loop graviton selfenergy in a locally de Sitter background". In: *Phys. Rev. D* 54 (1996), pp. 2621–2639. DOI: 10.1103/PhysRevD.54.2621. arXiv: hep-ph/9602317.

[100] Leonardo Senatore and Matias Zaldarriaga. "On Loops in Inflation". In: *JHEP* 12 (2010), p. 008. DOI: 10.1007/JHEP12(2010)008. arXiv: 0912.2734 [hep-th].

[101] Steven B. Giddings and Martin S. Sloth. "Semiclassical relations and IR effects in de Sitter and slow-roll space-times". In: *JCAP* 01 (2011), p. 023. DOI: 10.1088/1475-7516/2011/01/023. arXiv: 1005.1056 [hep-th].

[102] Takahiro Tanaka and Yuko Urakawa. "Loops in inflationary correlation functions". In: *Class. Quant. Grav.* 30 (2013), p. 233001. DOI: 10.1088/0264-9381/30/23/233001. arXiv: 1306.4461 [hep-th].

[103] Leonardo Senatore and Matias Zaldarriaga. "The constancy of ζ in single-clock Inflation at all loops". In: *JHEP* 09 (2013), p. 148. DOI: 10.1007/JHEP09(2013)148. arXiv: 1210.6048 [hep-th].

[104] S.P. Miao and R.P. Woodard. "Issues Concerning Loop Corrections to the Primordial Power Spectra". In: *JCAP* 07 (2012), p. 008. DOI: 10.1088/1475-7516/2012/07/008. arXiv: 1204.1784 [astro-ph.CO].

[105] D. Boyanovsky, Hector J. de Vega, and Norma G. Sanchez. "Quantum corrections to slow roll inflation and new scaling of superhorizon fluctuations". In: *Nucl. Phys. B* 747 (2006), pp. 25–54. DOI: 10.1016/j.nuclphysb.2006.04.010. arXiv: astro-ph/0503669.

[106] Jewel Kumar Ghosh et al. "Back-reaction in massless de Sitter QFTs: holography, gravitational DBI action and f(R) gravity". In: (Mar. 2020). arXiv: 2003.09435 [hep-th].

[107] Bharat Ratra. "Restoration of Spontaneously Broken Continuous Symmetries in de Sitter Space-Time". In: *Phys. Rev. D* 31 (1985), pp. 1931–1955. DOI: 10.1103/PhysRevD.31.1931.

[108] F.D. Mazzitelli and J.P. Paz. "Gaussian and $1/N$ Approximations in Semiclassical Cosmology". In: *Phys. Rev. D* 39 (1989), p. 2234. DOI: 10.1103/PhysRevD.39.2234.

[109] Robert Brandenberger et al. "Backreaction of super-Hubble cosmological perturbations beyond perturbation theory". In: *Phys. Rev. D* 98.10 (2018), p. 103523. DOI: 10.1103/PhysRevD.98.103523. arXiv: 1807.07494 [hep-th].

[110] B. Losic and W.G. Unruh. "Long-wavelength metric backreactions in slow-roll inflation". In: *Phys. Rev. D* 72 (2005), p. 123510. DOI: 10.1103/PhysRevD.72.123510. arXiv: gr-qc/0510078.

[111] S.P. Miao, N.C. Tsamis, and R.P. Woodard. "Invariant measure of the one-loop quantum gravitational backreaction on inflation". In: *Phys. Rev. D* 95.12 (2017), p. 125008. DOI: 10.1103/PhysRevD.95.125008. arXiv: 1702.05694 [gr-qc].

[112] D. Boyanovsky and R. Holman. "On the Perturbative Stability of Quantum Field Theories in de Sitter Space". In: *JHEP* 05 (2011), p. 047. DOI: 10.1007/JHEP05(2011)047. arXiv: 1103.4648 [astro-ph.CO].

[113] Tommi Markkanen and Arttu Rajantie. "Massive scalar field evolution in de Sitter". In: *JHEP* 01 (2017), p. 133. DOI: 10.1007/JHEP01(2017)133. arXiv: 1607.00334 [gr-qc].

[114] Paul R. Anderson, Emil Mottola, and Dillon H. Sanders. "Decay of the de Sitter Vacuum". In: *Phys. Rev. D* 97.6 (2018), p. 065016. DOI: 10.1103/PhysRevD.97.065016. arXiv: 1712.04522 [gr-qc].

[115] F. Finelli et al. "Generation of fluctuations during inflation: Comparison of stochastic and field-theoretic approaches". In: *Phys. Rev. D* 79 (2009), p. 044007. DOI: 10.1103/PhysRevD.79.044007. arXiv: 0808.1786 [hep-th].

[116] F. Finelli et al. "Stochastic growth of quantum fluctuations during slow-roll inflation". In: *Phys. Rev. D* 82 (2010), p. 064020. DOI: 10.1103/PhysRevD.82.064020. arXiv: 1003.1327 [hep-th].

[117] Vincent Vennin and Alexei A. Starobinsky. "Correlation Functions in Stochastic Inflation". In: *Eur. Phys. J. C* 75 (2015), p. 413. DOI: 10.1140/epjc/s10052-015-3643-y. arXiv: 1506.04732 [hep-th].

[118] Julien Grain and Vincent Vennin. "Stochastic inflation in phase space: Is slow roll a stochastic attractor?" In: *JCAP* 05 (2017), p. 045. DOI: 10.1088/1475-7516/2017/05/045. arXiv: 1703.00447 [gr-qc].

[119] Chris Pattison et al. "Stochastic inflation beyond slow roll". In: *JCAP* 07 (2019), p. 031. DOI: 10.1088/1475-7516/2019/07/031. arXiv: 1905.06300 [astro-ph.CO].

[120] David Polarski and Alexei A. Starobinsky. "Semiclassicality and decoherence of cosmological perturbations". In: *Class. Quant. Grav.* 13 (1996), pp. 377–392. DOI: 10.1088/0264-9381/13/3/006. arXiv: gr-qc/9504030.

[121] Claus Kiefer and David Polarski. "Why do cosmological perturbations look classical to us?" In: *Adv. Sci. Lett.* 2 (2009), pp. 164–173. DOI: 10.1166/asl.2009.1023. arXiv: 0810.0087 [astro-ph].

[122] Gert Aarts and Juergen Berges. "Classical aspects of quantum fields far from equilibrium". In: *Phys. Rev. Lett.* 88 (2002), p. 041603. DOI: 10.1103/PhysRevLett.88.041603. arXiv: hep-ph/0107129.

[123] Hannes Risken. "Fokker-planck equation". In: *The Fokker-Planck Equation*. Springer, 1996, pp. 63–95.

[124] G.W. Gibbons and S.W. Hawking. "Cosmological Event Horizons, Thermodynamics, and Particle Creation". In: *Phys. Rev. D* 15 (1977), pp. 2738–2751. DOI: 10.1103/PhysRevD.15.2738.

[125] Florian Gautier and Julien Serreau. "On the Langevin description of nonequilibrium quantum fields". In: *Phys. Rev. D* 86 (2012), p. 125002. DOI: 10.1103/PhysRevD.86.125002. arXiv: 1209.1827 [hep-th].

[126] Gerasimos Rigopoulos. "Thermal Interpretation of Infrared Dynamics in de Sitter". In: *JCAP* 07 (2016), p. 035. DOI: 10.1088/1475-7516/2016/07/035. arXiv: 1604.04313 [gr-qc].

[127] A Erldelyi et al. *Higher Transcendental Functions, Vol. 2*. 1955.

[128] Diana López Nacir, Francisco D. Mazzitelli, and Leonardo G. Trombetta. "To the sphere and back again: de Sitter infrared correlators at NTLO in 1/N". In: *JHEP* 08 (2019), p. 052. DOI: 10.1007/JHEP08(2019)052. arXiv: 1905.03665 [hep-th].

[129] Robert J. Hardwick et al. "The stochastic spectator". In: *JCAP* 10 (2017), p. 018. DOI: 10.1088/1475-7516/2017/10/018. arXiv: 1701.06473 [astro-ph.CO].

[130] Alexandre Giraud and Julien Serreau. "Decoherence and thermalization of a pure quantum state in quantum field theory". In: *Phys. Rev. Lett.* 104 (2010), p. 230405. DOI: 10.1103/PhysRevLett.104.230405. arXiv: 0910.2570 [hep-ph].

[131] Jérôme Martin and Vincent Vennin. "Non Gaussianities from Quantum Decoherence during Inflation". In: *JCAP* 06 (2018), p. 037. DOI: 10.1088/1475-7516/2018/06/037. arXiv: 1805.05609 [astro-ph.CO].

[132] Jerome Martin and Vincent Vennin. "Observational constraints on quantum decoherence during inflation". In: *JCAP* 05 (2018), p. 063. DOI: 10.1088/1475-7516/2018/05/063. arXiv: 1801.09949 [astro-ph.CO].

[133] A.D. Dolgov and V.S. Popov. "THE ANHARMONIC OSCILLATOR AND ITS DEPENDENCE ON SPACE DIMENSIONS". In: *Phys. Lett. B* 86 (1979), pp. 185–188. DOI: 10.1016/0370-2693(79)90815-3.

[134] A.K. Dutta and R.S. Willey. "EXACT ANALYTIC SOLUTIONS FOR THE QUANTUM MECHANICAL SEXTIC ANHARMONIC OSCILLATOR". In: *J. Math. Phys.* 29 (1988), p. 892. DOI: 10.1063/1.527986.

[135] A. Chatterjee. "Large n expansions in quantum mechanics, atomic physics and some O(n) invariant systems". In: *Phys. Rept.* 186 (1990), pp. 249–372. DOI: 10.1016/0370-1573(90)90048-7.

[136] Sidney R. Coleman, R. Jackiw, and H.David Politzer. "Spontaneous Symmetry Breaking in the O(N) Model for Large N*". In: *Phys. Rev. D* 10 (1974), p. 2491. DOI: 10.1103/PhysRevD.10.2491.

[137] David Campo and Renaud Parentani. "Inflationary spectra and partially decohered distributions". In: *Phys. Rev. D* 72 (2005), p. 045015. DOI: 10.1103/PhysRevD.72.045015. arXiv: astro-ph/0505379.

[138] David Campo and Renaud Parentani. "Decoherence and entropy of primordial fluctuations. I: Formalism and interpretation". In: *Phys. Rev. D* 78 (2008), p. 065044. DOI: 10.1103/PhysRevD.78.065044. arXiv: 0805.0548 [hep-th].

[139] Clifford Cheung et al. "The Effective Field Theory of Inflation". In: *JHEP* 03 (2008), p. 014. DOI: 10.1088/1126-6708/2008/03/014. arXiv: 0709.0293 [hep-th].

[140] Holger Gies and Stefan Lippoldt. "Renormalization flow towards gravitational catalysis in the 3d Gross-Neveu model". In: *Phys. Rev. D* 87 (2013), p. 104026. DOI: 10.1103/PhysRevD.87.104026. arXiv: 1303.4253 [hep-th].

Présentation de la thèse

La théorie quantique des champs en espace-temps courbe, c'est-à-dire en présence d'une géométrie non triviale, est considérée comme une bonne approximation d'une possible théorie de la gravité quantique, dans de nombreux contextes où les énergies typiques des processus sont très en deçà de l'échelle de Planck [1]. La description correcte de la production des inhomogénéités primordiales à partir des fluctuations quantiques dans l'Univers primordial comte parmi ses résultats les plus marquants. Cette approche aboutit au spectre des fluctuations de température dans le rayonnement diffus cosmologique (RDC) [2], et se manifeste également dans la formations des grandes structures de l'Univers. En effet, la phase d'inflation, introduite initialement comme une possible solution à des problèmes théoriques du modèle standard cosmologique [3–6], s'appuie sur une expansion exponentielle, qui amplifie les fluctuations quantiques initialement microscopiques à des échelles cosmologiques macroscopiques. Cette phase correspondant approximativement à un espace-temps de Sitter, l'étude des effets quantiques dans une telle géométrie est important à au moins deux titres. Sur un plan théorique, cette étude est motivée par le besoin d'une description cohérente des corrections d'ordre supérieur, pour comprendre le succès de la description actuelle. Dans le même temps, l'augmentation de la précision des expériences de cosmologie ouvre la perspective intéressante de tester des aspects quantiques fondamentaux.

Le calcul menant au spectre de puissance invariant d'échelle pour l'inflaton est aujourd'hui essentiellement basé sur une description linéarisée [7, 8]. Le traitement des ordres supérieurs dans le développement perturbatif est en principe requis par la présence de non-linéarités, sous la forme d'interactions de l'inflaton, ou simplement intrinsèques à la gravité dans la théorie de la relativité générale. Toutefois, le calcul de diagrammes à boucles dans une géométrie de Sitter pose des difficultés, directement liées au mécanisme d'amplification qui motive la phase d'inflation. Celles-ci se manifestent à travers une importante production de particules dans le secteur infrarouge (superhorizon) de la théorie [9–12], qui provoque des divergences problématiques dans le intégrales de boucles [11, 13, 14]. Ces dernières ne peuvent pas être traitées avec les outils habituels de la renormalisation perturbative, développée en espace plat, et sont plutôt le reflet d'effets non-perturbatifs et non triviaux dans l'infrarouge.

Le traitement correct de ces divergences est un sujet de recherche actif depuis une quarantaine d'années, avec un intérêt récemment renouvelé, et a conduit à une profusion d'approches non-perturbatives et d'études de ces non-linéarités. Une des pre-

mières techniques introduites dans ce contexte est le formalisme stochastique [15–18]. Ce dernier décrit la dynamique des modes super-horizon en termes d'une équation de Langevin, sourcée par les modes sortant de l'horizon au cours de l'expansion. Cette approche permet en fait de resommer les contributions logarithmiques dominantes du développement diagrammatique [11, 19, 20], et est donc capable de décrire des effets authentiquement non-perturbatifs. Des techniques de théorie des champs, initialement développées pour étudier des effets non-perturbatifs en espace-temps plats, ont en parallèle été adaptées et développées au cours des ans [21–42]. Parmi elles, les deux qui seront principalement utilisées au cours de cette thèse sont des développement en $1/N$ et le groupe de renormalisation fonctionnel (GRF) [43–45]. Ce dernier est particulièrement utile pour traiter la physique dans l'infrarouge, et est utilisé dans des situations très diverses, allant des phénomènes critiques [46, 47] à la gravité quantique [48]. Une étude systématique a été réalisée pour des champs scalaires tests en espace-temps de Sitter, dans l'approximation du potential local (APL) [39], et a obtenu des résultats identiques au formalisme stochastique dans la limite appropriée.

Les divergences séculaires, qui grossissent en fonction du temps cosmique, apparaissent comme des manifestations spécifiques fréquentes des divergences infrarouges dans le contexte cosmologique [13, 14]. Ce comportement apparaît également dans les théories quantiques des champs hors équilibre, comme un artéfact de calcul de l'approche perturbative, qui disparaît après une resommation appropriée [49–51], et des méthodes similaires ont été implémentées en espace-temps de Sitter [29, 34, 35]. Simultanément, dans de Sitter, ces contributions importantes des diagrammes à boucles pourraient conduire à une importante rétroaction sur la géométrie ambiante, et ont parfois été considérées comme l'origine d'une potentielle instabilité de cet espace-temps [10, 12, 52–62]. Ce type de rétroaction pourrait également fournir une résolution du problème de la constante cosmologique [63–65], via un mécanisme d'écrantage dynamique. Cependant, dans la logique de l'approche de la théorie des champs hors équilibre, ces contributions pourraient simplement être la conséquence d'un développement perturbatif invalide. Une des thématiques principales de cette thèse est d'étudier cette idée dans de Sitter en utilisant une généralisation appropriée du GRF appliqué aux champs tests. L'utilisation du GRF est motivée par le fait qu'il ne fait pas apparaître directement des divergences séculaires, mais plutôt des divergences infrarouges dans l'espace des moments. Ceci permet en particulier de considérer la stabilité au cours du flot de renormalisation, et non de la coordonnée temporelle, ce qui permet de préserver les symétries de de Sitter.

Même dans le cas des champs scalaires tests, les calculs explicites non-perturbatifs sont essentiellement limités à des fonctions à un point, et peu de résultats explicites existent pour des corrélateurs plus compliqués, avec une dépendance en plusieurs points d'espace-temps. Un autre objectif de cette thèse est le calcul de ces corrélateurs, qui donnent ensuite accès à des quantités physiques diverses, comme des temps de relaxation, de décohérence, ou des spectres de puissance.

Par exemple, le calcul du GRF dans l'APL permet d'obtenir la masse dynamique, qui mesure l'amplitude des fluctuations locales du champ au sein d'une région de Hub-

ble, mais donne une réponse incorrecte pour des quantités à temps inégaux, comme le temps d'autocorrélation. On explore donc le GRF au delà de l'APL, en particulier pour tester si les ordres supérieurs dans le développement en dérivées améliorent ce résultat. Le calcul dans la théorie des champs Lorentzienne se révèle difficile [40], notamment parce que l'on est obligé de calculer l'équation de flot pour la théorie complète avant de prendre la limite infrarouge. Une alternative possible est de considérer une théorie effective pour l'infrarouge, comme le formalisme stochastique. Il a été démontré que le GRF appliqué sur ce dernier donne des résultats identiques à la limite infrarouge de l'implémentation dans la théorie des champs initiale, dans l'APL [42]. Dans cette thèse, on poursuit cette démarche, et on généralise ce calcul en utilisant le fait que l'approche stochastique peut être vu comme un cas particulier du modèle A dans la classification de Hohenberg et Halperin [66]. Ce dernier a été étudié en détail en physique statistique, en particulier avec le GRF [67, 68]. Le point de départ est une formulation fonctionnelle de l'équation stochastique, que l'on obtient avec la procédure de Janssen-de Dominicis (JdD) [68–70]. Dans le contexte cosmologique, l'intégrale de chemin de JdD est unidimensionnelle, et peut être vue comme une mécanique quantique supersymétrique, qui a été récemment étudiée avec le FRG pour un champ scalaire unique [71]. En s'appuyant sur ces travaux existants, on calcule l'équation de flot pour un modèle $O(N)$ de champs scalaires tests au delà de l'APL, à l'ordre suivant dans le développement en dérivées. On vérifie que ce calcul reproduit le résultat de l'APL', qui inclus une renormalisation indépendante du champ pour le terme cinétique, et a été calculé pour la théorie des champs initiale [40]. La validité du développement en dérivées peut alors être étudiée via un développement $1/N$ de l'équation de flot, que l'on peut comparer à d'autres calcul en $1/N$, également traités dans cette thèse. La précision constatée pour le temps d'autocorrélation est autour de dix pourcent. La même précision est obtenue dans la comparaison dans le cas un champ unique ($N = 1$), avec des résultats numériques connus [18, 72].

Le résultat du calcul avec le GRF montre que l'obtention de formules analytiques au delà de l'APL est difficile. De plus, s'il est en principe possible d'améliorer la précision pour le temps d'autocorrélation en allant à des ordres supérieurs dans le développement en dérivées, on montre qu'il n'est pas à même de reproduire la bonne structure pour le propagateur à temps inégaux. Cette structure a toutefois été correctement obtenue par la résolution des équations de Schwinger-Dyson dans deux cas spécifiques [34, 35]. On applique donc cette méthode, directement à la formulation du formalisme stochastique en intégrale de chemin de JdD. On calcule les *self-energies* pour la théorie effective supersymétrique à une dimension, dans un développement perturbatif jusqu'à trois boucles, ou à l'ordre sous-dominant dans un développement $1/N$. La comparaison avec les résultats obtenus dans la théorie des champs initiale montre une correspondance parfaite pour le corrélateurs infrarouges, ce qui montre une équivalence non triviale avec le formalisme stochastique. Ce contexte offre également une méthode de calcul beaucoup plus simple pour les ordres supérieurs.

Enfin, on s'intéresse à la formulation de l'approche stochastique en termes d'une équation de Fokker-Planck, exprimée comme une équation au valeurs propres [18, 72–

74]. Ceci donne une explication naturelle à la structure du corrélateur que l'on observe à l'ordre sous-dominant [35], comme conséquence de la décomposition spectrale. Dans cet esprit, la résolution des équations de Schwinger-Dyson permet de trouver les première valeurs propres, par le calcul direct des corrélateurs. Par ailleurs, les expressions obtenues à l'ordre dominant dans le développement $1/N$ ont une structure particulièrement simple, qui indique la possibilité d'obtenir l'intégralité du spectre analytiquement. Ce dernier peut en principe être utilisé pour reconstruire n'importe quelle observable. On s'intéresse donc à la possibilité d'appliquer un développement $1/N$ directement au niveau de l'équation de Fokker-Planck, et on calcule explicitement les valeurs et fonctions propres à l'ordre sous-dominant (et sous-sous-dominant pour quelques quantités spécifiques). Pour tester la validité du développement $1/N$, on résout numériquement le problème aux valeurs propres pour un champ sans masse et pour une valeurs de N arbitraire incluant le cas limite où $N = 1$. La comparaison entre les résultats numériques et le développement $1/N$ montre un bon accord même pour des valeurs de N relativement basses, y compris pour $N = 1$ dans certains cas.

La thèse est organisée de la manière suivante. Dans le premier chapitre, on rappelle les raisons pour lesquelles on est amené à introduire une phase d'inflation dans le modèle standard de la cosmologie, qui peut être approximativement décrite par l'espace-temps de Sitter. On présente ensuite quelques aspects techniques concernant l'approche semi-classique, en particulier à propos de la quantification du champ scalaire libre massif, pour souligner un aspect central de la théorie des champs en espace-temps de Sitter, qui est l'amplification gravitationnelle des modes infrarouges. Le dernier outil que l'on introduit est le GRF, formulé dans le formalisme de l'action effective moyenne.

On s'intéresse ensuite à l'étude du problème de la rétroaction dans le second chapitre. On présente tout d'abord une extension minimale au cas de la théorie $O(N)$ de champs scalaires tests. Cela revient à considérer une métrique classique, mais renormalisée uniquement par les fluctuations quantiques des champs scalaires, où l'on ignore en particulier les fluctuations de la métrique comme le graviton. On dérive ensuite les équation d'Einstein semi-classiques, que l'on utilise pour calculer le flot de renormalisation du taux d'expansion de Hubble, dans la limite infrarouge. Le flot est dominé par le potentiel effectif, qui est calculé à partir d'une théorie à zéro dimension. Le GRF permet de considérer plusieurs conditions initiales, et on explore différents régimes, notamment Gaussien, ou profondément non-perturbatif, avec une possible brisure spontanée de symétrie au niveau classique. La limite où N est grand du flot de renormalisation est également discutée, et permet d'obtenir des formules analytiques simples qui permettent d'éclairer la physique mise en jeu.

Dans le troisième chapitre, après une brève dérivation du formalisme stochastique, on rappelle la procédure de JdD. Quelques conséquences générales pour les corrélateurs sont discutées, et on extrait plusieurs contraintes, valides dans l'infrarouge, qui donnent non seulement des interprétations intéressantes en termes de propriétés des systèmes thermiques, mais aussi des relations utiles dans les calculs présentés par la suite. Le GRF est ensuite implémenté, et on montre que le flot du potentiel effectif est capturé exactement dans l'APL. Le flot de l'action effective est ensuite calculé au sec-

ond ordre du développement en dérivées, et la convergence est discutée dans des cas spécifiques.

Finalement, le dernier chapitre s'intéresse à deux approches distinctes pour extraire des résultats analytiques pour les corrélateurs dans un développement $1/N$. Un premier calcul résout directement les équations de Schwinger-Dyson à l'ordre sous-dominant, en resommant une certaine classe de diagrammes à boucles. Le deuxième formule un développement $1/N$ de l'équation de Fokker-Planck, exprimée comme une équation aux valeurs propres. On calcule l'intégralité du spectre à l'ordre sous-dominant.